UNIVERSIDAD POLITÉCNICA DE VALENCIA

DEPARTAMENTO DE INGENIERIA MECÁNICA Y DE MATERIALES

DEVELOPMENT AND CHARACTERIZATION OF NOVEL NANOBIOCOMPOSITES CONTAINING VARIOUS NANOFILLERS TO IMPROVE BARRIER AND OTHER PHYSICAL PROPERTIES OF INTEREST IN FOOD PACKAGING AND COATING APPLICATIONS

TESIS DOCTORAL EUROPEA

Presentada por:

Mª Dolores Sánchez García

Dirigida por:

Dr. José María Lagarón Cabello

Valencia, Enero de 2011

INSTITUTO DE AGROQUÍMICA Y TECNOLOGÍA DE ALIMENTOS (IATA-CSIC)

Grupo de Nuevos Materiales y Nanotecnología

DEVELOPMENT AND CHARACTERIZATION OF NOVEL NANOBIOCOMPOSITES CONTAINING VARIOUS NANOFILLERS TO IMPROVE BARRIER AND OTHER PHYSICAL PROPERTIES OF INTEREST IN FOOD PACKAGING AND COATING APPLICATIONS

Memoria presentada por:

Mª Dolores Sánchez García

PARA OPTAR AL GRADO DE DOCTOR EN INGENIERÍA MECÁNICA Y DE MATERIALES

Valencia, Enero de 2011

Dr. José María Lagarón, Investigador Científico del Consejo Superior de Investigaciones Científicas en el Instituto de Agroquímica y Tecnología de Alimentos (IATA)

CERTIFICA

Que la presente memoria "Desarrollo y caracterización de nuevos nanobiocompuestos con propiedades barrera mejoradas de interés en aplicaciones de envasado alimentario y recubrimientos." constituye la tesis doctoral europea de Dña. Mª Dolores Sánchez García. Asimismo, certifica haber dirigido y supervisado tanto los distintos aspectos del trabajo como su redacción

Y para que conste a los efectos oportunos, firma la presente en Valencia a Enero de 2011

Fdo. José María Lagarón

Dedico este trabajo a

Mis padres y hermano, por su apoyo.
Mi marido Miguel, por su comprensión.
A nuestro futuro hijo, Miguel.

“Nuestra recompensa se encuentra en el esfuerzo y no en el resultado. Un esfuerzo total es una victoria completa.”
Mahatma Gandhi

AGRADECIMIENTOS

Estos casi cinco últimos años han sido para mí unos de los más importantes, intensos y asombrosos de mi trayectoria tanto profesional como personal.

En este tiempo he tenido la enorme suerte y satisfacción de conocer, aprender y trabajar con una persona que realmente admiro, mi director de tesis, Chema. Conocí a Chema con sólo 23 años, y durante estos 5 años, cada día que ha pasado me ha enseñado y transmitido toda su pasión, entusiasmo, motivación y entrega por la investigación. Ha sido un gran maestro, ejemplo y un gran hombre al que le estoy profundamente agradecida por todo lo que he aprendido a su lado, no sólo a nivel profesional sino también personal.

Durante esta etapa también he tenido la suerte de conocer a otras personas, que me han apoyado, ayudado y a las que también les doy las gracias por haber estado a mi lado. Me gustaría hacer una especial mención de agradecimiento para las siguientes compis, gracias Ajo por ser como eres, por tu gran corazón; a mi niña Patri por estar aconsejándome y ayudándome en todo momento; a mi cuqui (Sergi) por compartir codo con codo todo el trabajo, por nuestras risas y bueno momentos; a Amparín por sus consejos y su entusiasmo en todo lo que hace (también a su nene Marcos); a Antonio por sus charlas psicológicas; a Zipi y Zape (Marta y Merche) por sus risas y su buen rollo; a mis niñas Cari (Carol) y Graci, por nuestras risas en el oxtran y nuestros saludos todas las mañanas; a nuestro sueco David, por esos cuatro meses intensos; a toda la gente de Castellón de la UJI (LLuisot, Pilarín, etc…).

A todas mis compis de NBM, a mi niña Sabi, por ser tan especial…a mi cuqui Merche, que vuelvo a nombrar, por su alegría y su optimismo, a María por su motivación y exigencia en el trabajo, a Eugenia en especial por su compresión, apoyo y paciencia en todo momento, así como el resto de chicas NBM: a Pilar, por su agradable acogida; a Rosa, por sus ganas de ayudar, a Sandra, Amina, Cristina y Abi.

A toda la gente que he conocido durante mi estancia en Estocolmo; a Mikael por acogerme en su grupo de trabajo, al resto de compis y sobre todo a mis chicos suecos Fran y Steve, Mathew, a Julieta y Joakim, a Rosana y Gonzalo.

Así como la gente que conocí en mi estancia en Montreal, al Dr. Hoa por acogerme también en su grupo y por todo el trabajo que realizamos, a mi compis Nabeel, a mi niña mejicana Andrea, a mi amigo iraní Bijan, a Luis y Carolyne por su acogida.

También quisiera mencionar a mi hermano, al resto de mi familia; tíos (Lola, Juan, los Cañi…) primos, a mi abuela Eladia, a mis cuñadas y suegros, les agradezco todo su apoyo y confianza en mí.

Así como a mis amigas más cercanas que me han apoyado en todo momento; Marta, Natalia, Aran y Bárbara. Gracias por estar siempre ahí. También a Mariví, Marta (playa), Edurne, Paula, Estrella…

Pero especialmente quisiera darle las gracias a mis padres, porque siempre han confiado en mí y me han apoyado en todos los momentos de mi vida, porque realmente sabían lo importante que era para mí este esfuerzo de investigación. Gracias por ser los mejores.

Así como a una persona muy especial, que también ha vivido cada paso de mi tesis y ha sido mi compañero y cómplice en esta etapa de mi vida, Miguel, al que era mi novio cuando empecé con la tesis, ya mi marido y ahora el futuro padre de nuestro hijo Miguel Junior, el que también está acompañándome durante estos casi 8 últimos meses de esta etapa de mi tesis y le dedico todo mi esfuerzo realizado.

List of Publications

This thesis is the summary of the following papers:

1. M.D. Sanchez-Garcia, E. Gimenez and J.M. Lagaron. Comparative Barrier Performance of Novel PET Nanocomposites with Biopolyester Nanocomposites of Interest in Packaging Food Applications. Journal of Plastic Film and Sheeting 2007; 23 133-148.
2. M.D. Sanchez-Garcia, E. Gimenez and J.M. Lagaron. Development and Characterization of Novel Nanobiocomposites of Bacterial Poly(3-hydroxybutirate), Layered silicates and Poly(ε-caprolactone). Journal of Applied Polymer Science 2008; 108, 2787–2801.
3. M.D. Sanchez-Garcia, E. Gimenez and J.M. Lagaron. Mophology and Barrier Properties of Solvent Cast Composites of Thermoplastic Biopolymers and Purified Cellulose Fibers. Carbohydrate Polymers 2008; 71 235–244.
4. A. Fernández, M.D. Sánchez-García, M. Ankerfors and J.M. Lagaron. Effects of Ionizing Radiation in Ethylene-Vinyl Alcohol Copolymers and in Composites Containing Microfibrillated Cellulose. Journal of Applied Polymer Science. Journal of Applied Polymer Science 2008; 1, 126-134.
5. M.D. Sanchez-Garcia, E. Gimenez, M.J. Ocio and J.M. Lagaron. Novel Polycaprolactone nanocomposites containing thymol of interest in antimicrobial film and coating applications. Journal of Plastic Film and Sheeting 2008, 24, 239-251.
6. D. Nordqvist, M. Dolores Sanchez, M.S. Hedenqvist and Jose M. Lagaron. Incorporating amylopectin in poly(lactic acid) by melt blending using poly(ethylene-co-vinyl alcohol) as a thermoplastic carrier. (i) Morphological characterization. Journal of Applied Polymer Science 2009; 115, 3, 1315 – 1324.
7. M.D. Sanchez-Garcia, D. Nordqvist, M.S. Hedenqvist and Jose M. Lagaron. Incorporating amylopectin in poly(lactic acid) by melt blending using poly(ethylene-co-vinyl alcohol) as a thermoplastic carrier. (ii) physical properties. Journal of Applied Polymer Science 2011; 119, 3708–3716.
8. M.D. Sanchez-Garcia and J.M. Lagaron. Novel clay based nanobiocomposites of biopolyesters with synergistic barrier to UV light. Journal of Applied Polymer Science 2010; 118, 1, 188-199.
9. M.D. Sanchez-Garcia, L. Hilliou and J.M. Lagaron. Nanobiocomposites of Carrageenan, Zein and Mica of Interest in Food Packaging and Coating Applications. Journal of Agricultural and Food and Chemistry 2010; 58 11, 6884-6894.
10. M.D. Sanchez-Garcia and J.M. Lagaron. On the use of plant cellulose nanowhiskers to enhance the barrier properties of polylactic acid. Cellulose 2010; 17, 987–1004
11. M.D. Sanchez-Garcia, J.M. Lagaron, S.V. Hoa. Effect of addition of carbon nanofibers and carbon nanotubes on properties of thermoplastic biopolymers. Composites Science and Technology 2010; 70, 1095–1105.
12. M.D. Sanchez-Garcia, A. Lopez-Rubio and J.M. Lagaron. Natural Micro and Nanobiocomposites with Enhanced Barrier Properties and Novel Functionalities for Food Biopackaging Applications. Trends in Food Science and Technology 2010; 21; 528-536

13. M.D. Sanchez-Garcia, L. Hillou and J.M. Lagaron. Morphology and Barrier Properties of Solvent Cast Nanobiocomposites of κ/ι--carrageenan and Cellulose Nanowhiskers. Journal of Agricultural and Food and Chemistry 2010; 58, 12847–12857.

And the following Patent Application

14. Patente 200703100. Nuevos materiales nanocompuestos con propiedades de bloqueo de la radiación electromágnetica infrarroja, ultravioleta y visible y procedimiento para su obtención.

Desarrollo y caracterización de nuevos nanobiocompuestos con propiedades barrera mejoradas de interés en aplicaciones de envasado alimentario y recubrimientos.

RESUMEN

El desarrollo de nuevos biomateriales con propiedades a medida para aplicaciones en envases de alimentos, es un tema de gran interés actualmente, tanto a nivel académico como industrial. La presente tesis doctoral contiene el desarrollo y caracterización de nuevos biocompuestos y nanocompuestos de biopoliésteres y polisacáridos con diferentes micro y nano aditivos. El principal objetivo de este trabajo ha sido aportar nuevas soluciones, haciendo uso de aditivos naturales, para mejorar las propiedades barrera a gases y vapores de varios bioplásticos, manteniendo las buenas propiedades de la matriz e incluso añadiendo nuevas funcionalidades como el carácter antimicrobiano. El transporte de compuestos de bajo peso molecular a través de los materiales plásticos, (propiedades barrera), es un factor limitante importante para la aplicación de biopolímeros en envasado, recubrimientos y membranas. Por ello, diferentes micro y nanobiocompuestos han sido formulados, con refuerzos basados en nanoarcillas aptos para contacto alimentario, amilopectina, extractos naturales, microfibras y nanotubos de carbono, microfibras de celulosa y nanowhiskers de celulosa. A partir de este trabajo se han desarrollado nuevos nanobiocompuestos los cuales presentan mejor barrera a gases, vapores y luz UV y que a su vez son capaces de liberar de forma controlada sustancias naturales antimicrobianas. Este nuevo balance de propiedades de los compuestos puede ser un gran potencial para el diseño de nuevos materiales para envases y recubrimientos.

Development and Characterization of Novel Nanobiocomposites Containing Various Nanofillers to Improve Barrier and Other Physical Properties of Interest in Food Packaging and Coating Applications.

ABSTRACT

The development of novel biobased materials with tailored properties for food biopackaging applications is a topic of significant interest within academic and industrial laboratories. The current PhD thesis deals with the development and characterization of novel biocomposites and nanobiocomposites of biopolyesters, polysaccharides and proteins containing different micro and nanoadditives. The main aim of the work was to provide novel solutions, making use to the extent possible of natural additives, to enhance the gas and vapour barrier properties of the various biopolymers while retaining the good properties of the matrix and even adding novel functionalities such as antimicrobial character. The transport of low molecular weitght compounds through polymeric materials, i.e. the so-called barrier properties, is known to be a significant limiting factor for the widespread application of biopolymers in packaging, coating and membrane applications. To that end, different micro and nanobiocomposites were formulated which contained as reinforcing elements food contact complying nanoclays, amylopectin, natural extracts, carbon nanofibers and nanotubes, cellulose microfibers and cellulose nanowhiskers. From the work novel biocomposites were developed which exhibited enhanced gas, vapour and UV light barrier and which simultaneously were able to provide controlled release of natural antimicrobials. These new property balanced composites can have significant potential in the design of novel biopackaging and biocoating materials.

Desenvolupament y Caracterització de Nous Nanobiocompostos amb millors Propietats Barrera d'interés en aplicacions com Envasos d'Aliments i Recobriments.

RESUM

El desenvolupament de nous biomaterials amb propietats a mesura per a aplicacions en envasos d'aliments, es un tema de gran interés actualment, tant a nivell acadèmic com industrial. La present tesi doctoral conté el desenvolupament i caracterització de nous biocompostos i nanocompostos de biopolièsters i polisacàrids amb diferents micro i nano aditius. El principal objectiu d'aquest treball ha sigut aportar noves solucions, fent ús d'aditius naturals, per a millorar les propietats barrera a gassos i vapors de diversos bioplàstics, mantenint les bones propietats de la matriu i fins i tot afegint noves funcionalitats com el caràcter antimicrobià. El transport de compostos de baix pes molecular mitjançant els materials plàstics (propietats barrera), és un factor limitant important per a l'aplicació de biopolímers en envasat, recobriments i membranes. Per això, diferents micro i nanobiocompostos han sigut formulats, amb reforçaments basats en nanoarcilles aptes per al contacte alimentari, amilopectina, extractes naturals, microfibres i nanotubs de carboni, microfibres de cel·lulosa i nanowhiskers de cel·lulosa. A partir d'aquest treball s'han desenvolupat nous nanobiocompostos els quals presenten millor barrera a gassos, vapors i llum UV i que a la vegada són capaços d'alliberar de forma controlada substàncies naturals antimicrobianes. Aquest nou balanç de propietats dels compostos pot ésser un gran potencial per al diseny de nous materials per a envasos i recobriments.

CONTENTS

1. Introduction…… 1

1.1 Introduction to packaging……..... 1

1.2 Biodegradable polymers……..... 3

1.3 Nanotechnology to reinforce bioplastics……. 7

1.3.1. Nanoclays……... 7

1.3.2 Cellulosic nanomaterials..... 10

1.3.3 Carbon based nanomaterials..... 12

1.4 Properties of interest in biopackaging applications…….. 13

1.4.1 Barrier properties……..... 13

1.4.1.1 Introduction to mass transport properties…….. 13

1.4.1.2 Modeling mass transfer process…….. 14

1.4.1.3 Measuring mass transport properties……. 19

1.4.1.4 Factors influencing mass transport properties… 22

1.4.1.5 Barrier properties in nanobiocomposites for monolayer packaging: PLA, PCL, PHA and starch…..... 31

1.4.2 Thermal properties……... 35

1.4.3 Mechanical properties…….. 36

1.5 References……..... 40

2. Objectives……..... 48

3. Results…… 49

Chapter I. Nanobiocomposites based on nanoclays…….50

Paper I: M.D. Sanchez-Garcia, E. Gimenez and J.M. Lagaron Development and Characterization of Novel Nanobiocomposites of Bacterial Poly(3-hydroxybutirate), Layered silicates and Poly(ε-caprolactone). Journal of Applied Polymer Science, 2008; 108, 2787–2801 …….50

Paper II: M.D. Sanchez-Garcia, E. Gimenez and J.M. Lagaron. Comparative Barrier Performance of Novel PET Nanocomposites With Biopolyester Nanocomposites of Interest in Packaging Food Applications. Journal of Plastic Film and Sheeting 2007; 23 133-148……...…….83

Paper III: M.D. Sanchez-Garcia and J.M. Lagaron. Novel clay based nanobiocomposites of biopolyesters with synergistic barrier to UV light. Journal of Applied Polymer Science 2010; 118, 1, 188-199…….…….99

Paper IV : M.D. Sanchez-Garcia, L. Hilliou and J.M. Lagaron. Nanobiocomposites of Carrageenan, Zein and Mica of Interest in Food Packaging and Coating Applications. Journal of Agricultural and Food and Chemistry 2010; 58 11, 6884-6894.……125

Paper V: M.D. Sanchez-Garcia, E. Gimenez, M.J. Ocio and J.M. Lagaron. Novel Polycaprolactone nanocomposites containing thymol of interest in antimicrobial film and coating applications. Journal of Plastic Film and Sheeting 2008; 24, 239-251……...154

Chapter II. Nanobiocomposites based on micro and nano cellulose fibers…….....170

Paper VI: M.D. Sanchez-Garcia, E. Gimenez and J.M. Lagaron. Mophology and Barrier Properties of Solvent Cast Composites of Thermoplastic Biopolymers and Purified Cellulose Fibers. Carbohydrate Polymers 2008; 71, 235–244…….....171

Paper VII: M.D. Sanchez-Garcia and J.M. Lagaron. On the use of plant cellulose nanowhiskers to enhance the barrier properties of polylactic acid. Cellulose 2010; 17, 987–1004……...……195

Paper VIII : M.D. Sanchez-Garcia, L. Hilliou and J.M. Lagaron. Morphology and Barrier Properties of Solvent Cast Nanobiocomposites of κ/ι--carrageenan and Cellulose Nanowhiskers. Journal of Agricultural and Food and Chemistry 2010; 58, 12847–12857.....232

Chapter III. Nanobiocomposites based on Carbon nanotubes and Carbon Nanofibers……..259

Paper IX : M.D. Sanchez-Garcia, J.M. Lagaron, S.V. Hoa. Effect of addition of carbon nanofibers and carbon nanotubes on properties of thermoplastic biopolymers. Composites Science and Technology 2010; 70, 1095–1105.……...…….260

Chapter IV. Blends of biobased materials……...286

Paper X: D. Nordqvist, M. Dolores Sanchez, M.S. Hedenqvist and Jose M. Lagaron. Incorporating amylopectin in poly(lactic acid) by melt blending using poly(ethylene-co-vinyl alcohol) as a thermoplastic carrier. (i) Morphological characterization. Journal of Applied Polymer Science 2009; 115, 3, 1315 – 1324……...…….287

Paper XI: M.D. Sanchez-Garcia, D. Nordqvist, M.S. Hedenqvist and Jose M. Lagaron. Incorporating amylopectin in poly(lactic acid) by melt blending using poly(ethylene-co-vinyl alcohol) as a thermoplastic carrier. (ii) physical properties. Journal of Applied Polymer Science 2011; 119, 3708–3716……...……...307

4. Conclusions…….325

5. Annex……...331

1. Introduction

1.1 Introduction to Packaging

A food package has traditionally been considered a container to transport foodstuffs from the place where it had been obtained to where it was going to be retailed and consumed. Food packages are far more important nowadays, since the acceptability of food products is often determined by their preservation role.

The package has become the fifth P during the market analysis of a product: product, price, place, promotion and packaging. With time, more new functions have been added to packages, most of them during the last few decades. The principal function of packaging is protection and preservation of the content from external contamination. This function involves retardation of deterioration, extension of shelf-life, and maintenance of quality and safety of packaged food. Packaging protects foods from environmental influences such as heat, light, the presence or absence of moisture, oxygen, pressure, enzymes, spurious odors, microorganisms, insects, dirt and dust particles, gaseous emissions, and so on. All of these factors cause deterioration of foods and beverages. So, occasionally, the packages actually become more important or costly than the product they contain. Besides containing a product, the package also helps distribution and marketing, increases its quality and shelf-life, making it accessible to more consumers, includes information about the product and brand and can even be designed to reduce tampering and theft in the supermarkets. Furthermore, the extremely demanding markets of the developed countries are permanently asking for novel, sophisticated, ready-to-eat and stable products which retain to the extent possible the taste of the fresh product. It is not enough for the package to keep, or even improve the quality of its content, the large choice offered to consumers makes it necessary for the package also to look good, be ergonomic and make the product attractive to the consumer. In addition, an ideal package should be strong and light to make handling easy throughout the distribution chain, cheap enough to make the product competitive and, obviously, safe for the consumer. Furthermore, the modern vision in food packaging development is no longer focused on the passive role of packaging exploitation in the processing and preservation of foodstuffs and ensuring food integrity and safety. Today, packaging designs also aim at: The one-step transfer of the product directly “from the field to the table”, hence guaranteeing food freshness and safety; and the preparation of “ready-to-eat” food portions in microwaveable packaging containers (bowls and trays) supplying the consumer with warm food dishes.

Moreover, active and intelligent packaging can be considered as a further step in the optimization of packaging efficacy. Active packaging modifies the condition of the packed food without provoking any substantial variation in its quality and nutritional value, while improving its shelf-life and ultimately its safety. Intelligent packaging is meant to monitor the features of the packed food to provide indications of the quality status of the food during storage and handling. A combination of these two attributes in a single packaging material would then be desirable for the maintenance and quality control of the packed food.

Among the wide variety of materials currently utilized in food packaging technology, polymeric materials are taking a major share because of the versatility of their processing methods – extrusion (bubble and cast), injection and compression molding – and their interesting cost/performance ratios. There are various parameters determining the fortunes of natural, artificial or truly synthetic materials aiming to penetrate the food packaging market, notably parity of efficacy in food protection and hence cost/performance.

Using polymers to produce food packages presents even more advantages. They are light and cheap materials and can be heated in microwave ovens. The optical properties of the package (brightness and transparency) can also be adapted to the specific requirements of each product. Transparent packages allow the consumer to see the product, which in most cases produces a good impression. Furthermore filters and pigments can be added to protect the product from the light or from certain radiations. In addition, many polymers are printable, which makes it possible to use them as a way to give the consumer information, to identify the brand or to add an attractive design. Furthermore, polymeric packages can be produced as part of integrated processes where they are formed, filled and sealed in the same production line, making the process quick and cheap and can also be formed into an unlimited variety of sizes and shapes.

Designing a suitable polymeric package for almost every foodstuff would therefore seem to be perfectly possible. Such is the situation that a polymer-based option is available for almost every product and only social and environmental aspects or the cost of the package justify the use of non-polymeric packages.

The environmental drawbacks are mainly related to the extremely slow degradation rate of the most commonly-used polymers and with the fact that most of them are oil-derived products. Although package stability during the shelf-life of the product is an advantage, it turns into a disadvantage when the packages are rarely reused or recycled and the used containers generate huge volumes of residues. This problem has been attenuated by the creation and improvement of recycling systems in many developed countries, but it will only be solved with the introduction throughout the industry of biodegradable polymer resins which, in addition, should be obtained from renewable sources. The other main drawback of polymers for food packaging applications is that they are all permeable to the transport of low molecular weight compounds. The nature of this transport, the laws that govern it and its controlling factors will be discussed later.

1.2 Biodegradable polymers

The substantial increase in the use of plastics has also raised a number of environmental concerns from a waste management point of view. As a result, there is a strong research interest, pushed by authorities at national and international levels, and a concomitant industrial growing demand in the development and use of materials which can disintegrate and biodegrade through processes such as composting into carbon dioxide and water.

Among biodegradable materials, three families are usually considered: The first group includes; polymers directly extracted from biomass such as the polysaccharides chitosan, carrageenan, starch and cellulose and proteins such as gluten, soy and zein. A second family makes use of oil based monomers or of biomass derived monomers but uses classical chemical synthetic routes to obtain the final biodegradable polymer, this is the case of for instance polycaprolactones (PCL), polyvinyl-alcohol (PVOH) and copolymers (EVOH) and for the case of sustainable monomers of polylactic acid (PLA) [1-3]. The third family makes use of polymers produced by natural or genetically modified micro-organisms such as polyhydroxialcanoates (PHA) and polypentapectides [4].

The polymeric materials that are now attracting more commercial interest are some biodegradable polyesters, which can be processed by conventional processing equipment and that are being used in a number of monolayer and also multilayer applications already, particularly in the food packaging and biomedical field. The most widely studied thermoplastic sustainable biopolymers for monolayer packaging applications are starch, PHA and PLA. From these, starch and PLA biopolymers are without doubt the most interesting families of biodegradable materials because they have become commercially available (by for instance companies such as Novamont and Natureworks, respectively), are produced in a large industrial scale and also because they present an interesting balance of properties. Of particular interest in food packaging is the case of PLA due to its excellent transparency and relatively good water resistance. Water permeability of PLA is for instance much lower than that of proteins and polysaccharides but it is still higher than that of conventional polyolefins and PET. Its relatively high stiffness is usually reduced by addiction of plasticizers such as PCL and others but these also lead to a decrease in oxygen barrier and in transparency. Thus, the main drawbacks of this polymer regarding performance are still associated to low thermal resistance, excessive brittleness and insufficient barrier to oxygen and to water compared to for instance other benchmark packaging polymers like PET. It is, therefore, of great industrial interest to enhance the barrier properties of this material while maintaining its inherently good properties such as transparency and biodegradability. [5-11]

Finally, there are also other biomaterials with a high potential in food packaging applications, which are directly extracted from biomass such as gluten, zein prolamine obtained from corn and the polysaccharide chitosan typically obtained from the crustaceous chitin. These materials have excellent barrier properties to oxygen under dry conditions and are transparent (albeit zein is slightly colored). The main drawbacks of these families of materials are their inherently high rigidity, their difficult processability using conventional processing equipment and the very strong water sensitivity arising from their hydrophobic character, which leads to a strong plasticization affecting properties including the excellent oxygen barrier as relative humidity and water sorption increase in the material. The low water resistance of proteins and polysaccharides strongly handicap their use as monolayers in food packaging and aside few particular cases such as starch based materials and in smaller scale gluten and zein, most proteins and polysaccharides are better suited for coatings or multilayer systems. Nevertheless, chitosan and zein biopolymers exhibit two very interesting characteristics: One is that the chitosan displays antimicrobial properties[12-

[13] and the other that zein shows an unusually high water resistance compared to other similar biomaterials.[14] Furthermore, zein in a resin form can also be heat processed. In spite of that, and from an application point of view, it is of great relevance to diminish the water sensitivity of proteins and polysaccharides and to enhance the gas barrier of thermoplastic biopolyesters to make them suitable for monolayer and also for multilayer food packaging applications.

These biodegradable and renewable polymers, like for instance plasticised chitosan, can have excellent barrier properties to gases, albeit the barrier performance is dramatically reduced in the presence of moisture. However, other polymers like the PHAs have very high water barrier properties. So in principle, one could devise a biomass derived high barrier multilayer system where an inner layer of plasticized chitosan could be sandwiched between high moisture barrier PHA layers. An interesting property of some of these biobased polymers, e.g. PLA and starch, is that the permeability of carbon dioxide compared to that of oxygen (permselectivity) is higher than that of most conventional mineral oil based plastics. This is for instance of interest for some food packaging applications where high barrier to oxygen is required, but CO_2 generated by the product should be allowed to exit the package head space to avoid package swelling. However, some of these materials, still suffer from relatively high production costs and shortages in properties to compete with other conventional plastic materials now in the market. Figure 1 shows a general mastercurve representing oxygen permeability vs. the ratio cohesive energy density/fractional free volume for a number of plastics and the gas barrier properties at dry conditions for the bioplastics families for comparison purposes.

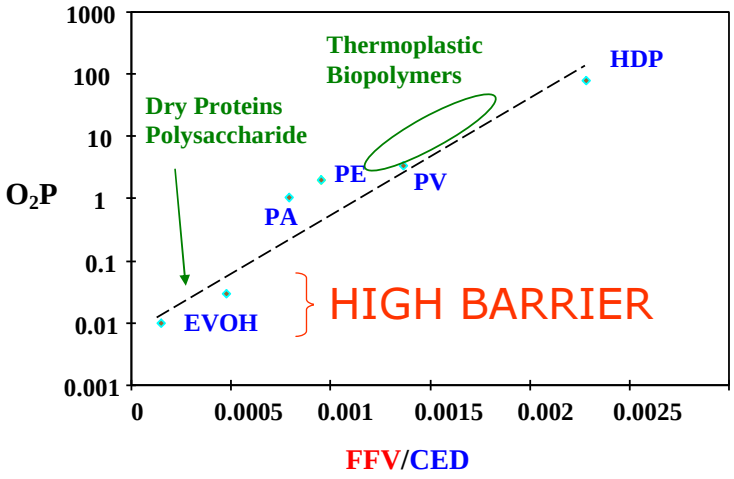

Figure 1. O_2P (cc mm/m^2 day atm) vs. the fractional free volume/cohesive energy density ratio for a number of polymers and biopolymers typically used in packaging applications

Therefore, for most biodegradable polymers it is required to improve some of their properties, such as gas barrier characteristics and mechanical properties, so that they can compete with greater advantage with petroleum-based materials. Therefore, modification of the biodegradable polymers through innovative technologies is a significant challenge for material scientists. Nanoreinforcement of these biodegradable polymers to prepare nanocomposites has already been proven to be an effective way to enhance these properties concurrently. So, these newly developed renewable and biodegradable polymer-based nanocomposites, that is, green nanocomposites, are the wave of the future are considered as the next generation of materials. In fact, renewability, has become a more important driving market force than even biodegradability, since renewable materials can lead to reduce the carbon foot print of packaging. In this respect biopolymers, i.e. renewable polymers, rather than just biodegradable polymers are currently of more important value for packaging.

1.3 Nanotechnology to reinforce biopolymers

Nanotechnology is defined as the controlled ability to manufacture products which are in at least one of the dimensions below 100 nm. For most applications of biodegradable polymers it is required to improve some of their properties, such as gas barrier characteristics and mechanical properties, so that they can compete with greater advantage with petroleum-based materials. Therefore, modification of biodegradable polymers through innovative technologies is a significant challenge for material scientists. Nanoreinforcement of these biodegradable polymers to prepare nanocomposites or composites has already been proven to be an effective way to enhance these properties concurrently. So, these newly developed biodegradable polymer-based nanocomposites or composites, that is, green nanocomposites, are the wave of the future and considered as the next generation materials.

1.3.1 Nanoclays

The commonly used layered silicates for the preparation of polymer/layered silicate nanocomposites belong to the same general family of 2:1 layered- or phyllosilicates. [15,16] Their crystal structure consists of layers made up of two tetrahedrally coordinated silicon atoms fused to an edge-shared octahedral sheet of either aluminum or magnesium hydroxide. The layer thickness is around 1 nm, and the lateral dimensions of these layers may vary from 30 nm to several microns or larger, depending on the particular layered silicate. Stacking of the layers leads to a regular Van der Waals gap between the layers called the interlayer or gallery. Isomorphic substitution within the layers (for example, Al^{3+} replaced by Mg^{2+} or $Fe^{2+,}$ or Mg^{2+} replaced by Li^{1+}) generates negative charges that are counterbalanced by alkali and alkaline earth cations situated inside the galleries. This type of layered silicates are characterized by a moderate surface charge known as the cation exchange capacity (CEC), and generally expressed as mequiv/100 g. This charge is not locally constant, but varies from layer to layer, and must be considered as an average value over the whole crystal.

Montmorillonite, hectorite, and saponite are the most commonly used layered silicates. Layered silicates include in their structure two types of crystalline cells: tetrahedral-substituted and octahedral-substituted. In the case of tetrahedrally substituted layered silicates the negative charge is located on the surface of silicate layers, and hence, the polymer matrices can interact more readily with these than with octahedrally-substituted material. Details regarding the structure for the 2:1 layered silicates, for example MMT, are provided in Figure 2.

Two particular characteristics of layered silicates that are generally considered for the preparation of nanocomposites are the ability of the silicate particles to disperse into individual layers and to be modified at the surface through ion exchange reactions with organic and inorganic cations. These two characteristics are, of course, interrelated since the degree of dispersion of layered silicate in a particular polymer matrix depends on the interlayer cation.

To render layered silicates miscible with biodegradable polymer matrices, one must convert the normally hydrophilic silicate surface to an organophilic one, making the intercalation of many biodegradable polymers possible. Generally, this can be done by ion-exchange reactions with cationic surfactants including primary, secondary, tertiary, and quaternary alkylammonium or alkylphosphonium cations.
Alkylammonium or alkylphosphonium cations in the organosilicates lower the surface energy of the inorganic host and improve the wetting characteristics of the polymer matrix, and result in a larger interlayer spacing. Additionally, the alkylammonium or alkylphosphonium cations can provide functional groups that can react with the polymer matrix, or in some cases initiate the polymerization of monomers to improve the adhesion between the inorganic and the polymer matrix.[18, 19]

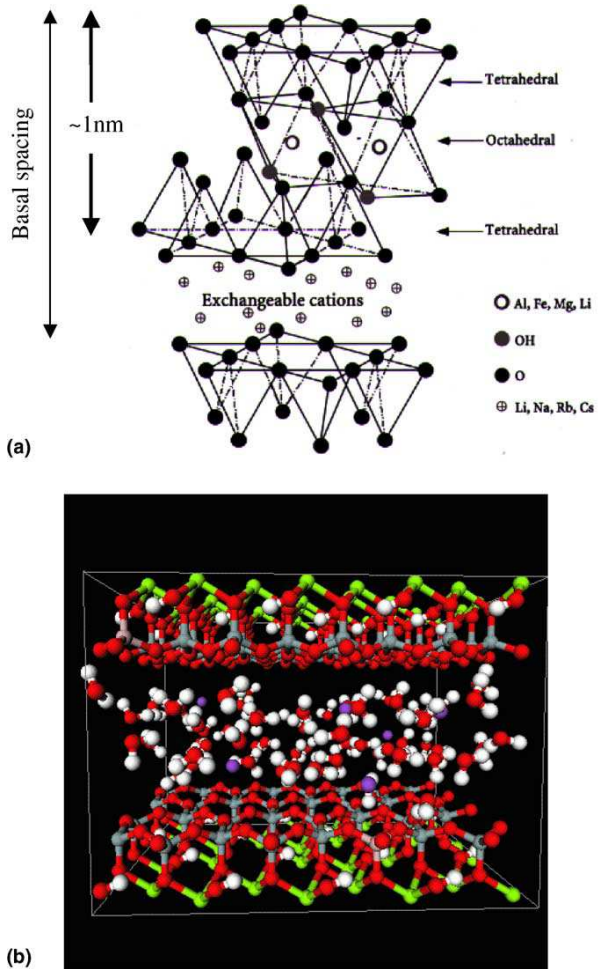

Figure 2. (a) Structure of 2:1 phyllosilicates. [17] Reproduced from Sinha Ray and Okamoto by permission of Elsevier Science Ltd., UK. (b) 3D crystal image of MMT.

The impact on properties by reinforcement of biopolymers with organically modified layered nanoclays has been described above. Thus, it is known that the addition of low contents of nanoclays (less than 10 wt.-%), leads to a remarkable increase in rigidity (elastic modulus)[20, 21], thermal and dimensional stability, and in the barrier properties to gases and vapours[22, 23, 19] without compromising other properties like toughness or transparency. Moreover, addition of nanoclays to bioplastic matrices such as chitosan or methyl cellulose has also been proven not to compromise the biodegradability of the composite materials during composting experiments. [24]

1.3.2 Cellulosic materials

Cellulose, the building material of, for instance, the long fibrous cell walls in green plants, is a highly strong natural polymer with formula $(C_6H_{10}O_5)n$, consisting of a linear chain of several hundred to over ten thousand β(1→4) linked D-glucose units. Cellulose fibers are inherently a low cost and widely available material. Moreover, they are environmentally friendly and easy of recycling by combustion and require low energy consumption in manufacturing. All of this makes cellulosic nanofillers an attractive class of nanomaterial for elaboration of low cost, lightweight, and high-strength nanocomposites.[25, 26] Basically two types of nanoreinforcements can be obtained from cellulose – microfibrils and nanowhiskers. [27]

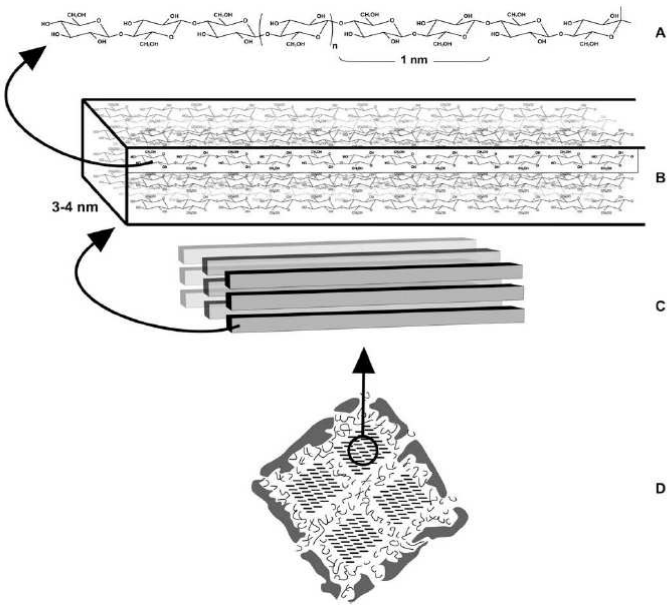

Figure 3. Internal structure of a cellulose microfibril: (A) a cellulose chain; (B) an elementary fibril containing bundles of cellulose chains; (C) parallel elementary fibrils; (D) four microfibrils held together by hemicellulose and lignin. (Adapted from Ramos, L. P. (2003). [28])

Figure 3 presents a schematic model of the structure of a microfibril. The microfibrils have nanosized diameters (2–20 nm, depending on the origin), and lengths in the micrometer range.[27, 29] Each microfibril is formed by aggregation of elementary fibrils, which are made up of crystalline and amorphous parts. The crystalline parts, which can be isolated by several treatments, are the whiskers, also known as nanocrystals, nanorods, or rodlike cellulose microcrystals[30] , with lengths ranging from 500 nm up to 1–2 µm, and about 8–20 nm or less in diameter [30, 31], resulting in high aspect ratios. The main method used to obtain cellulose whiskers has been acid hydrolysis, consisting basically in removing the amorphous regions present in the fibrils leaving the crystalline regions intact; the dimensions of the whiskers after hydrolysis depend on the percentage of amorphous regions in the bulk fibrils, which varies from source

to source.[32] Cellulose nanowhiskers (CNW) are not yet fully exploited commercially although they are commercially available.

Reinforcement of some of these bioplastics with lignocellulosic fibers has been previously carried out with the overall aim of increasing its biodegradation rate and to enhance mechanical properties, i.e. this route led to considerable improvements in the composites tensile strength.[33]However, to the best of our knowledge, there is very little literature on the use of these reinforcing fibres to modify the barrier properties of such biopolymers. In the area of synthetic polymers, Fendler et al. first reported an increase in the oxygen and limonene barrier properties of HDPE composites containing varying amounts of highly purified alpha cellulose fibers as a filler and maleic anhydride grafted polyethylene as a compatibilizer, concluding that 20 wt.-% was the optimum fiber loading level in terms of overall property balance. [34] This pioneering paper stated for the first time the potential for this type of cellulosic microfibers to enhance, in addition to the well reported mechanical properties, the barrier properties of the polymer matrix. Lignocellulosic materials are thus suitable fillers or reinforcing agents for biodegradable matrices since they exhibit a number of interesting properties such as a renewable nature, wide variety of feedstocks available, non-food agricultural based economy, low energy consumption, low cost, low density, high specific strength and modulus, comparatively easy processability due to their nonabrasive nature (allowing high filling levels and significant cost savings) and highly reactive surface, which can be used for grafting specific groups.[35]

Additionally, reinforcement of biopolymers with dispersed cellulose nanowhiskers (CNW) has been reported to increase mechanical properties, improving the thermal stability of the materials.[36, 37] However, very little is known about the effect of the CNW on the barrier properties of nanocomposites in general and of PLA in particular.

1.3.3 Carbon Based namomaterials

Carbon nanotubes (CNTs) are an extremely important class of nanostructured materials due to their unique mechanical, electrical and thermal properties. CNTs are the third allotropic form of carbon and were synthesized for the first time by Iijima in 1991.[38] Their exceptional properties depend on the structural perfection and high aspect ratio (typically ca 300–1000). Carbon nanotubes (CNTs) may consist of a one-atom thick single-wall nanotube (SWNT), or a number of concentric tubes called multiwalled nanotubes (MWNT), having extraordinarily high aspect ratios and elastic modulus.[39] The typical diameters of SWNTs are in 0.7–1.5 nm range, of MWNTs in the 10–50 nm range, and for carbon nanofibers (CNF) in the 60–200 nm range. In SWNT and MWNT, graphitic planes are parallel to the tube axis, while in CNF, graphitic planes make a small angle to the fiber axis. [40]

These type of fillers have been added to polymers and in particular to biopolymers with the overall aim of increasing the biodegradation rate, enhance mechanical properties and increase the thermal and electrical conductivity for different applications such us biomedical, automotive, packaging and electronics.[41-44]

However, very little is known about the effect of these nanofillers on the barrier properties to gases and water vapour of bioplastics

1.4 Properties of interest in biopackaging applications

1.4.1 Barrier properties.

1.4.1.1 Introduction to mass transport properties

When the transport of a molecule takes place from one side of a polymer film to the other, this process is referred to as permeation. This phenomenon takes place when a polymer film separates two environments with different concentrations of a compound. In this case, the low molecular weight substance receives the name of permeant and the phenomenon is usually characterized by the permeability coefficient (P). Permeation is a complex mechanism which involves the ingress of the permeant into the polymer by a sorption process on the high pressure (high concentration) side of the package wall, its diffusion through the polymer towards the low pressure side and its desorption on the low pressure side. The permeability (P) coefficient becomes thus the product of the solubity (S) and diffusion (D) coefficients related to sorption and diffusion processes, respectively. Often, the gain or loss of substances (environmental gases, water, food components…) causes dramatic changes in the product, affecting considerably its shelf-life. Chemical reactions, changes in flavour profile or morphological changes in water sensitive products are just a few examples of the negative effects that mass transfer can cause. Another mass transfer process that may result detrimental from a product quality view point is the sorption or scalping of product components to the packaging materials.

However, the most concerned mass transport phenomenon that can take place is the migration of packaging elements into the product. The term migration usually refers to the transfer of undesired substances (mostly residues and polymer additives) from the plastic container to the package foodstuff, with negative effects on the product. When this process involves substances which have been intentionally added to the polymer matrix for subsequent delivery to the food, as in some active packages, it is known as controlled release.

Migration compounds mainly include residual monomers, plastic processing additives and molecules that have been sorbed by the plastic container during previous use or recycling process. Packaging migration is important in the food industry because it can change organoleptic properties and even cause certain levels of toxicity within the food. For this latter reason, migration has become the focus of food packaging legislation in many countries and experimental procedures for its measurement are usually set out in the regulations. [45]
The controlled release of active substances from a matrix was first developed by the pharmaceutical industry. Although the use of carriers to transport a drug through the human body and to release it when specific locations are reached is common, the use of this technology in the food packaging industry is relatively new. It usually consists of a packaging material which contains active substances incorporated in its structure or in an independent element on such a way that they are released during storage,

continuously supplying the product with a controlled dose. The types of active substances being release include among others natural antioxidants and other bioactive ingredients and antimicrobial substances.

1.4.1.2 Modeling mass transfer processes

The permeation of low-molecular weight chemical species through a polymeric matrix is generally envisaged as a combination of two processes, i.e. solution and diffusion[46]. A solution-diffusion mechanism is thus applied, which can be formally expressed in terms of permeability (P), solubility (S) and diffusion (D) coefficients as follows:

$$P = D \cdot S \qquad \text{(Eq. 1)}$$

Where the diffusion coefficient, D, characterizes the average ability of the dissolved penetrant to move among the polymer segments comprising the film. The solubility coefficient, S, is thermodynamic in nature and is related to slope of the equilibrium sorption isotherm of the penetrant of interest, so a large value of S implies a large tendency for the penetrant to dissolve, or "sorb", into the polymer [47].

1.4.1.2.1 Diffusion

Thus, the movement of low molecular weight substances through polymers has generally been described through the free-volume theory. According to this theory, the movement of low molecular weight permeants through a polymer can be simplified as follows: A permeant molecule will only enter the polymer if the movements of the chains permits the opening of a hole in the polymer's structure and the energy of the permeant becomes smaller inside the hole. A new jump takes only place if the energy of the molecule is lowered in the new hole (and so on successively, jumping from hole to hole it reaches equilibrium).

The characteristics of this transport are determined by the nature of the permeant and the kind of interactions it can establish with the polymer matrix. Usually, diffusion can be described by the law of Fick.

This occurs when the rate of diffusion is much lower than the relaxation rate of the polymer and the diffusion coefficient is constant [48]. In this case, the movement of the penetrant across the polymer is described quantitatively using Fick´s laws of diffusion. When diffusion takes place through a polymer film, Fick´s first law expresses the transfer rate of the diffusing substance per unit of area (F) in the steady state as:

$$F = -D\frac{\partial c}{\partial x} \qquad \text{(Eq. 2)}$$

where c is the solute concentration in the polymer, x the direction of diffusion, and D the diffusion coefficient.

In the unsteady-state, the concentration of the solute in the polymer changes during the experiment following Fick´s second law:

$$\frac{\partial C}{\partial t} = \frac{\partial}{\partial t}\left(D\frac{\partial C}{\partial x} \right) \quad \text{(Eq. 3)}$$

To determine the diffusion coefficient, it is necessary to solve equation (3) by applying the boundary limits which best describe the experimental conditions. Solutions to the most common situations have been compiled by Crank.[49]

The most frequent case takes place when, at the beginning of the experiment (t=0), both sides of a previously equilibrated infinite layer of polymer are exposed to an environment with a new and constant concentration of the diffusing substance. If the polymer is initially free of permeant, the thickness of the film is homogenous and constant during the experiment, the mass gained by the film can be described using the following equation as a function of the diffusion coefficient:

$$\frac{M_t}{M_\infty} = 1 - \sum_{n=0}^{\infty} \frac{8}{(2n+1)^2\pi^2} \exp\left(\frac{(2n+1)^2\pi^2 Dt}{l^2} \right) \quad \text{(Eq. 4)}$$

Where M_t and M_∞ are respectively the uptake at a time t and when equilibrium is reached and l is the film thickness.

Sometimes it is analytically easier to monitor the desorption of the substance from a film. In this case, the film is previously equilibrated by exposing both sides of a constant concentration of the solute. At the beginning of the test, the sample is put in a sorbate-free environment. After changing the boundary conditions, equation 4 becomes equation 5, a general expression used to fit desorption curves.

$$\frac{M_t}{M_\infty} = \sum_{n=0}^{\infty} \frac{8}{(2n+1)^2\pi^2} \exp\left(\frac{-(2n+1)^2\pi^2 Dt}{l^2} \right) \quad \text{(Eq. 5)}$$

In both cases, a plot of the weight uptake versus time yields a curve that increases or decreases exponentially until it reaches its equilibrium value at $M_t/M_\infty=1$ or 0. Although the most exact way to obtain the diffusion coefficient is to fit these curves, the use of simplified solutions is generally accepted.

One of the most frequently-used approaches to simplify the analysis of sorption experiments is based on the proportionality between M_t/M_∞ and $\sqrt{t}$ in the initial section of the sorption process. When $0 < M_t/M_\infty \leq 0.5$, the mass transport process can be described by the following expression, know as the short time solution:

$$\frac{M_t}{M_\infty} = \frac{4}{l}\sqrt{\frac{D}{\pi}}\sqrt{t} \qquad \text{(Eq. 6)}$$

When this equation is used, the value of the diffusion coefficient is given by the fit of a plot of M_t/M_∞ versus $\sqrt{t}$ to a straight line.

When only the data closer to sorption equilibrium are considered (i.e. those where $M_t/M_\infty \geq 0.5$), the fit can be carried out using only the first term of the equation 3, which receives the name of long time solution (equation 7).

$$\frac{M_t}{M_\infty} = 1 - \frac{8}{\pi^2}\exp\left(\frac{-D\pi^2 t}{l^2}\right) \qquad \text{(Eq. 7)}$$

To obtain the diffusion coefficient, this expression is usually represented in the logarithmic form, equation 8, and the kinetic parameter is estimated from the fit to a straight line of a plot of the first term versus time:

$$\ln\left(1 - \frac{M_t}{M_\infty}\right) = \ln\left(\frac{8}{\pi^2}\right) - \frac{D\pi^2}{l^2}t \qquad \text{(Eq. 8)}$$

The error when the diffusion coefficient is obtained by using equations 6 and 8 instead of the complete equation is usually below 0.1%. [50]

1.4.1.2.2 Sorption

The sorption of low molecular weight compounds into a homogenous polymer is usually classified in the following main categories:

In rubbery polymeric structures, Henry's law is often used to describe the sorption of non-interacting compounds.[51] This basic law postulates that the concentration of solute in the polymer (C_i) is proportional to its partial pressure (p_i), both parameters being related by the solubility coefficient (S), i.e. $C=S_i \cdot p_i$.

In semi-crystalline polymers, it is often necessary to use the dual sorption model to characterize the sorption isotherm. This model, proposed by Barrer et al. [52] considers the co-existence of molecules specifically and non-speciafically sorbed onto the polymer matrix. While the sorption isotherm of the former is described using a Langmuir type isotherm, that of non-specifically adsorbed molecules is described by Henry´s sorption model.[53]

$$C = C_D + C_H = S_i \cdot p_i + \frac{C_H' \cdot b}{1 + p_i \cdot b} \qquad \text{(Eq. 9)}$$

Where C_D is the amount of solute non-specifically sorbed, C_H is the amount of the solute specifically bonded within the polymer and $C´_H$ and b are the hole saturation and hole affinity constants.

When some polymeric samples are exposed to environments with high activities of certain solutes, a positive deviation from Henry´s law can sometimes be observed. This positive deviation of Henry´s equation, which receives the name of plasticization, was first described by Vieth et al. [54] who considered it a consequence of the exposure of more binding sites after the swelling of the polymer network. When water activity is sorbed in polar polymers, the positive deviations are usually very strong, giving a clear concave upward shape to the curve. In these cases, sorption occurs not only through normal dissolution but also through the formation of immobilized cluster of water.[55]

When plasticization of the polymer takes place, the term C_D is not described using Henry´s law, but it can be estimated using a modified version of the Flory-Huggins equation. [56]

$$\ln(P) = \ln\left(\frac{C_D}{\rho + C_D}\right) + \left(1 - \frac{C_D}{\rho + C_D}\right) + \chi\left(1 - \frac{C_D}{\rho + C_D}\right) \quad \text{(Eq. 10)}$$

where ρ is the density of the permeant and χ the Flory-Huggins interaction parameter.

1.4.1.2.3 Permeation

Permeation across films is usually estimated in the steady state, when a constant flow of permeant has been established across a film of thickness l. With these boundary conditions, equation 2 reduces to:

$$F = -D\frac{\partial c}{\partial x} = -D\frac{C_1 - C_0}{l} \qquad \text{(Eq. 11)}$$

where C_1 and C_0 are the concentrations of the solute at each surface of the polymer film.

Applying Henry's law, these concentrations can be expressed in terms of the partial pressure of the solute in the gaseous phases to which the two surfaces of the films are exposed:

$$F = -D\frac{\partial c}{\partial x} = -D\frac{C_1 - C_0}{l} = -D \cdot S\frac{\rho_1 - \rho_0}{l} = D \cdot S\frac{\Delta p}{l} \quad \text{(Eq. 12)}$$

The product of the diffusion and solubility coefficients is known as the permeability coefficient (P) and can be defined using equation 1:

$$P = D \cdot S = \frac{F \cdot l}{\Delta p} = \frac{q \cdot l}{A \cdot t \cdot \Delta p} \qquad \text{(Eq. 13)}$$

where q represents the quantity of permeant (volume or mass) passing through the polymer film, t the time and A the effective area.

Permeation is a basic characteristic of the polymer materials used in package design. Besides the permeability coefficient, permeation can also be characterized using the following magnitudes. [51]:

Mass flow rate: $F = \frac{q}{A \cdot t}$ (Eq. 14)

Permeance: $R = \frac{q}{A \cdot t \cdot \Delta p}$ (Eq. 15)

1.4.1.3 Measuring mass transport properties

1.4.1.3.1 Sorption based methods

When both sides of a polymer film are exposed to a known constant partial pressure (or concentration) of a gaseous (or liquid) sorbate, the initially "dry" polymer takes up sorbate until the system reaches equilibrium. In these conditions, equation 4 describes the evolution of the relative sorbate uptake with time, while the equilibrium gain at different values of the sorbate activity can be used to obtain the sorption isotherm. As mentioned before, similar comments are applicable if the desorption of a solute from a previously equilibrated sample is monitored (equation 5).

Several analytical procedures based on sorption or desorption of a solute can be used to measure the mass transport properties of polymers. These methods are: gravimetric method, thermal desorption or purge and trap method, supercritical fluid extraction (SFE), headspace analysis: solid phase micro-extraction (SPME) and optical methods.

However, in the thesis sorption has been estimated by gravimetric methods. Gravimetry is probably the oldest and simplest method for determining mass transport properties from sorption or desorption experiments. By recording the weight and plotting it against time, sorption curves are obtained. The fit of these curves to any of the equations 4-8 is then used to obtain the diffusion coefficient as described above. The solubility coefficient can be estimated from the weights of the "dry" and "equilibrated" sample and the penetrant concentrations or pressure in the surrounding media; repeating the procedure at different penetrant concentrations allows the sorption isotherm to be obtained.

The main drawback of this technique is that, since it is unspecific it cannot be used to study the mass transfer properties of polymers simultaneously exposed to sorbate

mixtures. Additionally, to monitor the weight uptake, the sample has to be removed from the liquid, cleaned and weighed rapidly and returned to the assay cell, momentarily changing the boundary conditions of the experiment.

1.4.1.3.2 Permeation measurements

In this type of assay, the rate at which one or more volatiles cross through a polymer film separating two phases with different permeant concentrations is monitored. In most testing methods, the film sample separates two chambers which are initially filled with the same atmosphere composition. The permeant concentration in one of the chambers is modified at the beginning of the experiment, and maintained constant thereafter, and the amount of permeant exchanged between the cambers is measured. The experiment finishes when the flow of penetrant is constant, i.e. the steady state has been attained. The permeation through the film can be determined by substituting this constant flow in any of the equations 12-14.

By solving Fick´s second law with the boundary conditions of a permeation experiment, the evolution of the flow of permeant (F_t) coming out of the film during the transition state can be describes by equation 15:

$$\frac{F_t}{F_\infty} = \left(\frac{4}{\sqrt{\pi}}\right)\left(\sqrt{\frac{l^2}{4Dt}}\right)\sum_{n=1,3,5..}^{\infty} \exp\left(\frac{-n^2 l^2}{4Dt}\right) \qquad \text{(Eq. 15)}$$

Where F_∞ is the flow rate of the permeant at equilibrium.[57]
Different procedures can be used to estimate diffusion coefficient from this equation. This simplest approach is substituting the time required to reach half of the flow rate at equilibrium ($t_{1/2}$), as equation 16:

$$D = \frac{l^2}{7.205 t_{1/2}} \qquad \text{(Eq. 16)}$$

The permeation measurements can be measured by gravimetric methods and non-gravimetric methods.

The gravimetric methods are usually carried out with commercial permeation cups, normalized according to ASTM E96-95 (ASTM, 1996), known as the “cup method”. The cups consist of a reservoir that can be filled with the permeant or used as deposit for silica gel (that provides 0%RH) and closed with a film of the polymer material to be tested and left in a desiccator with a controlled humidity. If the concentration of the permeants remains constant on both sides, when the system reaches the steady state a plot of the weight loss or gain of the cup versus time will take the shape of a straight line; its slope is used to obtain the permeability value. When the permeant is water, a standard method is available to determine the water vapour transmission rate based on this technique.[58]

The main drawback of this method is that it is difficult to determinate time 0; therefore the diffusion coefficient cannot be obtained.

Non-gravimetric methods are, for instance, used when the flow is very small and measuring the weight changes of the cell is not possible, or when more than one compound is transported. To overcome these drawbacks, the permeant flow is directed to specific detectors of different kinds, depending on the permeant: electrochemical detectors are used for oxygen, infrared detector for water vapour and carbon dioxide and GC is applicable for almost all types of permeants substances.[59] If the boundary conditions of the experiments are well selected, most of these methods will also provide information that will allow the determination of the diffusion coefficient to be obtained through equations 15 and 16.

1.4.1.4 Factors influencing mass transport properties

1.4.1.4.1 The polymer

The chemical composition of the polymer is usually the key factor in defining its transport properties. As an example, Table 1 presents typical permeability data to oxygen and water vapour for conventional and novel biodegradable plastics used in packaging. The differences in gas permeability, i.e. which vary between materials by several order of magnitude, are primarily related to the influence of chemistry.

Table 2 shows as an example how the oxygen barrier of different polymeric materials with a chemical structure based on the repetition of CH_2-CHX units changes by various orders of magnitude with the X substituent.[60] As it can be seen, while the lowest oxygen permeability values are obtained when the repeating unit contains strongly self-interacting chemical groups (OH or CN), the presence of apolar or voluminous groups produces polymers with lower oxygen barrier. It is also well-know that the transport of low molecular weight substances takes place through only the amorphous region of the semi-crystalline polymers, where intermolecular interactions are mainly produced by secondary forces, mostly van der Waals unions or hydrogen bonds. Thus, the nature of these pendant groups, and consequently the strength of their interactions, will play a determining role in the transport through the polymer.

Table 1. Water permeability (at 38ºC and 90%RH) and Oxygen permeability (23ºC) of a number of commercial plastics and multilayer structures. (Data was gathered, unless otherwise stated from reference 11.

Material	Water P 10^{18} Kg m/(m^2 s Pa)	Oxygen P 10^{21} m^3 m/(m^2 s Pa)	
		0%RH	75%RH
PVOH	485000	0.17	900
EVOH	17000	0.77	91
PAN	2420	1.9	
PAN (70%AN)	8250	10.5	31
PVDC	30.53	4.5	
PA6	20600	52	225
aPA (amorph.)	2420	83	60
PET	2300	135	
PP	726	6750	
PC	19400	10500	
LDPE	1200	21500	
LCP	10	0.42	
PET/PVDC	170	17.5	
PA/PVDC	160	18.2	
PP/PVDC	43	25	
PET-met.	58	3.5	
PET/AlOx/PE	21	7	15
PET/SiOx/PE	16	4.9	
PA/SiOx/PE	32	7.7	
PP/SiOx/PE	13	81	
[61]PLA	12600	2250	2209
[62]PLA			1750
[61]PHB	1689	230	
[62]PHB			5100
[61]PHBV	6900	1590	3010
[61]PCL	26600	4380	7850
[63]PCL		934	
[64]PCL		1960	

Table 2. Relative oxygen permeability of polymer materials based on the repetition of CH_2-CHX

Polymer	X unit changes	Relative O_2 Permeability
PVOH	OH	1
PAN	CN	4
PVC	Cl	800
PP	CH_3	15000
PS	C_6H_5	42000
PE	H	48000

Furthemore, the chemistry of the polymer also determines the affinity between a potential permeant and the polymer matrix. If both have similar chemical groups, the solubility of the permeant in the polymer will be greater than when the polymer repeals the permeant.

Two physical parameters of the polymer that have a big effect on barrier properties are cohesive energy and free volume. Both parameters are also directly related with its chemical composition.

The cohesive energy of a substance in the condensed state is defined as the increase in internal energy per mole of substance if all the intermolecular forces are eliminated. This parameter quantifies the strength of the interaction between molecules and the changes that take place when different chemical groups are added to the polymer chain. The best barrier properties are obtained when this value is high, either because the unions between groups are very strong or because there are many of them.

The free volume gives information about the microcavities in a polymeric material used by the permeant molecules to diffuse through the matrix. The free volume is constantly redistributed by changes in the configuration of the polymer chains, making it possible for the permeant molecules to jump from one cavity to the next. In spite of these continuous changes, both the size and the distribution of the microcavities scarcely change with time. These two characteristics also determine the barrier behaviour of the material, as a material with very small cavities homogenously distributed will have a greater permeability to small molecules than other with bigger cavities concentrated in one region of the matrix, even if the total free volume of the second is greater.

1.4.1.4.2 Polymer morphology

Although fully amorphous polymers like aPA are used in food packaging applications, the most usual morphologies are semicrystalline ones like EVOH copolymers and HDPE. In the latter case, highly organized polymer chains form crystals which co-exist with amorphous regions where the chains have a less ordered configuration. In this case, the polymer matrix can be considered an amorphous structure filled with impermeable polymer crystals. The size, orientation and shape of the crystals will affect transport through the polymer matrix. In addition, the presence of these

crystalline blocks affects the surrounding polymer chains. As the contact between the crystals and the amorphous phase is very intimate, the former constrict the movement of the non-crystalline fraction, reducing its segmental mobility, which becomes smaller than in amorphous regions not surrounded by polymer crystal or in fully amorphous polymers. [65, 66]

The number, size, composition and structure of the crystalline fraction is affected by the thermal history of the polymer, i.e. its processing conditions and any thermal treatments it may have received. Both can be optimized to increase its barrier properties. For instance, successive annealing processes can increase the quality of previously formed crystals or even form new ones consequently improving the barrier properties of the material.[67, 68]

Certain processing conditions can produce orientation of the film, to which the following effects are usually attributed: (a) orientation-induced crystallization, (b) orientation of the existing crystals in the strain direction and (c) increased order in the amorphous region, hence reducing the free volume. All these changes typically lead to improvements in the barrier properties of the polymer, as Zhang et al. observed when comparing the limonene barrier properties of oriented and non-oriented EVOH films.[69]

The degree of cross-linking of a polymer refers to the number of chemical unions formed between its macromolecules. Among other things, increasing the degree of cross-linking increases the viscosity of the melted polymer, its tensile strength and its resistance to environmental stress cracking and affects the transport of low molecular weight substances through it.[70, 71] On increasing the cross-linking density, the jump of a permeant molecule requires more energy, as reflected by the reduction in the diffusion coefficient. [72] However, the restriction imposed on the macromolecules makes chain packing more difficult, reducing the number and size of the polymer crystals and also increasing the free volume of the polymer [73] with negative effects on its barrier properties.

1.4.1.4.3 Polymer Blends: The case of permeable fillers.

Blending polymers is a feasible route to access the desired balance of properties by controlling the polymer phase interaction or/and morphology in monolayer barrier systems.[74] The most commonly used case is to blend polymers with other polymers which have higher barrier properties. The barrier properties of these blends seem to follow a relationship (see equation 17) in good general agreement with that proposed by Maxwell and extended by Roberson (see equation 17) for spheres of a low oxygen barrier phase (e.g. aPA), but with higher water resistance, dispersed in a high oxygen barrier (e.g. EVOH), but with lower water resistance, continuous matrix. [75] This simple model appeared to closely reflect, albeit with a slight positive deviation, the case of the dispersed morphology found in EVOH/PA blends.[74]

$$P_{EVOH/aPA} = P_{EVOH}\left[\frac{P_{aPA} + 2P_{EVOH} - 2V_{aPA}\left(P_{EVOH} - P_{aPA}\right)}{P_{aPA} + 2P_{EVOH} + V_{aPA}\left(P_{EVOH} - P_{aPA}\right)}\right] \quad (17)$$

1.4.1.4.4 Fillers and additives: Case of impermeable fillers

The effect that adding fillers to the polymer matrix will have on transport properties depends, among other things, upon the nature of the filler and its degree of adhesion to and compatibility with the polymer.

When the polymer is loaded with inert impermeable fillers, among other changes in its properties the diffusion coefficient is usually reduced, due to an increase in the tortuosity of the path required for the permeant to traverse the polymer thickness. To reduce the diffusion coefficient of low molecular weight molecules, the most frequent nanofiller used are exfoliated and/or intercalated clay layers (with aspect ratios of the order of 10^3). [76] In this case, the best improvement is expected when clay plates with a large surface area are well dispersed in the polymer and oriented perpendicular to the direction of transport. In addition, introducing the nanoclays inside the amorphous region usually may lead to similar effects as the presence of crystals, e.g. reducing chain mobility.

Thus, by simple application of models such as the one of Nielsen (see Figure 4), and for the case of laminar structures with high aspect ratios (aspect ratios L/2W of 180), the model predicts permeability reductions of the matrix of up to ca. one order of magnitude for fractional volumes (ϕ) of layered nanoclay additions of ca. 0.05.

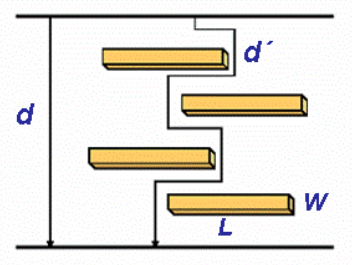

$$\frac{P_{nano}}{P_{matrix}} = \frac{1-\phi_{clay}}{1+\frac{L}{2W}\phi_{clay}}$$

Figure 4. Schematics showing the tortuosity effect imposed by layered nanoclays to the transport of low molecular weight components through a film and a typical model equation that takes this effect into account in the permeability coefficient.

In this technology, it is reckoned that the presence of exfoliated layers of nanoclay (the clay platelets are oriented so that the two edges of equal length, L, are perpendicular to the direction of transport and the third edge, of width W, is parallel to the direction of transport) in the polymer results in enhancement of the so-called tortuosity (or detour) factor, i.e. (1 + (L/2W) Φclay). The equation in Figure 4 shows a simple formalism to model permeability of systems comprising impermeable plates of a layered filler oriented perpendicular to the permeant transport direction and evenly dispersed across the polymer matrix. The use of other models such as the one of Cussler predicts even higher permeability reductions but most experimental data with barrier improvements below 10 fold fit better the above Nielsen model.[77]

However, when the fillers are not inert to the sorbates (somes clays), their highly hydrophilic nature increases the amounts of water and of other polar compounds sorbed by the composite materials. On the other hand, these molecules may be immobilized by the filler and after being adsorbed they may not play an active role in the transport. [78] Problems can also appear when the affinity between the polymer and the filler is not good. In this case their addition usually increases the free volume of the resulting material and, therefore, reduces the barrier properties of the composite.

1.4.1.4.5 Temperature

It is well known that temperature affects many of the properties of polymers. Temperature-induced changes in barrier properties are of an exponential nature. In the case of diffusion, the D value increases exponentially with temperature, in agreement with the Arrhenius law (equation 18), since activation energies (E_D) are always positive. This phenomenon is related to the greater mobility of polymer chains at higher temperatures, which reduces the energy needed by the permeant molecules to jump to the next active site, and to an increase in the free volume of the polymer. [79]

$$D = D_0(e^{\frac{-E_D}{RT}}) \qquad \text{(Equation 18)}$$

In the case of the solubility coefficient, the exponential dependence on T is described by Van't Hoof's Law (equation 19). The enthalpy of solution (AH_S) values are usually positive, although negative values have also been reported. [80] In this case, in spite of the larger number of molecules that can be accommodated in the active sites produced by the greater mobility of the polymer chains and the bigger free volume size, the volatility of the sorbates also affects their partition equilibrium between the polymer and the outer medium. [81]

$$S = S_0(e^{\frac{-AH_S}{RT}}) \qquad \text{(Equation 18)}$$

Finally, as permeability combines sorption and diffusion, its changes with temperature depends on the values of E_D and AH_S as shown in equation 20. Since the values of E_D are usually greater than absolute value of AH_S, the permeation equation is considered to be an Arrhenius type expression, the temperature dependence being described through the activation energy of permeation (E_P):

$$P = D_0(e^{\frac{-E_D}{RT}})S_0(e^{\frac{-AH_S}{RT}}) = D_0S_0(e^{\frac{-E_D-AH_S}{RT}}) = P_0(e^{\frac{-E_P}{RT}}) \qquad \text{(Equation 20)}$$

The temperature also affects the state of the polymer, being the transport properties of the polymer affected by it. In the melted polymer, the crystalline regions disappear and transport takes place across the entire matrix, which behaves like a liquid. In this case, all the polymer volume is available for the permeant, which increases its solubility, and the blocking effect of the crystals disappears, which reduces tortuosity and makes diffusion easier. Also, the polymer chains are in constant movement, which facilitates the jumps of the permeant molecules.

Changes associated with the glass transition, i.e. with the passage of the polymer from the glassy to the rubbery state, take place as a result of the relaxation or increased mobility of the chain segments in the amorphous phase of the polymer. Above the glass transition temperature (T_g) the amorphous phase of the polymer is in the rubbery state, below this temperature it is in the glassy state. In the rubbery state, relaxation times are shorter and, after the sorption of permeant molecules, a new equilibrium state is reached faster. As a result, diffusion is faster when the polymer is in the rubbery state.

1.4.1.4.6 The permeant

Characteristics of the permeant like molecular size, shape and chemical nature usually affect its transport properties.

Increasing the molecular size in homologous series of permeants (alkanes, esters, aldhehydes or alcohols) generally reduces the diffusion and solubility coefficients values of the permeants, mainly for steric reasons. Only when solutes are in the form of vapour the higher solubilities do correspond to the larger molecules, as a consequence of their greater condensabilities. [82-86] The shape of the permeant molecules is also important, as flattened or elongated molecules will diffuse faster through the polymer than spherical ones with the same molecular volume. [87, 88] The nature of the permeant also affects its transport properties, as described above in the effect of chemistry.

If the affinity between the permeant and the polymer is very high it can sometimes cause plasticization of the polymer. In this case, sorption leads to a decrease in the self-association between adjacent macromolecules in the amorphous region. The initial hydrogen bonding and van der Waals forces are replaced by polymer-sorbate interactions, increasing chain mobility and free volume, reducing the T_g and raising the diffusion and solubility coefficients of the solute. Plasticization depends on the penetrant concentration, which has to be above certain limit for it to take place. [89, 29] However, while outstanding affinity between the sorbate and the polymer and large uptakes are necessary, sometimes they are not sufficient to produce plasticization of the polymer, as described in the case of aPA. [90]
When a complex matrix like a foodstuff is placed inside a polymeric package the polymer will be in contact with a large number of solvents simultaneously and the transport properties of one solute are often affected by the presence of the other co-solvents.

Water is the main component of many foodstuffs and also the most frequently-reported co-solvent. In hydrophilic polymers like the EVOH copolymers, water-induced plasticization at high moisture levels has been reported to increase the permeability to hydrophobic and apolar solvents like limonene and oxygen [91, 69] . However, as described before in the case of the aPAs, the presence of water can also have a positive effect on the barrier properties of the material.

Another co-solute whose effect has been widely described in the literature is limonene, the main component of orange juice flavor. The effect of this terpene on the

barrier performance of apolar polyolefins is similar to that of water on polar EVOH copolymers. The presence of high concentrations of limonene has been reported to double permeability of ethyl-butyrate through HDPE and to increase that of ethyl acetate through bi-axially oriented polypropylene by up to forty times. [92]

The simultaneous transport of a group of co-solvents with similar transport properties has usually been described as a competition between them for the active sites, resulting in the transport of certain compounds being reduced and this of the rest increased. [93] However, positive synergist effects have also been reported, as in the case of toluene/methanol mixtures. [94]

1.4.1.5 Barrier properties of Nanobiocomposites of PLA, PCL, PHA and Starch

Within the polymer/clay nanocomposite technologies, the case of the biocomposites containing biopolymers and clays is one of the most significant novel developments. Biopolymers typically considered for thermoplastic monolayer and also multilayer applications are PLA, PCL, PHA and starch. These materials have, however, a number of property shortages in barrier, thermal and mechanical performance when compared to conventional plastics currently used. The use of clay based nanoadditives to boost their performance, particularly in barrier properties, is perhaps one of the most lively areas of current and future research and, therefore, this paragraph pays special attention to review the current status of the literature regarding the enhancement in barrier properties of thermoplastic biocomposites. Concerning PLA, two techniques are frequently used to produce nanocomposites of this material namely, solution-casting [95, 96] and melt mixing. [87-97] The works claim for the PLA nanocomposites improvements in material properties such as storage modulus, flexural modulus, flexural strength, heat distortion temperature, but also in gas barrier properties [104-114] compared to neat PLA.

Maiti et al. [108] postulated that the barrier properties of non-interacting gases in nanocomposites primarily depends on two factors: One is the dispersed silicate particles aspect ratio and the other is the extent of dispersion of these within the polymer matrix. As mentioned above, when the degree of dispersion of the layered organoclay is maximum an exfoliated morphology is attained and the barrier properties solely depend on the particles aspect ratio. Table 3 summarizes the reported improvements in oxygen and water permeability of nanocomposites of PLA and of other thermoplastic biopolymers. Recently, Sinha Ray et al. [75] claimed reductions in oxygen permeability of ca. 65% for PLA+4 wt.-% of synthetic fluorine mica prepared by melt mixing. Nanocomposites with similar clay contents (4-7 wt.-%), but with a different kind of clay showed less improvements in oxygen permeability, i.e. ranging from 6% to 56%. [84, 104, 105, 110, 112-114] In summary, the barrier properties of PLA were found to strongly depend upon clay type, organic modification of the clay, clay content, clay aspect ratio, clay interfacial adhesion and clay dispersion.

In the case of PHAs, Gardolinski JE et al. [115] described the formulation of PHB nanocomposites. However, due to the high thermal instability of the polymer, the commercial applications of PHB have been extremely limited (see Table 3).

Due to the mentioned instability of the PBH copolymer, researchers have mainly used lower melting temperature copolymers of PHB, such as poly(3-hydroxybutyrate-co-3-hydroxyvalerate) (PHBV) with improved chemical stability and good physical properties but with lower barrier properties. Again solution-casting [116, 119-120] and melt mixing [117-120] routes were explored for the nanocomposites of this biopolymer.

In the case of PCL four methodologies have been used to prepare nanocomposites of PCL namely, in-situ polymerization[23, 121-125], solution casting [126], melt mixing [19, 127-135] and a master batch method. [129]

Table 3 summarizes the reported oxygen and water barrier improvements of these nanocomposites. Gorrasi G et al. [134] prepared nanocomposites of PCL with MMT by melt mixing. The barrier properties were studied for water vapour and dichloromethane as an organic solvent. Although, the water sorption increased with increasing the MMT content, the diffusion parameters of the samples showed much lower values in exfoliated systems. Messersmith, PB et al. [19] prepared nanocomposites with an organically modified mica-type silicate. The nanocomposite exhibited a significant reduction in water vapour permeability, which showed a linear dependence with silicate content. The significant decrease in water permeability observed for this system is of great importance in evaluating PCL and PCL nanocomposites for use in food packaging, protective coatings, and other applications where efficient polymeric barriers are needed. The significant improvement in both barrier and mechanical properties of PCL nanocomposites could be attributed to the fine dispersion state of organoclay in the PCL matrix and the strong interaction between the organic modifier and the matrix.

In starch, also solution-casting [138, 142] and melt-mixing [136-141] are the nanocomposite technologies applied. In most cases, given the higher sensitivity of this material towards water sorption, a reduction in this parameter has been attempted.

Park, H.M. et al. [135-136] prepared nanocomposites of starch-organoclays by melt intercalation, with different natural montmorillonite (Na+ MMT; Cloisite Na+) and different organically modified MMT. The barrier properties to water vapour in the nanocomposites were found to be higher than in the pure starch. In general, for the preparation of nanocomposites by solution casting the addition of a plasticizer has been considered as a necessary condition. Kampeerapappun, P. et al. [138] prepared starch/MMT films by casting, using chitosan as a compatibilizing agent in order to disperse the clay in a starch matrix. Others nanocomposites [141-142] of starch were prepared via different addition sequences of plasticizer and clay (Na-MMT) by the solution method. Nanocomposites of starch with clay generally led to a decrease in hydrophilicity for the systems.

Huang, M.-F. et al.[138] and Huang, M. et al.[140] prepared nanocomposites of starch-ethanolamineactivated montmorillonite by melt mixing. From the results, the water-absorption of the nanocomposites was also found to be reduced. Bagdi, K. et al. [139] prepared nanocomposites of thermoplastic starch and layered silicates organophilized with different surfactants, by the melt mixing method. The equilibrium water uptake in an atmosphere of 50% relative humidity decreased by about 0.5–1.0% for

composites containing 5 vol% of silicate. The largest decrease in water adsorption was observed in the case of the neat NaMMT, for which laminate exfoliation was reported.

Table 3. Reductions (%) in oxygen and water vapour permeability reported for nanocomposites of thermoplastic biopolymers.

Matrix	Type of clay	Clay content	O_2 Permeability	H_2O Permeability
[104] PLA	Organically-Modified-MMT	4%	12%	
[104] PLA	Organically-Modified-MMT	5%	15%	
[104] PLA	Organically-Modified-MMT	7%	19%	
[105] PLA	MMT	4%	14%	
[105] PLA	MMT-Modified	4%	12%	
[105] PLA	Saponite	4%	40%	
[105] PLA	Synthetic Fluorine Mica	4%	65%	
[110] PLA	MMT-layered silicate	5%	48%	50%
[112] PLA	MMT-modified	5%	46%	
[113] PLA	Bentonite	5%	6%	
[114] PLA	Hexadecylamine-MMT	4%	42%	
[114] PLA	Hexadecylamine-MMT	6%	56%	
[114] PLA	Hexadecylamine-MMT	10%	58%	
[114] PLA	Dodecytrimetil ammonium bromide-MMT	4%	41%	
[114] PLA	Dodecytrimetil ammonium bromide-MMT	6%	55%	
[114] PLA	Dodecytrimetil ammonium bromide-MMT	10%	58%	
[114] PLA	Cloisite 25A (Organically-Modified-MMT)	6%	45%	
[114] PLA	Cloisite 25A (Organically-Modified-MMT)	10%	56%	
[132] PCL	Organically modified mica-type silicate	1.1%		11%
[132] PCL	Organically modified mica-type silicate	2.5%		39%
[132] PCL	Organically modified mica-type silicate	3.6%		59%
[132] PCL	Organically modified mica-type silicate	4.8%		80%
[133] PCL	Cloisite 30B (Organically-Modified-MMT)	2%	35%	
[133] PCL	Cloisite 30B (Organically-Modified-MMT)	5%	50%	
[133] PCL	Cloisite 30B (Organically-Modified-MMT)	10%	57%	
[133]PCL	Cloisite 93B (Organically-Modified-MMT)	2%	21%	
[133] PCL	Cloisite 93B (Organically-Modified-MMT)	5%	34%	
[133] PCL	Cloisite 93B (Organically-Modified-MMT)	10%	44%	

Despite the fact that there are many studies in the literature that report about barrier enhancements in polymer and biopolymer matrices, it is clear from the modeling results that the expected improvements are not yet experimentally attained or reproducible. This is the result of lack of (i) complete exfoliation of the nanofiller, (ii) good compatibility between filler and matrix and/or (iii) good purification and appropriate selection of raw materials and surface modifications. In general, there is still a need for a deeper understanding of the composition-structure-processing-properties relationships in nanoclay based nanobiocomposites both at a lab and at an industrial scale. Moreover, due to the fact that most of the extensive studies related to nanoclays have been carried out using very few nanoclay grades (based mostly on MMT), in many cases from the same commercial supplier, there is still a lot of room for variation and maturation in the nanoclay based composites area.

1.4.2 Thermal properties of nanobiocomposites

Crystallization is one of the most effective processes used to control the properties of polymeric materials. Crystal formation includes two stages, namely nucleation and crystal growth.

In the case of nanocomposites based on clays, although it is well established that nanometer sized clay platelets are effective nucleating agents, different effects have been reported on the linear growth rate and the overall crystallization rate of crystals, depending on the type of polymer. [143] Di Maio et al. [144] studied the isothermal crystallization of PCL/clay nanocomposites and noticed that the dispersed clay platelets acted as nucleating agents in the PCL matrix. In general, by DSC analysis after isothermal crystallization, the authors observed a reduction of the melting temperature and enthalpy with increasing clay content, indicating a reduced degree of crystal perfection and crystallinity. This was attributed to the confinement of chains and segments in the presence of clay, hindering the segmental rearrangement during crystallization and restricting the formation of more perfect crystals in the polymer matrix. Ke and Yongping [147] conducted DSC analysis on intercalated PET/o-MMT nanocomposites. They found a reduction of T_g in the composite compared to the pure matrix, which they attributed to the plasticizing effect of o- MMT. However, they noticed that by increasing the o-MMT content the T_g also increased. Furthermore, they observed that the cold crystallization point of pure PET was at 150 ºC, while for the nanocomposite it decreased to 130 ºC. This result suggested that adding o-MMT into PET is favorable to its crystallization. So, as a summary, the general reported tendency of the clays in the polymer is to act as a nucleating agent and to promote crystallinity.

In the case of nanocomposites based on fibers, the cellulose filler does not have a generic role in the biocomposites thermal properties. Thus, depending on the biomaterial, they have been found to act as impairments to crystal development, as for PCL and PHBV, or as a nucleating agent, as for PLA. Different roles were also observed depending on the type or the origin of the cellulose. [146, 147]

1.4.3 Mechanical properties of nanocomposites

The mechanical properties of films depend on the type of film-forming material and especially on its structural cohesion. Cohesion is the result of a polymer's ability to form strong and/or numerous molecular bonds between polymeric chains, thus hindering their separation. This ability depends on the structure of the polymer and specially its molecular strength, geometry, phase structure, molecular weight distribution and the type and position of its lateral functional groups. The mechanical properties are also linked with the film-forming conditions, e.g. type of process and solvent, cooling or evaporation rate, etc [148] and of course of the addition of nanofillers. The mechanical properties are usually evaluated by tensile tests. [149, 150] The properties typically evaluated in tensile tests are tensile strength, elongation at break and elastic

modulus, and also yield stress and strain and toughness. Tensile strength is defined as the maximum tensile stress which a material can sustain and is taken to be the maximum load exerted on the test specimen during the test. Elongation at break is the maximum change in the length of the test specimen before breaking and is expressed as the percent change of the original length of the material between the grip of the test machine. Elastic modulus (Young's modulus) is defined as the ratio of stress to strain in the initial linear part of the stress-strain curve. It is a fundamental measurement of inherent stiffness of a single film since it is nearly independent of dimensions and stress from small strains. [150]

The materials can be classified in four types on the basis of stress-strain curves.[151] A hard brittle material such as an amorphous polymer far below its glass transition temperature (T_g) usually has an initial slope indicative of very high modulus, moderate strength, a low elongation at break, and a low area under the stress-strain curve. Hard and strong polymers have high modulus of elasticity, high strength, and elongation at break of approximately 5 per cent. The shape of the curve often suggests that the material breaks where a yield point might be expected. Hard and tough behaviour is shown by polymers that have high yield points and high modulus, high strengths and large elongations. Polymeric materials that are soft and tough show low modulus and yield values, moderate strength at break, and very high elongation ranging from 20 to 1000 per cent. Since the mechanical properties of films are strongly influenced by their environmental RH, film samples should be conditioned in a specified RH prior to the experiments.

In the case of the nanocomposite materials. The first mechanism that has been put forward to explain the reinforcing action of conventional reinforcements, such as fibers or clays, is schematically depicted in Fig. 5. That is, rigid fillers are naturally resistant to straining due to their higher modulus. Therefore, when a relatively softer matrix is reinforced with such fillers, the polymer, particularly that adjacent to the filler particles, becomes highly restrained mechanically. This enables a significant portion of an applied load to be carried by the filler, assuming, of course, that the interfacial bonding between the two phases is adequate. [152] From this mechanism it becomes obvious that the larger the surface of the filler in contact with the polymer, the greater the reinforcing effect that it will show. This could partly explain why layered silicates, having an extremely high specific surface area (on the order of $800 m^2/g$) should impart dramatic improvements in modulus even when present in very small amounts in a polymer. In fact, the low silicate loading required in nanocomposites to produce significant property improvements, is probably their most distinguishing characteristic. In most conventionally filled polymer systems, the modulus increases linearly with the filler volume fraction, whereas for nanocomposites much lower filler concentrations increase the modulus sharply and to a much larger extent.[153]

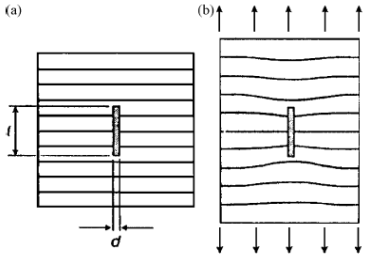

Figure 5. Reinforcement mechanism in composite materials.

In general, the addition of an organically modified layered silicate in a polymer matrix results in significant improvements of Young's modulus, as has been reported in many studies. [154-159] for a number of different materials. For example, Gorrasi et al.[160] reported an increase from 216 to 390 MPa for a PCL nanocomposite containing 10 wt.-% of ammonium-treated montmorillonite, while in another study [161] , Young's modulus was increased from 120 to 445 MPa with addition of 8 wt.-% ammonium treated clay to PCL. Similarly, in the case of nylon 6 nanocomposites obtained through the intercalative ring opening polymerization of ε-caprolactam, a large increase in the Young's modulus at rather low filler content has been reported, whatever the method of preparation: Polymerization within organo-modified montmorillonite, polymerization within protonated ε-caprolactam swollen montmorillonite or polymerization within natural montmorillonite in the presence of ε -caprolactam and an acid catalyst. [165] However, exceptions to this general trend have also been reported. Bharadwaj RK et al. showed in crosslinked polyester/OMLS nanocomposites, a decrease in modulus with increasing clay content; in fact, the drop for the 2.5 wt.-% nanocomposite was greater than expected. To explain this phenomenon, it was proposed that the intercalation and exfoliation of the clay in the polyester resin serve to effectively decrease the number of crosslinks from a topological perspective.[163]

Apart from the modulus, the addition of clays in a polymer matrix usually also increases the tensile strength compared to that of the neat polymer material. For example, Shelley et al. [164] reported a 175% improvement in yield stress accompanied by a 200% increase in tensile modulus for a nylon 6 nanocomposite containing 5 wt.-% clay.

Regarding toughness or impact resistance of the material, in general, the addition of an organically modified layered silicate to a polymer matrix results in little or no change in toughness upon clay intercalation/exfoliation [167, 168]. For example, Liu X et al. reported that while the tensile strength and modulus of PP nanocomposites increased rapidly with increasing clay content from 0 to 5 wt.-%, the notched Izod impact strength was constant, within experimental error, in the clay content range between 0 and 7 wt.-%[167]. In fact, toughness improvements upon good clay dispersion have also been reported [25, 169].

For nanocomposites based on cellulosic nanofillers, it has also been reported that a significant improvement in modulus is typically observed. [25, 169-173]

For example, Helbert et al. [25] reported that a poly(styrene-co-butyl acrylate) latex film containing 30 wt.% of straw cellulose whiskers presented a modulus more than a thousand times higher than that of the bulk matrix. According to Jordan et al. [174], and the same as with nanoclays, the addition of nanoreinforcements with poor interaction with the matrix causes the elongation and the strength of the material to decrease.

So, as a summary the influence of the degree of exfoliation and the adequate morphology of the fillers (clays or fibers) leads to the expected improvement in tensile modulus and strength. Other factors that may play a crucial role in the improvement of nanocomposite mechanical properties include the organic modification of the clay and the addition of compatibilizers to the polymer matrix. [175-176] The extent of improvement of nanocomposite mechanical properties will also depend directly upon the average length of the dispersed filler particles (clays of fibers), since this determines their aspect ratio and, hence, their surface area. [177-178] In general, nanocomposite materials, particularly with good morphology and exfoliated structures present significant improvements in modulus and strength, whereas contradictory results are reported concerning their elongation and toughness.

1.5 References

1. K. Petersen, P.K. Nielsen, G. Bertelsen, M. Lawther, M.B. Olsen, N.H. Nilsson, G. Mortensen. Trends in Food Science and Technology 10, 52-68 (1999)
2. V.K. Haugaard, A.M. Udsen, G. Mortensen, L. Hoegh, K. Petersen, F. Monahan. Ed. C.J. Weber, Copenhagen (2001).
3. I. Arvanitoyannis, E. Psomiadou, C.G. Biliaderis, H. Ogawa, H. Kawasaki, O. Nakayama. Starch/Stärke 49, 306 (1997)
4. J. Reguera, J. M. Lagaron, M. Alonso, V. Reboto, B. Calvo, J.C. Rodriguez-Cabello. Macromolecules, 36, 8470-8476, (2003)
5. M.F. Koening, S.J. Huang. Polymer 36, 1877 (1995)
6. C. Bastiolo, V. Bellotti, G.F. Del Tredici, R. Lombi, A. Montino, R. Ponti; Int. Pat. Appl WO 92/19680 (1992)
7. E.S Park, M.N. Kim, J.S. Yoon. J. Polym. Sci.: Part B Polym. Phys. 40, 2561 (2002)
8. H. Tsuji, T. Yamada. J. Appl. Polym. Sci. 87, 412 (2003)
9. S. Jacobsen, PH. Degée, H.G. Fritz, PH. Dubois, R. Jérome. Polym. Eng. Sci. 39, 1311 (1999)
10. S. Jacobsen, H.G. Fritz. Polym. Eng. Sci. 36, 2799 (1996)
11. C.C. Chen, J.Y. Chueh, H. Tseng, H.M. Huang, S.Y. Lee. Biomaterials 24, 1167 (2003)
12. H. Möller, S. Grelier, P. Pardon, V. Coma. J. Agric. Food Chem., 52, 6585-6591 (2004)
13. C. Dong and M. S. Chinnan. Critical Review in Food Science and Nutrition, V44, 4, 223- 237, (2004)
14. Y. Wang, G.W. Padua, Journal of Agricultural and Food Chemistry 52 (10): 3100-3105, 19, (2004)
15. R.E. Grim. Clay mineralogy. New York: McGraw-Hill; 1953;
16. S.W. Brindly, G. Brown, editors. Crystal structure of clay minerals and their X-ray diffraction. London: Mineralogical Society; 1980
17. S.S. Ray, M. Okamoto. Prog Polym Sci;28:1539–641 (2003)
18. A. Blumstein. J Polym Sci A;3:2665–73 (1965)
19. Pb. Messersmith, Ep. Giannelis. J Polym Sci Pol Chem; 33 (7): 1047-1057 (1995)
20. T.M. Wu, C.Y. Wu. Polymer Degradation and Stability 91(9): 2198-2204 (2006)
21. J.H. Lee, Y.H. Lee, D.S. Lee, Y.K. Lee, J.D. Nam. Polymer Korea 29(4): 375-379 (2005)
22. S.S. Ray, K. Yamada, M. Okamoto, K. Ueda. Polymer 44:857–866; (2003)
23. P.B. Messersmith, E.P. Giannelis. Chem Mater; 5:1064–6. (1993)
24. J.M. Lagaron, A. Fendler. Journal of Plastic Film and Sheeting, 25, 1, Pages 47-59 (2009)
25. W. Helbert, C.Y. Cavaillé, A. Dufresne. Polymer Composites, 17(4), 604–611 (1996)
26. P. Podsiadlo, S.Y. Choi, B. Shim, J. Lee, M. Cuddihy, N. A. Kotov. Biomacromolecules, 6, 2914–2918 (2005)
27. M.A.S. Azizi Samir, F. Alloin, A. Dufresne. Biomacromolecules, 6, 612–626 (2005)
28. L.P. Ramos. Química Nova, 26(6), 863–871 (2003)
29. K. Oksman, A.P. Mathew, D. Bondeson, I. Kvien. Composites Science and Technology, 66(15), 2776–2784 (2006)
30. M.A.S. Azizi Samir, F. Alloin, J.Y. Sanchez, A. Dufresne, Polymer, 45, 4149–4157 (2004)
31. M.M.D. Lima, R. Borsali. Macromolecular Rapid Communications, 25(7), 771–787 (2004)
32. D.J. Gardner, G.S. Oporto, R. Mills, M.A.S. Azizi Samir, Journal of Adhesion Science and Technology, 22, 545–567 (2008)

33. V. Tserki, P. Matzinos, N.E. Zafeiropoulos, C. Panayiotou. Journal of Applied Polymer Science 100: 4703-4710 (2006)
34. A. Fendler, M.P. Villanueva, E. Gimenez, J.M. Lagaron. Cellulose 14:427–438 (2007)
35. W.J. Orts, J. Shey, S.H. Imam, G.M. Glenn, M.E. Guttman, J.F. Revol. Journal of Polymers and the Environment 13(4): 301-306 (2005)
36. L. Petersson, I. Kvien, K. Oksman. Composites Science and Technology 67, 2535–2544; (2007)
37. I. Kvien, S.T. Bjørn, K. Oksman. Biomacromolecules 6, 3160-3165 (2005)
38. S. Iijima, Nature 354:56 (1991)
39. X. Zhou, E. Shin, K.W. Wang, C.E. Composites Science and Technology, 64(15), 2425–2437 (2004)
40. H. Ma, J. Zeng, M.L. Realff, S. Kumar, D.A. Schiraldi. Compos Sci Tech,;63:1617–28 (2003)
41. E.C. Chen, T.M. Wu. Polymer Degradation and Stability 92, 1009-1015; (2007)
42. K. Chrissafis, G. Antoniadis, K.M. Paraskevopoulos, A. Vassiliou, D.N. Bikiaris. Composites Science and Technology 67, 2165–2174. (2007).
43. M. Lai, J. Li, J.,Yang, J. Liu, X. Tong, H. Cheng. Polym Int 53:1479–1484; (2004)
44. K. Saeed, S.Y. Park. Journal of Applied Polymer Science, Vol. 104, 1957–1963 (2007)
45. R.J. Hernández, R. Gavara. Plastics Packaging. Methods for Studying Mass Transfer Interactions. Pira International Surrey (UK) (1999)
46. J. Crank, G.S. Park, Diffusion in Polymers, Ed. Academic New York, (1968)
47. Koros, J. Willian. Barrier Polymers and Structures. ACS Symposium Series. (1984)
48. N.E. Schlotter, P.Y. Furlann. Polymer 33 (16) (1992) 3323
49. J. Crank. The mathematics of Diffusion. Oxford, Ed Clarendon (1975)
50. J.M. Vergaud. Liquid Transport Processes in Polymeric Materials: Modelling and Industrial Applications. Prentince Hall, Englewood Cliffs (1990)
51. S.C. George, S. Thomas Progress in Polymer Science 26 985(2001)
52. R.M. Barrer, J.A. Barrier, J. Slater, Journal of Polymer Science 27 (115) 177 (1958)
53. W.R, Vieth, J.M. Howell, J.H. Hsieh. Journal of Membrane Science 1-177 (1976)
54. W.R. Vieth, A.S. Douglas, R. Bloch, Journal of Macromolecular Science-Ohysics B3 737 (1969)
55. W.R. Vieth, J.M. Howell J.H. HsiehJournal of Membrane Science 1-177 (1976)
56. S.J. Metz, N.F.A van der Vegt, M.H.V. Mulder, M Wessling. Journal of Physics Chemistry: Part B 107, 13629 (2003)
57. R. Gavara, R.J. Hernández. Journal of Plastic Film and Sheeting 9(2) 126 (1993)
58. ISO 2528; 1995, Sheet materials, Determination of water vapour transmission rate, Gravimetric (dish) method.
59. Q. Zou, B. Guthrie, K.R. Cadwallader. Packaging Technology and Science 17, 175 (2004)
60. J.M. Lagarón, R. Catalá, R. Gavara. Materials Science and Technology 20 1(2004)
61. M.D. Sanchez-Garcia, E. Gimenez ,J.M. Lagaron. Journal of Plastic Film and Sheeting 23 133-148 (2007)
62. K. Petersen, P.V. Nielsen, M.B. Olsen, Starch, 53, 8, 356 (2001)
63. S.K. Young, G.C. Gemeinhardt, J.W. Sherman, R.F. Storey, K.A. Mauritz, D.A. Schiraldi, A. Polyakova, A. Hiltner, E. Baer Polymer, 43, 23, 6101-6114 (2002)
64. I. Olabarrieta, D. Forsström, U.W. Gedde, M.S. Hedenqvist, Polymer 42, 4401-4408 (2001)
65. R.H. Boyd, Polymer Engineering and Science 19 1010 (1979);
66. M. Hedenqvist, A. Angelstock, L. Edsberg, P.T. Larsson, U.W. Gede. Polymer 37 , 2887, (1996)
67. J.P. Gorce, S.J. Spells, Polymer 45 3297 (2004);
68. C. Sammon, N. Everall, J. Yarwood, Macromolecular Symposia 119, 189 (1197)

69. Z. Zhang, L.T. Lim, M.A. Tung. Journal of Applied Polymer Science 79, 1949 (2001)
70. A.G. Andrepoulus, E.M. Kapourius, Journal of Applied Polymer Science 31 (4) 1061(1986)
71. R.W. Appleby, W.K. Busfield, Polymer Communication Guildford 27 (2) 45 (1986)
72. R.M. Barrer, G. Skirrow, Journal of Polymer Science 3 549 (1948)
73. H.A. Khonakdar, J. Morshedian, U. Wagenknecht, S.H. Jafari, Polymer 44 4301 (2003)
74. D.R. Paul, C.B. Bucknall. Editors Polymer Blends, Volume 2: Performance, John Wiley & Sons, New York (US) (2000)
75. J.M. Lagaron, E. Gimenez, V. Del-Valle, B. Altava, R. Gavara, Macromolecular Symposia, 198, 473, (2003)
76. T.J. Pinnavaia, G.W. Beall. Editors "Polymer-clay nanocomposites" Johnm Willey and Sons Inc, New York (2001)
77. A.A. Gusev, H.R. Lusti. Advanced Materials 13 (21), pp. 1641-1643, (2001)
78. A.D. Drozdov, JdeC. Christiansen, R.K. Gupta, A.P. Shah, Journal of Polymer Science: Part B: Polymer Physics 41 476 (2003)
79. L. Nicolas, E. Drioli, H.B. Hopfenbergand, D. Tidone. Polymer 18 1137 (1977)
80. J. Brandrupand, E.H. Immergut. Polymer handbook 3rd edition. John Willey and Sons Inc, New York (2001) 1989
81. Zhou, Q, K.R. Cadwallader, Journal of Agricultural and Food Chemistry 52 6271 (2004)
82. G.W. Halek, J.P. Luttmann, In: Food Packaging Interactions 2, ed. by JH Hotchkiss, Washington DC, ACS 1991;
83. L. Safa, B. Abbes, Packaging Technology and Science 15, 55; (2002)
84. D. Kim, J.M. Caruthers, N.A. Peppas, Macromolecules 26, 8, 1841 (1993)
85. A. Benghalem, A. Oughilas, A. Leboukh, Polymer 44 4381; (2003)
86. W.H. Jiang, H. Liu, S.J. Han, European Polymer Journal 37, 1705 (2001),
87. A.R. Berens, H.B. Hopfenberg, Journal of Membrane Science 10 (2-3), 283; (1982)
88. N. Yi-Yan, R.M. Felder, W.J. Koros, Journal of Applied Polymer Science 25 (8), 1755, (1980)
89. Q. Zhou, B. Guthrie, K.R. Cadwallader, Packaging Technology and Science 17, 175, (2004)
90. R.J. Hernández, J.R. Giacin, E.A. Grulke, Journal of Membrane Science 65, 187, (1992)
91. Zhang, Z.; Britt, I.J. and Tung, M.A. Journal of Applied Polymer Science 82, 2001, 1886
92. T.J. Nielsen, J.R. Giacin, Packaging Technology and Science 7 (5), 247, (1994)
93. J. Letinski, G.W. Halek, Journal of Food Science 57 (2) 481 (1992)
94. C. Gagnard, Y. Germain, P. Keraudren, and B. Barriere, Journal of Applied Polymer Science 92 676 (2004)
95. N. Ogata, G. Jimenez, H. Kawai, T. Ogihara. J Polym Sci Part B: Polym Phys 35:389–396 (1997)
96. S. Bandyopadhyay, R. Chen, E.P. Giannelis. Polym Mater Sci Eng; 81:159–60 (1999)
97. S.S. Ray, K. Yamada, M. Okamoto, K. Ueda. Nano Lett; 2:1093–6 (2002)
98. S.S. Ray, P. Maiti, M. Okamoto, K. Yamada, K. Ueda. Macromolecules; 35:3104–10 (2002)
99. S.S. Ray, K. Yamada, A. Ogami, M. Okamoto, K. Ueda Macromol Rapid Commun; 23:493–7 (2002)
100. S.S. Ray, K. Yamada, M. Okamoto, A. Ogami, K. Ueda. Chem Mater; 15:1456–65 (2003)
101. S.S. Ray, M. Okamoto, K. Yamada, K. Ueda. Nanocomposites 2002 proc. San Diego, USA.
102. K. Yamada, K. Ueda, S.S. Ray, M. Okamoto. Kobun Robun; 59:760–5 (2002).

103. S.S. Ray, M. Okamoto, K. Yamada, K. Ueda. Macromol Rapid Comm;23 (16): 943-947 (2002)
104. S.S. Ray, M. Okamoto, K. Yamada, K. Ueda. Polymer; 44:857–66 (2003)
105. S.S. Ray, K. Yamada, M. Okamoto, Y. Fujimoto, A. Ogami, K. Ueda. Polymer; 44:6633–46 (2003)
106. S.S. Ray, M. Okamoto. Macromol Rapid Commun; 24:815–40, (2003)
107. S.S. Ray, K. Yamada, M. Okamoto, K. Ueda. J Nanosci Nanotech; 3:503–50, (2003).
108. P. Maiti, K. Yamada, M. Okamoto. Chem Mater 14 (11): 4654-4661(2002)
109. S.S. Ray, K. Yamada, M. Okamoto et al. Polymer;44 (3): 857-866 (2003)
110. C. Thellen, C. Orroth, D. Froio et al. Polymer; 46 (25): 11716-11727 (2005)
111. G. Gorrasi, L. Tammaro, V. Vittoria et al. J Macromol Sci Phys B; 43 (3): 565-575 (2004)
112. J.M. Lagaron, L. Cabedo, D. Cava et al. Food Additives and Contaminants : 22 (10) 994-998 (2005)
113. L. Petersson, K. Oksman. Compos Sci Technol; 66 (13): 2187-2196 (2006)
114. J.H. Chang, Y.U. An, G.S. Sur.Journal of Polymer Science Part B: Polymer Physics. 2003; 41, 94-103
115. J.E. Gardolinski , L.C.M. Carrera , M.P. Cantao ,F. Wypych. Journal of Materials Science; 35 (12): 3113-3119, (2000)
116. G.X. Chen, G.J. Hao, T.Y. Guo, M.D. Song, B.H. Zhang. J Appl Polym Sci; 93:655–61 (2004)
117. P. Maiti, C.A. Batt, E.P. Giannelis. Polym Mater Sci Eng; 88:58–9 (2003)
118. W.M. Choi, T.W. Kim, O.O. Park, Y.K. Chang, J.W. Lee. Journal of Applied Polymer Science; 90, 525–529 (2003)
119. G.X. Chen, G.J. Hao, T.Y. Guo, M.D. Song, B.H. Zhang. Journal of Materials Science Letters 21, 1587 – 1589 (2002)
120. S.F. Wang , C.J. Song , G.X. Chen , T.Y. Guo , J. Liu , B.H. Zhang , S. Takeuchi. Polymer Degradation and Stability 2005; 87 (1): 69-76
121. D. Knani, A.L. Gutman, D.H Kohn. J Polym Sci Part A: Polym Chem; 31:1221–32 (1993).
122. A.S. Sawhney, P.P. Chandrashekhar, J.A. Hubbell. Macromolecules 1993; 26:581–7.
123. P. Cerrai, M. Tricoli, F.A.M. Paci. Polymer; 30:338–43 (1989)
124. D.R. Wilson, R.G. Beaman. J Polym Sci Part A-1;8:2161–70 (1970)
125. G. Jimenez, N. Ogata, H. Kawai, T. Ogihara. J Appl Polym Sci; 64:2211–20 (1997)
126. Y. Di, S. Iannace, E.D. Maio, L. Nicolais. J Polym Sci Part B: Polym Phys; 41:670–8 (2003)
127. B. Lepoittevin, M. Devalckenaere, N. Pantoustier, M. Alexandre, D. Kubies, C. Calberg, et al. Polymer; 43:4017–23 (2002)
128. 1B. Lepoittevin, N. Pantoustier, M. Devalckenaere, M. Alexandre, C. Calberg, R. Jerome, et al. Polymer; 44:2033–40 (2003)
129. I. Gonzalez, J.I. Eguiazabal, J. Nazabal. Polym Eng Sci; 46 (7): 864-873 (2006)
130. L. Cabedo, J.L. Feijoo, M.P. Villanueva et al. Macromol Symp 233: 191-197 (2006)
131. B.Q. Chen, J.R.G. Evans. Macromolecules; 39 (2): 747-754 (2006)
132. Y.W. Di, S. Iannac, L. Sanguigno, L. Nicolais. Macromol Symp; 228: 115-124 (2005)
133. M. Avella, F. Bondioli, V. Cannillo M.E. Errico, A.M. Ferrari and B. Focher. Mater Sci Tech-Lond; 20 (10): 1340-1344 (2004)
134. G. Gorrasi, M. Tortora, V. Vittoria et al. J Polym Sci Pol Phys; 42 (8): 1466-1475 (2004)
135. H.M. Park, W.K. Lee, C.Y. Park, W.J. Cho, C.S. Ha. Journal of Materials Science 38 (5), 909-915, (2003)
136. H.M. Park, X. Li, C.Z. Jin, C.Y. Park, W.J. Cho, C.S. Ha. Macromolecular Materials and Engineering 287 (8), pp. 553-558, (2002)

137. P. Kampeerapappun, D. Aht-ong, D. Pentrakoon, K.Srikulkit. Carbohydrate Polymers 67 (2), pp. 155-163, (2007)
138. M.F. Huang, J.G. Yu, X.F. Ma, P. Jin. Polymer 46 (9), pp. 3157-3162, (2005)
139. K. Bagdi, P. Müller, B. Composite Interfaces 13 (1), pp. 1-17, (2006)
140. M. Huang, J. Journal of Applied Polymer Science 99 (1), pp. 170-176,(2006)
141. J.K. Pandey, R.P. Singh. Starch/Staerke 57 (1), pp. 8-15, (2005)
142. H.M. Wilhelm, M.R. Sierakowski, G.P. Souza, F. Wypych, Carbohydrate Polymers 52 (2), pp. 101-110, (2003)
143. Z. Wu, C. Zhou, R. Qi, H. Zhang. J Appl Polym Sci;83:2403–10 (2002)
144. D.E. Maio, S. Iannace, L. Sorrentini, L. Nicolais. Polymer; 45:8893–900 (2004)
145. Z. Ke, B. Yongping. Mater Lett;59:3348–51 (2005)
)
146. M.A.S. Azizi Samir, F. Alloin, J.Y. Sanchez, A. Dufresne, Polymer, 45, 4149–4157 (2004).
147. A.P. Mathew, A. Dufresne. Biomacromolecules, 3(3), 609–617, (2002).
148. S. Guilbert, N. Gontard, L.G.M. Gorris. Food Science and Technology, 29, 10-17 (1996).
149. B. Cuq, N. Gontard, J.L. Cuq, S. Guilbert. Journal of Agricultural and Food Chemistry, 44, 1116-1122 (1996).
150. T.H. McHugh, J.M. Krochta. Journal of Agricultural and Food Chemistry, 42, 841-845 (1994)
151. A. Blaga. Properties and Behaviour of Plastics, Canadian Building Digest, 157, 4 (1973)
152. T.D. Fornes, D.R. Paul. Polymer;44:4993–5013 (2003)
153. S.S. Ray, M. Okamoto. Prog Polym Sci; 28:1539–641(2003)
154. T.D. Fornes, P.J. Yoon, H. Keskkula, D.R. Paul. Polymer;42:9929– 40; (2001)
155. N. Hasegawa, M. Kawasumi, M. Kato, A. Usuki, A. Okada J Appl Polym Sci;67:87–92 (1998)
156. S. Peeterbroeck, M. Alexandre, R. Jerome, Ph. Dubois. Polym Degrad Stabil;90:288–94 (2005)
157. B. Finnigan, D. Martin, P. Halley, R. Truss, K. Campell Polymer;45:2249–60, (2004).
158. L.A. Goettler.. Ann Tech Confr Soc Plast Eng:1980 2 (2005)
159. Y. Kojima, A. Usuki, M. Kawasumi, A. Okada, T. Kurauchi, O. Kamigaito. J Appl Polym Sci;49:1259–64 (1993).
160. G. Gorrasi, M. Tortora, V. Vittoria, E. Pollet, B. Lepoittevin, M. Alexandre, et al. Polymer;44:2271–9 (2003)
161. M. Tortora, V. Vittoria, G. Galli, S. Ritrovati, E. Chiellini. Macromol Mater Eng; 287: 243–9 (2002).
162. A.S. Zerda, A.J. Lesser. J Polym Sci Polym Phys;39:1137–46 (2001)
163. R.K. Bharadwaj, A.R. Mehrabi, C. Hamilton, C. Trujillo, M.F. Murga, A. Chavira. Polymer;43:3699–705 (2002)
164. J.S. Shelley, P.T. Mather, K.L. DeVries. Polymer;42:5849–58 (2002)
165. Liu X, Wu Q. PP/clay nanocomposites prepared by grafting melt intercalation. Polymer 2001;42:10013–9,
166. Liu LM, Qi ZN, Zhu XG. Studies on nylon-6 clay nanocomposites by melt-intercalation process. J Appl Polym Sci 1999;71:1133–8.
167. Liu X,Wu Q. Polyamide 66/clay nanocomposites via melt intercalation. Macromol Mater Eng 2002;287:180–6;
168. LeBaron PC, Wang Z, Pinnavaia TJ. Polymer–layered silicate nanocomposites: an overview. Appl Clay Sci 1999;15:11–29.
169. A. Bhatnagar, M. Sain. Journal of Reinforced Plastics and Composites, 24(12), 1259–1268 (2005)

170. Q. Wu, M. Henriksson, X. Liu, L.A. Berglund. Biomacromolecules, 8, 3687–369 (2007)
171. T. Zimmermann, E. Pöhler, T. Geiger. Advanced Engineering Materials, 6(9), 754–761. (2004).
172. A. Dufresne, D. Dupeyre, M.R. Vignon. Journal of Applied Polymer Science, 76(14), 2080–2092 (2000)
173. A. Dufresne, M.R. Vignon. Macromolecules, 31, 2693–2696. , (1998)
174. J. Jordan, K.I., Jacob, R. Tannenbaum, M.A. Sharaf, I. Jasiuk, Materials Science & Engineering A, 393(1–2), 1–11, (2005).
175. C. Zhao, H. Qin, F. Gong, M. Feng, S. Zhang, M. Yang. Polym Degrad Stabil;87:183–9, (2005)
176. J. Xiong, Y. Liu, X. Yang, X. Wang. Polym Degrad Stabil;86:549–55 (2004)
177. S.S. Ray, M. Okamoto. Prog Polym Sci;28:1539–641 (2003)
178. Y. Kojima, A. Usuki, M. Kawasumi, A. Okada, Y. Fukushima, T. Karauchi, et al. J Mater Res;6:1185–9 (1993)

2. Objectives

The main objective of this Phd thesis was to develop and characterized novel biocomposites reinforced with various nanofillers in order to better or balance the **physical properties of some biopolyesters and polysaccharides of recent interest in food packaging and coating applications.**

To fulfill the above overall objective, the following partial objectives were proposed:

- Development of new nanobiocomposites from various biopolymers using different processing methods and different contents of food contact complying nanoclays, cellulose microfibers, cellulose nanowhiskers, carbon nanotubes, carbon nanofibers and amylopectine.

- Characterization of the morphology, of the thermal and mechanical properties, and a more exhaustive characterization of the mass transport properties to different permeants for these nanobiocomposites and in comparison with the properties of the petroleum-based polyester benchmark PET.

- Development and/or characterization of additional functionalities such as UV barrier, electrical conductivity and controlled release of natural extracts with antimicrobial and antioxidant properties.

3. Results

Chapter I.

Nanobiocomposites based on nanoclays.

<u>PAPER I:</u> Development and Characterization of Novel Nanobiocomposites of Bacterial Poly(3-hydroxybutirate), Layered silicates and Poly(ε-caprolactone).

Abstract

Polyhydroxybutyrate (PHB) is generally considered to be a very uneasy biopolymer to handle because of significant instability during melt processing and some excessive brittleness. This work studied the morphological, thermal, and barrier properties of novel meltmixed nanobiocomposites of PHB, poly(e-caprolactones) (PCL), and layered phyllosilicates based on commercial organomodified kaolinite and montmorillonite clay additives. The addition of PCL component to the blend was seen to reduce oxygen permeability but it was also found to lead to a finer dispersion of the clay. The addition of highly intergallery swollen organomodified montmorillonite clays to the PHB blend led to a highly dispersed morphology of the filler, but this simultaneously increased to a significant extend the melt instability of the biopolymer. Nevertheless, the organomodified kaolinite clay, despite the fact that it was found to both lead to less dispersed and irregular morphology, particularly for higher clay loadings, it led to enhanced barrier properties to oxygen, D-limonene, and water. D-limonene and specially wáter molecules were, however, found to sorb in both hydrophobic and hydrophilic sites of the filler, respectively, hence diminishing the positive barrier effect of an enlarged tortuosity factor in the permeability. Mass transport properties were found to depend on the type of penetrant and modeling of the permeability data to most commonly applied formalisms was not found to be satisfactory because of factors such as morphological alterations, heterogeneity in the clay dispersion, and penetrant solubility in the filler.

Key words: biopolymers; packaging applications; barrier properties; nanocomposites; polyhydroxybutyrate

Introduction

In the last decades, there has been a significant increase in the amount of plastics being used in packaging applications. In fact, the largest application for plastics today is packaging, and within the packaging niche, food packaging amounts has the largest plastics demanding application. This substantial increase in use has also raised a number of environmental concerns from a waste management point of view.[1–3] As a result, there is a strong research interest, pushed by authorities at national and international levels, and a parallel industrial growing demand in the development and use of materials which can disintegrate and biodegrade through processes such as composting into carbon dioxide and water.

Among biodegradable materials, three families[1–4] are usually considered: polymers directly extracted from biomass such as the polysaccharides starch, chitosan, and cellulose and proteins such as gluten, soy protein, and zein. A second family comprises oil based monomers or biomass derived monomers, but uses classical chemical synthetic routes to obtain the final biodegradable material, this is the case of for instance poly(e-caprolactones) (PCL), polyvinyl-alcohol (PVOH) and for the case of sustainable monomers polylactic acid (PLA). The third family comprises polymers produced by natural or genetically modified microorganisms such as polyhydroxylalcanoates and polypeptides.[5] Recently, surface modified clays have been studied as advanced additives to improve or balance thermal,mechanical, fire resistance, surface, or conductivity properties of nanocomposites because of its high surface to volume ratios and the subsequent intimate contact that they promote with the matrix at low filler additions.[5] Aside from the enhancement in these properties, these clay platelets with very few nanometers (ideally one nanometer in fully exfoliated systems) in thickness have the potential to uniquely reduce the matrix permeability to gases and vapors, while maintaining largely unmodified interesting properties of the matrix such as toughness or transparency. The enhanced gas barrier properties of polymer nanocomposites are now finding some specific applications, in fields such as membranes and in packaging materials and containers for a wide variety of food and beverage products.[6,7] Kaolinite ($Al_2Si_2O_5(OH)_4$) is a naturally occurring 1 : 1 phyllosilicate containing a gibbsite (aluminum hydroxide) octahedral layer and a silicon oxide tetrahedral sheet. This asymmetric structure allows the formation of hydrogen bonds between consecutive layers, providing a large cohesive energy. As a consequence of the high layer-to-layer interactions, the intercalation of the polymer chains in between the kaolinite platelets is greatly impeded, being thus a necessary layer for surface chemical treatment to facilitate the intercalation and further exfoliation of the clay. The treatment usually consists of an intercalation of chemical agents such as poly(ethylene glycol), n-methyl formamide, 1- methyl-2-pyrrolidone, 6-aminohexanoic acid, methanol, octadecylamine, or even polyhydroxybutyrate (PHB) (Ref. 8 and therein). Montmorillonite, unlike kaolinite, is strongly prone to swelling with increasing water content and is, therefore, a highly hydratable naturally occurring 2 : 1 phyllosilicate consisting of a central gibbsite octahedral layer between two external silica tetrahedral sheets. Isomorphous substitution of the Al^{3+} within the layers by for instance Fe^{2+} or Mg^{2+} yields a positive charge deficiency (characterized

by the so-called cation exchange capacity), which is balanced by hydrated cations (Na^{1+}, Li^{1+}, Ca^{2+}) at the interlayer.[9] Water molecules are, therefore, more strongly present in montmorillonite clays. Blends of thermoplastic biodegradable polymers, such PCL, PLA, and PHB, and the pure clay materials are typically incompatible; as a result, incorporation of an organic modifier onto the clay surface, to mediate between the polarity of the hydrophilic clay surface and that of the more hydrophobic polymer, has been widely adopted for compatibilization and for ease of exfoliation of the clay platelets into the polymer matrix during processing. Thus, as expected, the organoclay dispersability within a polymer matrix has been found to depend on factors such as type and quantity of surfactant, type of clay employed, as well as on the processing conditions. In the latter respect, the most interesting method for preparing polymer-based nanocomposites is the melt compounding route. This route is most adequate for rapid industrial implementation of the technology because of the wide availability of melt processable equipment and applications.[9–12] Biodegradable thermoplastic polyesters are melt processable biomaterials that present a number of excellent and promising properties in a number of uses, including packaging, automotive, and biomedical applications. Among them, bacterial biopolymers such as poly(3-hydroxybutyrate) (PHB) and its copolymers with valerate (PHB/HV) present good thermal, permselectivity, and mechanical properties. However, PHB suffers from relatively medium to low barrier to gases and water vapor, lack of transparency, brittleness and, more importantly, low melt stability.[13,14] A feasible strategy to decrease the inherent brittleness of thermoplastic biopolymers is by blending with PCL.[4,15–18] PCL is also a biodegradable polyester obtained by ring-opening polymerization from the Ɛ-caprolactone. The PCL is a semicrystalline polymer with low tensile strength, high elongation at break (above 400%), and processing temperatures similar to biopolyesters, therefore, it is expected to act as a plasticizing agent when blending it with for instance the PLA and PHB polymers. A potential drawback of these materials is the increase in gas permeability exhibited by the blends because of the poorer gas barrier properties of PCL. Nanocomposites of PCL have already been found to decrease by up to 50% the oxygen permeability of the polymer and to exhibit enhanced thermal and mechanical stability.[19] Previous work in our group in nanobiocomposite blends of an amorphous poly(lactic acid), PCL, and a food contact complying modified kaolinite were found to lead to a unique balance of thermal, mechanical, and barrier properties.[20,21]

Solvent casting nanocomposites of PHB with organically modified montmorillonite having as surfactants organic quaternary ammonium salts have previously been reported.[22] These solution cast composites displayed intercalated morphologies and exhibited improved thermal stability, except for contents of clay in excess of 6%. Not many blending works have, however, been carried out with PHB by direct melt compounding because of its melt instability.[13,14] However, a recent study showed that melt blending of PHB with various plasticizers has been proven to be a feasible route to enhance the biopolymer melt stability as determined by DSC.[13] Nanocomposites via melt compounding have only been developed for PHB/HV copolymers.23 The results showed that good dispersion of the fillers and enhanced temperature and rate of crystallization were achieved. PHB/HV copolymers have lower melting temperature and, therefore, can overcome the low melt stability of the neat PHB, but have as drawback low crystallization kinetics and lower barrier properties. It would, therefore, be highly desirable to find alternative and viable routes to retain or enhance the superior physical properties of the homopolymer PHB via melt compounding. The

objective of the current study is consequently to study the feasibility of the melt blending nanocomposites route to yield property enhanced PHB materials. Thus, the current study reports on the preparation and characterization of the morphology and barrier properties of novel property enhanced nanobiocomposite blends of PHB with organically modified kaolinite and montmorillonite layered silicates and with PCL as a plasticizing element. A discussion about the polymer morphology and its thermal and barrier properties is also carried out at the light of the most commonly considered models for permeability reduction in nanocomposites.

Experimental

Materials

The bacterial PHB grade was purchased from Goodfellow Cambridge Limited, U.K., in powder form. The supplied PHB material with density 1.25 g/cm^3 is a melt-processable semicrystalline thermoplastic
polymer made by biological fermentation from renewable carbohydrate feedstocks. Polycaprolactone (PCL) grade FB100 was kindly supplied in pellet form by Solvay Chemicals, Belgium. This grade has a density of 1.1 g/cm^3 and a mean molecular weight of 100,000 g/mol. A food contact complying phyllosilicate experimental grade (Nanoter^{TM} 2212) based on an organophilic surface modified kaolinite was kindly supplied by NanoBioMatters S.L., Spain. This grade was mainly used throughout the paper for generation of the biocomposites unless otherwise stated. A second food contact complying phyllosilicate experimental grade (Nanoter^{TM} 2000) based on an organophilic surface modified montmorillonite and designed for dispersion in polyolefins and polyesters was also supplied by NanoBioMatters S.L. No further details of sample preparation and modification were disclosed by the manufacturer. Cloisite^{TM} 20A, a montmorillonite grade chemicallymodified with dimethyl, dihydrogenatedtallow ~ 65% C18/~ 30% C16/~5% C14, quaternary ammonium salt was purchased from Southern Clay Products Incorporation, US.

Preparations of blends

Prior to the mixing step, the PBH and clays were dried at 70ºC and the PCL at 45ºC under vacuum for 24 h to remove sorbed moisture. Neat PHB, PHB blends, as well as PHB nanocomposites were melt-mixed in an internal mixer (16 cm^3 Brabender Plastograph) during a mixing time of 6 min at a temperature of 182ºC. The mixing was performed at a rotor speed of 60 rpm, which ensured that the melt temperature did not surpass 190ºC at any moment during the mixing time. The batch was extracted from the mixing chamber manually and allowed to cool to room temperature in air. The resulting material was dried at 50ºC at the above-mentioned conditions. The samples were finally transformed into sheets (0.7 and 0.1 mm thick) by compression molding in a hot-plate hydraulic press at 185ºC and 2 MPa of pressure during 4 min. The polymer sheets were eventually allowed to cool to room temperature under pressure. All the measurements and experiments were carried out on these polymer sheets.

The composition of the bioblends obtained in this work was (PHB/PCL) 100 : 0, term throughout the paper as PHB, and 80 : 20 wt/wt termed PHB-Blends. The clay loading of the nanobiocomposite samples was 1 and 4% wt/wt. Table I gathers the

nomenclature and corresponding composition of the PHB nanocomposites used throughout the paper.

Table I. Description of the samples used

Samples code	Composition
PHB-Blend	PHB/PCL, 80:20 wt/wt
4%NanoterPHB	4% wt of NanoterTM 2212 based on Kaolinite in neat PHB
1 or 4%NanoterPHB-Blend	1 or 4% wt of NanoterTM 2212 based on Kaolinite in PHB-Blend
4%NanoterMmtPHB-Blend	4% wt of NanoterTM 2000 based on Montmorillonite in PHB-Blend
4%CloisitePHB-Blend	4% wt of CloisiteTM 20A based on Montmorillonite in PHB-Blend

Oxygen transmission rate

The oxygen permeability coefficient was derived from oxygen transmission rate (OTR) measurements recorded using an Oxtran 100 equipment (Modern Control, Minneapolis, MN). During all experiments temperature and relative humidity were held at 24ºC and 0%RH and at 24ºC and 80%RH humidity. 80% relative humidity was generated by a built-in gas bubbler and was checked with a hygrometer placed at the exit of the detector. To avoid sample humidity equilibration during the actual oxygen transmission rate test at 80%RH and the subsequent fluctuations on barrier during the test, the samples were preconditioned at this RH by storage in a dessicator set up at this RH by appropriate salt solution. The experiments were done in duplicate at 0%RH an in quintuplicate at 80%RH, because the latter conditions are closer to real applications. As more data was accumulated at 80%RH, diffusion and solubility coefficients were also estimated at this humidity. The samples were purged with nitrogen for a minimum of 20 h, prior to exposure to a 100% oxygen flow of 10 mL/min, and a 5 cm^2 sample area was measured by using an in-house developed mask. Permeability (P) and diffusion (D) coefficients were estimated from fitting the OTR-time curve to the first six sum terms of the following solution of the Fick's second law:[24]

$$OTR(t) = \frac{Pp}{l}\left[1 + 2\sum_{n=1}^{\infty}(-1)^n \exp(-\frac{D\pi^2 n^2 t}{l^2})\right] \qquad (1)$$

In eq. (1), Pp is the oxygen partial pressure and l is the film thickness. The diffusion coefficient can also be calculated using the ''half-time'' method and yielded no significant differences. In this method the diffusion coefficient can be estimated from the following equation:[25]

$$D = \frac{l^2}{7.1999 \cdot t_{1/2}} \qquad (2)$$

where $t_{1/2}$ is the time for reaching an OTR value which is half that at the equilibrium.

Gravimetric measurements

Direct permeability to D(+)-limonene of 95% purity (Panreac Química, Spain) was determined from theslope of the weight loss-time curves at 24ºC and 40% RH. The films were sandwiched between the aluminum top (open O-ring) and bottom (deposit for the permeant) parts of a specifically designed permeability cell with screws.[26] A Viton rubber O-ring was placed between the film and the bottom part of the cell to enhance sealability. Then the bottom part of the cell was filled with the permeant and the pinhole secured with a rubber O-ring and a screw. Finally, the cell was placed in the desired environment and the solvent weight loss through the film was monitored and plotted as a function of time. Cells with aluminum films were used as control samples to estimate solvent loss through the sealing. Cells clamping polymer films but with no solvent were used as blank samples to monitor water uptake. Solvent permeation rates were estimated from the steady-state permeation slopes. Organic vapor weight loss was calculated as the total cell loss minus the loss through the sealing and plus the water weight gain. The tests were done in duplicate. The solubility and diffusion coefficients of D-limonene were estimated by gravimetry during desorption experiments at 24ºC and 40%RH using an analytical balance Voyager1 V11140 (Bradford, US). Thus, at saturation conditions, checked by observing no changes in successive weight uptake measurements of the specimens dipped in the aroma compound, the samples were thoroughly wiped with a tissue to remove the excess of aroma vapor condensed over the film surface (this step is considered as time zero) and were periodically weighted until they yielded constant weight. D values were obtained from fitting the experimental data versus time to the first six sum terms of the corresponding solution of Fick's second law [see eq. (3)] during desorption experiments.[27] Solubility was determined from equilibrium uptake measurements.

$$\frac{M_t}{M_e} = \frac{8}{\pi^2}\sum_{n=0}^{\infty}\frac{1}{(2n+1)^2}\exp\left\{\frac{-D(2n+1)^2\pi^2 t}{l^2}\right\} \qquad (3)$$

In eq. (3), M_t is the sample weight at time t and M_e is the sample weight at saturation or equilibrium conditions.

FTIR measurements

Diffusion coefficients to water could not be determined by conventional gravimetric methods because of lack of sensitivity of the gravimetric method and were, therefore, alternatively determined by FTIR transmission spectroscopy during desorption from equilibrated specimens as described more in detail elsewhere.[27] To do so, the measuring chamber was continuously purged with a high flow rate stream of dry N_2 to maintain a zero concentration level of the vapors at the polymer film. During desorption, previously equilibrated samples were removed from the water, quickly

wiped with a dry tissue to remove the excess of water vapor condensate from the surface, (this step is consider as time zero) and were immediately placed inside the measuring chamber to follow the desorption of the permeants. All FTIR experiments were carried out at 24ºC and in duplicate. Diffusion coefficients were estimated by mathematical fitting of the desorption data to the first six sum terms of the corresponding solution of Fick's
second law:

$$\frac{A_t}{A_e} = \frac{8}{\pi^2}\sum_{n=0}^{\infty}\frac{1}{(2n+1)^2}\exp\left\{\frac{-D(2n+1)^2\pi^2 t}{l^2}\right\} \qquad (4)$$

In eq. (4), A_t and A_e are the absorbances (OH stretching band centered at 3400 cm^{-1}) at a given time t and at saturation or equilibrium sorption conditions, respectively.

DSC measurements

Differential scanning calorimetry (DSC) of PHB and its biocomposites was performed on a Perkin-Elmer DSC 7 (Waltham, MA) thermal analysis system on typically 7 mg of material at a scanning speed of 10ºC/min from room temperature to the melting point using N_2 as the purging gas. Before evaluation, the thermal runs were subtracted analogous runs of an empty pan. The crystallinity of the samples was
estimated using as the heat of fusion for an infinity crystal of PHB 146 J/g[28] and for this of PCL 136 J/g.[29] The DSC equipment was calibrated using indium as a standard.

SEM measurements

For scanning electron microscopy (SEM) observation, the samples were fractured in liquid nitrogen and mounted on bevel sample holders. The fracture surface of the different samples was sputtered with Au/Pd in a vacuum. The SEM pictures (Hitachi S4100) (Hitachi High Technologies, Wokingham, UK) were taken with an accelerating voltage of 10 keV on the sample thickness.

TEM measurements

Transmission electron microscopy (TEM) was performed using a JEOL 1010 (Jeol, Tokyo, Japan) equipped with a digital Bioscan (Gatan) image acquisition system. TEM observations were performed on ultra-thin sections of microtomed thin biocomposite sheets.

X-Ray experiments

Wide angle X-ray experiments (WAXS) were performed using a Siemens D5000D equipment (Germany). Radial scans of intensity versus scattering angle (2θ) were recorded at room temperature in the range 2 to 28º(2θ) (step size = 0.03º(2θ), scanning rate = 8s/step) with identical settings of the instrument by using filtered Cu Kα radiation (λ = 1.54Å),an operating voltage of 40 kV, and a filament current of 30 mA. To calculate the clay basal spacing Bragg's law (λ = 2dsinθ) was applied.

Statistical analysis

One-way analysis of variance (ANOVA) was performed using XLSTAT-Pro (Win) 7.5.3 (Addinsoft, NY). Comparisons between treatments were evaluated using the Tukey test.

Results and Discussion
Morphological results in PHB-Kaolinite nanocomposites

Figure 1 shows SEM pictures from some of the samples taken using three different magnifications. From this Figure it can be seen that the PHB-Blend contains a very fine dispersion of the PCL phase in the matrix. Albeit, some debonding is observed at the polymer interphase, a closer inspection of the phase morphology shows that there is interfacial adhesion between the dispersed PCL phase and the biopolymer matrix. The two polymers are, therefore, not miscible as further suggested by observation of two melting points at around the same temperature as in the neat components (see later), but somewhat compatible due to the observed interfacial contact. A similar two phase morphology is also observed for the 4%NanoterPHB-Blend. However, for this particular sample, additional phases displaying clay particles or aggregates are not discernible from the SEM pictures, suggesting that the clay may be well dispersed across the polymer morphology. On the other hand and unlike the latter 4%NanoterPHB-Blend, the 4%NanoterPHB sample (with no PCL) does clearly exhibit a highly dispersed but irregular in size two-phase morphology, where clay particles can be easily spotted across the biopolymer matrix. A closer inspection into this sample [See Fig. 1(D,G)] indicates the presence of some mineral aggregates, i.e. tactoids, ranging in size from few tens of nanometers up to about one micron in thickness with some apparent weak adhesion at the interphase. Surprisingly and as stated earlier, this segregated morphology is not seen in the biocomposite containing kaolinite clay and PCL. It would appear, from the SEM pictures, as if the organomodified clay could be more easily compatibilized and dispersed during blending in the presence of this more viscoelastic blending component. The reason for this could be related to a better dispersion of the clay in the PCL phase or/and to the particular melt stabilization that the PCL component induces to the blend as will be later derived from the DSC experiments.

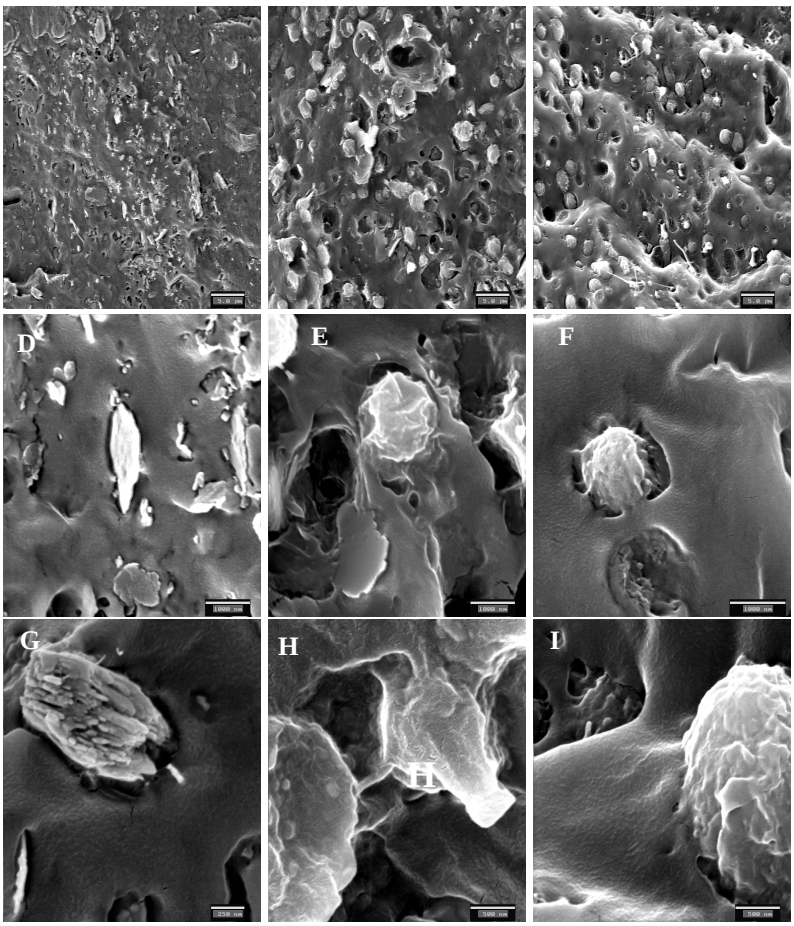

Figure 1. SEM pictures with increasing magnification of the samples 4%NanoterPHB (A, D and G with scale markers of 5 µm, 1 µm and 250 nm, respectively), 4%NanoterPBH-Blend (B, E and H showing scale markers of 5 µm, 1 µm and 500 nm, respectively) and PHB-Blend (C, F and I with scale markers of 5 µm, 1 µm and 500 nm, respectively).

Figure 2 shows the WAXS patterns of the above samples and, additionally, it shows the diffraction patterns of the 1%NanoterPHB-Blend and of the unmodified (raw clay) and surface modified kaolinite (Nanoter^{TM} 2212) based clays. From this figure, it can be easily seen that the modified clay shows a dominant (001) diffraction peak at angle 7.8º indicating that the intergallery or basal space of the natural
clay with peak at 12.4º has been expanded from 0.7 nm up to, at least, 1.13 nm as a result of the organicmodification and that most of the natural clay has undergone the intercalation. On the other hand, in the diffractograms of the biocomposites in Figure 2, only one clay peak can be discerned, which is located at about the same position as in the unmodified clay; no clay peak is, however, discerned in the 1%NanoterPHB-Blend. These observations indicate that during the melt mixing process, partial or total clay agglomeration or platelet collapse has taking place within the polymer matrix for

the samples with 4% Nanoter^{TM} 2212 loadings, due to probably losses of surfactant at the clay surface during the relatively extensive mixing cycle. In spite of that, the presence of the natural clay peak is clearly stronger (and at exactly the same position as in the natural clay) in the 4%NanoterPBH sample than in the 4%NanoterPBH-Blend sample, suggesting that a better dispersion of the organomodified clay may have been achieved through the use of the PCL component in the blends. Of course, it is difficult to discriminate how much of the originally modified clay has agglomerated and how much has been dispersed (intercalated or/and exfoliated) in any of the samples because there is no internal standard. Nevertheless, from the comparative intensity and shape of the clay peaks in Figure 2, from the SEM results and from the TEM results that follow it seems reasonable
to assume that a fraction of the clay has been, at the least, intercalated within the polymer matrix. Thus, from the above, it is inferred that a better compatibilization of the organomodified clay with the PHB/ PCL blend occurs. The sample with 1% clay loading could, however, be even more dispersed in the matrix since no trace of clay peak is observed in Figure 2.

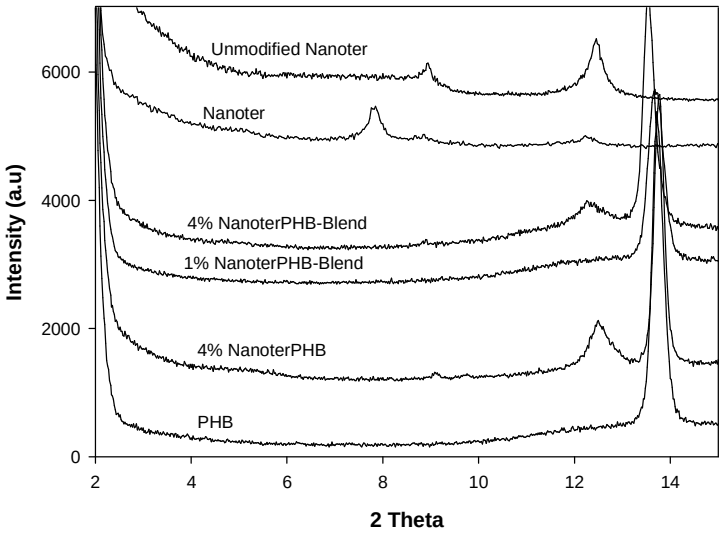

Figure 2. X-ray diffractograms of the unmodified (raw mineral) and modified kaolinite clays and of the various PHB nanobiocomposites.

Overall, the WAXS results point again that the NanoterPHB-Blends seem to have a more favorable morphology in terms of dispersion than the NanoterPHB samples. Figure 3 shows some TEM results taken on specimens of the 4%NanoterPHB-Blend and 1%NanoterPHB-Blend. This figure indicates that the former sample displays a highly dispersed irregular morphology consisting of intercalated thin tactoids with different sizes and some completely exfoliated (see white arrows) layered clay particles of different size and platelet orientation. Interestingly, it is observed that the smaller clay particles appear also fractured, whereas the intercalated particles are more

prone to remain in larger sizes in the platelets direction. Regarding particle aspect ratio, it is difficult to estimate accurate values given the dispersion in sizes,
platelet shape, and particles orientation, but the lowest aspect ratios (L/W) that were estimated from the pictures are for the biggest particles and ranges from around 8 to 40. A combination of appropriate surface modification and sufficiently high shear forces in the melt during polymer processing is usually required to generate extensive ratios exfoliation/ intercalation in nanocomposites; however, fully exfoliated systems are very seldom achieved via conventional melt blending routes in thermoplastic polyesters. The sample 1%NanoterPHB-Blend appears to show, however, more dispersed clay morphology, in which some exfoliated platelets (white arrows) and
some intercalated laminates can be observed.

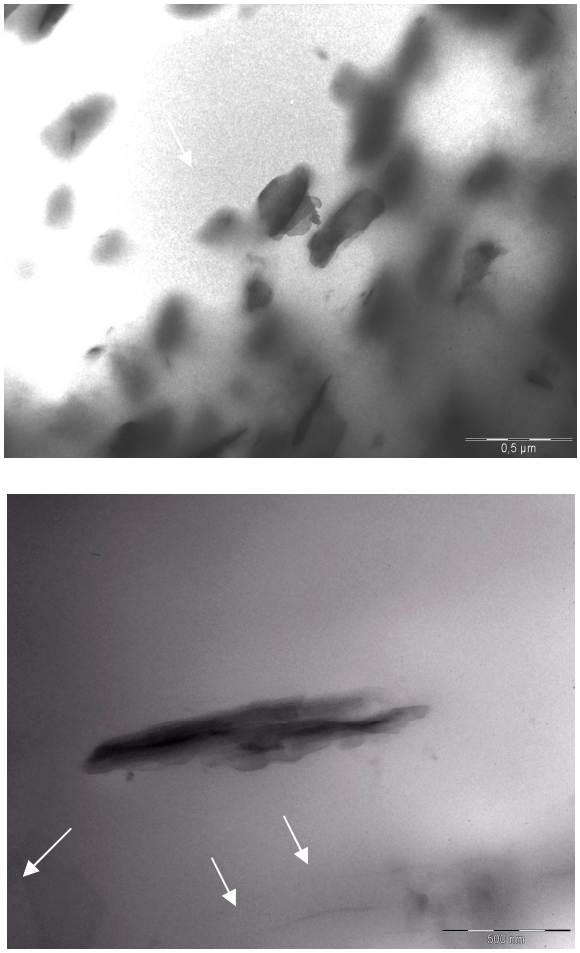

Figure 3. TEM pictures of 4%NanoterPHB-Blend sample (A showing scale markers of 0.5 lm) and of 1%NanoterPHB-Blend sample (B with scale markers of 0.5 lm).

Thermal properties of PHB-Kaolinite nanocomposites

The crystallinity and melting point of the blends were measured by DSC and the results are gathered in Table II. From this table, it can be seen that the melting point is not greatly altered in the clay containing samples but that the crystallinity (corrected for the biopolymer content in the composite) increases. The latter result adds to similar nucleating observations reported in previous works for PHB/ HV nanocomposites,[23] and suggests that the clay can act as a heterophase nucleating agent, hence promoting higher crystallinity in the matrix. In spite of that, Table II suggests that the melting point is either not affected or is slightly reduced (see later Fig. 7) for the more dispersed 4%NanoterPHB-Blend. Changes in melting point are the result of many factors such as changes in molecular orientation, crystal thickness, and crystal perfection. An increase in the latter factors leads to increased melting points.[30] Nevertheless, despite the fact that the crystallinity goes up in the nanocomposites the melting point is either unaffected or slightly reduced. A reduction in crystal size could explain a small decrease in melting point, but also some polymer degradation and chain scission due to melt processing.[13] It should be borne in mind that the natural PHB homopolymer used is a nonstabilized material which is even more unstable than commercial formulations of this or than PHBV copolymers. Albeit, the changes in the melting point of the samples are probably not meaningful because they are very small and, perhaps, within the experimental error of the technique, interestingly, the PHB-Blend appears to show slightly higher melting point than the neat PHB. This may indicate that the PCL plasticizing phase component could tend to act as a stabilizing agent for the biopolymer. In light of the cited previous work,[13] which indicated that processing of PHB should be carried at temperatures below T_m +15ºC to avoid polymer degradation, the samples were not allowed to surpass during melt mixing 190ºC by using a relatively low torque during processing. Of course, the use of a relatively low processing torque has a drawback that the impairment in the ability of the systems to exfoliate further due to the lower shear forces generated in the melt. More evident support to prove the instability of the homopolymer PHB arises from the crystallization and remelting behavior of the samples. Thus, further DSC crystallization experiments obtained by cooling at 10ºC/min the fresh molten samples after 1 min in the melt at 188ºC in the presence of a nitrogen purge, indicated that the crystallization temperature (T_c) for the PHB-Blend specimen was 121.0ºC, but for the 4%NanoterPHB-Blend it became 112ºC. This decrease in the crystallization point of the blend strongly suggests that thermal exposure of the nanobiocomposites results in lower crystallization rate due to most likely molecular degradation and further decrease in molar mass and, subsequent, depletion in nucleation density.[13] Further, degradation with successive heating cycles is revealed by data gathered after a second heating run at 10ºC/min following crystallization of the samples. These results yielded for the PHB-Blend a melting temperature of 175.7ºC and a crystallinity for the PHB fraction of 63% and for the 4%NanoterPHB-Blend a melting temperature of 173.4ºC and a crystallinity for the PHB fraction of 57%. As a result, the nanocomposite blend shows with increasing thermal aging, even in the presence of an inert gas, a much larger decrease in melting point compared to data gathered for the first heating of the sample in Table II, but also a decrease in melting enthalpy with extensive thermal exposure in accordance with results and degradation behavior reported earlier. This behavior is most likely related to a filler assisted acceleration in thermal degradation for the polymer. Since, the

mechanism of degradation for this biopolymer is thought to occur by esterification reaction between hydroxyl and carboxyl groups,[13] and as clay particles are inorganic hard particles which furthermore exhibit some hydroxyl and other potentially reactive moieties and impurities, the effect of a highly disperse filler may consequently be to facilitate the latter chemistry or other chemical and/or chain scission mechanisms (see later in the paper).

Table II. DSC melting point and melting enthalpy of the samples. The values for the PCL fraction in the blend are given between brackets.

Sample	**M_p (^oC)**	**PHB Melting Enthalpy (J/g)**	**PHB crystallinity(%)**
PHB-Blend	176 (64)	93 (60)	64 (44)
4% NanoterPHB-Blend	175 (65)	99 (53)	68 (39)
PHB	175	94	64
4% NanoterPHB	175	103	71
PCL	62	52	38

PHB-montmorillonite nanocomposites

In view of the above results and since more aggressive processing conditions were precluded in the internal mixer, an alternative route of blending with higher intergallery swollen clay systems was considered to aim fully exfoliated morphologies. It is well reported that organomodified montmorillonite has a higher intergallery spacing, even as a natural clay, compared to kaolinite and, therefore, it should in principle be more easily dispersible within the polymer matrix. In this context, further blending of PHB was similarly carried out with 20% (w/w) of PCL but alternatively with a 4% wt of Cloisite 20A and with a 4% Wt of a highly swollen organophylic montmorillonite (Nanoter 2000) (see Table I). Figures 4 and 5 show SEM and TEM results of these nanocomposites and Figure 6 shows the WAXS diffraction patterns of the composites and of the two commercial clays.
Surprisingly, nanocomposites with both of the above clay systems yielded extremely soft and fragile materials with hardly any mechanical consistency suggesting that these organophylic montmorillonite grades under the same blending conditions undergo
extensive molecular degradation (see DSC and ATRFTIR results below). Figure 4 reveals that the SEM morphology of both nanocomposites is coarser and flaky at the fracture surface compared to that of the unfilled blend. This particular microscopic discontinuous morphology is responsible for the macroscopic spongy and soft character of the material. However, no filler particles can be seen, fact that indicates that a good dispersion of the clay must have been achieved in both systems. Figure 5 shows some TEM pictures of the
4%CloisitePHB-Blend revealing the presence of larger length (due to the higher aspect ratio of the montmorillonite) in layers of apparently nonoriented clay particles, which are more highly dispersed across the polymer morphology than was observed in Figure 3, although still the system does not show a fully exfoliated morphology. Nanometric thin clay platelets can, however, be clearly discerned to be randomly dispersed across the polymer matrix.

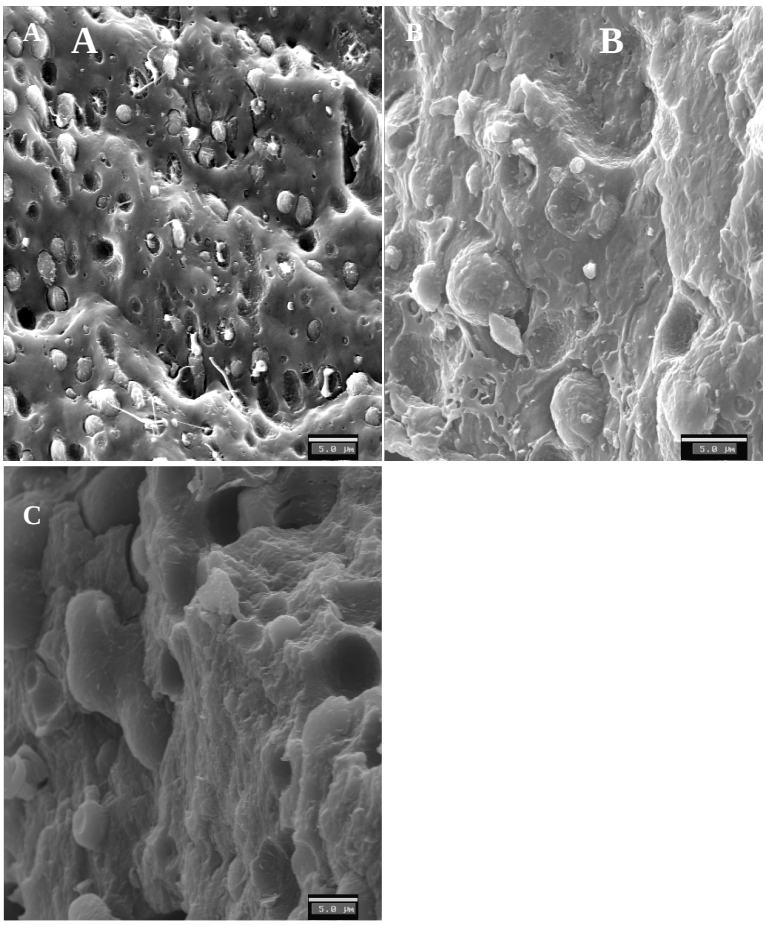

Figure 4. SEM pictures of samples PHB-Blend (A), 4%CloisitePHB-Blend (B), and 4%NanoterMmtPHB-Blend (C). The pictures show scale markers of 5 µm.

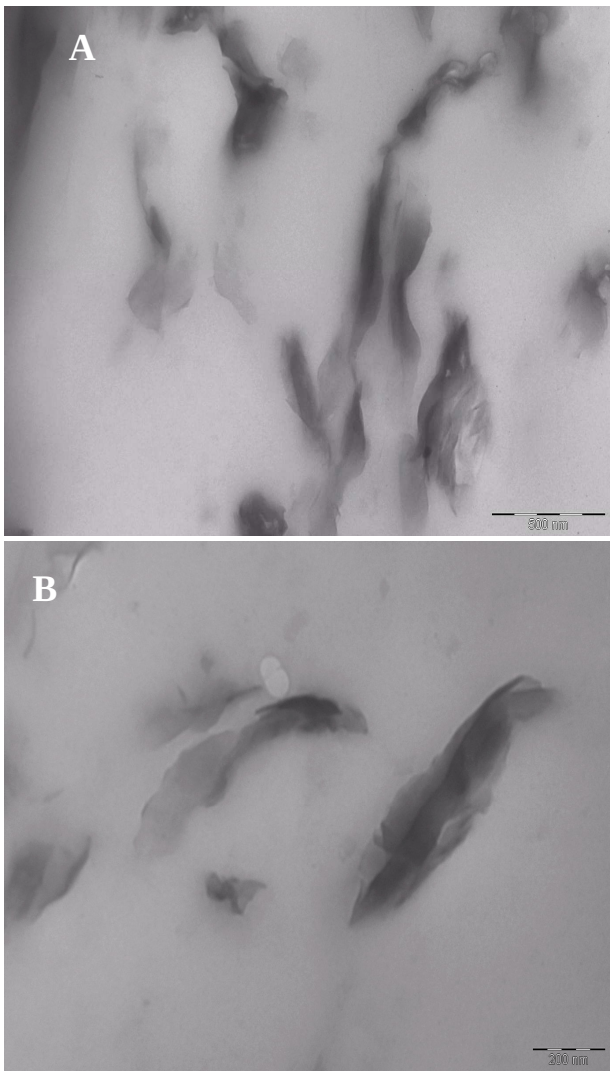

Figure 5. TEM picture of the 4%CloisitePHB-Blend. Scale markers are 0.5 µm for picture A and 0.2 µm for picture B.

Interesting observations are also derived from the X-ray patterns in Figure 6: In the montmorillonite based samples, while Cloisite 20A clay shows an intergallery spacing of d_{001}= 24.6Å, the Nanoter Mmt grade shows a spacing of d_{001}= 39.40Å, indicating that the latter clay is more effectively swollen or expanded. Other two peaks, besides the most intense one at 2θ 2.3^{o}, are observed at angles 4.6^{o} and 6.9^{o}, which are associated to the second and third order diffraction features, respectively. This highly ordered and stacked layered modified structure should of course lead to more easily dispersable clay morphologies in polymers and biopolymers, and further work is being carried out at present to evaluate its capacity to design more advanced nanocompo sites. Figure 6 clearly indicates that in neither of the nanobiocomposites the clay peaks

are discerned, suggesting again that a good clay dispersion across the biopolymer matrix must have been achieved for both systems. Nevertheless, it is worth noting that even when no clay basal peak is observed in the diffractograms of the nanobiocomposites in Figure 6, not fully randomly dispersed exfoliated morphologies are suggested by the TEM experiments. As a result, caution should be taken when assumptions are made regarding the existence of randomly dispersed platelet systems on the sole bases of lack of basal peaks in the X-ray experiments.

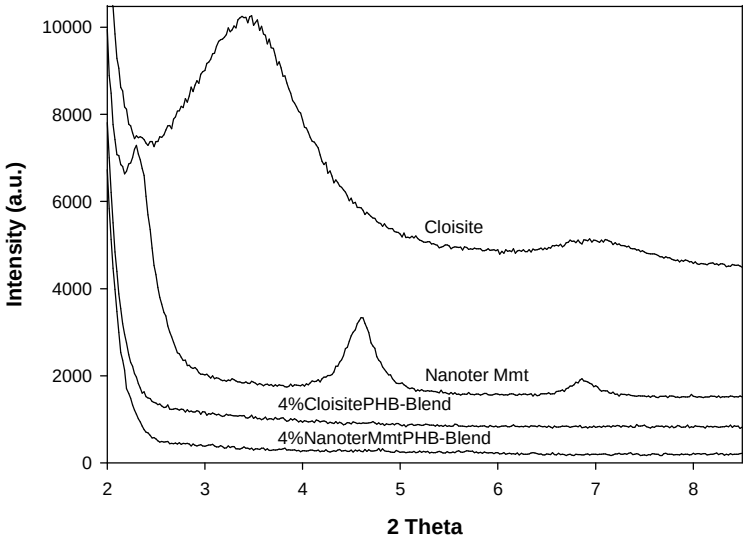

Figure 6 X-ray patterns of two montmorillonite-based surface modified clays and of their correspondent PHB-Blend biocomposites.

Finally, Figure 7(a) shows the DSC melting thermograms of the unfilled and filled nanocomposites revealing melting features of both the PCL, at ~60ºC, and the PHB, at ~ 176ºC, fractions. From this figure, the two composites containing montmorillonite exhibit a multiple melting endotherm (with two peaks) of noticeable lower melting point than both the unfilled blend and their kaolinite counterparts, suggesting that most likely extensive degradation of the
PHB matrix has taken place during compounding with these particular clays. This is further substantiated by the ATR-FTIR spectra plotted in Figure 7(b).

Figure 7(b) indicates that clear differences can be seen between the PHB-Blend and its nanocomposites depending on whether organomodified kaolinite or

montmorillonite clays are used. In the 4%NanoterPHB- Blend, there are some peaks, i.e. at 100º and 3700 cm^{-1}, which arise from the presence of the clay in the blend (see arrows). However, by comparison of the latter sample with the PHB-Blend there are some spectral changes such as the disappearance of a band at 700 cm^{-1} and some small changes in the relative intensity of bands in the range from 1000 to 150 cm^{-1} and in the group of bands around 2950 cm^{-1}. On the other hand, much bigger and different

alterations are observed for the 4%CloisitePHB-Blend sample (the strong montmorillonite peak at 1008 cm^{-1} is not discernible in the spectrum). This sample shows large spectral variations in the band envelop from 1000 to 1500 cm^{-1}, which clearly point to, at the least, chemical alterations in the material. More recent work making use of gel permeation chromatography measurements (GPC) and other techniques carried out in this and in PHBV nanocomposites indicated strong molecular weight decrease, particularly in the presence of organomodified montmorillonite clays
(will be published elsewhere). All of these changes strongly point to the hypothesized molecular degradation mechanism, most notably in the 4%CloisitePHB- Blend, and molecular weight reductions. The particular degradation behavior for the montmorillonite nanocomposites could be related to the different nature of the clay, e.g., sorbed water, specific clay surface chemistry and higher aspect ratio but it is probably also related to the higher degree of molecular
dispersion achieved for these particular systems, which promotes a more intimate contact between clay and polymer.

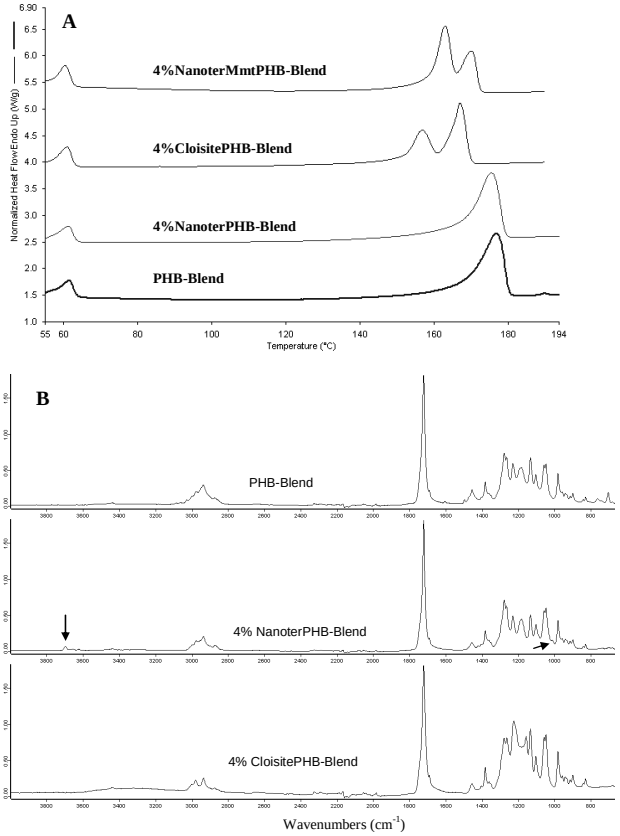

Figure 7 (A) DSC melting endotherms of from top to bottom, 4%NanoterMmtPHB-Blend, 4%CloisitePHB-Blend, 4%NanoterPHB-Blend and PHB-Blend. **(B)** ATR-FTIR spectra of from top to bottom, PHB-Blend, 4%NanoterPHB-Blend and

4%CloisitePHB-Blend. The arrows indicate the presence of clay peaks in the middle spectrum.

Mass transport properties of PHB-Kaolinite nanocomposites

Figure 8 shows, as an example, the oxygen transmission rate curves at 0%RH of the 4%NanoterPHBBlendand of the unfilled PHB-Blend. From this Figure,it is seen that the equilibrium transmission rate is higher in the unfilled blend than in the nanocomposite indicating that a lower permeability is reached in the nanocomposite systems, and that the diffusion appears faster in the unfilled blend. Table III shows the oxygen permeability coefficients at dry (0%RH) and at 80% RH for the various samples. From this Table III, it is seen that the oxygen permeability is most largely reduced, i.e. by ~43%, at 0%RH in the 4%NanoterPHB-Blend compared to the 4%NanoterPHB sample. This supports the morphology data discussed earlier, which displayed a more dispersed morphology for the composite containing PCL. The 1%NanoterPHB-Blend shows a permeability reduction at 0%RH of ~ 10%. Table III also shows that at a higher relative humidity, i.e. 80%RH, the oxygen barrier is somewhat lower in the neat polymer compared to dry conditions; however, increasing RH does not seem to enhance so apparently the oxygen permeability of the composites compared to their performance in dry. At 80%RH a 46% decrease in oxygen permeability is observed in the filled blend compared to the unfilled material, which is slightly higher than that measured at 0%RH. From an applied view point, Table III also teaches that although the PHB blend has higher permeability than both the neat PHB and petroleum-based amorphous polyethylene terephthalate (PET), the 4% clay loaded nanocomposite clearly maintains the barrier of the neat PHB polymer and outperforms the barrier properties of PET at dry and at high relative humidity conditions.

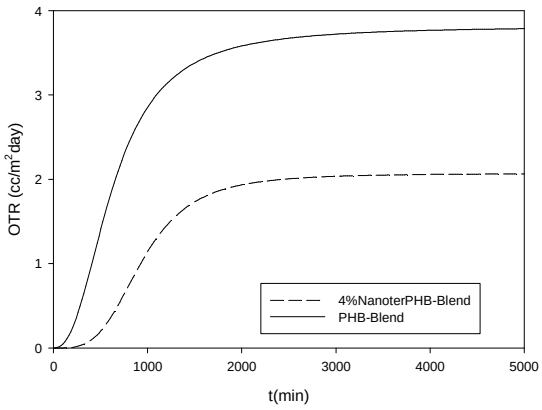

Figure 8. Oxygen transmission rate curve of the PHB-Blend and of the 4%NanoterPHB-Blend.

Table 3. Oxygen permeability of the various samples at 0%RH and at 80%RH and estimated diffusion and solubility coefficients at 80%RH for the blends. The permeability of a PET commercial film measured under the same conditions is also

reported for comparison purposes. The a, b and c and A and B letters correspond to the ANOVA statistical analysis of the data that indicate that with a 95% level of confidence the values are significantly different.

Sample	PO_2 (m^3 m/m^2 s Pa) 24°C, 0%RH	PO_2 (m^3 m/m^2 s Pa) 80%RH	DO_2 (m^2/s) 80%RH	SO_2 (m^3/m^3 Pa) 80%RH
PHB-Blend	[a]4.2±0.0005 e^{-19} (14.6 e^{-19})* (4.0 e^{-19})†	[a]5.2±0.004 e^{-19}	[a]1.1±0.01e^{-12}	[a]4.7±0.05e^{-7}
1%NanoterPHB-Blend	[b]3.8±0.3 e^{-19}	[b]3.9±0.1 e^{-19}	[b]1.0±0.02e^{-12}	[b]3.9±0.2e^{-7}
4%NanoterPHB-Blend	[c]2.4±0.3 e^{-19}	[c]2.8±0.2 e^{-19}	[c]0.8±0.01e^{-12}	[c]3.5±0.3e^{-7}
PHB	[A]2.3±0.002 e^{-19}	-	-	-
4%NanoterPHB	[B]1.8±0.3 e^{-19}	-	-	-
PCL	58.0 e^{-19}	-	-	-
PET	3.3 e^{-19}	3.8 e^{-19}		

*Calculated using the rule of mixtures; †Calculated using the model of Maxwell as extended by Roberson

Figure 9 shows examples of the application of the Nielsen and Fricke models [eq. (2)] to different aspect ratios (W/L) of layered particles. The model of Nielsen[31] [see eq. (5)] and other ulterior refinements such as the one of Fredrickson and Bicerano,[32] describe systems in which the layered i.e., thin, flat, and squared particles are perfectly oriented with length and width perpendicular to the permeant transport direction and are homogeneously diluted in the polymer matrix.

$$\frac{P_{nano}}{P_{neat}} = \frac{1 - V_{clay}}{1 + \frac{L}{2W} \cdot V_{clay}} \qquad \text{Equation 5}$$

In equation 1, L/W is the aspect ratio of the platelets and V_{clay} the volume fraction of the clay filler.

The model of Fricke [33] describes oblate randomly oriented spheroids uniformly distributed across the matrix (see Equations 6 and 7).

$$\frac{P_{nano}}{P_{neat}} = \frac{1 - V_{clay}}{\tau} \qquad \text{Equation 6}$$

$$\frac{W}{L} = \frac{1}{0.785 - \sqrt{0.616 - \frac{\frac{V_{clay}}{\tau - 1}}{\frac{V_{clay}}{\tau - 1} + 3}}} \qquad \text{Equation 7}$$

In Equation 6, τ is the tortuosity factor, which increases with increasing impedance efficiency of the clay filler. Equation 7 relates within this model the volume fraction of clay and the aspect ratio to the tortuosity factor.

Figure 9 additionally plots the experimental oxygen permeability data measured at 80%RH. The results seem to best fit the Nielsen model for aspect ratios of the layered particles around 100, and the Fricke model for particles of aspect ratios around 250. However, the best fitting to these models appear to overestimate the actual aspect ratio of the particles morphology, at least this of the biggest ones, as observed by TEM in Figure 3. Thus, it should be taken into account that there are a number of morphological factors that these simple models obviate. The main factors disregarded, besides the fact that these particles are not perfectly aligned or completely random, are the morphological changes in the matrix or blending components (mainly crystallinity, crystalline morphology, relative humidity effect, molecular degradation and molar mass reduction, and amorphous and interfacial changes) and do not account for heterogeneity in the aspect ratio of the filler experimentally observed in Figure 3.

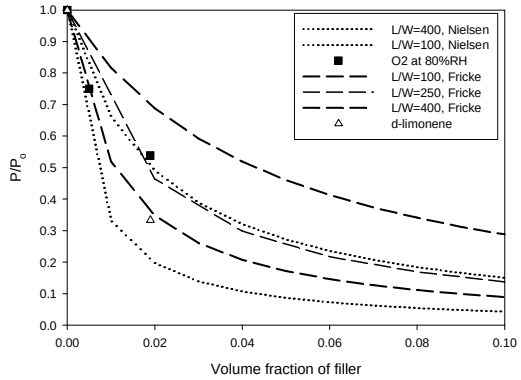

Figure 9. Experimental permeability data of the PHB-Blends to oxygen at 80%RH and d-limonene and, theoretical, permeability vs. filler content curves resulting from application of the formalisms of Nielsen and Fricke to several clay platelet aspect ratios.

Another interesting observation from Table 3 is that the permeability of the unfilled PHB-Blend is lower than that expected from application of the simple rule of mixtures of the pure PHB and PCL components, however, this approaches more closely the permeability value predicted by application of the model of Maxwell as extended by Robertson (see equation 8) [34,35].

$$P_{Blend} = P_{PHB}\left[\frac{P_{PCL} + 2P_{PHB} - 2V_{PCL}\left(P_{PHB} - P_{PCL}\right)}{P_{PCL} + 2P_{PHB} + V_{PCL}\left(P_{PHB} - P_{PCL}\right)}\right] \quad \text{Equation 8}$$

Equation 8 describes the permeability of blend systems in which both matrix (PHB) and blending components (PCL) are permeable, and in which the blending component are spheres evenly distributed across the matrix as is observed from Figures 1C, 1F or 1I.

Table III also shows the estimated diffusion and solubility coefficients for the blends at 80%RH. The solubility coefficient was easily derived from the well-known simple relation P = DS. The estimated diffusion and solubility coefficients are seen to decrease in the composites with the incorporation of clay and with increasing clay content in the matrix
as expected. In the case of diffusion, the presence of platelets is thought to increase the tortuosity (τ) or detour factor in the materials leading to slower diffusion processes and, therefore, to lower permeability. Nevertheless, the diffusion coefficient is seen to be reduced by only 27%, whereas the permeability is reduced by 46%. Therefore, the solubility parameter must also have a significant role in the biocomposites. The solubility coefficient is indeed seen to decrease from observation of Table III. However, the solubility decrease is higher than would be expected from simple application of eq. (9).

$S_{nano} = S_{neat} (1-V_{clay})$ Equation 9

In this equation, S_{nano} means solubility of the nanocomposite, S_{neat} solubility of the matrix and V_{clay} is the volume fraction of clay. The equation is derived from Equations 5 or 6, which subsequently derived from the well-known solubility model developed for semicrystalline polymers in which a solubility decrease is expected to occur with increasing the crystallinity fraction [Ref. 7 and therein, Ref. 25]. Thus, while only ca. 0.5% and 2% reductions in solubility would be expected for 1 and 4% wt/wt of clay loadings, the experimental reduction values are of 17% and 25%, respectively. The latter results highlight that simple models cannot be applied to describe complex systems such as those described in the paper, in which morphological changes, molar mass reduction, polymer degradation, relative humidity and crystallinity increase factors take place.

Figure 10 shows water desorption curves of unfilled and filled blends as obtained from FTIR spectroscopy data recorded during desorption from equilibrium saturation conditions. From the data in Figure 10, a diffusion coefficient can be easily estimated which is gathered in Table IV. From this table, the diffusion coefficient of water in the biocomposite is seen to be reduced by ~ 72% compared to the unfilled
polymer blend during desorption. Nevertheless, the solubility was seen to increase in the composite blend. Thus, the FTIR band area of the water band at 3400 cm^{-1} corrected for sample thickness (A3400/L (μm)) was found to be 1.95 for the PHB-Blend, whereas for the 4%NanoterPHB-Blend was 3.00. This means that the nanocomposite uptakes ~ 54% more water than the unfilled blend due to likely the existing hydrophilic sites of the filler. On the whole, as the water permeability is the product of D and S, this meaningful transport parameter is expected to be lower since the reduction in diffusion is seen larger than the 54% increase in solubility.

Table IV. Water diffusion coefficient as determined by FTIR and d-limonene direct permeability, diffusion and solubility coefficients as determined by gravimetry in the blends. The a and b letters correspond to the ANOVA statistical analysis of the data that indicate that with a 95% level of confidence the values are significantly different.

Sample	D_{Water} (m^2/s)	$P_{Limonene}$ (kg m/m^2 s Pa)	$D_{Limonene}$ (m^2/s)	$S_{Limonene}$ (kg/kg Pa)
PHB-Blend	$^{a}1.1\pm0.08\ e^{-17}$	$^{a}0.9\pm0.05\ e^{-15}$	$^{a}0.02\pm0.002\ e^{-10}$	$^{a}1.13\pm0.16\ e^{-5}$
4%NanoterPHB-Blend	$^{b}0.3\pm0.04\ e^{-17}$	$^{b}0.3\pm0.1\ e^{-15}$	$^{b}0.008\pm0.001\ e^{-10}$	$^{b}1.44\pm0.11\ e^{-5}$

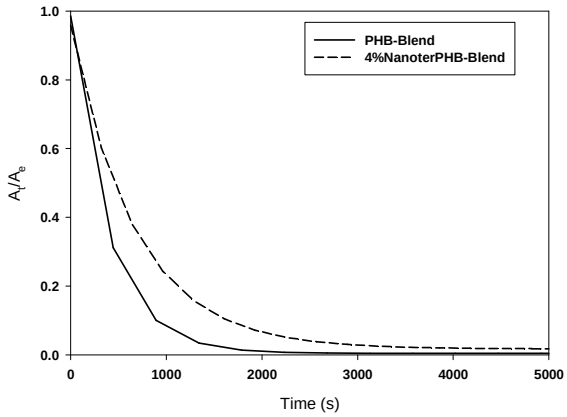

Figure 10. Water desorption curves as follow by FTIR vs. time for PHB-Blend and for 4%NanoterPHB-Blend film specimens.

Figure 11 shows limonene weight loss experiments for the two blends. From the slope of such curves, direct permeability results can be easily derived that are presented in Table IV. Table IV also presents the estimated diffusion coefficient of limonene and its solubility coefficient as determined by weight uptake measurements for the blends. From the results, a reduction in permeability of ~ 67% and in the diffusion coefficient of 60% is observed in the biocomposite for this particular organic vapor. On the other hand, the limonene solubility shows the opposite behavior and increases in the nanocomposite by ~ 27%. This is likely the result of the affinity of the organophylic sites of the filler for this less hydrophilic component. Figure 9 also plots the permeability decrease for this component versus the modelling work. From the modeling work a higher barrier effect compared to that for oxygen is observed which is best described in the model of Fricke by an aspect ratio of about 400.

Overall, the biocomposites exhibit increased gas, aroma, and water vapor barrier performance. However and in accordance with previous works,[36,37] the barrier effect was seen to be penetrant dependent. Conversely, these barrier results are in disagreement with most commonly considered models which simply relate

permeability reduction to filler shape and volume fraction. In the above experiments, the tortuosity factor related to the diffusion process appears to be larger for the vapor interacting molecules, which on the other hand have increased solubility as expected.

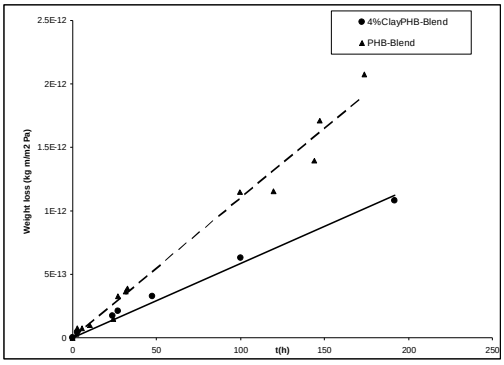

Figure 11. d-limonene direct permeability (weight loss vs. time) results for PHB-Blend and for 4%NanoterPHB-Blend film specimens.

Concluding Remarks

This article reports morphology data, thermal, and barrier properties of novel nanobiocomposites comprising PHB, PCL as plasticizing element and three commercial organomodified clays based on kaolinite and montmorillonite phyllosilicates. PHB is known to be a very rigid and melt unstable material; however, it does exhibit somewhat better oxygen barrier than its petroleum based counterpart PET.[38] Thus, the underlying objective of this work was to provide an understanding for the relation between structure and properties for nanocomposites of PHB and to develop novel PHB composites with enhanced barrier properties of interest in rigid food packaging applications for food and beverage trays and containers. From the results, it was found that indeed nanocomposites of PHB with highly swollen clay systems (based on montmorillonite) led to highly dispersed morphologies in the biopolymer. However, the montmorillonite systems simultaneously resulted in extremely soft materials of probably no use in most packaging applications because of extensive polymer degradation of the biopolymer as suggested by DSC and ATR-FTIR results. Similar nanocomposites with a less swollen organomodified clay (based on kaolinite) led to a less dispersed and irregular morphology. Surprisingly, this characteristic was found to generate a novel biomaterial with enhanced crystallinity and barrier properties, due to the clay reinforcing effect.

The addition of the PLC to the PHB was found to lead to a nonmiscible but compatible interphase blend, and this component appeared to increase compatibilization with the organophylic clay. The barrier properties of the systems were not seen to fit the most widely applied models such as those of Nielsen and Fricke for oriented and random dispersion of the fillers, in that barrier enhancements were found to depend on the penetrant and did not clearly match morphological observations in terms of aspect ratio. The reason for this disagreement must be attributed to limitations of the models to account for factors such as polymer

morphology and crystallinity alterations, irregular morphology and orientation of the filler platelets, chemical alterations in the matrix, and solubility of the penetrants in the filler.

References

1. Petersen, K.; Nielsen, P. K.; Bertelsen, G.; Lawther, M.; Olsen, M. B.; Nilsson, N. H.; Mortensen, G. Trends Food Sci Technol 1999, 10, 52.
2. Haugaard, V. K.; Udsen, A. M.; Mortensen, G.; Hoegh, L.; Petersen, K.; Monahan, F. In Biobased Packaging Materials for the Food Industry—Status and Perspectives; Weber, C. J., Ed.; KVL Department of Dairy and Food Science: Copenhagen, 2001.
3. Arvanitoyannis, I.; Psomiadou, E.; Biliaderis, C. G.; Ogawa, H.; Kawasaki, H.; Nakayama, O. Starch/Starke 1997, 49, 306.
4. Shuai, X.; He, Y.; Na, Y.; Inoue, Y. J Appl Polym Sci 2001, 80, 2600.
5. Reguera, J.; Lagaron, J. M.; Alonso, M.; Reboto, V.; Calvo, B.; Rodriguez-Cabello, J. C. Macromolecules 2003, 36, 8470.
6. Lagaron, J. M.; Catala´, R.; Gavara, R. Mater Sci Technol 2004, 20, 1.
7. Lagaron, J. M.; Cabedo, L.; Cava, D.; Feijoo, J. L.; Gavara, R.; Gimenez, E. Food Additives Contaminants 2005, 22, 994.
8. Cabedo, L.; Gimenez, E.; Lagaron, J. M.; Gavara, R.; Saura, J. J. Polymer 2004, 45, 5233.
9. Krishnamoorti, R.; Vaia, R. A.; Giannelis, E. P. Chem Mater 1996, 8, 1728.
10. Giannelis, E. P. Appl Organometal Chem 1998, 12, 675.
11. Vaia, R. A.; Giannelis, E. P. Macromolecules 1997, 30, 8000.
12. Dennis, H. R.; Hunter, D. L.; Chang, D.; Kim, S.; White, J. L.; Cho, J. W.; Paul, D. R. Polymer 2001, 42, 9513.
13. El-Hadi, A.; Schanabel, R.; Straube, E.; Mu¨ ller, G.; Riemschneider, M. Macromol Mater Eng 2002, 287, 363.
14. Bucci, D. Z.; Tavares, L. B. B.; Sell, I. Polym Test 2005, 24, 564.
15. Koening, M. F.; Huang, S. J. Polymer 1995, 36, 1877.
16. Bastiolo, C.; Bellotti, V.; Del Tredici, G. F.; Lombi, R.; Montino, A.; Ponti, R. Int. Pat. Appl WO 92/19680 (1992).
17. Park, E. S.; Kim, M. N.; Yoon, J. S. J Polym Sci Part B: Polym Phys 2002, 40, 2561.
18. Tsuji, H.; Yamada, T. J Appl Polym Sci 2003, 87, 412.
19. Di, Y.; Iannac, S.; Sanguigno, L.; Nicolais, L. Macromol Symp 2005, 228, 115.
20. Feijoo, J.; Cabedo, L.; Gimenez, E.; Lagaron, J. M.; Saura, J. J Mater Sci 2005, 40, 1785.
21. Cabedo, L.; Feijoo, J. L.; Villanueva, M. P.; Lagaron, J. M.; Jimenez, E. Macromol Symp 2006, 233, 191.
22. Lim, S. T.; Hyun, Y. H.; Lee, C. H.; Choi, H. J. J Mater Sci Lett 2003, 22, 299.
23. Choi, W. M.; Kim, T. W.; Park, O. O.; Chang, Y. K.; Lee, J. W.J Appl Polym Sci 2003, 90, 525.
24. Hiltner, A.; Liu, R. Y. F.; Hu, Y. S.; Baer, E. J Polym Sci Part B: Polym Phys 2005, 43, 1047.
25. Crank, J. The Mathematics of Diffusion, 2nd ed.; Oxford Science Publications: Oxford, 1975.
26. Lagaron, J. M.; Powell, A. K.; Bonner, J. G. Polym Test 2001, 20, 569.
27. Cava, D.; Catala, R.; Gavara, R.; Lagaron, J. M. Polym Test 2005, 24, 483.
28. Barham, P. J.; Keller, A.; Otun, E. L.; Holmes, P. A. J Mater Sci 1984, 19, 2781.
29. Crescezi, V.; Mazini, G.; Calzolari, G.; Borri, C. Eur Polym Mater 1972, 8, 449.
30. Bershtein, V. A.; Egorov, V. M. Differential Scanning Calorimetry of Polymers; Ellis Horwood: New York, 1994.
31. Nielsen, L. E. J Macromol Sci (Chem) A 1967, 1, 929.

32. Fredrickson, G. H.; Bicerano, J. J Chem Phys 1999, 110, 2181.
33. Krook, M.; Morgan, G.; Hedenqvist, M. S. Polym Eng Sci 2005, 45, 136.
34. Hopfenberg, H. B.; Paul, D. R. In Polymer Blends; Paul, D. R.; Newman, S., Eds.; Academic Press: New York, 1978.
35. Lagaron, J. M.; Gime´nez, E.; Altava, B.; Del-Valle, V.; Gavara, R. Macromol Symp 2003, 198, 473.
36. Takahashi, S.; Goldberg, H. A.; Feeney, C. A.; Karim, D. P.; Farell, M.; O'Leary, K.; Paul, D. R. Polymer 2006, 47, 3083.
37. Merkel, T. C.; He, Z.; Pinnau, I.; Freeman, B. D.; Meakin, P.; Hill, A. J. Macromolecules 2003, 36, 6844.
38. Cava, D.; Gimenez, T.; Gavara, R.; Lagaron; J. M. J Plast Film Sheeting 2006, 22, 265.

<u>PAPER II:</u> Comparative Barrier Performance of Novel PET Nanocomposites With Biopolyester Nanocomposites of Interest in Packaging Food Applications.

Abstract

Poly(ethylene terephthalate) (PET) is one of the polymers most widely used in the packaging industry. However, it is highly desirable to enhance its barrier properties for applications, such as carbonated drinks and other rigid and flexible packaging applications. The nanocomposites route offers unique possibilities to enhance the properties of this material, provided that adequate thermally resistant and legislation complying nanoadditives are used. This study presents novel PET nanocomposites with enhanced barrier properties to oxygen, water, and limonene based on a new specifically developed food-contact-complying highly swollen montmorillonite grade, and, furthermore, presents and discusses morphological data. Moreover, given the current interest in the packaging industry to replace this material by other biopolyesters, a comparative barrier performance of PET nanocomposites versus that of biopolymers, such as poly(lactic acid) (PLA), polyhydroxyalkanoates (PHB, PHBV), and polycaprolactones (PCL) and their corresponding nanocomposites is also reported.

Key words: PET, food packaging, composites, barrier properties, biopolyesters.

Introduction

Poly(ethylene Terephthalate) (PET) is widely used due to its high transparency, high dimensional stability, and good thermal and mechanical properties. It is also frequently applied to produce fibers, films, and packaging materials which require intermediate barrier properties. Nevertheless, in many applications it is highly desirable to further enhance some properties, such as barrier properties for food packaging and beverages applications. A feasible way to do this is by using nanocomposites containing layered phyllosilicates [1].
Poly(ethylene terephthalate)–montmorillonite (MMT) nanocomposites with enhanced barrier properties have been reported previously in the literature. Some authors have reported ~25% oxygen permeability reductions for PET+1%MMT by using in situ interlayer polymerization [2]. More recently, some authors have even claimed to obtain ~94% oxygen permeability reductions for PET+5%MMT nanocomposites by using in situ polymerization [3]. Finally, ~50% water vapor permeability reduction for PET–MMT nanocomposites by melt blending in a rheometer was also reported [4].
Natural and organo-modified MMTs have thus been researched to a significant extent as reinforcing materials for polymers due to their high aspect ratio and unique intercalation/exfoliation characteristics by several processing routes. The most useful route to prepare PET-MMT
nanocomposites is possibly the melt-compounding process because of its cost effectiveness and its enabling immediate implementation by converters using currently available processing machinery. However, due to the high temperatures needed for processing PET, the PET nanocomposites have become a major technological challenge due to potential degradation of the clay's organic modification during processing. In addition to this, legislation barriers are also imposing restrictions for MMT additives, because most commercially available organo-modified MMTs are not currently allowed for food contact. Poly(ethylene terephthalate) is also facing a substantial threat arising from the increasing implementation of biodegradable and/or renewable biopolyesters, such as poly(lactic acid) (PLA), polycaprolactones (PCL), and polyhydroxyalkanoates (PHA). The reason for this is that
these materials have excellent and promising properties that may replace conventional non-biodegradable polymers in a number of applications, including packaging, automotive, and biomedical applications[5].

The objective of this study was to characterize the morphology and barrier properties of a novel food-contact-complying PET nanocomposite containing a 'highly swollen' organo-modified MMT grade. The study also reports comparative barrier data of PET and some biodegradable biopolyesters and of their corresponding nanocomposites.

Materials and Methods
Materials

The PET resin used was a film extrusion grade supplied by the converter Neoplastica, Spain. No further details about the characteristics of the materials were provided. The bacterial PHB grade was purchased from Goodfellow Cambridge Limited, UK, in powder form. The supplied PHB material with density 1.25 g/cm^3 is a melt-processable semi-crystalline thermoplastic polymer made by biological fermentation from renewable carbohydrate feedstocks. A melt-processable semi-crystalline

thermoplastic polyhydroxybutyrate with 12 mol% valerate (PHBV) copolymer made by biological fermentation from renewable carbohydrate feedstocks was also purchased from the same manufacturer in pellet form. The PCL grade FB100 was supplied in pellet form by Solvay Chemicals, Belgium. This grade has a density of 1.1 g/cm^3 and a mean molecular weight of 100,000 g/mol.

The semicrystalline PLA used was a film extrusion grade manufactured by Natureworks, USA (with a D-isomer content of ~2%). The molecular weight had a number-average molecular weight (Mn) of ~130,000 g/mol, and the weight-average molecular weight (Mw) was ~150,000 g/mol.

A highly swollen food-contact-complying Nanoter^{TM} 2000 grade based on modified MMT was supplied by NanoBioMatters S.L., Spain. No further details on sample surface modification were disclosed by the manufacturer. The Nanoter^{TM} grade was characterized to be a very fine white powder with an average 3 m particle size. When the Nanoter 2000 grade was used with PHB and PHB/PCL resins, due to extensive hydrolytic degradation of the biopolymer, the compounds were extremely soft and thus of no use in packaging applications. Therefore, for the PHB and PHB/20% PCL nanocomposites a second food-contact-complying phyllosilicate grade called Nanoter^{TM} 2212 based on an organophilic surface modified kaolinite [6] supplied by NanoBioMatters S.L., Spain, was used.

Preparation of Nanocomposites

Prior to mixing, PET was dried at 60ºC, under vacuum for 24 h to remove sorbed moisture in an oven under vacuum. PHBV, PLA, and PCL were dried at 70, 70, and 508C, respectively. The polymers as well as the nanocomposite blends were prepared by melt-blending in an internal mixer (16cm3 Brabender Plastograph) for 4 min at 260ºC
for PET and for 5min at 1758C for PHBV, PLA, PHB, and PHB/20% PCL. The mixer was run at 60 rpm. The batch was manually removed from the mixing chamber and allowed to cool to room temperature in air. The resulting material was dried at the abovementioned conditions. The samples were compressed into sheets (0.7 and 0.1mm thick) in a hot-plate hydraulic press as follows:

- PET at 255ºC and 2MPa for 2 min.
- The biopolymers at 175ºC and 2MPa for 4 min.

The PET polymer sheets were crash cooled from the melt by rapid immersion in an ice bath. The biopolymer sheets were allowed to cool to room temperature under pressure. All the measurements and experiments were carried out on these polymer sheets. The nanobiocomposite samples clay loading was 5wt% unless otherwise stated.

Oxygen Transmission Rate

The oxygen permeability coefficient was derived from oxygen transmission rate (OTR) measurements recorded using an Oxtran 100 equipment (Modern Controls Inc., Minneapolis, MN, US). During all experiments temperature and relative humidity

(RH) were held at 24ºC and 0% RH and at 24ºC and 80% RH. Relative humidity of 80% was generated by a built-in gas bubbler and was checked with a hygrometer placed at the exit of the detector. To avoid sample humidity equilibration during the actual OTR test at 80%RH and the subsequent fluctuations on barrier during the test, the samples were preconditioned at this RH by storage in a desiccator set at this RH by an appropriate salt solution. The samples were then purged with nitrogen for a minimum of 20 h prior to exposure to a 100% oxygen flow of 10 mL/min, and a $5cm^2$ sample area was measured by using an in-house developed mask. The permeability (P) coefficient was estimated from the steady-state OTR curve versus time. The samples were measured at least in duplicate and the data quoted corresponds as usual in permeability testing of non-industrial samples to the lowest permeability value measured, as the scatter was rather small for the duplicates.

Gravimetric Measurements

Direct permeability to d-limonene of 95% purity (Panreac Química,
Spain) was determined from the slope of the weight loss–time curves at 24ºC and 40% RH. The films were sandwiched between the aluminium top (open O-ring) and bottom (deposit for the permeant) parts of a specifically designed permeability cell with screws. A Viton rubber O-ring was placed between the film and the bottom part of the cell to enhance sealability. Then the bottom part of the cell was filled with the permeant and the pinhole secured with a rubber O-ring and a screw. Finally, the cell was placed in the desired environment and the solvent weight loss through a film area of $0.001m^2$ was monitored and plotted as a function of time. Cells with aluminum films (with a thickness of ca. 10 m) were used as control samples to estimate solvent loss through the sealing. The permeability sensibility of the permeation cells was determined to be better than $0.01x10^{-13}$ kg m/s m^2 Pa based on the weight loss measurements of the aluminum cells. Cells clamping polymer films but with no solvent were used as blank samples to monitor water uptake. Solvent permeation rates were estimated from the steady-state permeation slopes. Organic vapor weight loss was calculated as the total cell loss minus the loss through the sealing plus the water weight gain. The tests were done in triplicate and average values and standard errors are provided.

DSC Measurements

Differential scanning calorimetry (DSC) of PET and its nanocomposites was performed on a Perkin-Elmer (USA) DSC 7 thermal analysis system on typically 7mg of material at a scanning speed of 10ºC/min from room temperature to the melting point of the PET. Before evaluation, the thermal runs were subtracted from similar runs of an empty pan. The DSC equipment was calibrated using indium as a standard. Typically one sample of each material was tested.

SEM Measurements

For scanning electron microscopic (SEM) observation, the samples were fractured in liquid nitrogen and mounted on bevel sample holders. The fracture surface of the different samples was sputtered with Au/Pd in vacuum. The scanning electron

micrographs (Hitachi S4100, Tokyo, Japan) were taken with an accelerating voltage of 10 keV on the sample thickness.

TEM Measurements

Transmission electron microscopy (TEM) was performed using a JEOL 1010 (Jeol Ltd, Akishima, Japan) equipped with a digital Bioscan (Gatan) image acquisition system. TEM observations were performed on ultra-thin sections of microtomed nanocomposite sheets.

X-Ray Experiments

Wide angle X-ray experiments (WAXS) were performed using a Siemens D5000D equipment. Radial scans of intensity versus scattering angle (2θ) were recorded at room temperature in the range 2 to 28º(2θ) (step size = 0.03º(2θ), scanning rate = 8s/step) with identical settings of the instrument by using filtered Cu Kα radiation (λ = 1.54Å), an operating voltage of 40kV, and a filament current of 30mA. To calculate the clay basal spacing, Bragg's law (λ = 2dsinθ) was applied.

Results and Discussion
Morphology

Figure 1 shows scanning electron micrographs taken in criofractured cross-section specimens of the samples. The SEM examination reveals that a homogeneous distribution of the clays in the PET matrix and good interfacial adhesion must have been achieved for 5 wt% clay contents since no filler agglomerates and/or phase discontinuity can be discerned in the reinforced sample by this technique.

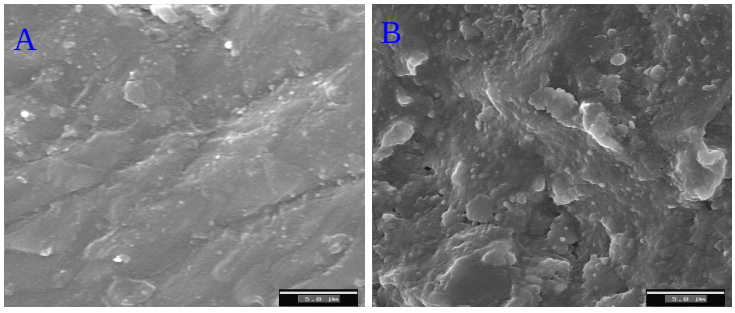

Figure 1. Scanning electron micrographs of the cross section of: (A) A film prepared by melt blending of pure PET and (B) A film prepared by melt blending of PET with 5%Nanoter content.

Figure 2 shows a typical TEM picture taken on specimens of the PET with 5 wt% Nanoter nanocomposite where the clay particles can be easily discerned. In nanocomposites, TEM and WAXS experiments are often used to discriminate the morphology of the nanofiller dispersion, since clay nanoparticles with high levels of dispersion, i.e., highly fractured tactoids, cannot be usually discerned by conventional

SEM experiments. Figure 2 is representative of the morphology attained in the nanocomposite and indicates that this specimen does indeed exhibit a highly dispersed morphology consisting of exfoliated and some very thin intercalated layered clay nanoparticles. From the figure, the filler appears to be evenly dispersed across the matrix and remains in the nanometer range in the thickness direction. The corresponding WAXS patterns of the nanocomposite samples did not show evidence of the clay basal peaks, suggesting further that a very high dispersion in terms of intercalation and exfoliation of the filler has been achieved in the system (see Figure 3).

Curiously, it is observed that the smallest (in length) clay particles appear more exfoliated but fractured, whereas the intercalated thicker particles are more prone to remain in larger sizes in the length direction. It is well-known that a combination of appropriate surface modification and high sheer forces in the melt during polymer processing, such as these generated in typical twin screw extruders, often lead to best results in terms of morphology in nanocomposites.
In spite of the fact that the current study made use of moderate sheer forces in the processing of the nanocomposites to potentially reduce processing-induced degradation in the systems, the morphology appears to still be quite favorable.

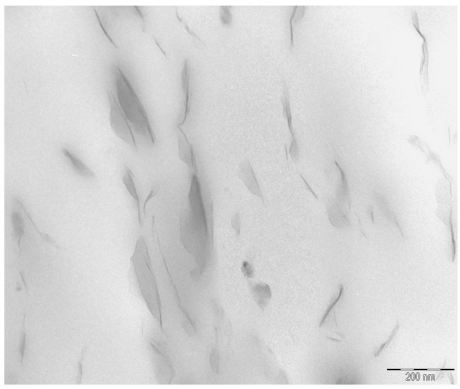

Figure 2. TEM photograph taken in a specimen of the PET+5%Nanoter sample.

X-Ray Experiments

Figure 3 shows the WAXS patterns of the neat PET, PET+5%Nanoter and of the Nanoter grade. The Nanoter MMT shows a basal spacing of d001=39.4 Å, indicating that the latter clay is very effectively swollen or expanded. The unmodified MMT was reported by the manufacturer to have a d basal spacing of d001=11.9Å. Moreover, the modified clay shows two more peaks, besides the most intense one at 2theta 2.3^{o}, at angles 4.6^{o} and 6.9^{o}. These diffraction peaks which decrease in intensity with increasing 2theta are associated to the second and third order diffraction features of

the clay, respectively. This highly expanded, ordered and stacked layered modified structure is thought to lead to more easily dispersable clay morphologies in polymers and biopolymers. Figure 3 also indicates that the PET+5%Nanoter sample shows no clay peaks in the range scanned, pointing that a high dispersion of the clay has been promoted across the polymer matrix as was anticipated by the SEM and TEM experiments.

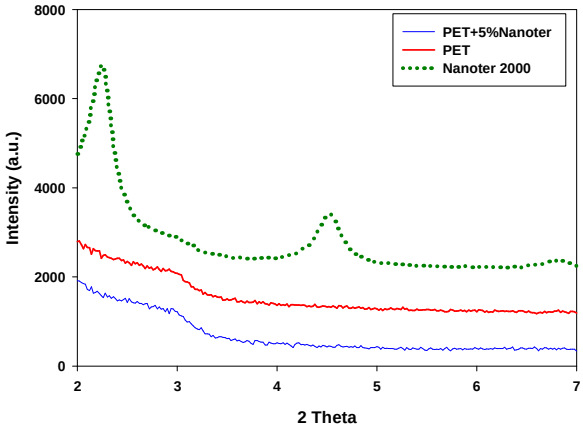

Figure 3. X-ray patterns of neat PET, PET+5%Nanoter and of the Nanoter powder.

Thermal Properties

Melting temperature (T_m), heat of fusion (ΔH_m), glass transition temperature (T_g) and heat capacity increment (ΔC_p), corrected for the matrix content in the nanocomposite, were determined from the DSC first heating runs of the samples. The data is gathered in Table 1 for all the samples. From the results, the enthalpy of fusion (calculated as the difference between the melting enthalpy and the cold crystallization enthalpy) appears to increase slightly in the PET+5%Nanoter sample. The polymer Tg is higher in the nanocomposite and the jump in heat capacity is also slightly higher. The overall results suggest that crystallinity is not strongly affected in the PET+5%Nanoter sample. Moreover, the thermal resistance, i.e. Tg, of the polymer is enhanced by ca. 3ºC with the addition of Nanoter. In principle, crystallization of the nanocomposites is positive from a barrier perspective, since crystals are typically impermeable systems, but it may also impose additional rigidity and hence fragility to the nanocomposites mechanical performance.

Table 1. DSC melting point, melting enthalpy, glass transition temperate and heat capacity jump.

	T_m (ºC)	ΔH_m (J/g)	Tg (ºC)	ΔC_p (J/gºC)
PET	245	18	69	0.3
PET-5%Nanoter	245	22	72	0.4

Mass Transport Properties

Figure 4 shows, as an example, the OTR curves at 0%RH of the PET+5%Nanoter sample and of the neat PET processed under the same conditions. From this figure, it is seen that the equilibrium transmission rate is higher in the unfilled blend than in the nanocomposite indicating that a lower permeability is clearly reached
in the nanocomposite systems, and that the diffusion is clearly faster in the unfilled blend. Table 2 shows the calculated oxygen permeability coefficients, water permeability, and limonene permeability for the samples of PET. From this table, it is seen that the oxygen permeability of the nanocomposite of PET is reduced by ~55% at 0%RH in the 5%Nanoter compared to the pure PET sample. The table also shows that at higher RH (80%), the oxygen barrier is somewhat lower in the neat polymer compared to dry conditions and the permeability reduction is ~35%. A previous study [8] reported that the oxygen permeability for PET is of ~$4.11x10^{-19}$ m^3 m/s m^2 Pa when measured at 0% RH, a value which is similar to the permeability measurement taken in the laboratory.

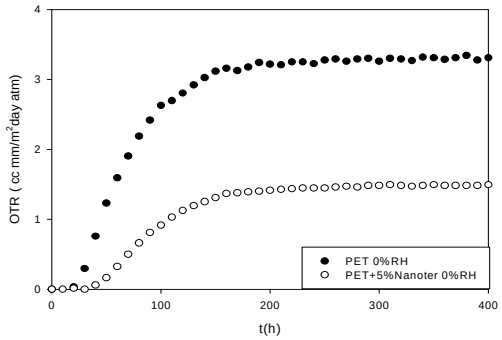

Figure 4. Oxygen transmission rate curve of the pure PET and of the PET+5%Nanoter at 0%RH.

Water and limonene direct permeability were also evaluated for the PET and for their nanocomposites and are summarized in Table 2. This table also shows water and limonene permeability measured in samples containing 1 wt% of clay. Films of PET with 1%wt Nanoter have a limonene permeability decrease of 26% compared to the unfilled material, but the sample with 5%wt Nanoter content has a reduction in limonene permeability of ca. 68%. A reduction in water permeability of ~43% is observed in the nanocomposite of PET with 1%wt Nanoter but films of PET with 5%wt Nanoter have a reduction in water permeability of only 14%. The reason for the latter counterintuitive behavior in the water permeability behavior could be related to

the inherent MMT clay hygroscopicity. Previous studies reported that the PET limonene permeability is about $0.0000048x10^{-13}$ kg m/s m^2 Pawhen measured at 23ºC and 40 Pa [7]. The reason for the large disagreement with the limonene permeability data could be related to the different origins of the two samples (extruded vs. un-oriented compression molded specimens) and the fact that the polymer grade, the test conditions used, and the differences in partial pressure used for testing were largely different. Since the differences in partial pressure gradient used for testing was much smaller than the ones reported here, the sample is expected to be much less plasticized by the component ingress. On the other hand, the PET water permeability was earlier reported to be about $0.028x10^{-13}$ kg m/s m^2 Pa when measured at 37.8ºC and 100%RH [9], a value which is similar to the one measured in the laboratory. This is likely to be so because the test conditions were more alike for the evaluation of the transport properties of this permeant.

Table 2. Oxygen permeability at 0%RH and at 80%RH and D-Limonene and water permeability .

	PO_2 (m^3m/m^2sPa) at 24ºC, 80%RH	PO_2 (m^3m/m^2sPa) at 24ºC, 0%RH	P limonene (Kg m/s m^2 Pa)	P water (Kg m/s m^2 Pa)
PET	4.26 e^{-19}	3.78 e^{-19}	1.17±0.15 e^{-13}	0.03±0.01 e^{-13}
PET+1%Nanoter	-	-	0.87±055 e^{-13}	0.017±0.002 e^{-13}
PET+5%Nanoter	2.81 e^{-19}	1.69 e^{-19}	0.37±0.07 e^{-13}	0.026±0.0009 e^{-13}
Literature Value PET	(at 85%RH) [8]4.45 e^{-19}	[5]4.11 e^{-19}	[7]0.0000048 e^{-13} 23ºC and 40Pa	[9]0.028±0.00015 e^{-13} 37.8ºC and 100%RH
PLA	22.09 e^{-19}	22.56 e^{-19}	-	0.126±0.010e^{-13}
PLA+5%Nanoter	15.4 e^{-19}	19.55 e^{-19}	-	0.104±0.009e^{-13}
Literature Value PLA	[10]17.5 e^{-19}	-	-	-
PHBV	-	15.69 e^{-19}	1.99±1.01e^{-13}	0.069±0.003e^{-13}
PHBV+5% Nanoter	-	11.53 e^{-19}	1.27±0.08e^{-13}	0.032±0.002e^{-13}
PHB	-	2.24 e^{-19}	0.0885 e^{-13}	0.017±0.0009e^{-13}
PHB+5% Nanoter	-	1.78 e^{-19}	0.01±0.0005e^{-13}	0.016±0.00003e^{-13}
PHB/20%PCL	5.19 e^{-19}	4.2 e^{-19}	-	0.025±0.0003e^{-13}
PHB/20%PCL+5% Nanoter	2.80 e^{-19}	2.4 e^{-19}	-	0.021±0.0005e^{-13}

Figure 5 shows the comparative oxygen permeability data for PET and several thermoplastics biopolymers and their nanocomposites at 0%RH. Further details about the biopolymers morphology, thermal and mechanical and other relevant properties will be published elsewhere, e.g., [6]. Table 2 also compares the barrier performance of these biopolyesters and their corresponding nanobiocomposites. All the biopolymer specimens were obtained by slow cooling from the melt (unlike PET that was rapidly quenched) and thus had enhanced
crystallinity [6]. From the permeability results, only PHB and PHB nanocomposites show lower oxygen permeability than the pure PET. The PHB nanocomposite has the lowest oxygen permeability value of all biodegradable materials, and becomes closer to the PET nanocomposite. The PHB/20% PCL nanocomposite also shows lower

oxygen permeability than the pure PET. The biodegradable materials (PHBV and PLA) have higher oxygen permeability compared to PET, and their nanobiocomposites have better oxygen barrier than the neat biopolymers. Figure 6 compares water and limonene permeability for PET and biodegradable polymers and their nanocomposites. Table 2 also compares the vapor barrier performance of the biopolyesters and their corresponding nanobiocomposites. PHB and the PHB nanocomposite show better water and aroma (limonene) barrier compared with PET. The PHB nanocomposite has the lowest water permeability and the limonene permeability values of it are much lower than that of the PET nanocomposite. The PHBV nanocomposite has water permeability similar to the neat PET and the limonene permeability of this nanocomposite is also close to that of the neat PET.
In summary, the PHB and PHB/20% PCL nanobiocomposites show the best barrier properties of all biopolyesters. These materials additionally show lower water and limonene permeability than both pure PET and the PET nanocomposite. For oxygen permeability the PET nanocomposites show the best barrier performance of all the materials considered.

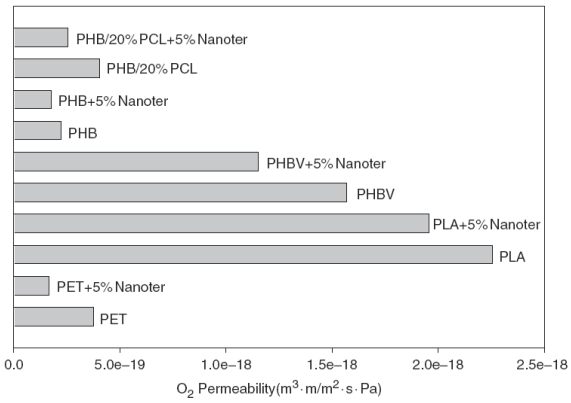

Figure 5. Oxygen permeability of pure PET and of PET+5%Nanoter and of the biopolyesters and their nanocomposites containing 5 wt.-% Nanoter at 0%RH.

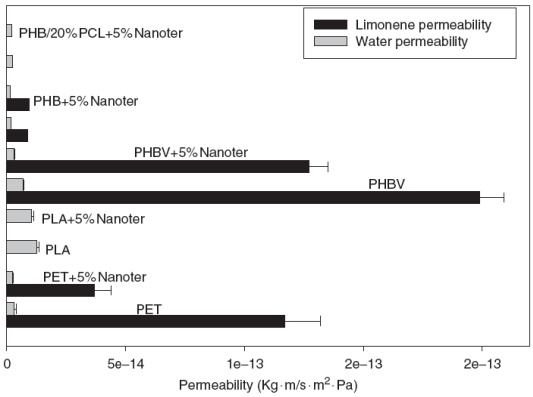

Figure 6. Limonene and water permeability of pure PET and PET+5%Nanoter and of the biopolyesters and their nanocomposites containing 5 wt.-% Nanoter.

References

1. Hao, J., Lu, X., Liu, S., Lau, S.K. and Chua, Y.C. (2006). Synthesis of Poly(ethylene terephthalate)/Clay Nanocomposites using Aminododecanoic Acid-modified Clay and a Bifunctional Compatibilizer, J. Appl. Polym. Sci., 101(2): 1057–1064.
2. Ke, Z. and Yongping, B. (2005). Improve the Barrier Property of PET Film with Montmorillonite by in situ Interlayer Polymerization, Materials Letters, 59(27): 3348–3351
3. Choi, W.J., Kim, H.-J., Yoon, K.H., Kwon, O.H. and Hwang, C.I. (2006). Preparation and Barrier Property of Poly(ethylene terephthalate)/Clay Nanocomposite using Clay-supported Catalyst, J. Appl. Polym. Sci., 100(6): 4875–4879.
4. Vidotti, S.E., Chinellato, A.C., Boesel, L.F. and Pessan, L.A. (2004). Poly (ethylene terephthalate)-organoclay Nanocomposites: Morphological, Thermal and Barrier Properties, J. Metastable and Nanocrystalline Materials, 22(1): 57–64.
5. Cava, D., Gimenez, E., Gavara, R. and Lagaron, J.M. (2006). Comparative Performance and Barrier Properties of Biodegradable Thermoplastics and Nanobiocomposites versus PET for Food Packaging Applications, J. Plas. Film and Sheeting, 22(4): 265–274.
6. Sanchez-Garcia, M.D., Gimenez, E. and Lagaron, J.M. Morphology and Barrier Properties of Novel Nanobiocomposites of Bacterial Poly(3-hydroxybutirate), Poly("-caprolactone) and Layered Silicates, Carbohydrate Polymers, In Press, DOI: 10.1016/j.carbpol.2007.05.041.
7. Auras, R., Harte, B. and Selke, S. (2005). Sorption of Ethyl Acetate and d-limonene in Poly(lactide) Polymers, J. Sci. Food Agric., 86(4): 648–656.
8. Hua, Y.S., Prattipatia, V., Mehtab, S., Schiraldia, D.A., Hiltner, A. and Baer, E. (2005). Improving Gas Barrier of PET by Blending with Aromatic Polyamides, Polymer, 46(8): 2685–2698.
9. Rafael, A., Auras, S., Singh, P. and Singh, J.J. (2005). Evaluation of Oriented Poly(lactide) Polymers vs. Existing PET and Oriented PS for Fresh Food Service Containers, Packgg. Technol. Sci., 18(4): 207–216.
10. Petersen, K., Nielsen, P.V. and Olsen, M.B. (2001). Physical and Mechanical Properties of Biobased Materials, Starch, 53(8): 356.
11. Hiltner, A., Liu, R.Y.F., Hu, Y.S. and Baer, E. (2005). Oxygen Transport as a Solid-state Structure Probe for Polymeric Materials: A Review, J. Polym. Sci.: Part B: Poly. Phys., 43(9): 1047–1063.

Paper III. **Novel Clay Based Nanobiocomposites of Biopolyesters with synergistis Barrier to UV light**

Abstract

This paper presents novel solvent cast biocomposites of poly(lactic acid) (PLA), polyhydroxybutyrate-co-valerate (PHBV) and polycaprolactone (PCL) with enhanced barrier properties to UV light, oxygen, water and limonene by means of incorporating an organomodified mica based clay grade. The TEM results suggested a good clay dispersion but with no exfoliation in the three biopolyesters. In conformity with the crystallinity data, which was found to generally increase with increasing filler content, oxygen but specially water and d-limonene permeability coefficients were seen to decrease to a significant extent in the biocomposites and an optimum property balance was found for 5 wt.-% of clay loading in the three biopolymers. With increasing clay content, the light transmission of these biodegradable biocomposites decreased by up to a 90% in the UV wavelength region due to the specific UV blocking nature of this clay and the higher blocking efficiency was found to be for 1 and 5 wt.-% clay loading. As a result, these new biocomposites can have significant potential to develop films, coatings and membranes with enhanced gas and vapour barrier properties and UV blocking performance.

Keywords: Clay-based composites, Barrier properties, Biopolyesters.

Introduction

Protection against light is a basic requirement to preserve the quality of many products such as packaged foods. Metal and paper, being opaque to the transmission of light, automatically provide this function. On the other hand, plastic films are often transparent materials to UV and Visible radiation of short wavelengths. Therefore, the protection of light sensitive goods such as fruit and vegetable juices, vitamin and sport drinks, dairy products and edible oils from UV-radiation when packaged in plastic containers has been widely investigated [1-3].

The primary wavelengths of interest in, for instance, food packaging applications are those that fall between 200 and 2,200 nm. This section of the electromagnetic spectrum can be divided into three components: the ultraviolet (UV) range (100–400 nm); the visible spectrum (400–700 nm); and the near-infrared range (700–2,200 nm). Ultraviolet radiation accounts for only 3% of the total radiation that reaches earth, but it causes chemical reactions, weathering of polymers, fading of certain colouring and even eye and skin damage. For this reason, UV light blocking is a very demanded property in polymers and also in the newcoming renewable and biodegradable polymers with interest in multisectorial applications.

Biodegradable and/or sustainable materials present a number of excellent properties for a number of applications, including packaging, automotive and biomedical fields. Thermoplastic biopolymers, such as poly(lactic acid) (PLA), polyhydroxyalkanoates (PHA) and polycaprolactones (PCL), exhibit an excellent balance between barrier and mechanical properties, are water resistant and can be processed using conventional plastics machinery. Moreover, for the case of the first two, they originate from renewable resources, i.e. maize and micro-organisms, respectively. Composites of biopolymers, often called nanobiocomposites, containing highly dispersed naturally derived layered additives, typically montmorillonite (MMT), are proving to be an excellent technology to design new materials with enhanced key properties while retaining the “bio” characteristics. Nanocomposites of biodegradable materials containing between 1 and 5 wt.-% of MMT have been claimed to exhibit significant improvements in barrier [4-9] and in mechanical properties [10-11] and have been reported to be able to disperse to a very little amount the UV-visible radiation [12], probably due to the reduced scattering phenomena caused by the highly dispersed clay nanolayers. Petersson, L et al. also reported some reduction of the light transmitted by nanocomposites of PLA containing 5 wt.-% of MMT compared to pure PLA [12]. Nevertheless, the idea of using nanoclays has always been aimed to minimize the impact in optical properties of the reinforcing filler and hence, being this the main reason for the characterization of the UV-Vis spectra of nanocomposites.

Some earlier works also reported the UV-Vis transmission spectra of polymer nanocomposites based in MMT containing between 3 and 10% of the clay inside oil-derived polymers such as nylon[13], polyimide[14], PVC[15], polyvinyl alcohol[16-17] and other commodities[18]. There are also other works which reported some reduction of the UV-Vis transmission in polyvinyl alcohol containing between 0.5-10 wt.-% content of Red Mud [19] and also in PMMA containing 1 to 5 wt.-% content of 10-undecenoate

intercalated layered double hydroxides[20]. In spite of this, there is no previous literature regarding the use of clay based systems as an intended route to generate UV blocking properties in films or coatings, as well as in the use of non-MMT clays to enhance the properties of bioplastics.

In this study, the morphology, UV-Vis blocking efficiency, color and gas and vapour barrier properties as a function of clay content of novel mica based biocomposites of solvent cast PLA, PCL and PHBV are presented and discussed.

Materials and methods
Materials

The bacterial polyhydroxyalcanoate grade was purchased from Goodfellow Cambridge Limited, U.K., in pellet form. The supplied material was a melt-processable semi-crystalline thermoplastic PHBV (polyhydroxybutyrate with 12 mol% of valerate) copolymer made by biological fermentation from renewable carbohydrate feedstocks. The polycaprolactone (PCL) grade FB100 was kindly supplied in pellet form by Solvay Chemicals, Belgium. This grade has a density of 1.1 g/cm^3 and a mean molecular weight of 100,000 g/mol. The semicrystalline poly(lactic acid) (PLA) used was a film extrusion grade produced by Natureworks (with a D-isomer content of approximately 2%). The molecular weight had a number-average molecular weight (M_n) of ca. 130,000 g/mol, and the weight-average molecular weight (M_w) was ca. 150,000 g/mol.

A proprietary food contact commercial laminar phyllosilicate grade termed NanoBioTer® AC11 based on a mica (so-called through the paper clay) containing 30 wt.-% (as determined by TGA) of an organophilic modification was kindly supplied in powder form by NanoBioMatters Ltd., Paterna, Spain. The clay grade was characterized to be a very fine slightly brown powder and no further details of sample preparation and modification were disclosed by the manufacturer.

Preparations of blends

Prior to the mixing step, the PHBV, PLA and the filler were dried at 70ºC and the PCL at 45ºC under vacuum for 24 hours to remove sorbed moisture.

Solution-cast film samples of the biodegradable materials containing 1, 5 and 10 wt.-% of the clay filler were prepared with a dry film thickness of around 100 μm, using chloroform as a solvent. Organoclay solutions in chloroform were heavily mixed using a homogenizer (Ultraturrax T25 basic, Ika-Werke, Germany) for five minutes and were then stirred with the polymer at 40ºC during 30 min and subsequently cast onto Petri dishes to generate films after solvent evaporation at room temperature conditions**.**

TEM measurements

Transmission electron microscopy (TEM) was performed using a JEOL 1010 (Jeol Ltd., Tokyo, Japan) equipped with a digital Bioscan (Gatan) image acquisition system. TEM observations were performed on ultra-thin sections of microtomed thin

biocomposite sheets. The films were embedded in epoxy resin (Durcupan ACM, Fluka) for the preparation of the sample and the resin with the sample was microtomed with cryogenic cutting conditions**.** The PCL specimens could not be successfully cut to generate clear TEM observations due to the high plasticity of the material even when cryogenic cutting conditions were used.

AFM measurements

AFM measurements were performed on PCL composites using an Agilent 5500 SPM system (provided by Scientec Ibérica, Spain) to investigate the morphology of the composite surfaces on both sides of the cast films. The images were scanned in tapping mode in air using commercial Si cantilevers with a resonance frequency of 320 kHz.

DSC measurements

Differential scanning calorimetry (DSC) of PCL, PHBV and PLA and its composites was performed on a Perkin-Elmer DSC 7 thermal analysis system on typically 7 mg of material at a scanning speed of 10^{o}C/min from room temperature to the melting point of these materials. The thermograms were corrected with these of an empty pan and the DSC equipment was calibrated with an indium standard. To calculate the Heat of Fusion of the PLA, as this biopolymer undergoes cold crystallization during heating, the melting peak was subtracted the cold crystallization peak. Crystallinity was estimated using the ratio between the heat of fusion of the studied material and the heat of fusion of an infinity crystal of same material, i.e. $\%X_c = \frac{\Delta H_f}{\Delta H_f^0} x100$ (Equation 1), where ΔH_f is the enthalpy of fusion of the studied specimen and ΔH_f^o is the enthalpy of fusion of a totally crystalline material. The ΔH_f^o fed to the equation was 93 J/g for PLA [21], 146 J/g for PHBV [22] and 136 J/g for PCL [7].

UV-VIS spectra

An UV–Vis spectrophotometer (Hewlett Packard 8452A Diode Array Spectropotometer) was used to measure the transmittance spectra of specially prepared thin films in the wavelength range 200–700 nm. Thin films of biodegradable materials and their composites of ca. 30 microns were specially prepared by casting over the surface of quartz cuvettes typically in UV-Vis. In all cases, the UV abortion signal of the films was normalized to exactly 30 microns of thickness for comparative purposes.

The yellow index (YI) was calculated from the transmittance values of the UV-Vis spectra. The YI was calculated using the following relationship[18]:

$$YI = \frac{T_{680} - T_{420}}{T_{560}} \qquad \text{Equation 2}$$

Where T_{680}, T_{420} and T_{560} are the transmission dates at the wavelength of 680nm, 420nm and 560nm, respectively.

Color measurements

Color parameters were determined in the reflective mode using a colorimeter, Minolta Chroma Meter CR-300 series.

Gravimetric measurements

Direct permeability to d(+)-limonene of 95% purity (Panreac Química, Spain) and direct permeability to water were determined from the slope of weight loss vs. time experiments at 24°C and 40%RH. The films were sandwiched between the aluminium top (open O-ring) and bottom (deposit for the permeant) parts of aluminium permeability cells. A Viton rubber O-ring was placed between the film and the bottom part of the cell to enhance sealability. Then the bottom part of the cell was filled with the permeant and the pinhole secured with a rubber O-ring and a screw. Finally, the cell was placed in the desired environment and the solvent weight loss through a film area of 0.001 m^2 was monitored and plotted as a function of time. Cells with aluminium films (with thickness of ca. 100 microns) were used as control samples to estimate solvent loss through the sealing. The permeability sensibility of the permeation cells was determined to be of ca. 0.01 10^{-13} Kg m/s m^2 Pa based on the weight loss measurements of the aluminium cells. Cells clamping polymer films but with no solvent were used as blank samples to monitor water uptake. Solvent permeation rates were estimated from the steady-state permeation slopes. Water vapour weight loss was calculated as the total cell loss minus the loss through the sealing. Organic vapour weight loss was calculated as the total cell loss minus the loss through the sealing and plus the water weight gain. The tests were done in duplicate for both permeants.

Oxygen transmission rate

The oxygen permeability coefficient was derived from oxygen transmission rate (OTR) measurements recorded using an Oxtran 100 equipment (Modern Control Inc., Minneapolis, MN, US). During all experiments temperature and relative humidity were held at 24 ºC and 80% R.H. 80% relative humidity was generated by a built in gas bubbler and was checked with a hygrometer placed at the exit of the detector. The experiments were done in duplicate. The samples were purged with nitrogen for a minimum of 20 h prior to exposure to a 100% oxygen flow of 10 ml/min, and a 5 cm^2 sample area was measured by using an in-house developed mask. Permeability (P) was estimated from fitting the OTR-time curve to the first six sum terms of the following solution of the Fick's second law [23]:

$$OTR(t) = \frac{Pp}{l}\left[1 + 2\sum_{n=1}^{\infty}(-1)^n \exp(-\frac{D\pi^2 n^2 t}{l^2})\right] \qquad \text{Equation 3}$$

In Equation 1, D is the diffusion coefficient, p is the oxygen partial pressure and l is the film thickness.

Results and discussion

Biocomposites Morphology

Figure 1 shows typical pictures of PLA and PLA biocomposite films containing 1, 5 and 10 wt.-% of the clay. From these pictures, it can be seen that while all samples remain transparent at 100 microns thickness, specially the PLA and PLA+1 wt.-% clay, the biocomposites exhibit some brownish color with increasing clay content due to the presence of this particular filler in the matrix.

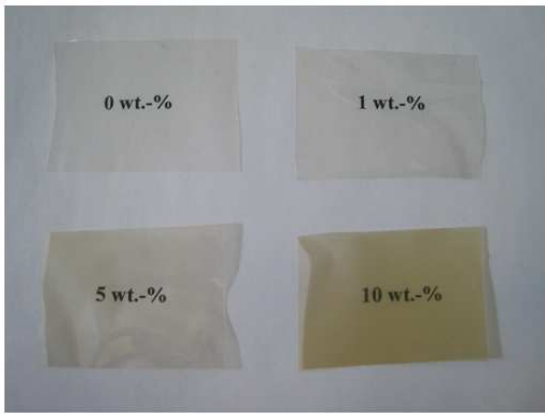

Figure 1. Typical photographs of 100 microns thickness films of PLA and of PLA containing 1, 5 and 10 wt.-% of clay.

Figure 2 shows some TEM images taken from the specimens of composites of PHBV, and PLA. The current PCL samples were more difficult to cut and observe with sufficient clarity due to the high plasticity exhibited by the polymer, which led to misleading wrinkles and to too thick cuts to discern clay morphology. The PLA and PHBV samples show, a dispersed clay morphology with long platelets, in which a considerable reduction of the original tactoids size is attained in all dimensions but especially in the thickness direction. In any case, no exfoliation was observed in the samples. Notwithstanding the above, most layered particles, particularly in the PHBV composites, are below 100 nm in thickness, typical upper size limit definition for a nanotechnology product. The remarkable observation from Figures 2, is the extremely large size of the platelets dispersed in the matrix. Filler dispersion seems higher for PHBV than for PLA and the particles appeared rather oriented. In any case, it is clear that the solution casting method used does not lead to completely exfoliated morphologies, since achieving fully exfoliated systems is very seldom obtained irrespective of the processing method, but still yields interesting submicro- and/or nano-biocomposites with enhanced properties as it will be shown. Particle size and dispersion seem better for PHBV than for PLA, and in all cases particle sizes are well below the micron in the thickness direction. Fractured particles along the layered axis are also observed due to the aggressive homogenization step.

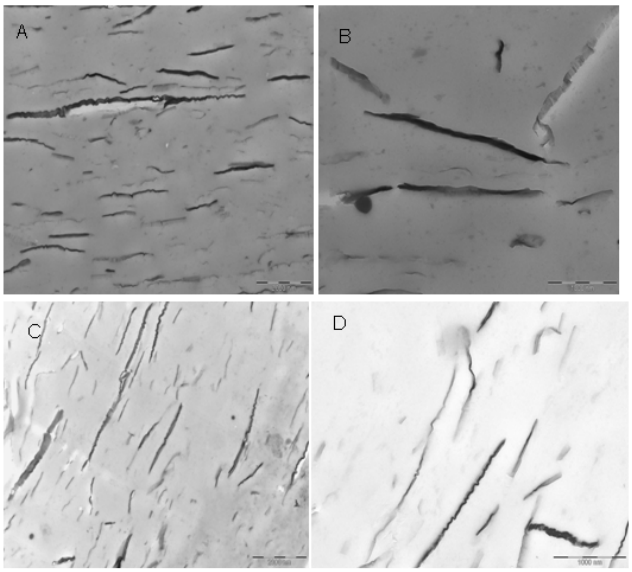

Figure 2. TEM pictures of A and B) PLA containing 5 wt.-% of clay and C and D) PHBV containing 5 wt.-% of clay. Scale markers are 2000 nm for the left pictures and 1000 nm for the right pictures.

Figure 3 shows the surface roughness (topographic image) of the PCL cast composite sample containing 5 wt.-% clay content by AFM. The image suggests that the extremely large particles are intercalated by the polymer and are greatly dispersed within this biopolymer matrix. This image also suggests that there appears to be a good adhesion of the filler to the biopolymer due to possibly the organophylic surface modification of the filler. Regarding particle thickness, the clay layers have typical thicknesses around 16 nm.

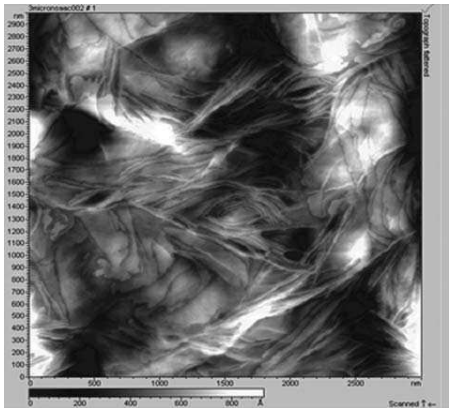

Figure 3 AFM topography picture of the 5 wt % clay PCL biocomposite.

Thermal properties

Melting temperature (T_m) and heat of fusion (ΔH_m) corrected for biopolymer content in the biocomposites were determined from the DSC thermograms of the samples. Figure 4 shows typical endotherms of the DSC first melting endotherms of the neat biopolymers and of the 5 wt.-% filler loaded biocomposites. Data from the first and the second heating runs are summarised in Table 1 for cast films of PCL with different clay filler contents. The first heating run is related to the original state of the material after solvent casting and is, therefore, more meaningful for correlation with physical properties, such as barrier properties. From this Table 1, the heat of fusion of PCL and, therefore, the crystallinity is seen to increase in the biocomposite during the first heating run of this biomaterial but the melting point is largely unmodified or changes very slightly, it drops by ca. 1^{o}C in the 5 wt.-% loaded composite. The latter result adds to similar nucleating observations reported in previous works for PHB/PCL nanocomposites[7], and suggests that the clay can act as a heterophase nucleating agent, hence promoting somewhat higher crystallinity in the matrix. The second heating run show lower values for both melting temperature and heat of fusion compared to the first run, due to possibly faster cooling and higher metastability compared to the solvent casting method. Table 1 shows that the values for the second heating run have the same comparative behaviour as the first heating.

Table 1. DSC melting point, melting enthalpy and crystallinity (%Xc) of PCL and of PCL biocomposites containing 1, 5 and 10 wt.-% of clay.

Sample	T_m (ºC) 1st heating	ΔH_m (J/g) 1st heating	$\%X_c$ 1st heating	T_m (ºC) 2nd heating	ΔH_m (J/g) 2nd heating
PCL	63.25±0.09	51.82±0.05	38	55.75±0.09	38.49±3.85
PCL+1 wt.-%	63.09±0.19	55.89±1.26	41	55.94±0.12	41.07±0.97
PCL+5 wt.-%	61.92±0.38	57.92±1.28	42	55.86±0.16	41.90±4.44
PCL+10 wt.-%	63.75±0.96	65.06±0.75	48	55.78±0.12	42.80±2.89

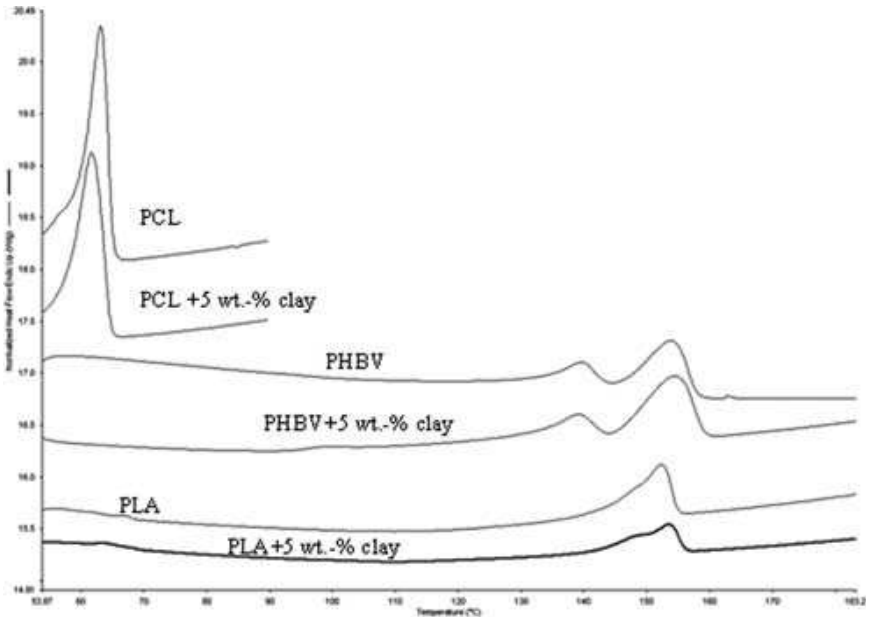

Figure 4 Normalized for total mass typical DSC thermographs of the biopolymers PCL, PHBV, and PLA and their biocomposites with 5 wt % clay in the first heating run.

Table 2 summarizes melting temperature (T_m), heat of fusion (ΔH_m) and the crystallization temperature (T_c) of the PHBV and their biocomposites during the first and second heating run. From this table, it can be seen that in the first heating curve, the melting point is not greatly altered in the clay containing samples and it is slightly increased for the 5 wt.-% loaded composite. But in the second heating run the melting point decreases with increasing clay content up to 16ºC with 10 wt.-% clay content due to possibly clay-induced polymer degradation, both hydrolytic and adiabatic[7, 24]. During the first and second heating runs, the melting enthalpy (corrected for the biopolymer content in the composite) decreases somewhat at low clay contents (1 wt.-%), however at 5 wt.-% of clay content, the enthalpy of fusion is the highest in the concentration range screened. Nevertheless, filler-induced crystallinity changes are very small for this biopolymer. The crystallization temperature is not altered in the clay containing samples, except for the 5 wt.-% of clay, where the crystallization increases by 4ºC.

Table 2. DSC melting point and melting enthalpy during the 1st and 2nd heating runs and crystallization temperature of PHBV and of PHBV biocomposites with 1, 5 and 10 wt.-% clay content.

Sample	T_m (ºC) 1st heating	ΔH_m (J/g) 1st heating	$\%X_c$ 1st heating	T_m (ºC) 2nd heating	ΔH_m (J/g) 2nd heating
PHBV	(139.86-153.87)± (0.23-0.00)	35.17±0.95	24	(146.45-157.28) ±(0.11-0.12)	37.42±0.87
PHBV+1 wt.-%	(138.85-152.94)± (1.20-1.31)	32.95±2.56	22	(143.45-153.45) ±(0.11-1.76)	37.23±2.03
PHBV+5 wt.-%	(138.86-154.28)± (0.23-0.35)	39.33±4.70	27	(140.45-150.95) ±(1.30-1.06)	39.14±6.97
PHBV+10 wt.-%	(138.53-154.20)± (0.47-0.82)	37.71±2.10	26	(130.70-143.37) ±(1.88-1.41)	35.47±0.40

The thermal behavior of PLA is different and more complex than that of the two previous biopolyesters, because PLA exhibits a cold crystallization process[25] similar to that typically observed for the petroleum-based polyester polyethylene terephthalate (PET). Table 3 presents the melting temperature (Tm), heat of fusion (ΔHm) and the cold crystallization temperature (Tcc) of the PLA and of their biocomposites in the first and second heating. From this Table 3, the heat of fusion during the first and second heating runs is seen to increase in the biocomposites and the melting point remains largely unmodified but it increases slightly for the 5 wt.-% loaded composite. A curious observation from this Table 3 is that while the pure PLA does not have a measurable melting endotherm in the second heating, so the polymer is in an amorphous state, the PLA biocomposites developed crystallinity. This suggests again that the clays act as a nucleating agent. However, from Table 3, the cold crystallization temperature increases particularly for the highest filler content, suggesting that the clay delays the cold crystallization process upon heating. Table 3 also shows that the T_g of these materials increases slightly with filler content, due to possibly clay-induced stiffening of the biopolymer amorphous phase. However, for the film of PLA with 10 wt.-% of clay the T_g increase is less than for the composites containing 1 and 5 wt.-% of clay. The reason for not observing a higher T_g rise for the samples with the highest filler loading must be attributed to further inefficiency of the clay as a reinforcing element due to clay extensive segregation and agglomeration.

Table 3. DSC melting point, melting enthalpy, cold crystallization temperature and Tg during the 1st and 2nd heating runs of PLA and of PLA biocomposites containing 1, 5 and 10 wt.-% of clay.

Sample	T_m (ºC) 1st heating	ΔH_m (J/g) 1st heating	T_{cc} (ºC) 1st heating	$\%X_c$ 1st heating	T_m (ºC) 2nd heating	ΔH_m (J/g) 2nd heating	T_{cc} (ºC) 2nd heating	T_g (ºC) 2nd heating
PLA	152.53±0.23	8.51±1.61	110.95±1.30	9.1	-	-	-	59.06±0.31
PLA+1 wt.-%	153.09±0.25	10.87±0.69	110.14±0.78	11.6	151.70±0.24	4.87±2.20	127.20±0.23	59.33±0.48
PLA+5 wt.-%	153.45±0.11	10.86±0.82	109.7±1.41	11.6	151.78±0.35	4.42±0.87	125.95±0.82	63.01±4.88
PLA+10 wt.-%	151.86±1.18	16.90±3.04	116.7±7.78	18.1	151.36±1.64	13.14±2.02	126.70±3.07	60.13±0.23

In conclusion, the clay has a generic role in the biocomposites thermal properties, of nucleation and promotion of some crystallinity, particularly for PCL and PLA. In principle, filler-induced crystallization of the biopolymers is positive from a barrier perspective, since crystals are typically impermeable systems to the transport of low

molecular weight compounds. Nevertheless, extensive crystallization may also promote, as a downside, excessive rigidity and hence fragility for the biopolymer mechanical performance.

Mass transport properties

Table 4 gathers the water, limonene and oxygen permeability coefficients of the materials and their biocomposites. A curious first observation from Table 4 regarding PCL is that the water permeability coefficient of 3.39 10^{-14} Kg m / s m^2 Pa is much higher than that of 0.023 10^{-14} Kg m / s m^2 Pa previously reported for toluene cast PCL[8]. The reason for the large disagreement could be related to the different origins of the two samples (lab scale material vs. industrial scale material production) and the fact that molecular weight, the solvent used and the differences in relative humidity gradient used for testing were totally different. Direct permeability for limonene in PLA was not reported, because the measurements yielded values below the sensitivity of the permeation cells; a previous study reported that the limonene permeability for PLA is of ca. 0.000002 10^{-13} Kg m / s m^2 Pa when measured at 45ºC and 258 Pa of vapour partial pressure gradient[26]. The previously reported water direct permeability of the PLA films at 1.80 10^{-14} Kg m / s m^2 Pa using chloroform as a solvent, is very similar to the one measured in our laboratory, due to the similar conditions of the produced film.

Table 4. Water, limonene and oxygen permeability coefficients of PLA, PHBV, PCL and their biocomposites.

	P_{water} (Kg m/s m^2 Pa)	**$P_{limonene}$ (Kg m/s m^2 Pa)**	**P_{oxygen} (m^3 m/s m^2 Pa) at 80%RH**
PLA	2.30±0.07e^{-14}	-	2.77±0.08e^{-18}
PLA+1 wt.-%	1.69±0.07e^{-14}	-	2.08±0.16e^{-18}
PLA+5 wt.-%	1.05±0.26e^{-14}	-	1.24±0.20e^{-18}
PLA+10 wt.-%	1.03±0.11e^{-14}	-	1.09±0.17e^{-18}
Literature value PLA	**[29]1.26 e^{-14}**	-	**[27 b]1.75e^{-18}**
Literature value PLA	**[30]1.80e^{-14}**		
PHBV	1.27±0.14e^{-14}	1.27±0.07e^{-13}	1.44±0.01e^{-18}
PHBV+1 wt.-%	0.49±0.03e^{-14}	0.72±0.23e^{-13}	1.53±0.01e^{-18}
PHBV+5 wt.-%	0.30±0.09e^{-14}	0.28±0.04e^{-13}	0.98 ±0.02e^{-18}
PHBV+10 wt.-%	0.60±0.20e^{-14}	2.25±0.18e^{-13}	2.33 ±0.03e^{-18}
Literature value PHBV[29]			**3.01 e^{-18}**
Literature value PHB[27]	-	-	**[b]5.10e^{-18}**
Literature value PHB[7]	-	-	**[c]0.23e^{-18}**
PCL	3.39±0.61e^{-14}	5.05±0.65e^{-13}	7.06e^{-18}
PCL+1 wt.-%	1.58±0.05e^{-14}	4.16±1.18e^{-13}	5.48 ±0.27e^{-18}
PCL+5 wt.-%	1.26±0.05e^{-14}	2.58±0.57e^{-13}	3.68 ±0.29e^{-18}
PCL+10 wt.-%	1.26±0.05e^{-14}	3.80±0.57e^{-13}	3.67e^{-18}
Literature value PCL	**[8a]0.023e^{-14}**	-	**[28d]1.9e^{-18}**

[a] At 35ºC, 75%RH and cast from toluene
[b] At 75%RH (commercial biobased material)

[c] At 24°C and 0%RH (obtained by melt blending)
[d] At 0%RH (solvent casting)

Figure 5A shows the plot of the water permeability of the neat PLA, PHBV and PCL and of their biocomposites with 1, 5 and 10 wt.-% content of clay. In the case of PLA, reductions of water permeability of ca. 27%, 54% and 55% were obtained for the cast films containing 1, 5 and 10 wt.-% of clay, respectively. The barrier improvement for the samples containing 5 and 10 wt.-% of clay content yielded similar barrier. Water barrier also increased with increasing clay content. In the case of PHBV, the film containing 1 wt.-% of clay shows a water permeability reduction of 61%, the one containing 5 wt.-% of clay shows a reduction of ca. 76%, but for the film PHBV+10 wt.-% of clay the reduction is of ca. 47%. In this case of the film containing 10 wt.-% of clay the water permeability reduction is lower than for films with 1 and 5 wt.-% filler content, possibly due to the clay content surpassing the solubility limit and detrimental agglomeration. For the case of PCL composites, films of this biodegradable polymer with 1, 5 and 10 wt.-% clay exhibit a water permeability decrease of 54%, 63% and 63%, respectively, compared to the unfilled material. The latter results are similar in trend to those of PLA.

Figure 5B shows the limonene permeability for neat PHBV and PCL and their biocomposites. In the case of the PHBV, a reproducible reduction in limonene permeability of ca. 78% is obtained for the sample containing 5 wt.-% of clay loading. However, further increase in clay content until 10 wt.-%, does not improve the barrier as shown for other permeants above, due to clay agglomeration. Films of PCL with 1, 5 and 10 wt.-% clay contents have a limonene permeability decrease of 18%, 49% and 25%, respectively, compared to the unfilled material. Thus, the lowest limonene permeability coefficient value is for the samples containing 5 wt.-% of clay in all materials. It is interesting to observe that, in general, crystallinity in the biocomposites increases by the nucleating effect promoted by the clays and, therefore, the induction of crystals as well as the nanodispersion of the clays yield the impermeable blocking elements that result in enhance barrier. Impermeable blocks in plastics are responsible for the increase in both detour and chain immobilization factors that enter in the denominator in the expression for the calculation of the diffusion coefficient and, therefore, result in decreased diffusion and hence in permeability. In this context, it is relevant to observe that the PHBV specimen containing 5 wt.-% of clay exhibits somewhat higher crystallinity compared to the 1 and 10 wt.-% samples and it is precisely this specimen the one showing the biggest reductions in water and limonene permeability. Nevertheless, from all of the above results, it is the combination of the optimum clay loading, i.e. in the vicinity of 5 wt.-% which fills in the available free volume, and the positive morphology generated by such loading, the responsible factor behind the reported barrier enhancement.

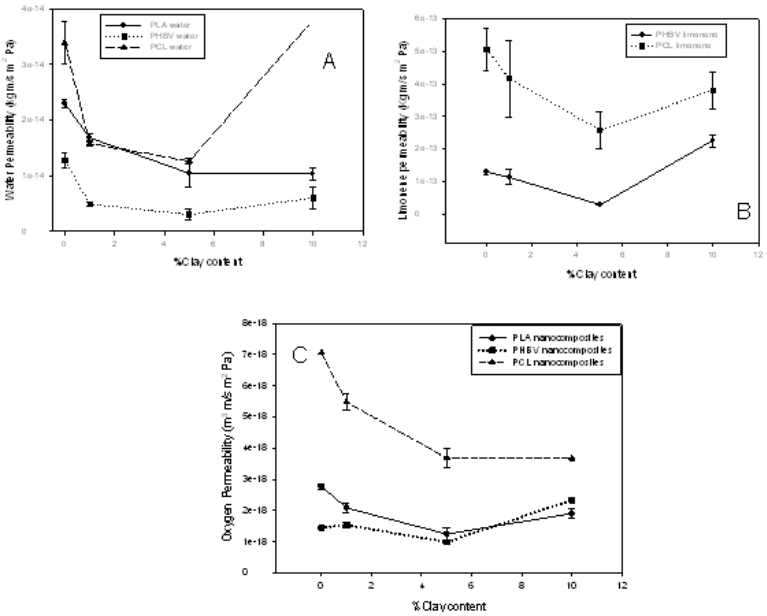

Figure 5. A) Water permeability coefficient of PLA, PHBV and PCL and their biocomposite with 1, 5, and 10 wt.-% of clay. B) Limonene permeability coefficient of PHBV and PCL and their biocomposites with 1, 5, and 10 wt.-% clay content. C) Oxygen permeability coefficient of PLA, PHBV and PCL and their biocomposites with 1, 5, and 10 wt.-% clay content.

Table 4 gathers the oxygen permeability measurements carried out in the samples. The permeability value reported in the literature for PLA of $1.75e^{-18}$ m^3m/sm^2Pa measured at 75%RH [27] is of the same order of magnitude as the value of $2.77e^{-18}m^3m/sm^2Pa$ measured in our lab at 80%RH. For the PLA composites containing 1, 5 and 10 wt.-% of filler an oxygen permeability reduction of 25%, 55% and 60% respectively was observed, compared to the unfilled material (see Figure 5C).

For the case of the PHBV, the reported value for PHB of $5.10e^{-18}m^3m/sm^2Pa$ measured at 75%RH[27] is higher than the value obtained in our laboratory at 80%RH of $1.44e^{-18}m^3m/sm^2Pa$ for the PHBV. On the other hand previous measurements on melt mixed PHB followed by compression moulding provided a value of $0.23e^{-18}m^3m/sm^2Pa$[7]. The variation could arise from the different material origin, i.e. homopolymer vs. copolymer, processing conditions of the two materials and the difference in relative humidity gradient used for testing. A reduction in oxygen permeability of 32% is measured for the film of PHBV containing 5 wt.-% of clay. Increasing filler content to 10 wt.-% does not result in further barrier increase (see Figure 5C).

The previously reported oxygen permeability of PCL is of $1.9e^{-18}m^3m/sm^2Pa$ at 0%RH[28], which is lower than the value of $7.06e^{-18}m^3m/sm^2Pa$ measured at 80%RH in our laboratory. The reason for the discrepancy in the absolute permeability value is

again related to the different origin and processing conditions to the materials and for the difference relativity humidity used for the testing. For the PCL composites, a reduction in oxygen permeability of ca. 22%, 48% and 48% was measured in the films containing 1, 5 and 10 wt.-% of clay, respectively (see Figure 5C).

It is a general observation that composites containing 5 wt.-% of the filler exhibit the highest oxygen barrier performance for the lowest filler content. These results are also in good accordance in relative terms with permeability for the other permeants and with the thermal data discussed above, i.e. crystallinity rise due to clay-induced nucleation. The overall barrier results indicate that the barrier performance is the result of a good balance between polymer structural morphology (crystalline phase content and morphology) and filler loading, when the filler loading goes beyond the clay solubility limit in the polymer, it agglomerates and even when in some cases higher crystallinity is observed, it creates no further enhancement in barrier but in some cases opposite behaviour.

Figure 6 presents what we termed as the Clay Barrier Efficiency (CBE) for each biomaterial and permeant. This factor is calculated by dividing the penetrant permeability drop in percent between the sample crystallinity as determined by DSC during the first heating run, also as a percentage. This CBE factor highlights the barrier effect of the clay in the biomaterials and separates this from any crystallinity rise measured. From the results, the clay is more efficient at 5 wt.-% content for all the biomaterials tested and appears to reinforce more efficiently PHBV and PCL against water and limonene permeation and less to oxygen. It is curious that in PHBV, the permeability for the biocomposite filled with 1 wt.-% of clay is more inefficient for oxygen than for the other biopolymers and the effect is reproducible.

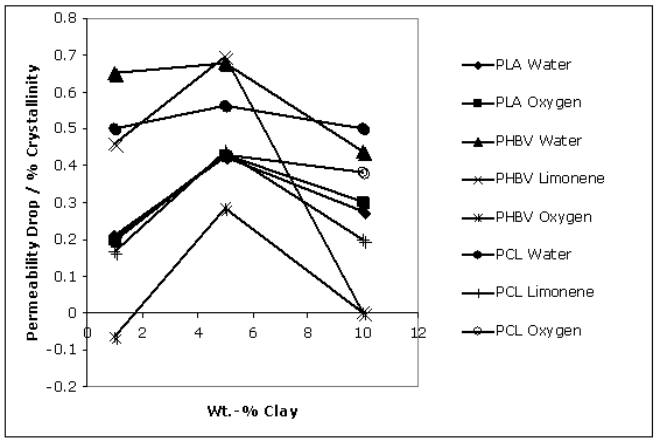

Figure 6. Clay barrier efficiency (CBE) plot for each biomaterial and permeant**.**

UV-VIS spectra

Figure 7 shows the normalized UV-Vis spectra to 30 microns thickness of unfilled PLA, PHBV and PCL and of their biocomposites. The UV region is classified in three zones: UVC (100-280nm), UVB (280-320) and UVA (320-400nm).

Figure 7A shows the transmission spectra of PLA with increasing clay content (1, 5, 10 and 20 wt.-% of clay). The UV-VIS transmission spectra show a reduction with increasing clay content in the films. From the results (Figure 7A), the transmittance of the pure PLA in the region of UVC can be of a maximum of 10%. The corresponding PLA biocomposites show a reduction in transmittance to around 0%, i.e. a complete blocking to the passage of radiation, with 20 wt.-% clay content in the composite. More relevant regions for protection are the UVB and UVA regions, where the pure PLA has a transmittance of around 100%, thus the PLA is virtually transparent in this range as it is in the visible range. Films of PLA containing 20 wt.-% of clay content reach transmission values below 15% of transmittance in this region (UVB-UVA), yielding a very efficient blocking effect, which decreases in the visible range where transparency is still highly appreciated. It is clear that 20 wt.-% filler content is perhaps too high a loading to use, since it does negatively affect to the transmission in the visible range and will be unlikely to yield an optimum property balance. Nevertheless, and as it was the case with the barrier performance, the ratio of protection is still very efficient at 5 wt.-% of clay addition, yielding 10 wt.-% not so strong differentiating benefits. Thus, low clay contents (1 and 5 wt.-%) in the PLA matrix lead to significant reductions in the UV light transmission, while retaining transparency to a significant extent due to a higher clay dispersion in the matrix (see Table 5).

In the case of PHBV, Figure 7B shows the transmission spectra of the biocomposites with 1, 5, 10 and 20 wt.-% clay content. The blocking effect of PHBV in the UV-Vis region is higher than the PLA transmission since PHBV is a translucent material. Similar as with the transmission spectra of PLA, with increasing of clay content, the UV-Vis transmittance decreases to a significant extent in the UV region and is more efficient for contents of 5 wt.-% of clay. Figure 7C shows the transmission spectra of PCL and of its biocomposites with different clay contents (1, 5, 10 and 20 wt.-%). PCL is also a very translucent material. In the UV region, the reduction in transmittance is very low compared to other biodegradable materials such as PHBV and PLA. In the visible zone, films of PCL containing 20 wt.-% of clay reduce transmittance to a significant extent.

As a summary, the highly transparent PLA, but also the translucent PHBV, underwent the highest UV barrier effect due to the addition of this clay. The higher barrier to filler loading ratio efficiency was observed to be for the 1 and 5 wt.-% clay content samples (see Table 5). Light blocking was higher in the UV range as required and lower in the visible range for these two biopolyesters.

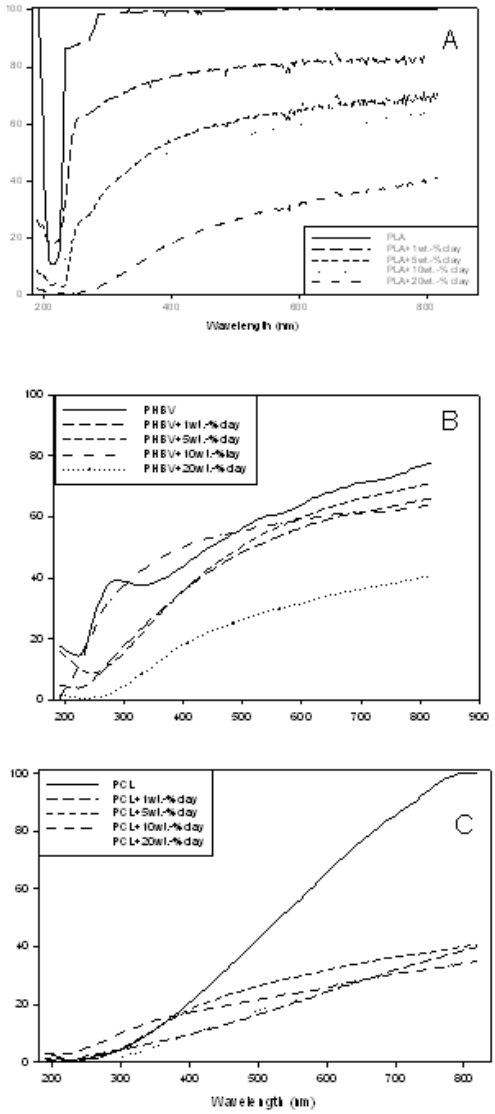

Figure 7. UV–Vis spectra normalized to 30 microns vs. clay content of cast films of PLA, PHBV and PCL biocomposites.

Table 6 gathers the Yellowness Index (YI) for the biocomposites. The yellowness index describes the color changes of a sample from clear or white towards yellow. The yellowness index is dependent on the thickness of the sample; in this case the measurements were taken on 30 microns thickness cast films. As it can be seen from Table 6, the YI of the biocomposites of PLA, PHBV and PCL increases with increasing filler content, and the YI data of PCL (YI =1.5) is higher than that of

PHBV (YI=0.5) and of PLA (YI=0), due to the known opacity of PCL and the transparency of the PLA.

Color measurements

The luminosity, L*, measures the clarity at which a color is perceived in the CIELAB color system. It is determined by a percentage of the light reflected by the colored object. The co-ordinates of chromaticity are often termed “a” and “b” in this color representation system. The co-ordinate “a” defines the red/green axis (+a and -a), and “b” represents the yellow/blue axis (+b and -b).

Table 6 gathers the color parameters, i.e. the parameter L* and coordinates “a” and “b”, taken in the samples. From the results, the luminosity has a similar trend in all of the three biopolymers. This parameter decreases with increasing clay content as expected from the above. The coordinate “a” decreases to negatives values with increasing clay content. Films containing clays turned color towards green. In the case of the coordinate “b”, this value increases with increasing clay content, i.e. towards yellow. Figure 8 shows the effect of increasing clay content in the three materials on the level of color generated in the biocomposites. The level of color intensifies with increasing clay content as expected but not in a linear manner. The graph shows a good correlation between color index and the optimum dispersion of the organoclay in the matrix, being dispersion deteriorated beyond 5 wt.-% due to agglomeration and therefore yielding stronger color index. Thus, the optical luminosity and the color of these biocomposites results primarily from addition of the clay but the level of these parameters is also related to dispersion of the clays. In this context, the color study is consistent with all previous data.

In summary, the biocomposites of PLA, PHBV and PCL, show a decrease in luminosity, lightness and clarity with increasing of clay content and a change of color towards yellow and green.

Table 6. Yellow index (YI) and L*, a and b parameters of PLA, PHBV, PCL and of their biocomposites.

	YI	L*	a	b
PLA	0	96.03±0.13	0.37±0.011	2.30±0.19
PLA+1% clay	0.12	95.42±0.33	0.14±0.04	3.58±0.10
PLA+5% clay	0.24	93.19±0.26	-0.69±0.05	9.63±0.57
PLA+10% clay	0.21	87.29±1.43	-0.71±0.14	19.22±1.53
PHBV	0.49	97.07±0.14	-0.21±0.04	3.83±0.14
PHBV+1% clay	0.50	96.23±0.07	-0.46±0.01	6.25±0.07
PHBV+5% clay	0.48	93.06±1.23	-0.65±0.18	9.51±1.68
PHBV+10% clay	1.10	88.22±0.48	-0.82±0.40	22.12±0.78
PCL	1.45	95.93±0.27	0.10±0.04	2.22±0.09
PCL+1% clay	1.62	96.43±0.22	-0.17±0.05	4.99±0.32
PCL+5% clay	0.70	93.70±0.63	-0.83±0.06	11.22±0.83
PCL+10% clay	1.39	84.39±0.63	-0.30±0.06	25.10±0.77

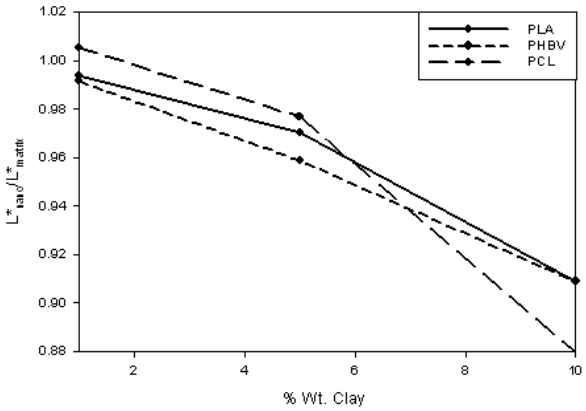

Figure 8. The effect of clay content on the biocomposites color index

Conclusions

The present study successfully developed novel PHBV, PCL and PLA-layered silicate biocomposites by a solvent casting method, wherein an organically modified mica based filler was nicely distributed to a nanoscale level within the biodegradable matrixes. No exfoliation of the filler was achieved in any of the matrices but in all cases extremely long platelets with thickness in the nanoscale were observed by TEM and AFM techniques. All the biocomposites formulated exhibited improvements in properties such as gas (oxygen) and vapour (water and limonene) permeability and exhibited considerable barrier to the transmission of UV light due to the specific blocking effect of the finely dispersed mica filler. In conformity with the DSC crystallinity data, property that generally increased with increasing filler content, oxygen but specially water and d-limonene permeability coefficients were seen to decrease to a significant extent in the biocomposites. In the case of the barrier properties, it was observed that PLA, PHBV and PCL containing 5 wt.-% of clay, led to a water permeability reduction of ca. 54%, 76% and 63% and reductions in oxygen permeability of ca. 55%, 32% and 48%, respectively, compared with the unfilled material. Reductions in limonene permeability of ca. 78% and 49%, for the films of PHBV and PCL with 5 wt.-% of clay were also observed. Clay barrier efficiency plots, correcting for crystallinity, indicated that 5% was indeed the optimum clay loading used, being 1% not sufficient (given the lack of exfoliation and sufficient dispersion) and 10% beyond the clay solubility limit where agglomeration and property drop occur. For the UV light transmission, films of PLA and PHBV with 5 wt.-% of clay showed a decrease in the transmission of the damaging UV light of up to ca. 75% at 250nm wavelength. In the visible light transmission range, a reduction of ca. 32%, 10% and 66% was observed at 650 nm wavelength for the PLA, PHBV and PCL with 5 wt.-% of clay films, respectively. As a result, the increased barrier properties of the biocomposites developed to UV light, water, limonene and oxygen

highlights the excellent potential of these novel biomaterials for film and coating applications.

References

[1] Van Aardt M, Duncan SE, Marcy JE., Long TE, and Hackney CR. Effectiveness of Poly(ethylene terephthalate) and High-Density Polyethylene in Protection of Milk Flavor. Journal of Dairy Science 2001, 84 (6): 1341-1347.

[2] Conrad KR, Davidson VJ, Mulholland DL, Britt I.J, Yada S. Influence of PET and PET/PEN blend packaging on ascorbic acid and color in juices exposed to fluorescent and UV light. Journal of Food Science 2005, 70 (1): E19-E25.

[3] Goldhan G, Rieblinger K. Natural dyes for optimum light protection of sensitive foods. European Food and Drink Review 2002 : No. 3, Autumn, 69, 71-72.

[4] Sinha Ray S, Yamada K, Okamoto M, Ueda K. New polylactide/layered silicate nanocomposites. 2. Concurrent improvements of material properties, biodegradability and melt rheology. Polymer 2003; 44:857–66.

[5] Sinha Ray S, Yamada K, Okamoto M, Fujimoto Y, Ogami A, Ueda K. New polylactide/layered silicate nanocomposites: 5. Designing of materials with desired properties. Polymer 2003; 44:6633–46.

[6] Jin-Hae Chang, Yeong Uk An, Gil Soo Sur. Poly(lactic acid) nanocomposites with various organoclays. I. Thermomechanical properties, morphology, and gas permeability. Journal of Polymer Science Part B: Polymer Physics. 2003; 41, 94-103.

[7] Sanchez-Garcia MD, Gimenez E and Lagaron JM. Morphology and Barrier Properties of Novel Nanobiocomposites of Bacterial Poly(3-hydroxybutirate), Poly(ε-caprolactone) and Layered silicates. Journal of Applied Polymer Science 2008, Vol. 108, 2787–2801.

[8] Messersmith Pb, Giannelis Ep. Synthesis and Barrier Properties of Poly(Epsilon-Caprolactone)-Layered Silicate Nanocomposite. Journal of Polymer Science Polymer Chemistry 1995; 33 (7): 1047-1057.

[9] Di, YW, Iannac, S, Sanguigno, L, et al. Barrier and mechanical properties of poly(caprolactone)/organoclay nanocomposites. Macromolecular Symposia 2005; 228: 115-124.

[10] Wu, TM, Wu, CY. Biodegradable poly(lactic acid)/chitosan-modified montmorillonite nanocomposites: Preparation and characterization. Polymer Degradation Stability 2006, 91 (9): 2198-2204.

[11] Lee JH, Lee YH, Lee DS, Lee YK, Nam JD. Thermal and mechanical properties with hydrolysis of PLLA/MMT nanocomposite. Polymer Korea 2005, 29 (4): 375-379.

[12] Petersson L, Oksman K. Biopolymer based nanocomposites: Comparing layered silicates and microcrystalline cellulose as nanoreinforcement. Composites Science and Technology 2006, 66 (13): 2187-2196.

[13] Fornes TD, Yoon PJ, Paul DR. Polymer matrix degradation and color formation in melt processed nylon 6/clay nanocomposites. Polymer 2003, 44 7545–7556.

[14] Yeh JM, Chen CL, Kuo TH, Su WFH, Huang SY, Liaw DJ, Lu HY, Liu CF, Y.H. Yu. Preparation and Properties of (BATB–ODPA) Polyimide–Clay Nanocomposite Materials. Journal of Applied Polymer Science, 2004, Vol. 92, 1072–1079.

[15] Wan Chaoying, Zhang Yong, Zhang Yinxi. Effect of alkyl quaternary ammonium on processing discoloration of melt-intercalated PVC-montmorillonitecomposites. Polymer Testing 2004, 23, 299–306

[16] Strawhecker KE and Manias E. Structure and Properties of Poly(vinyl alcohol)/Na+ Montmorillonite Nanocomposites. Chemistry of Materials 2000, 12, 2943-2949.

[17] Jaime C. Grunlan, Ani Grigorian, Charles B. Hamilton, Ali R. Mehrabi. Effect of Clay Concentration on the Oxygen Permeability and Optical Properties of a Modified Poly(vinyl alcohol). Journal of Applied Polymer Science, 2004, 93, 1102–1109.

[18] Yoon PJ, Hunter DL, Paul DR. Polycarbonate nanocomposites: Part 2. Degradation and color formation. Polymer 2003, 44, 5341–5354.

[19] Bhat AH, Banthia AK. Preparation and Characterization of Poly(vinyl alcohol)-Modified Red Mud Composite Materials. Journal of Applied Polymer Science 2007, Vol. 103, 238–243.

[20] Guo-An W, Cheng-Chien W, Chuh-Yung C. The disorderly exfoliated LDHs/PMMA nanocomposites synthesized by in situ bulk polymerization: The effects of LDH-U on thermal and mechanical properties. Polymer Degradation and Stability 2006, 91, 2443-2450.

[21] Liu X, Dever M, Fair N, and Benson RS. Thermal and Mechanical Properties of Poly(lactic Acid) and Poly(ethylene/butylene Succinate) Blends. Journal of Environmental Polymer Degradation 1997, Vol. 5, No. 4.

[22] Barham PJ, Keller A, Otun EL. Holmes, P. A. Crystallization and morphology of a bacterial thermoplastic: poly-3-hydroxybutyrate Journal of Materials Science 1984, 19, 2781.

[23] Crank J. “The Mathematics of Diffusion”, Second Ed., Oxford Science Publications, Oxford, 1975

[24] Cabedo L, Plackett D, Giménez E and Lagarón JM. Studying the degradation of polyhydroxybutyrate-covalerate during processing with clay based nanofillers. Journal of Applied Polymer Science. APP- 2008-03-1044.R1. Accepted 2008

[25] Mathew A, Oskman K, and Sain M. The Effect of Morphology and Chemical Characteristics of Cellulose Reinforcements on the Crystallinity of Polylactic Acid. Journal of Applied Polymer Science 2006, 101, 300-310.

[26] Auras R, Harte B, and Selke S. Sorption of ethyl acetate and d-limonene in poly(lactide) polymers. Society of Chemical Industry. Journal of the Science of Food Agriculture 2005, 0022–5142.

[27] Petersen K, Nielsen PV, and Olsen MB. Physical and mechanical properties of biobased materials. Starch 2001, 53, 8, 356.

[28] Olabarrieta I, Forsström D, Gedde UW, and Hedenqvist MS. Transport properties of chitosan and whey blended with poly(ε-caprolactone) assessed by standard permeability measurements and microcalorimetry. Polymer 2001, 42, 4401-4408.

[29] Cava D, Gimenez E, Gavara R and Lagaron JM, Journal of Plastics films and sheeting 2006, 22, 265.

[30] Jong-Whan Rhim, Seok-In Hong, Chang-Sik Ha. Tensile, water vapor barrier and antimicrobial properties of PLA/nanoclay composite films. Food Science and Technology 2009, 42, 612–617.

PAPER IV: Nanobiocomposites of Carrageenan, Zein, and Mica of Interest in Food Packaging and Coating.

Abstract

The present study presents the development and characterization of biocomposites of a red algae derived carrageenan, mica and their blends with zein prolamine obtained by solvent casting. The morphology of the blends was characterized by scanning and transmission electron microscopy (SEM and TEM), optical microscopy and atomic force microscopy (AFM). Mechanical behaviour, water barrier, water uptake and UV-VIS protection of the cast films were also investigated. The results indicated that addition of 10 wt.-% glycerol to the blends resulted in a better dispersion of the additive and for that reason in a better improvement for the studied properties. The composites were seen coloured but transparent and exhibited the ability to block the UV-VIS radiation due to the characteristic absorbing properties of the filler. Nevertheless, the main conclusion from the work is that the nanocomposites were seen to act as a reinforcing plasticizer and also led to significantly reduced water permeability and uptake. The clay was found to be more efficient in the latter aspect than the zein prolamine as an additive. As a result, these novel carragenan based biocomposites can have significant potential to develop packaging films and coatings for shelf-life extension of food products.

Keywords: Carrageenan; food hydrocolloids; nanocomposites; packaging; coatings

Introduction

Biopolymer films have been the focus of worldwide attention for the past few decades because they offer favourable environmental advantages in terms of sustainability and compostability compared to conventional synthetic polymeric films. Edible and biodegradable natural polymer films offer alternative packaging with lower environmental costs. The search for new renewable resources for the production of edible and biodegradable packaging materials and coatings has steadily increased in recent years. In particular, non-conventional sources of carbohydrates have been extensively studied. There are various unique carbohydrates that are found in marine organisms that represent a largely unexplored source of valuable materials. These non-conventional and underexploited renewable materials can be used as an interesting alternative to produce edible films and coatings.

The biopolymers studied in this work to produce edible films and coatings were κ/ι-hybrid carrageenan extracted from Mastocarpus stellatus, an underexploited red algae present in the Portuguese marine coast [1-4]. Carrageenans are water-soluble polymers with a linear chain of partially sulfated galactans, which present high potentiality as film-forming material. Carrageenans are structural polysaccharides from red seaweed and have been used extensively in foods, cosmetics, and pharmaceuticals[5]. Carrageenan biopolymer extracted from Mastocarpus stellatus seaweeds was shown to be a κ/ι-hybrid carrageenan[1] with gel properties comparable to commercial k-carrageenan gel formers [2,3]. The use of carrageenan as edible films and coatings are already used in the food industry on fresh and frozen meat, poultry and fish to prevent superficial dehydration[6], ham or sausage casings[7], granulation-coated powders, dry solid foods, oily foods[8], etc., but also manufacturing soft capsules [9, 10] and especially nongelatin capsules [11]. Polysaccharide and protein film materials are characterized by high moisture permeability, low oxygen and lipid permeability at lower relative humidities, and compromised barrier and mechanical properties at high relative humidities[12].

In order to tailor the properties and improve the water resistance of these biopolymers, it is often desirable to combine with, for instance, other biopolymers more resistance to water or with the addition of nanoclays. In the case of the addition of nanoclays, these layers are known to form impermeable shields. As a consequence, it is expected that the nanocomposite carbohydrate film will have substantially reduced water vapor permeability, thus helping to solve one of the long-standing drawbacks in the use of biopolymer films, i.e. water plasticization[13]. Indeed, Lagaron et al. [13] showed that the dispersion of mica nanoclay layers into the biopolymer matrix greatly improved the overall water barrier without measurable impact in the biodegradability of the matrix, thus turning them into industrially attractive materials. Moreover, the addition of glycerol to carrageenan has permited to obtain more usable film forming materials**.** Plasticizers are very important components to tailor the physicochemical properties of biopolymers. In principle, addition of plasticizers results in a decrease in the intermolecular forces along the polymer chains, which

consequently improve flexibility, extensibility, toughness and tear resistance of biopolymer films. To enhance the barrier properties of biopolymer films, a high crosslink density has often been promoted. As a result, an increase in the plasticizer concentration normally causes an increase in the water permeability of hygroscopic or hydrophilic films due to a reorganization of the macromolecular network and a subsequent increase in free volume. Indeed, some studies have reported that the addition of plasticizers yield marked increases in permeability and diffusion coefficients of gas or water vapour [14-15]. But this effect depends on the glycerol content in the polymer. In fact, it has been reported that a decrease in water permeability takes place for low additions of glycerol, between 5-10%, but that increasing the glycerol content increases the water permeability [16-17].

In this work, carrageenan was also combined with zein, other biopolymer from the group of alcohol soluble proteins (prolamines) found in the corn endosperm. The film-forming properties of zein have also been recognized for decades and are the basis for most commercial utilization of zein. Even when zein is a protein, it presents unusually high resistance to water. Zein films are also brittle and plasticizers are often recommended. Zein-based films show great potential for uses in edible coatings and biobased packaging[18]. In a preliminary study, Arora and Padua developed nanocomposites of zein and reported a water vapour permeability decreased of ca. 50% with the addition of kaolinite clays[19]. In some studies, zein was blended with other proteins such as gluten[20], starch[21] and soy protein[22]. These were reported to exhibit enhanced mechanical performance as a result of blending. Corradini et al. reported a decrease in water uptake with the addition of zein in starch films plasticized with glycerol[23].

However, very little is known about the development and characterization of carrageenan nanocomposites. Daniel-Da-Silva et al. reported the production of polysaccharide i-carrageenan used in the production of macroporous composites containing nanosized hydroxyapatite, with application in bone tissue engineering[24]. Gan et al. also reported a new injectable biomaterial carrageenan/nano-hydroxyapatite/collagen for bone surgery[25]. To be best of our knowledge, the addition of nanoclays in the pure carrageenan and the study of the barrier properties of these nanocomposites have not been reported yet.

In this context, the overall objective of this work was the development of novel renewable and biodegradable carrageenan-based food packaging films with improved barrier properties, especially with enhanced water and UV-light resistance. To do so, blends of carrageenan extracted from a Portuguese red algae with a water resistant zein prolamine and/or with nanoclays were developed and characterized for the first time.

Experimental

Materials

Details about the recovery of κ/ι hybrid carrageenan biopolymers from *M. stellatus* seaweeds can be found elsewhere[1,2,5]. The polysaccharide used in the present study was obtained through a hot extraction process performed during 2 h at 95ºC and a pH of 8 on alkali-treated M. stellatus seaweeds. The resulting powder was then purified

by mixing 1 g of isolated product with 49 ml hot distilled water during 1 h and subsequent centrifugation performed at sequence cycles at 10^4 rpm and 40ºC during 40 min. The supernatant was finally recovered and used for film forming by casting.

Zein from corn (grade Z3625) purchased from Sigma-Aldrich (Madrid, Spain) was used as received without further purification. Glycerol was used as plasticizer and was supplied by Panreac Quimica S.A. (Spain)

A food contact complying NanoBioTer® grade based on purified natural mica clay was kindly supplied by NanoBioMatters S.L., (Paterna, Spain). No further details of sample preparation and modification were disclosed by the manufacturer.

Preparation of nanocomposites

Solution-cast film samples of the purified carrageenan with (1, 5, 10 and 20) wt.-% clay and 10 wt.-% glycerol content were prepared with a dry film thickness of around 50 μm. Nanoclay dispersions in water were simply mixed in a homogenizer (Ultra-turrax T25 basic, Ika-Werke, Germany) for two minutes and were then stirred with the carrageenan during 30 min and, subsequently, cast onto Petri dishes to generate films of ca. 50 μm after solvent evaporation at room temperature conditions.

Solution-cast 50 microns thickness film samples of the nanocomposites of carrageenan containing 5 wt.-% clay, 20 wt.-% of zein and 25 wt.-% of glycerol were also prepared. A solution of zein in water:ethanol (70/30, v/v) was first prepared and then added to a suspension of nanoclays in carrageenan prepared as described above. The solution was then stirred for 30 min and, subsequently cast onto Petri dishes. The nanocomposites of zein and of carrageenan-zein blends were only obtained with 5 wt.-% of clay, due to the fact that the best property balance was found for compositions around or below this loading level.

Optical light polarized microscopy

Polarized light microscopy (PLM) examinations using an ECLIPSE E800-Nikon with a capture camera DXM1200F- Nikon were carried out on both sides of the cast samples.

SEM measurements

For scanning electron microscopy (SEM) observation, the samples were criofractured after immersion in liquid nitrogen, mounted on bevel sample holders and sputtered with Au/Pd in a vacuum. The SEM pictures (Hitachi S4100) were taken with an accelerating voltage of 10 keV on the sample thickness.

TEM measurements

Transmission electron microscopy (TEM) was performed using a JEOL 1010 equipped with a digital Bioscan (Gatan) image acquisition system. TEM observations were very difficult to perform due to solubility and difficult handling of the films.

However, some pictures were taken on microdrops of the solution cast directly onto the TEM observation grids.

AFM measurements

Atomic force microscopy (AFM) measurements were performed using an Agilent 5500 SPM system (provided by Scientec Iberica, Spain) to investigate the morphology of the nanocomposite surfaces on both sides of the cast films. The images were scanned in tapping mode in air using commercial Si cantilevers with a resonance frequency of 320 kHz.

Gravimetric measurements

Water permeability was determined from the slope of the weight gain–time curves at 24°C. The films were sandwiched between the aluminium top (open O-ring) and bottom (deposit for the silica gel that provides 0%RH) parts of a specifically designed permeability cell with screws and placed inside a desiccator at 75%RH. A Viton rubber O-ring was placed between the film and the bottom part of the cell to enhance sealability. The solvent weight gain through the film was monitored and plotted as a function of time. Cells with aluminium films were used as control samples to estimate water gain through the sealing. Solvent permeation rates were estimated from the steady-state permeation slopes. Water vapour weight gain was calculated as the total cell weight gain minus the gain through the sealing. The tests were done in duplicate.

For the water uptake, samples were dried in a desiccator at 0%RH until constant weight. They were then allowed to saturate in moisture inside desiccators at 11%, 54% and 75% RH and monitored during sorption until constant weight (indicating water uptake). These experiments were done in triplicate.

Tensile test

Tensile test was measured at 10 mm/min according to ASTM Standard D638 in stamped dogbone-shaped specimens of the samples, using an Instron Testing Machine (Model 4469; Instron Corp., Canton, MA). The tensile tests were carried out at ambient conditions, i.e. typically 21 ºC and 60%RH, and the tests were done in quadruplicate. The samples were preconditioned in a desiccator at 60%RH before testing.

UV-VIS Spectra

An UV–Vis spectrophotometer (Hewlett Packard 8452A Diode Array Spectropotometer) was used to measure the absorbance and transmittance spectra of the films in the range 200–700 nm wavelength light. UV-Vis spectra were taken in thin films of biodegradable materials and their nanocomposites cast directly onto the surface of a quartz cuvette. The measurements were later normalized to an average thickness of 30 microns for all the samples to allow comparison between materials.

Results and Discussion

Morphology

Polarized optical light microscopy photographs were aimed at the characterization of the dispersion of the glycerol-phase and the nanoclays in the biodegradable matrixes. Figure 1 shows the optical micrographs of the carrageenan castings with and without glycerol and with different clay contents. In Figure 1A, films of pure carrageenan exhibit some spots, most likely as a consequence of some residues. However, Figure 1B indicates that clay tactoids (5 wt.-%) can be clearly observed in the nonplasticized carrageenan matrix. Figures 1 C, D, E and F show micrographs of the carrageenan containing 10 wt.-% of glycerol and 0, 1, 5 and 20 wt.-% of clay content, respectively. A first observation from these images is that an apparent better dispersion of the clay occurs in the presence of glycerol (compare Figures 1B and 1E). Thus, the presence of glycerol permits to increase the compatibility and hence dispersion between the clay and the biopolymer in the nanocomposites. From these images, it can also be seen that with increasing clay content from 1 wt.-% to 20 wt.-% the clay agglomerates (compare Figures 1D and 1F). Mica has very large platelets which upon dispersion, even if this is poorer than with other more conventional nanoclays, should provide high shielding efficiency in terms of low molecular weight species diffusion[13]. In principle, this is the reason why it becomes relatively easy to observe big tactoids by optical microscopy since the platelets length and width dimensions should tend to naturally seat during film forming parallel to the casting dishes due to gravitational and surface energy forces[26].

Figure 1G shows a picture taken in the blend of carrageenan containing 20 wt.-% zein and 10 wt.-% glycerol. This picture shows a clear phase segregation of most likely the zein phase in the polysaccharide matrix. However, Figure 1H, shows that the ternary blend is better dispersed in the presence of the nanoclay.

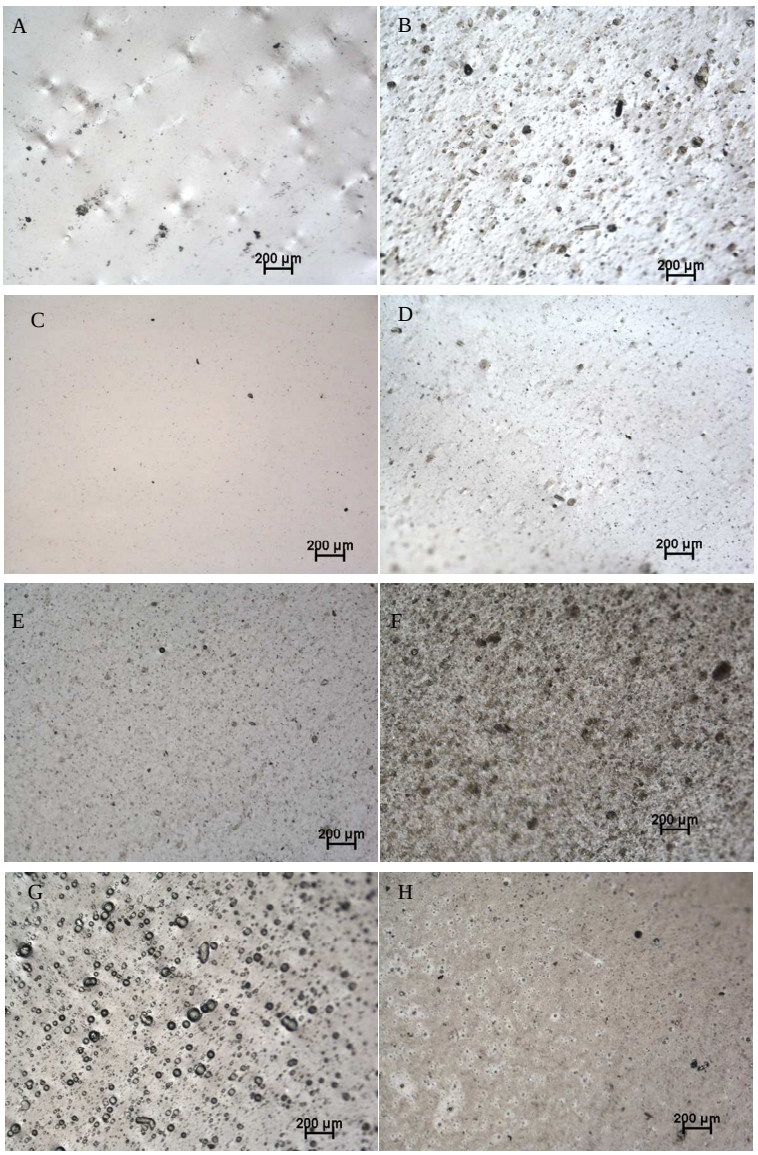

Figure 1. Optical micrographs of: (A) Carrageenan, (B) carrageenan with 5 wt.-% clay content, (C) carrageenan with 10 wt.-% glycerol content, (D) carrageenan with 1 wt.-% clay content and 10wt.-% glycerol content, (E) carrageenan with 5 wt.-% clay content and 10wt.-% glycerol content, (F) carrageenan with 20 wt.-% clay content and 10wt.-% glycerol content, (G) carrageenan with 20 wt.-% zein content and 10wt.-% glycerol content, (H) carrageenan with 20 wt.-% zein content and 5 wt.-% clay content and 10wt.-% glycerol content. The scale marker is 200 microns in all the micrographs.

Figure 2 shows a picture with higher magnification taken in a film of carrageenan containing 10 wt.-% of glycerol and 5 wt.-% of clay. From Figure 2A, it can be clearly

observed that glycerol forms a separates phase at the microscale within the carrageenan matrix which is very homogeneously dispersed. Curiously, clay platelets are observed to be displayed inside glycerol particles and at the interphase between the glycerol and the matrix (see arrows), suggesting again a higher affinity for the glycerol, which may then act as a compatibilizer for the filler (see Figure 2B).

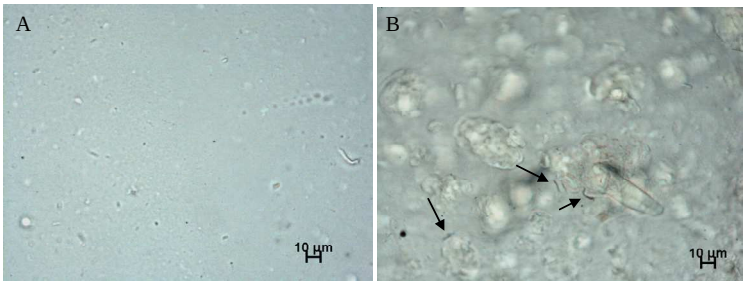

Figure 2. Typical optical micrographs of: (A) Carrageenan with 10 wt.-% glycerol content, (B) carrageenan with 5 wt.-% clay content and 10wt.-% glycerol content. The scale marker is 10 microns in the micrographs.

Figure 3 shows the scanning micrographs of the cross-section of these biopolymer blends. For pure carrageenan, a homogenous film morphology is observed (see Figure 3A). In the case of carrageenan with 5 wt.-% clay content and 10 wt.-% glycerol (see Figure 3B), the presence of the clay cannot be discerned. However, from Figure 3C it can be seen that in the carrageenan-zein blend, which phase separate, there seems to be a strong interfacial adhesion between the biopolymer matrix and the protein. The two polymers are, therefore, not miscible, but compatible due to the observed interfacial contact. A similar morphology is also observed for the nanocomposite of the carrageenan-zein blend (see Figure 3D). Figure 3E, shows the morphology of pure zein with analogous morphology as the zein composites with clay, suggesting a fine dispersion and adhesion of the nanoclay in the zein matrix (see Figure 3F).

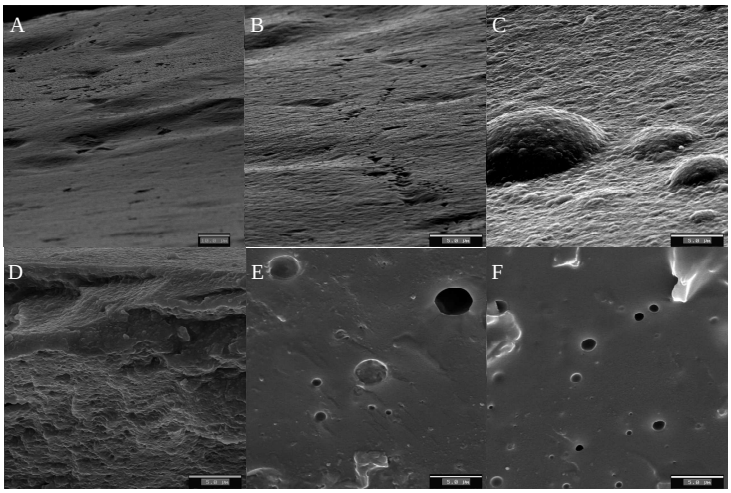

Figure 3. Scanning electron micrographs of the cross section of: (A) carrageenan (scale marker is 10 microns), (B) carrageenan with 5 wt.-% clay content and 10 wt.-% glycerol content (scale marker is 5 microns), (C) carrageenan with 20 wt.-% zein content and 10 wt.-% glycerol content (scale marker is 5 microns) and (D) carrageenan with 5 wt.-% clay content and 20 wt.-% zein content and 10 wt.-% glycerol content (scale marker is 5 microns) and (E) zein with 10 wt.-% glycerol content and (F) zein with 5 wt.-% clay content and 10 wt.-% glycerol content (scale marker is 5 microns).

Figure 4 shows some TEM results taken on specimens of plasticized carrageenan containing 5 wt.-% of the nanoclay. This figure indicates a highly dispersed irregular morphology consisting of intercalated tactoids with thickness in the nanorange, i.e. below 100 nanometers, and some exfoliated nanoclay platelets most probably fractured.

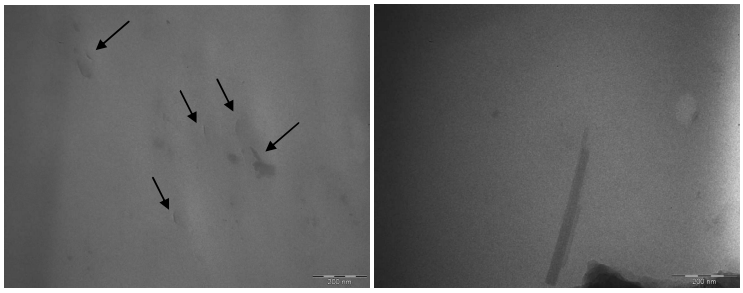

Figure 4. Transmission electron micrographs of plasticized carrageenan containing 5 wt.-%clay. (scale marker is 200 nm).

Finally, Figure 5 shows the surface roughness of a carrageenan cast film containing 5 wt.-% nanoclay content and 10 wt.-% of glycerol as measured by AFM. From observation of this Figure, it can be seen that the nanoclay contains large platelets strongly intercalated and dispersed at the nanolevel but not to an individual platelet level, which would have meant exfoliation, across the matrix. This image also shows that there appears to be a good adhesion of the nanofiller to the biopolymer.

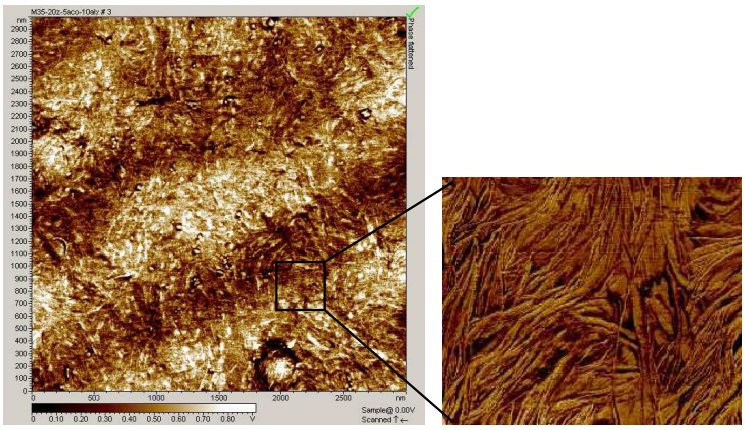

Figure 5. AFM picture of plasticized carrageenan containing 5 wt.-% clay and 10 wt.-% glycerol

Mechanical properties

Specimens of carrageenan, zein and blends of carrageenan-zein and of their nanocomposites with glycerol were measured in tensile testing experiments, in order to evaluate the effect of adding nanoclays and zein on the mechanical properties of these biopolymers. Mechanical parameters such as tensile strength, Young modulus and elongation at failure are presented in Figure 6. Figure 6 shows that the stiffness, strength, toughness but also the elongation at failure has a general trend of increasing in the materials with increasing clay content in the materials. This suggests a reinforcing-plasticizing effect of the nanoclay in the material which in turn allow a better mechanical handling of the films.

In Figure 6A, the tensile strength carrageenan is seen to increase with nanoclay content, this behaviour has been reported in different studies with nanoclays[27-28]. This suggests that the nanoclays act to reinforce the material as expected. Addition of nanoclays to carrageenan resulted in an increase in the tensile strength of ca. 39% and 146% for the films of carrageenan with 10 and 20 wt.-% nanoclay, respectively compared to carrageenan containing 1 wt.-% of filler content. Nanocomposites with 1 wt.-% of filler are referenced because pure carragenan films could not be tensile tested even with 10 wt.-% of glycerol due to excessive fragility. This was expected as earlier studies[2-4] reported a Young modulus as low as 25 MPa and a strain at break as low as 3.5% for a pure carrageenan film. The increase in tensile strength with further addition

of clay is attributed to a good nanoclay dispersion of these nanocomposites. This behaviour is in contrast with the work by Majdzadeh-Ardakani et al., who reported that the addition of high nanoclay loadings into the starch matrix led to the appearance of clay stacks, non exfoliated morphologies and even aggregates that deteriorated the mechanical properties and decreased the tensile strength of the higher loaded specimens[29]**.** Curiously, in zein cast films, albeit the error bars are relatively high the tensile strength appeared to decrease in the film with 5 wt.-% nanoclay compared to the pure zein, due to most likely the poorer morphology of the nanocomposites with zein.

The addition of zein to the carrageenan films increased the tensile strength by up to 72% compared to the carrageenan matrix. Kim et al. reported an analogous behaviour, i.e. the addition of zein to gluten increased the mechanical properties until the content of zein reached 20–22%. Further increase in zein content lowered the mechanical properties[20]. Pol et al. also showed that the tensile strength of soy protein laminates films increased (within a 95% confidence level) with increasing the relative content of zein in the laminates[22].

Nanocomposite of the blends carrageenan-zein seemed to exhibit similar tensile strength, albeit the error bar is relatively high, but carragenan improved this property with the addition of zein, at least compared to the nanocomposite of carrageenan with 1 wt.%.

Young's modulus, expressing the stiffness of the material, showed a general trend of increasing values in the nanocomposites, albeit this was not seen for some samples. Figure 6B shows the Young modulus of these biopolymers as a function of nanoclay content. The Young's modulus generally increased in carragenan with increasing clay content, in line with the typical behaviour in nanocomposites[30-31].Thus, an increase in Young modulus of 70% for the film of carrageenan with 20 wt.-% nanoclay compared to carrageenan with 1 wt.-% content was observed. Addition of zein to the carrageenan seemed to increase the Young modulus in agreement with the above cited previous work[20]. However, the rigidity of the nanocomposites of this blend was reduced with increasing clay content similarly as with the composites of zein.

Elongation at failure for these biopolymers and their nanocomposites are presented in Figure 6C. For pure carrageenan, it can be observed an increase of up to 132% for the film of carrageenan with 20 wt.-% nanoclay compared to carrageenan with 1 wt.-% content. Elongation at failure was seen to increase in all cases in accordance with previous works[27-28]. Toughness was, in accordance with the above, seen to increase with clay presence and content in the biopolymers (see Figure 6D). This is a very positive finding from an applied view-point because the extreme rigidity of these biomaterials restricts to a considerable extent its usability.

In summary, tensile strength, Young modulus, elongation at failure and thoughness increased with increasing clay loading in the case of carrageenan**,** due to the good dispersion of the clays in the carrageenan. However, in the case of the nanocomposites of carrageenan-zein the rigidity was not enhanced, possibly due to phase separation

and the very different mechanical response of the two biopolymers and the lower affinity of the zein for the nanoclay.

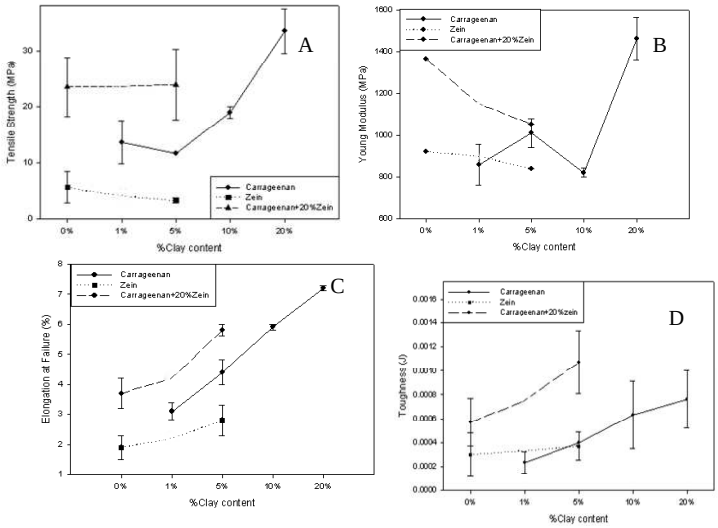

Figure 6. A) Tensile strength (MPa), B) Young modulus E (MPa), C) elongation at failure (%) and D) Toughness (J) as a function of nanoclay content for carrageenan, zein and blends of carrageenan-zein.

Barrier properties

Table 1 gathers all the barrier data (direct permeability and solvent uptake) that has been measured in the neat biopolymers and in their biocomposites and also gathers permeability values reported in the literature for the neat biopolymers.

First observation from Table 1 regarding pure carrageenan is that the water permeability coefficient of 6.86 10^{-14} Kg m / s m^2 Pa is really similar to the 6.7 10^{-14} Kg m / s m^2 Pa previously reported for this κ/ι-carrageenan[4]. An interesting observation is the effect of glycerol in the barrier properties, Table 1 indicates that the water permeability decreased by ca. 32% with the addition of 10 wt.-% of glycerol, as expected for low additions of glycerol to the matrix. Talja et al. reported that the water permeability of potato starch-based films was higher without plasticizer than with 20 wt.-% of glycerol at all RH gradients. However, the films plasticized with 30 or 40 wt.-% of glycerol exhibited increased water permeability[16]. The increase in water permeability for plasticizer-free potato starch-based films was attributed by the authors to the presence of microcracks in the pure biopolymer film. The carrageenan samples studied here did not show evidences of microcracks upon careful inspection. Guo et al. also reported that cellulose acetate films with plasticizer contents of 5 to 10 wt.-% (w/w, solids) had lower water permeability than films without plasticizer. They attributed this behaviour to a decreased molecular mobility of cellulose acetate in the presence of plasticizers[32].

Table 1 and Figure 7A teach that the water permeability show minimum values for specimens containing 1 and 5 wt.-% of nanoclay. From the results, a decrease in the water permeability of ca. 86%, 83%, 61% and 61% for the films of plasticized carrageenan containing 1wt.-%, 5wt.-%, 10wt.-% and 20wt.-% of clay, respectively, were seen compared with the unfilled plasticized material. So, the addition of the clays to the plasticized carrageenan films enhances considerably the water barrier properties. Nevertheless, addition of higher nanoclay contents (10 and 20wt.-% of clay) results in lower reductions in water permeability, due to most likely nanoclay agglomeration which results in a reduction in the nanoclay barrier efficiency due to creation of preferential paths for diffusion. These results are not in coincidence with a recent paper that used the same type of mica-based nanoclay but in methyl cellulose and chitosan[13]. In the latter materials, higher loadings of clay, i.e. 20 wt.-% were needed to achieve similar water permeability reductions, however these materials did not make use of glycerol as plasticizer. From the morphology results reported above, glycerol enhances the nanoclay dispersion in carrageenan. In fact Table 1 indicates that if 5 wt.-% of nanoclay is added to carrageenan without glycerol, the permeability reduction is smaller, i.e. 31% in permeability drop, suggesting that the dispersion is indeed poorer.

The water uptake of the carrageenan films and of their related nanobiocomposites at different humidities is also summarized in Table 1. A general observation is that the water uptake increased for all samples with increasing RH, as expected[16]. Also the presence of glycerol increased the water uptake but only at medium-high %RH. The uptake was higher at higher %RH. The same behaviour was reported by Zeppa et al. [33]. Thus, glycerol was seen to decrease the water uptake at low activity but increased it at high activity. This phenomenon has been attributed to potential interactions between the hydroxyl groups of carrageenan and the hydroxyl groups of glycerol resulting in less sorption sites for water molecules [16, 33].

Interestingly, the films of plasticized carrageenan containing 1, 5, 10 and 20.-wt% of clay exhibited clearly lower uptakes at 75%RH, i.e. ca. 56%, 56%, 61% and 65%, respectively, compared with the unfilled plasticized material. At 54%RH, higher reductions of 85%, 90%, 81% and 61% were observed with increasing clay content (see Figure 8A). However, at 11%RH the nanocomposites took up more moisture than the unfilled material most likely by moisture being preferentially sorbed at the nanoclay surface. The significantly lower water uptake at medium high relative humidities, but especially at medium, must be related to a water solubility reduction due to the presence of the nanoclays filling the available free volume in the biopolymer matrix as moisture begins to plasticize the biopolymer.

Tabla 2 and Figure 7B also show the water permeability of plasticized zein films. A first observation is that the water permeability of zein containing 25 wt.-% of glycerol is 7.41 10^{-14} Kg m/s m^2 Pa, whereas a film of pure zein was reported by Parris et al. to be of 30.34 10^{-14} Kg m/s m^2 Pa[34] by Ghanbarzadeh et al. of 53.50e^{-14} Kg m/s m^2 Pa in a compression molded zein film[35]. The reason for the disagreement could be related to the different origin, testing conditions, composition and processing of the films. From the results the water permeability of the plasticized zein film is seen higher than the water permeability of the pure plasticized carrageenan. Moreover, addition of zein to carrageenan in the presence of glycerol did not outperform in barrier properties

plasticized carrageenan. However, the nanocomposites of carrageenan-zein show a reduction in the water permeability of 18% compared to the plasticized carrageenan, Hence, the nanoclay seems a more efficient element than zein to reduce the water permeability of carrageenan.

In terms of the water uptake of zein (see Figure 8B), it is observed that the water resistance in terms of uptake of the polymer is much higher than that of carrageenan, as expected. Thus, the water uptake of zein containing 25 wt.-% glycerol measured at 11%, 54% and 75%RH is 66%, 61% and 48%, respectively, smaller than plasticized carrageenan. In good accordance, blends of carrageenan containing 20 wt.-% of zein show a reduction in uptake of 15%, 30% and 19%, respectively, compared to plasticized carrageenan. Again, in the case of the nanocomposites of the blend, a reduction in the water uptake at 11%, 54% and 75%RH of ca. 60%, 40% and 33%, respectively, were seen compared to the plasticized carrageenan films.

Nielsen[36] developed an expression to model the permeability of a two-phase film in which impermeable square plates are dispersed in a continuous conducting matrix. The plates are oriented so that the two edges of equal length, L, are perpendicular to the direction of transport: and the third edge, the thickness W, is parallel to the direction of transport. This expression is:

$$P = P_m\left(1-\phi_d\right)/\left[1+\left(L/2W\right)\phi_d\right] \qquad \text{(equation 1)}$$

where P is the permeability of the composite, P_m, is the permeability of the matrix, and Φ_d is the volume fraction of the impermeable filler. The $(1 - \Phi_d)$ term accounts for volume exclusion and the $(1 + (L/2W)\ \Phi_d)$ term for tortuosity. Note that this model does not account for permeation through the dispersed phase.

A more realistic system to consider is one in which a discontinuous low-permeability phase is present in a high-permeability matrix. Maxwell[37] developed a model to describe the conductivity of a two-phase system in which permeable spheres are dispersed in a continuous permeable matrix. Fricke[38] extended Maxwell's model to describe the conductivity of a two-phase system in which permeable ellipsoids are dispersed in a more permeable continuous matrix. This model describes the permeability of a two-phase system in which lower permeability elongated ellipsoids (P_d) are dispersed in a more permeable continuous matrix (P_m).

According to the latter model, the permeability of a composite system consisting of a blend of the two materials in which the dispersed phase (Φ_2 is the volume fraction of the dispersed phase) is distributed as ellipsoids can be expressed as follows[39]**:**

$$P = (P_m + P_dF)/(1+F) \qquad \text{(equation 2)}$$

where

$$F = [\Phi_2/1 - \Phi_2][1/(1+(1-M)(P_d/P_m-1))] \qquad \text{(equation 3)}$$

$$M = \cos\theta / \sin^3\theta\,[\theta - 1/2 \sin 2\theta] \qquad \text{(equation 4)}$$

and

$$\cos \theta = W/L \qquad \text{(equation 5)}$$

Where ρ_{clay} = 2.7 g/ml, $P_d \approx 0$, P_m=100 and L/W was taken as 8 and 100.
W is the dimension of the axis of the ellipsoid parallel to, and L the dimension perpendicular to, the direction of transport, and θ is given in radians.

Figure 9 shows the experimental permeability values for the plasticized carrageenan system and modelling results using the Nielsen model and Fricke extended Maxwell´s models. The Fricke modelling results for the higher aspect ratios best fit the data at lower filler volumes (between 1 and 5 wt.-% of clay). However, higher clay loading contents (between 10 and 20 wt.-% of clay) do not follow the modelling trend suggesting as explained above that agglomeration of the nanoclay decreases the barrier efficiency.

Table 1. Water permeability, water %uptake at 11%, 54% and 75%RH for carrageenan and carrageenan-zein films and their nanocomposites.

	P water (Kg m/s m^2 Pa)	**Water Uptake (%) 11%RH**	**Water Uptake (%) 54%RH**	**Water Uptake (%) 75%RH**
Carrageenan	6.86±0.041e-^{14}	5.12	10.90±0.29	17.02±0.34
Carrageenan+5%clay	4.74±0.023e-^{14}	4.99±0.38	9.44±0.34	16.35±0.43
Carrageenan+10%glycerol	4.65±0.542e-^{14}	3.62±0.32	12.41	26.03±0.62
Carrageenan+1%clay+10%glycerol	0.65±0.19e-^{14}	3.71±1.26	1.84±2.72	11.35±1.64
Carrageenan+5%clay+10%glycerol	0.81±0.52e-^{14}	5.57	1.21	11.36±0.29
Carrageenan+10%clay +10%glycerol	1.82±0.35e-^{14}	5.28±1.33	2.39±0.07	10.18±1.05
Carrageenan+20%clay+10%glycerol	1.80±0.03e-^{14}	7.75±4.37	4.79±0.62	9.21±0.20
Carrageenan+20%Zein+10%glycerol	5.65±0.248e-^{14}	3.06±0.29	8.66±0.29	21.14±0.98
Carrageenan+20%Zein+5%clay+10%glycerol	3.81±0.056e-^{14}	1.44±0.39	7.55±0.52	17.42
Zein+10%glycerol		1.68	3.74±0.57	9.77±0.80
Zein+5%clay+10%glycerol		1.67±0.25	3.61±0.54	6.04±0.511
Zein+25%glycerol	7.41e-^{14}	1.22±0.16	4.83±0.70	13.39±0.52
Zein+5%clay+25%glycerol	7.71±0.776e-^{14}	2.39	5.99±0.72	9.37
k/i-carrageenan literature Value[13]	**6.7e-^{14}**			
Zein literature Value[33]	**30.36e^{-14}**			
Zein literature Value[34]	**53.50e^{-14}**			

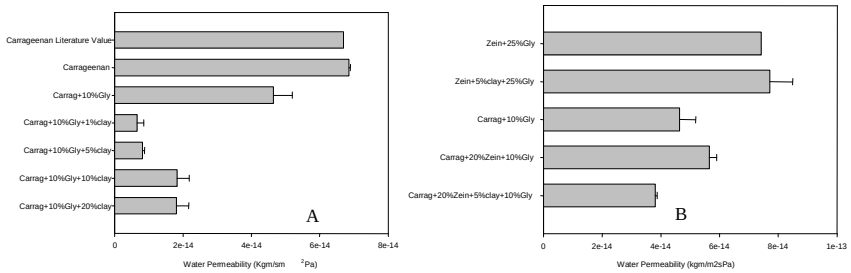

Figure 7. Water direct permeability for (A) films of carrageenan and their nanocomposites (B) films of carrageenan/zein blends and their nanocomposites.

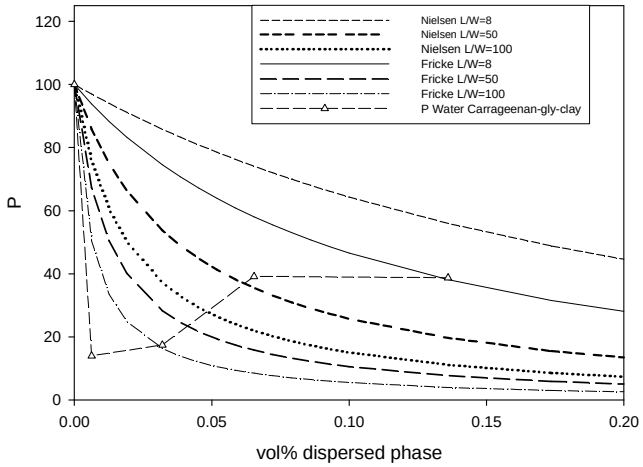

Figure 8. Experimental normalized permeability values and modelling results assuming different aspect ratios.

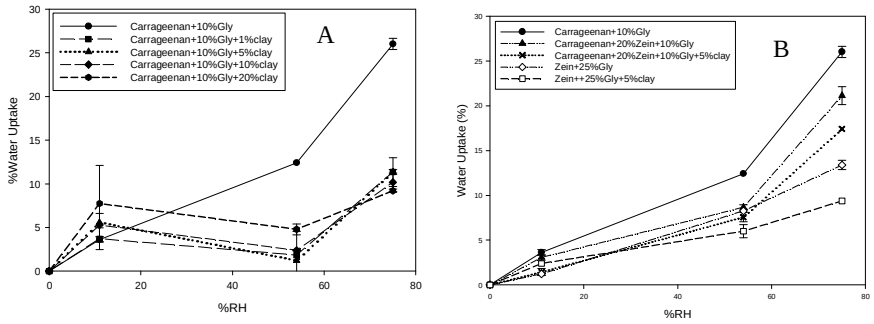

Figure 9. Water uptake (%) at 11%, 54% and 75%RH for: (A) The films of carrageenan and their nanocomposites (B) the films of carrageenan and zein and their nanocomposites

UV-VIS

Figure 10 shows the visual appearance of the plasticized carrageenan composite films. From this Figure an increase in colouring of the sample and a reduction in transparency was observed with increasing clay content, particularly for the sample containing 20 wt.-% of filler. Nevertheless, low filler contents still exhibit good contact transparency.

Figure 11 shows the normalized transmittance for the UV-VIS spectra of the nanocomposite films of plasticized carrageenan with 30 microns thickness. The UV region is typically classified in three zones: UVC (Ultraviolet C) (100-280nm), UVB (Ultraviolet B) (280-320) and UVA (Ultraviolet A) (320-400nm) .

From Figure 11 a clear reduction in UV-VIS transmittance with increasing clay content in the films was observed. From the results, the transmittance of the pure carrageenan in the region of UVC is around 30%. A complete shielding of UVC occurs for the selected thickness at 10 and 20 wt.-% clay loading in the carrageenan film. Films of carrageenan containing 20 wt.-% of nanoclay led to reductions in the transmission of light in the UVB-UVA of ca. 95-100%. In the visible region, pure plasticized carrageenan has a transmittance of 85%, whereas the film of plasticized carrageenan containing 20 wt.-% of clay has very little transmittance.

It is clear that 20 wt.-% filler loading is perhaps too high a loading since it does negatively affect the transmission in the visible range and will be unlikely to yield optimum property balance. Nevertheless, and as it was observed with the barrier performance, the ratio of protection is still very efficient at nanoclay loadings of 5 wt.-%, yielding the 10 wt.-% filler not so strong differentiating benefits. Thus, low nanoclay contents (5 wt.-%) in the carrageenan matrix led to significant reductions in the UV light transmission (see Table 2), while retaining transparency to a significant extent.

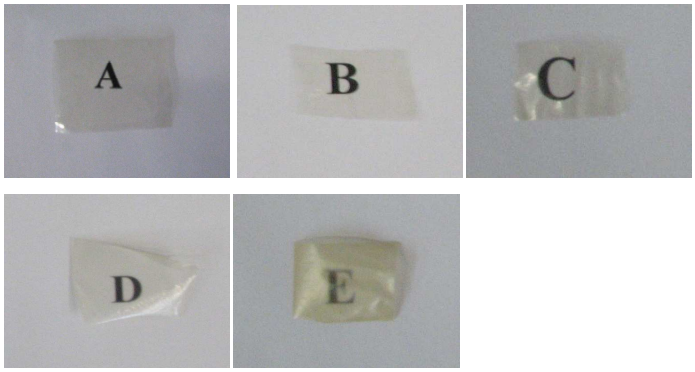

Figure 10. Typical photographs of ca. 30 microns thickness films of plasticized carrageenan containing: A) 0 wt.-% of clay, B) 1 wt.-% of clay, C) 5 wt.-% of clay, D) 10 wt.-% of clay and E) 20 wt.-% of clay.

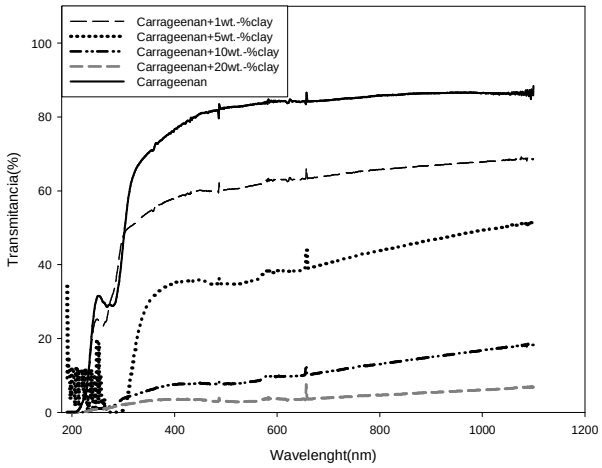

Figure 11. UV–Vis spectra of 30 microns films of plasticized carrageenan nanocomposites containing 0, 1, 5, 10, and 20 wt.-% of nanoclay.

Table 2. UV-Vis blocking ($\%T_{nanocomposite}$-$\%T_{pristine}$) at 300nm (UV) and 600nm (Visible) wavelengths per wt.-% of nanoclay in plasticized carrageenan nanocomposites.

Wt.-% filler	Blocking at 300nm %T/wt.-%clay	Blocking at 600nm %T/wt.-%clay
1	0	21.26
5	8.92	8.06
10	4.14	7.45
20	2.19	4.03

Conclusions

Successful blends of carrageenan with zein prolamine and a mica clay additive were obtained by solution casting using glycerol as a plasticizer. From the results, addition of glycerol to the carrageenan nanocomposite films permitted to obtain a good dispersed morphology of the inorganic additive, especially at low filler contents. Addition of zein to the plasticized carrageenan films showed phase separation but with strong adhesion suggesting that the two polymers are not miscible but are compatible. Tensile strength, Young modulus, elongation at failure and toughness increased with increasing clay loading for the plasticized carrageenan composites**,** due to the good dispersion of the clays in the matrix. However, for the carrageenan-zein composites the rigidity was not enhanced, possibly due to the mentioned phase separation, the very different mechanical response of the two biopolymers and the lower affinity of the zein for the nanoclay. Interestingly, the addition of nanoclays (1 or 5 wt.-%) to the plasticized carrageenan decreased significantly the water permeability by ca. 86 and 83%, respectively. The water uptake was also reduced by up to ca. 90% in samples with low nanoclay contents at high relative humidity, suggesting that the observed lower water permeability may be strongly contributed by a nanoclay induced solubility drop effect. Additionally, low nanoclay contents (1 or 5 wt.-%) in the carrageenan matrix led to significant reductions in the UV-VIS light transmission, while retaining transparency. These results suggest that these blends can have significant potential in food packaging and coating applications where enhanced water resistance and permeability and increase flexibility can provide more usability for the polysaccharide.

References

(1) Hilliou, L.; Larotonda, F.D.S.; Abreu, P.; Ramos, A.M; Sereno, A.M; Gonçalves M.P. Effect of extraction parameters on the chemical structure and gel properties of kappa/iota-hybrid carrageenans obtained from Mastocarpus stellatus. Biomolecular Engineering, 2006, 23: 201-208.

(2) Hilliou, L.; Larotonda, F.D.S.; Sereno, A.M.; Gonçalves, M.P. Thermal and viscoelastic properties of κ/ι-hybrid carrageenan gels obtained from the Portuguese seaweed Mastocarpus stellatus. Journal of Agricultural and Food Chemistry. 2006, 54 (20), pp. 7870-7878. ANTIGUO 24

(3) Hilliou, L.; Gonçalves, M.P.. Gelling properties of a kappa/iota-hybrid carrageenan: effect of concentration and steady shear. International Journal of Food Science & Technology, 2007, 42: 678-685.

(4) Larontonda, F. D. S.; Hilliou, L.; Goncalves, M. P.; Sereno, A. M. – From Low Value renewable Resources to green Biomaterials for Edible Coating Applications. In Recent Advances In Research on Biodegradable Polymers and Sustainable Composites (vol. 3); A. Jiménez, G. E. Zaikoz (Eds.), 2008, p. 19. ISBN 978-1-60692-155-5.

(5) De Ruiter, G. A.; Rudolph, B. Carrageenan biotechnology. Trends Food Sci. Technol. 1997, 8, 389-395.

(6) Shaw, C.; Secrist, J.; Tuomy, J. Method of extending the storage life in the frozen state of precooked foods and product produced. U.S. Patent 1980, 4,196,219.

(7) Macquarrie, R. Edible film formulation. U.S. Patent 0155200 A1, 2002.

(8) Ninomiya, H.; Suzuki, S.; Ishii, K. Edible film and method of making same. U.S. Patent 1997, 5,620,757.

(9) Tanner, K.; Getz, J.; Burnett, S.; Youngblood, E.; Draper, P. Film forming compositions comprising modified starches and iota-carrageenan and methods for manufacturing soft capsules using same. U.S. Patent 0081331 A1, 2002.

(10) Bartkowiak, A.; Hunkeler, D. Carrageenan–oligochitosan microcapsules: optimization of the formation process. Colloids Surf. B: Biointerfaces. 2001, 21, 285-298

(11) Fonkwe, L.; Archibald, D.; Gennadios, A. Nongelatin capsule shell formulation. U.S. Patent 0138482 A1, 2003.

(12) Brody, A.L.. Edible packaging. Food Technol. 2005, 59, 65.

(13) Lagaron, J.M.; Fendler, A. High water barrier nanobiocomposites of methyl cellulose and chitosan for film and coating applications. Journal of Plastic Film and Sheeting. 2009, Volume 25, Issue 1, Pages 47-59.

(14) Tihminlioglu, F.; Atik, I.D.; Özen, B. Water vapor and oxygen-barrier performance of corn–zein coated polypropylene films. Journal of Food Engineering. 2010, 96 342–347.

(15) Guilbert, S.; Gontard, N.; Gorris, L. G. M. Prolongation of the shelflife of perishable food products using biodegradable films and coatings. Food Science and Technology. Lebensmittel-Wissenschaft & Technologie. 1996, 29, 10-17.

(16) Talja, R.A.; Helén, H.; Roos, Y.H.; Jouppila, K. Effect of various polyols and polyol contents on physical and mechanical properties of potato starch-based films. Carbohydrate Polymers. 2007, 67, 288–295.

(17) Schou, M.; Longares, A.; Montesinos-Herrero, C.; Monahan, F.J.; O'Riordan, D.; O'Sullivan, M. Properties of edible sodium caseinate films and their application as food wrapping, Lebensmittel-Wissenschaft und-Technologie. 2005. 38, 605–610.

(18) Padua, G.W.; Rakoronirainy, A.; Wang, Q. Zein-based biodegradable packaging for frozen foods. In: Conference Proceedings. The Food Biopack Conference. 2000, Denmark 27-29, pp. 84-88.

(19) Arora, A.; Pádua, G.W. Review: Nanocomposites in Food Packaging. Journal of Food Science. 2010, 75 (1), pp. R43-R49.

(20) Kim, S. Processing and properties of gluten/zein composite. Bioresource Technology. 2008, 99, 2032–2036

(21) Corradini, E.; De Medeiros, E.S.; Carvalho, A.J.F.; Curvelo, A.A.S.; Mattoso, L.H.C. Mechanical and Morphological Characterization of Starch/Zein Blends Plasticized with Glycerol. Journal of Applied Polymer Science. 2006, 101, 4133–4139.

(22) Pol, H.; Dawson, P.; Acton, J. ; Ogale, A. Soy Protein Isolate/Corn-Zein Laminated Films: Transport and Mechanical Properties. Journal of food science. 2002, 67, nr. 1.

(23) Corradini, E.; de Carvalho, A.J.F.; Curvelo, A.A da S.; Agnelli, J.A.M.; Mattoso, L.H.C. Preparation and Characterization of Thermoplastic Starch/Zein Blends. Materials Research. 2007, Vol. 10, No. 3, 227-231.

(24) Daniel-Da-Silva, A.L.; Lopes, A.B.; Gil, A.M.; Correia, R.N. Synthesis and characterization of porous κ-carrageenan/calcium phosphate nanocomposite scaffolds. J Mater Sci. 2007, 42:8581–8591.

(25) Gan, S.-L.; Feng, Q.-L. Preparation and characterization of a new injectable bone substitute-carrageenan/nano-hydroxyapatite/collagen. Acta Academiae Medicinae Sinicae. 2006, 28 (5), pp. 710-713.

(26) Olabarrieta I.; Gällstedt, M.; Ispizua, I.; Sarasua, J.R.; Hedenqvist, M.S. Properties of Aged Montmorillonite-Wheat Gluten Composite Films. J. Agric. Food Chem. 2006, 54, 1283-1288.

(27) Wang, N.; Zhang, X.; Han, N.; Bai, S.. Effect of citric acid and processing on the performance of thermoplastic starch/montmorillonite nanocomposites Carbohydrate Polymers. 2009, 76, 68–73.

(28) Chang, J-H.; Uk-An, Y.; Sur, G.S. Poly(lactic acid) nanocomposites with various organoclays. I. thermomechanical properties, morphology, and gas permeability. J Polym Sci Part B: Polym Phys. 2003, 41:94–103.

(29) Majdzadeh-Ardakani, K.; Navarchian, A.H.; Sadeghi, F. Optimization of mechanical properties of thermoplastic starch/clay nanocomposites. Carbohydrate Polymers. 2010. 79, 547–554.

(30) Soundararajah, Q.Y.; Karunaratne, B.S.B; Rajapakse, R.M.G.; Montmorillonite polyaniline nanocomposites: Preparation, characterization and investigation of mechanical properties. Materials Chemistry and Physics. 2009, 113, 850–855.

(31) Ganguly, A.; Bhowmick, A. K. Effect of polar modification on morphology and properties of styrene-(ethylene-co-butylene)-styrene triblock copolymer and its montmorillonite clay-based nanocomposites. Mater Sci. 2009, 44:903–918.

(32) Guo, J. H. Effects of plasticizers on water permeation and mechanical properties of cellulose acetate: antiplasticization in slightly plasticized polymer film. Drug Development and Industrial Pharmacy. 1993, 19(13), 1541–1555.

(33) Zeppa C.; Gouanve, F.; Espuche, E. Effect of a Plasticizer on the Structure of Biodegradable Starch/Clay Nanocomposites: Thermal, Water-Sorption, and Oxygen-Barrier Properties. Journal of Applied Polymer Science. 2009, Vol. 112, 2044–2056.

(34) Parris, N.; Dickey, L.C.; Kurantz, M.J.; Moten, R.O.; Craig, J. C. Water vapor permeability and solubility of zein/starch hydrophilic films prepared from dry milled corn extract. Journal of Food Engineering. 1997, Volume 32, Issue 2, Pages 199-207.

(35) Ghanbarzadeh, B.; Musavi, M.; Oromiehie, A.R.; Rezayi, K.; Razmi Rad, E.; Milani, J. Effect of plasticizing sugars on water vapor permeability, surface energy and microstructure properties of zein films. Food Science and Technology. 2007, Volume 40, Issue 7, Pages 1191-1197.

(36) Nielsen, L. W. J. Macromol Sci.1967, Al, 929.

(37) Maxwell, J. C. Electricity and Magnetism. 1891, Vol. 1, 3rd., Dover. New York.

(38) Fricke, H. A Mathematical Treatment of the Electric Conductivity and Capacity of Disperse Systems I. The Electric Conductivity of a Suspension of Homogeneous Spheroids. Phys. Rev.1924, 24, 575.

(39) Paul D.R.; Bucknall, C.B. Polymer Blends. 2000,Volume 2: Performance.

PAPER V: Novel Polycaprolactone Nanocomposites containing Thymol of interest in antimicrobial film and coating applications.

Abstract

It is well-known that the nanocomposites technology can significantly enhance, among others, the thermal, mechanical, and barrier properties of plastics. It is also known that most bioplastics, including the thermoplastic biopolymers, have lower than desired levels for certain properties which makes their use in certain packaging applications problematic. The combination of active technologies such as antimicrobials and nanotechnologies such as nanocomposites can synergistically lead to bioplastic formulations with balanced properties and functionalities for their implementation in packaging applications. The present work presents the development and characterization of novel nanocomposites of polycaprolactone with enhanced barrier properties and with controlled-release of the biocide natural extract thymol. The antimicrobial nanocomposites of biodegradable materials were prepared in solution by a casting method. The morphology of the biocomposites was visualized by transmission electron microscopy and by atomic force microscopy, the thermal properties were investigated by differential scanning calorimetry and the relative uptake (solubility) and kinetics (diffusion) of the released biocide were determined by Attenuated Total Reflection Fourier Transformed Infrared spectroscopy. Water, oxygen, and limonene barrier properties were also enhanced in the biocomposites.

Keywords: nanocomposites, biodegradable materials, antimicrobial properties.

Introduction

Active Technologies in packaging have been defined as systems in which the product, the package, and the environment interact in a positive way to extend shelf-life or to achieve some characteristics that
cannot be obtained otherwise [1]. The main aim of active packaging technologies is to change the conditions of packaged food in order to extend the shelf-life [2]. This practice can improve food safety and sensory properties, while maintaining the quality of packaged food. Active packaging techniques for conservation and improving quality and safety of foods and of other products can be divided into three classes: (i) absorbing systems; (ii) releasing systems; and (iii) other speciality systems for temperature, ultraviolet light and microwave management [3]. Antimicrobial activity can be realized by adding antimicrobial (AM) agents to a packaging system during manufacturing or by using AM polymeric materials [4]. There are three typical systems of AM agent activity: (i) absorption; (ii) immobilization; and (iii) release systems. The release system allows the migration of the AM agent into the food or the headspace inside the package to inhibit the growth of microorganisms. Controlled release packaging is a new generation of packaging materials that can release active compounds at different controlled rates suitable for enhancing the quality and safety of foods during extended storage. The substances that are possible to include in the release packaging are nutrients, antimicrobials, antioxidants, enzymes, flavors, and biocides components. The incorporation of antimicrobial substances in the releasing packaging permit the gradual migration of the antimicrobial to the food during storage and distribution of the foods. The antimicrobial packaging is effective in minimizing the superficial contamination of foods such as meats, fruits, vegetables, etc. The antimicrobial substances used in food packaging that migrate to the food should be in accordance with the food additives and active food contact legislation, which is currently under preparation in the European Union area [5]. In this work, we present the formulation of novel antimicrobial nanocomposites of polycaprolactone (PCL) as a way to control solubility and diffusion of the natural biocide agent thymol. Thymol is a phenolic monoterpene that has received considerable attention as an antimicrobial agent with very high antifungal activity and very low Minimum Inhibitory Concentration (MIC) values [6] and is also an excellent food antioxidant [7].

Materials and Methods

Materials

The PCL grade FB100 was kindly supplied in pellet form by Solvay Chemicals, Belgium. This grade has a density of 1.1 g/cm^3 and a mean
molecular weight of 100,000 g/mol. A proprietary (patent pending) food contact compliant commercial laminar phyllosilicate grade termed NanoBioTer^R AC11 based on a natural mica modified with a food contact surfactant, which is listed by EU and FDA, legislations, was kindly supplied in powder form by NanoBioMatters S.L., Paterna, Spain.

The antimicrobial agent thymol (#89330) was purchased from Fluka Chemie, (Buchs, Switzerland), in powder form. The purity of this material was ~ 99.0% and the molecular weight was 150.22 g/mol.

Preparation of Nanocomposites

Solution-cast film samples of the biodegradable material (PCL) containing 1, 5, and 10 wt% filler contents and 10 wt% of thymol (related to the weight of PCL) were prepared with a dry film thickness of around 100 mm. The proprietary biocide nanobiocomposite solutions in chloroform, which were provided by NanoBioMatters S.L., were homogenized for 2 min, stirred at 40ºC for 30 min and, then cast onto Petri dishes to generate films after solvent evaporation at room temperature conditions.

TEM Measurements

Transmission electron microscopy (TEM) was performed using a JEOL 1010 equipped with a digital Bioscan (Gatan) image acquisition system at 5 kv. The films were embedded in epoxy resin and TEM observations in the cross section were performed on thin sections, i.e., ca. 70 nm, of ultramicrotomed nanocomposite sheets.

AFM Measurements

AFM measurements were performed using an Agilent 5500 SPM system (provided by Scientec Ibérica, Spain) to investigate the morphology of the nanocomposite surfaces on both sides of the cast films. The images were scanned in tapping mode in air using commercial Si cantilevers with a resonance frequency of 320 kHz.

DSC Measurements

Differential scanning calorimetry (DSC) of PCL and its nanocomposites was performed on a Perkin–Elmer DSC 7 thermal analysis system on typically 7mg of material at a scanning speed of 10ºC/min from room temperature to the melting point of the PCL. The DSC equipment was calibrated using indium as a standard. The thermograms were corrected with an empty pan.

Gravimetric Measurements

Direct permeability to water and d(±)limonene of 95% purity (Panreac Química, Spain) was determined from the slope of the weight loss–time curves at 24ºC and 40%RH. The films were sandwiched between the aluminum top (open O-ring) and bottom (deposit for the permeant) parts of a specifically designed permeability cell with screws. A Viton rubber O-ring was placed between the film and the bottom part of the cell to enhance sealability. Then the bottom part of the cell was filled with the permeant and the pinhole secured with a rubber O-ring and a screw. Finally, the cell was placed in the desired environment and the solvent weight loss through a film area of 0.001m^2 was monitored and plotted as a function of time. Cells with aluminium films (with thickness of ca. 100 mm) were used as control samples to estimate solvent loss through the sealing. The permeability sensitivity of the permeation cells was

determined to be better than $0.01x10^{-13}$ kg m/sm^2 Pa based on the weight loss measurements of the aluminium cells. Cells clamping polymer films, but with no solvent, were used as blank samples to monitor water, uptake. Solvent permeation rates were estimated from the steady-state permeation slopes. Organic vapor weight loss was calculated as the total cell loss minus the loss through the sealing and plus the water weight gain. The tests were done in triplicate and average values and standard errors are provided. For the case of water permeability the cells containing liquid water were stored in a desiccator at 0%RH and weighed over time.

Oxygen Transmission Rate

The oxygen permeability coefficient was derived from oxygen transmission rate (OTR). The OTR is defined as the quantity of oxygen gas passing through a unit area of the parallel surface of a plastic film per unit time under predefined oxygen partial pressure, temperature, and relative humidity. The OTR was measured using an Oxtran 100 (Modern Control Inc., Minneapolis, MN, US). The oxygen
permeability coefficient is the product of the permeance (the ratio of the OTR to the difference between the partial pressure of oxygen on the two sides of the films) and the film thickness. During all experiments temperature and relative humidity were held at 24ºC and 80%RH humidity. Eighty percent of relative humidity was generated by a built-in gas bubbler and was checked with a hygrometer placed at the exit of the detector. To avoid sample humidity equilibration during the actual OTR test at 80%RH and the subsequent fluctuations on barrier during the test, the samples were preconditioned at this RH by storage in a desiccator set up at this RH by appropriate salt solution.
The experiments were done in duplicate and the samples were purged with nitrogen for a minimum of 20 h, prior to exposure to a 100% oxygen flow of 10 mL/min, and a 5cm^2 sample area was measured by using an in-house developed mask. Permeability (P) coefficient was estimated from fitting the OTR-time curve to the first six sum terms (n) of the following solution of the Fick's second law:

$$OTR(t) = \frac{Pp}{l}\left[1 + 2\sum_{n=1}^{\infty}(-1)^n \exp(-\frac{D\pi^2 n^2 t}{l^2})\right] \quad (1)$$

Where Pp=oxygen partial pressure, l=film thickness, D=diffusion coefficient, t=time.

ATR Measurements

Thymol release kinetics and the diffusion coefficients to thymol were determined by ATR reflection spectroscopy during desorption of the antimicrobial substance. In order to do so, the nanobiocompositesthymol solutions were cast on the surface of the ATR crystal to follow the kinetics of release of this substance. All ATR experiments were carried out at 24ºC. Data fitting to a suitable model is required to derive a quantitative measure of diffusion kinetics from experimental curves obtained using ATR-FTIR spectroscopy. To obtain D-values from these sorption curves, the experimental curves must be fitted to the appropriate solution of Fick's second law of

diffusion for the case of a plane sheet (Equation (2)) modified to suit an ATR experiment (Equation (3)) as proposed by Fieldson et al. [8]:

$$\frac{M_t}{M_\infty} = 1 - \sum_{n=0}^{\infty} \frac{8}{(2n+1)^2 \pi^2} \exp\left[\frac{-D(2n+1)^2 \pi^2 t}{4L^2}\right] \quad (2)$$

$$\frac{A_t}{A_\infty} = 1 - \frac{8\gamma}{\pi\left[1-\exp(-2\gamma L)\right]} \sum_{n=0}^{\infty} \left[\frac{\exp\frac{-D(2n+1)^2\pi^2 t}{4L^2}\left[\frac{(2n+1)\pi}{2L}\exp(-2\gamma L) + (-1)^n (2\gamma)\right]}{(2n+1)\left(4\gamma^2 + \frac{(2n+1)\pi}{2L}\right)}\right] \quad (3)$$

Where

A_t and A_∞ =the spectral absorptions at a time t and equilibrium, respectively, the spectral absorptions at a time t and equilibrium, respectively, d_p=the penetration depth of the evanescent field, γ=1/dp, D=the diffusion coefficient, L=the film thickness.

However, in an analogous manner to that described in previous works [9], a simplified approach was used to determine D values, which is based on an observed initial 'lag' time (normalized to path length L), during which little sorption occurs within the evanescent field, followed by a pseudo-Fickian behavior predicted from Equation (3) at short times.

$$\frac{A_t}{A_\infty} = \frac{2}{L}\left(\frac{D}{\pi}\right)^n t^n \quad (4)$$

$$n = 0.5$$

In Equation (4), A_t and A_∞ are the absorbances (of the thymol ring vibration band at 807 cm^{-1}) at a given time t and at saturation or equilibrium sorption conditions, respectively.

Results and Discussion

Morphology

Figure 1(a) shows a typical TEM image for one of the specimens of PCL+5 wt% NanoBioTer™ AC. From the picture a large dispersion of the filler particles and partial exfoliation of the platelets to particle thickness in the nano-range can be observed. Figure 1(b) shows the surface roughness of a similar cast sample by AFM. From this picture it can be seen that the particles are largely dispersed and intercalated by the biopolymer. This image also shows that there appears to be a good adhesion of the filler to the biopolymer due to the appropriate surface modification of the filler.

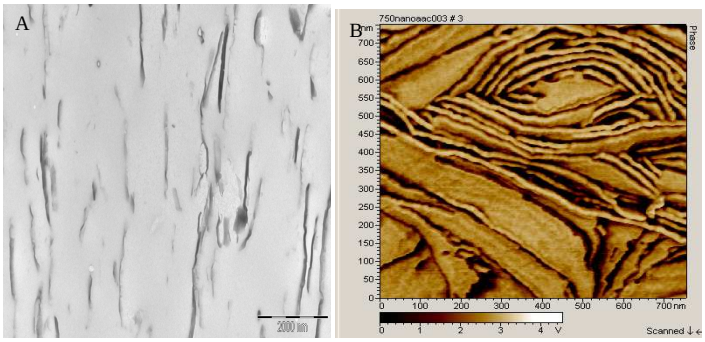

Figure 1. A) TEM picture of the 5 wt.-% AC11 PCL composite. Scale markers are 2000nm. B) AFM picture of the same.

Thermal Properties

Melting temperature (T_m) and heat of fusion (ΔH_m) corrected for biopolymer content in the nanobiocomposites were determined from the DSC thermograms of the samples. These are summarized in Table 1 for cast films of PCL with different AC11 filler contents. From Table 1, it is seen that the heat of fusion of the biomaterial tends to increase with clay addition. The differential increase between 1 and 5 wt% clay loading may not be statistically significant. The PCL melting point is seen to remain largely unmodified. The latter result adds to similar nucleating observations reported in previous works for PHB/PCL nanocomposites [10], and suggests that the clay can act as a heterophase nucleating agent, hence promoting somewhat higher crystallinity in the matrix.

Table 1. DSC melting point and melting enthalpy of the neat films of PCL and of their nanocomposites with 1, 5 and 10 wt.-% AC11 content prepared by solving casting

Sample	Tm (ºC)	ΔHm (J/g)
PCL	63.25±0.09	55.94±4.40
PCL+1% AC11	63.09±0.19	60.17±1.79
PCL+5% AC11	61.86±0.29	62.55±1.38
PCL+10% AC11	63.91±0.92	69.71±0.0

Mass Transport Properties

Table 2 summarizes the water, d-limonene, and oxygen permeability of PCL and of the nanocomposites. A curious observation from Table 2 is that the water permeability coefficient of $0.34x10^{-13}$ kg m/sm^2 Pa is much higher than that of $0.0023x10^{-13}$ kg m/sm^2 Pa previously reported for toluene cast PCL [11]. The reason for the disagreement could be related to the different origins of the two samples (lab scale solvent cast material vs. industrial scale material production) and the fact that

molecular weight, the solvent used for the casting and the differences in relative humidity gradient used for testing were totally different.

From the results, films of PCL with 1 wt% AC11 filler content havea water permeability decrease of 53% compared to the unfilled material and the films with 5 and 10 wt% of AC11 filler contents have the same water permeability reduction of 63%. In the case of the limonene permeability, films of PCL with 1, 5, and 10 wt% AC11 filler contents have a limonene permeability decrease of 18, 49, and 25%, respectively, compared to the unfilled material. The lowest limonene permeability value is for the sample with 5 wt% AC11 filler content.

Table 2 shows the oxygen permeability of PCL and their nanocomposite measured at 80% RH. Films of PCL with 1 wt% AC11 filler contents show an oxygen permeability reduction of ca. 22% compared to the unfilled material and the films with 5 and 10 wt% AC11 filler contents have the same oxygen permeability reduction of 48%. In general, films with 5 wt% AC11 filler content show the lowest permeability value. This observation may indicate that there must be a balance in the nanobiocomposites between the content of filler used, which has in itself barrier capacity, the morphology of the nanocomposite samples and the possibility of a permeability deterioration that may be caused by filler agglomeration (clay solubility limit).

	P water (Kg m/s m^2 Pa)	P limonene (Kg m/s m2 Pa)	P oxygen (m3 m/s m2 Pa)
PCL	$0.34\pm0.061e^{-13}$	$5.05\pm0.65e^{-13}$	$7.06e^{-18}$
PCL+1% AC11	$0.16\pm0.005e^{-13}$	$4.16\pm1.18e^{-13}$	$5.48\pm0.27e^{-18}$
PCL+5% AC11	$0.12\pm0.005e^{-13}$	$2.58\pm0.57e^{-13}$	$3.68\pm0.28e^{-18}$
PCL+10% AC11	$0.12\pm0.001e^{-13}$	$3.80\pm0.57e^{-13}$	$3.67e^{-18}$
[11]PCL Literature Value	$0.0023e^{-13}$		

Table 2. Water and D-Limonene permeability for PCL and their nanocomposites prepared by casting.

ATR Measurements

The IR spectrum of the thymol type is very similar to that of the corresponding chemo type of basil, recently described elsewhere [12]. The most intense peaks at 738 and 807 cm^{-1} are assigned to ring vibrations of the thymol chemistry [13]. Systematic release studies were performed for thymol incorporated in the nanocomposite of the biodegradable material for a time period of up to 2 weeks. Figure 2(a)
shows the decrease of the band (C-Cl stretching) associated to the chloroform [14] compound as the film forms and the subsequent release of thymol from the formed film as followed by the decrease of the band at 807 cm^{-1} over time. The spectra also show a concomitant

increase of the PCL signal in the ATR evanescent field due to polymer deswelling (thickness reduction) as thymol is released from the matrix and the polymer reduces free volume. Figure 2(b) shows, as an example, how the natural antimicrobial agent is released with slower kinetics due to the presence of the nanoclay. Figure 2(c) shows (see arrow) that before the release of thymol the nanocomposites have higher uptake or solubility of the natural antimicrobial than the neat polymer due to the presence of the nanoclay. The IR spectrum also shows some other differences in the bands between PCL spectra and PCL nanocomposite spectra as a result of overlapping with other thymol bands. Figure 3 shows how the natural antimicrobial agent uptake or solubility, referred to the above infrared band intensity for the neat material, is enhanced by the presence of the nanoplatelets. This is possibly due to retention over the surface of the apolar biocide agent. The thymol diffusion coefficient (Figure 4) is on the other hand seen to decrease with the addition of the nanoadditive in the biocomposite as expected from observation of Figure 2(b). This is likely the result of the larger tortuosity effect imposed to the diffusion of the biocide by the dispersed nanoclay. From the results, it is possible to observe a reduction in thymol diffusion coefficient of ca. 58% with regard to the unfilled material. These results confirm that it is feasible to control the uptake and release of thymol by incorporation of laminar nanoclays in bioplastics such as PCL.

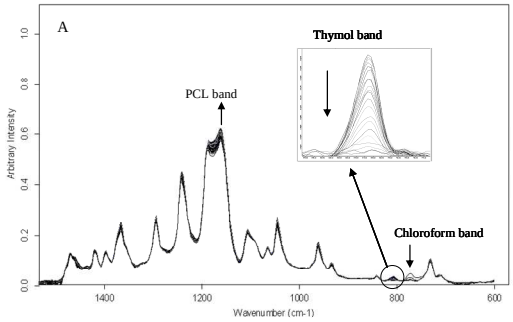

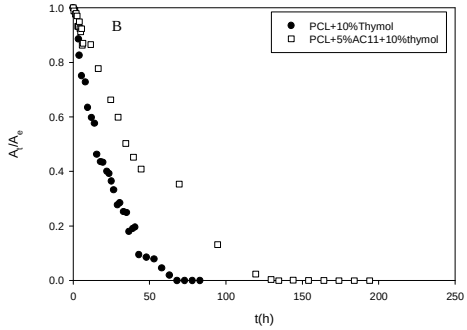

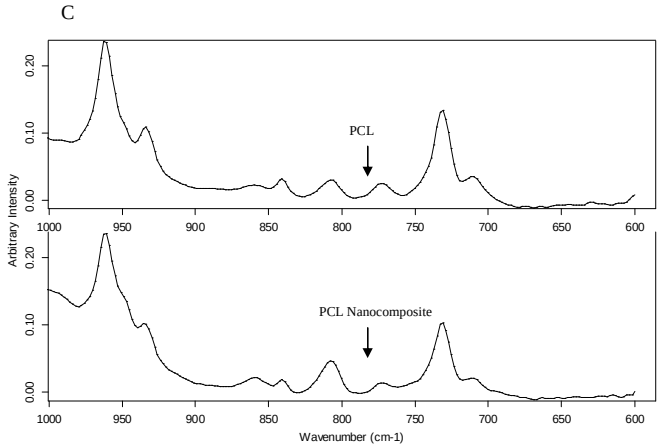

Figure 2. (a) ATR-FTIR spectra of the thymol release from neat PCL, (b) Normalized ATR desorption (A_t, absorbance at any time t during the desorption vs. Ae, initial equilibrium absorbance at time zero) kinetics of the release of thymol from the PCL matrix and PCL nanocomposites, (c) ATR-FTIR spectra of the thymol uptake before the release experiment for PCL and the nanocomposite of PCL. The two spectra in Figure 2(c) were stacked for easy of comparison.

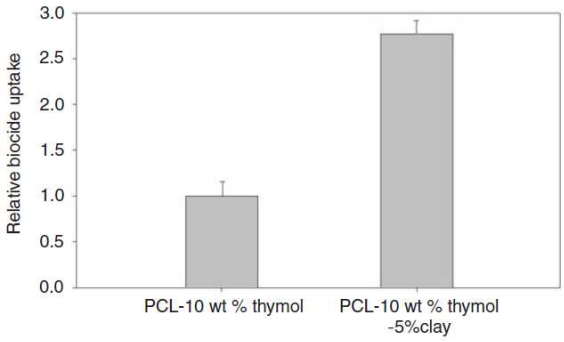

Figure 3. Relative uptake or solubility coefficient ($A_{composite}/A_{neat}$) of thymol as determined by ATR-FTIR spectroscopy in neat PCL matrix and in the nanocomposite.

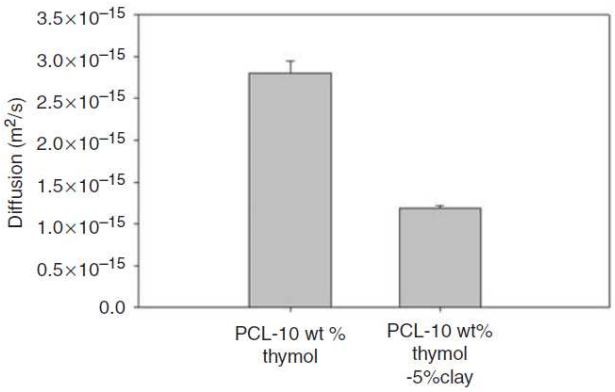

Figure 4. Diffusion coefficient (m^2/s) for the release of thymol from the PCL matrix and the PCL nanocomposite.

Summary

The addition of novel organoclays – based on mica – to biodegradable polymers is a very promising technology that can enhance the properties of biodegradable polymers and, therefore, enhance product quality and safety aspects in film and coating applications. In this context, functional nanoadditives with tailor made EU and FDA food contact approved surface modifications are shown to have significant potential to enhance barrier properties of these biomaterials in food contact and other applications. Moreover, these nanoadditives can also help to enhance the solubility of natural biocides in the biopolymer matrix and to control the release of natural antimicrobials with interest in the design of novel active antimicrobial film and coating systems.

Acknowledgments

The authors would like to acknowledge the EU integrated project SUSTAINPACK for financial support. NanoBioMatters S.L., Paterna (Spain) and the Spanish MEC project MAT2006-10261-C03 are also acknowledged for financial support. Finally, M.D.S.G. would like to thank the FPI program of the GV associated to the MEC project MAT2003-08480-C3 for the research grant.

References

1. Miltz, J., Passy, N. and Mannhwim, C.H. (1995). Trends and Applications of Active Packaging Systems. In: Ackerman, P., Ja¨gerstad, M. and Ohlsson, P. (eds), Food and Packaging Materials - Chemical Interaction, pp. 201–210,
The Royal Society of Chemistry.

2. Ahvenainen, R. (2003). Active and Intelligent Packaging. In: Ahvenainen, R. (ed.), Novel Food Packaging Techniques, Woodhead Publishing Limited,
Cambridge, UK.

3. Han, J.H. (2003). Antimicrobial Food Packaging. In: Ahvenainen, R. (ed.), Novel Food Packaging Techniques, Woodhead Publishing Limited, Cambridge, UK.

4. Hotchkiss, J.H. (1997). Food Packaging Interactions Influencing Quality and Safety, Food Addit. Contam., 14(6-7): 601–607.

5. Directive 2001/62/EC of the Official Journal of the European Communities relating to plastics materials and articles intended to come into contact with foodstuffs.

6. Thompson, D.P. (1989). Fungitoxic Activity of Essential Oil Components on Food Storagefungi, Mycologia, 81(1): 151–153.

7. Youdim, K.A. and Deanes, S.G. (2000). Effect of Thyme Oil and Thymol Dietary Supplementation on the Antioxident Status and Fatty Acid Composition of the Ageing Rat Brain, J. Nutrition, 83(1): 87–93.

8. Crank, J. (1975). The Mathematics of Diffusion, 2nd edn, Oxford, UK: Oxford Science Publications.

9. Sammon, C., Yarwood, J. and Everall, N. (2000). A FTIR-ATR Study of Liquid Diffusion Processes in PET Films: Comparison of Water with Simple Alcohols, Polymer, 41(7): 2521–2534.

10. Sanchez-Garcia, M.D., Gimenez, E. and Lagaron, J.M. (2008). Development and Characterization of Novel Nanobiocomposites of Bacterial Poly(3-hydroxybutirate), Layered silicates and Poly("-caprolactone), J. Appl. Polym. Sci., 108(5): 2787–2801.

11. Messersmith, P.B. and Giannelis, E.P. (1995). Synthesis and Barrier Properties of Poly(Epsilon-Caprolactone)-Layered Silicate Nanocomposite, J. Polym. Sci. Part A: Polym. Chem., 33(7): 1047–1057.

12. Schulz, H., Schrader, B., Quilitzsch, R., Pfeffer, S. and Kruger, H. (2003). Rapid Classification of Basil Chemotypes by Various Vibrational Spectroscopy Methods, J. Agric. Food Chem., 51(9): 2475–2981.

13. Schulz, H., Quilitzsch, R. and Kruger, H. (2003). Rapid Evaluation and Quantitative Analysis of Thyme, Origano and Chamomile Essential Oils byATR-IR and NIR Spectroscopy, J. Molec. Struct., 661–662: 299–306.

14. Roeges, N.P.G. (1994). A Guide to the Complete Interpretation of Infrared Spectra of Organic Structures, p. 94, England: John Wiley & Sons Ltd.

Chapter II.

Nanobiocomposites based on micro and nano cellulose fibers.

PAPER VI: Morphology and barrier properties of solvent cast composites of thermoplastic biopolymers and purified cellulose fibers

Abstract

This paper shows and discusses the morphology, thermal and transport properties of solvent cast biocomposites of poly(lactic acid) (PLA), polyhydroxybutyrate-co-valerate (PHBV) and polycaprolactones (PCL) containing purified alfa micro-cellulose fibers as a function of filler content. The SEM, optical microscopy and Raman imaging results indicate that a good dispersion of the fibers in the matrix was achieved for the three biopolymers. However, detrimental fiber agglomeration was clearly observed to take place for samples with fiber contents in excess of 5 wt%. The heat of fusion (related to crystallinity) of the semicrystalline PCL and PHBV biopolymers was seen to decrease, particularly in low fiber content biocomposites, but it seemed to increase slightly in the highly amorphous PLA biocomposites. In accordance with the morphology data, water and D-limonene direct permeability were seen to decrease to a significant extent in the biocomposites with low fiber contents. The permeability reduction was mostly related to a decrease in diffusivity but solubility was also found to be favorable. The main conclusion from this work is that purified cellulose fibers can also be used to enhance the barrier properties of thermoplastic biopolyesters of interest in, for instance, packaging and membrane applications.

Keywords: Cellulose fibers; Composites; Barrier properties; PLA; PCL and PHBV

Introduction

There is a growing worldwide interest pushed by governments and societies to increment the responsible use of renewable resources in commodity plastic products in order to reduce the waste associated to their use, particularly in packaging applications (Petersen et al., 1999; Haugaard et al., 2001). The use of biodegradable plastics and resources are seen as one of the many strategies to minimise the environmental impact of petroleum-based plastics. The biological base of these new biopolymers provides a unique opportunity to incorporate a highly demanded property of these materials, i.e. the compostability. It must be considered that among the plastic waste there are products with a high degree of contamination and recycling requires a high energy cost. Therefore, compostability is a very interesting property that guarantees that these new biomaterials will degrade mostly into carbon dioxide and water after disposal (Kijchavengkul, Auras, Rubino, Ngouajio, & Fernandez, 2006). These biodegradable materials present a number of excellent and promising properties in a number of applications, including packaging, automotive and biomedical sectors. Thus, thermoplastic biodegradable polymers, such as poly(lactic acid) (PLA), polyhydroxyalkanoate (PHA) and polycaprolactones (PCL), exhibit an excellent equilibrium of properties, i.e. they are processable using conventional plastics machinery and, for the case of the first two, they arise from renewable resources. PLA is a thermoplastic biopolyester produced from L-lactid acid, which typically comes from the fermentation of corn starch. Currently, PLA is being commercialized and being used as a food packaging polymer for short shelf-life products with common applications such as containers, drinking cups, sundae, and salad cups, overwrap and lamination films, and blister packages (Auras, Kale, & Singh, 2006). In PHAs (polyhydroxyalkanoates) family, the most widely used material is the polyhydroxybutyrate (PHB) and its copolymers with valerate. These microbial biopolymers are storage materials produced by a variety of bacteria in response to particular environmental stresses (Peoples & Sinskey, 1990). Polyhydroxybutyrate (PHB) is a naturally occurring b-hydroxyacid (a linear polyester). The homopolymer, poly(hydroxybutyrate) PHB, and its copolymer with hydroxyvalerate, PHBV, are biodegradable engineering thermoplastic polymers with important trade properties that make them suitable in many applications for which petroleum-based synthetic polymers are currently used. PHB polymers are already being used in small disposable products and in packaging materials (Rosa, Lotto, Lopes, & Guedes, 2004). Finally, PCL is a thermoplastic biodegradable polyester synthesized by chemical conversion of crude oil. PCL has good water, oil, solvent, and chlorine resistance, a low melting point, and low viscosity, and is easily processed using conventional melt blending technologies (Gross & Kalra, 2002). PCL is at this time being investigated for its use in biomedical utensils, pharmaceutical controlled release systems, and in biodegradable packaging (PigŁowski & Kiersnowski, 2006; Iannace, Luca, & Nicolais, 1990). In order to tailor the properties and reduce material costs, it is often desirable to combine bioplastic materials with other, ideally, more inexpensive substances, such as natural fibers (Bodros, Pillin, Montrelay,&Baley, 2007). Reinforcement of some of these bioplastics with lignocellulosic fibers has previously been carried out with the overall aim of increasing its biodegradation rate and to enhance mechanical properties, i.e. this route led to considerable improvements in the composites tensile strength (Tserki, Matzinos, Zafeiropoulos, & Panayiotou, 2006).

However, to the best of our knowledge there is not prior literature on the use of these reinforced biocomposites to modify the barrier properties of such biopolymers. Lignocellulosic materials appear to be suitable fillers or reinforcing agents for biodegradable matrices since they exhibit interesting properties such as a renewable nature, wide variety of feedstocks available throughout the world, nonfood agricultural-based economy, low energy consumption, low cost, low density, high specific strength and modulus, high sound attenuation of lignocellulosic- based composites, comparatively easy processability due to their nonabrasive nature, which allows high filling levels and significant cost savings, and finally relatively high reactive surface, which can be used for grafting specific groups (Orts et al., 2005). Thus, the use of lignocellulosic fibers derived from annually renewable resources as a reinforcing phase in polymeric matrix composites provides positive environmental benefits with respect to ultimate disposability and raw materials use. A major disadvantage of cellulose fibers is their hydrophilic character that makes them, in principle, sparingly miscible with less polar or nonpolar polymers (Mutje, Girones, & Lopez, 2006). Therefore, to develop such biocomposites with optimum properties, it has been customary to decrease the hydrophilicity of the lignocellulosic materials by chemical modification or to promote interfacial adhesion through the use of compatibilizers (Nitz, Semke, Landers, & Mulhaupt, 2001). The chemical modification is usually obtained through the use of reagents having functional groups that are capable of bonding to the hydroxyl groups of the lignocellulosic materials (Rana, Basak, Mitra, Lawther, & Banerjee, 1997; Ichazo, Albano, Gonzalez, Perera, & Candal, 2001). Another drawback of lignocellulosic fillers is their high moisture absorption and the resulting swelling and decrease in mechanical properties (Najafi, Tajvidi, & Chaharmahli, 2006.) Moreover, the processing temperature of composites is restricted to about 200 ºC because lignocellulosic materials exhibit significant degradation processes above this temperature. In spite of that, higher thermal stability, less color, more homogeneity and enhanced properties can be achieved by using highly purified alfa cellulose fibers. In the latter material, lignin and hemicellulose residues have been virtually eliminated from the natural fiber and, therefore, a more robust filler is thus generated (Malainine, Mahrouz, & Dufresne, 2004). Properties of fiber reinforced composites depend on many factors, for instance fiber/matrix adhesion, volume fraction of fiber, fiber aspect ratio, fiber orientation, and stress/transfer efficiency through the interface (Dufresne, Dupeyre, & Paillet, 2003). Fiber size and processing techniques have a significant incidence on the final properties of the composites, because they define the degree of fiber dispersion and their impact on matrix morphology. Fiber content in biodegradable polymers is also frequently associated with the degree of dispersion or agglomeration of the fibers, because high fiber contents in the matrix produce fiber agglomeration, caused by the tendency of the filler to form hydrogen bonding with each other (Tserki et al., 2006). As mentioned above, fiber dispersion has a stronger effect in themechanical properties of the composites, which can ultimately be reflected on other potential properties such as barrier properties. The presence of impermeable crystalline fibers is thought to increase the tortuosity or detour factor in the materials leading to slower diffusion processes and, hence, to lower permeability. To enhance barrier properties to gases and vapors the filler should be less permeable or impermeable and have optimum dispersion and a high aspect ratio (filler length/thickness ratio) (Lagaron, Catalá, & Gavara, 2004). Fiber size is also relevant because by reducing fiber size, high surface to volume ratio of the filler in the matrix is achieved, and this makes possible to

strongly impact properties with low additions of the reinforcing elements without detrimental impact on other important parameters such as crystallinity, optical properties and material toughness. The literature results show that composites with a smaller particle size and good dispersion have higher properties compared to others of greater size (Khalil, Shahnaz, Ratnam, Ahmad, & Fuaad, 2006).Current technologies allowto reduce fiber cross-section to the nanometer level as in the case of the so-called Micro Fibrillated Cellulose (MFC) (Lopez-Rubio et al., 2007) or in electrospun cellulose fibers (Huang, Zhang, & Kotaki, 2003). In summary, it is well known that cellulose fibers can enhance mechanical properties in as much as other synthetic fibers (Nabi Sahed & Jog, 1999), however, very little is known about their impact on barrier properties. Regarding the latter, only a previous work reported about reductions in oxygen permeability for PLA composites containing microcrystal cellulose (Petersson & Oksman, 2006). In this first study, the morphology and solvent barrier properties as a function of filler content of biocomposites of PLA, PCL and PHBV containing purified alfa cellulose fibers as reinforcing elements are presented and discussed.

Materials and Methods

Materials

The bacterial polyhydroxyalkanoate grade was purchased to Goodfellow Cambridge Limited, UK, in pellet form. The supplied material was a melt-processable semicrystalline thermoplastic PHBV (Polyhydroxybutyrate with 12 mol% of Valerate) copolymer made by biological fermentation from renewable carbohydrate feedstocks. The PCL grade FB100 was kindly supplied in pellet form by Solvay Chemicals, Belgium. This grade has a density of 1.1 g/cm3 and a mean molecular weight of 100,000 g/mol. The semicrystalline PLA used was a film extrusion grade manufactured by Natureworks (with a D-isomer content of approximately 2%). The molecular weight had a number–average molecular weight (Mn) of ca. 130,000 g/mol, and the weight–average molecular weight (Mw) was ca. 150,000 g/mol. A purified cellulose fiber grade from CreaFill Fibers Corp. (US), having an average fiber length of 60 lm and an average fiber width of 20 lm was used. According to manufacturer's specifications, these fibers had an alfa-cellulose content of >99.5% and an aspect ratio of ca. 3.

Preparation of the blends.

Solution-cast film samples of the biodegradables materials with 1, 2, 4, 5, and 10 wt% fiber contents were prepared with a dry film thickness of around 100 lm, using chloroform as a solvent. Fiber solutions in chloroform were mixed in a homogenizer (Ultraturrax T25 basic, Ika-Werke, Germany) for 2 min and were then stirred with the polymer at 40 ºC during 30 min and, subsequently, cast onto Petri dishes to generate films after solvent evaporation at room temperature conditions.

SEM measurements

For scanning electron microscopy (SEM) observation, the samples were cryofractured by hand after immersion in liquid nitrogen, mounted on bevel sample holders and sputtered with Au/Pd in a vacuum. The SEM pictures (Hitachi S4100) were taken with an accelerating voltage of 10 keV on the sample thickness.

AFM measurements

AFM measurements were performed using a Nano-Scope IIIa (Digital Instruments Inc.) to investigate the morphology on the top and fracture surfaces of the cast films in the biocomposites. The images were scanned in tapping mode in air using commercial Si cantilevers (Digital Instruments Inc.) with a resonance frequency of 320 kHz.

Optical light polarized microscopy

Polarized light microscopy (PLM) examinations using an ECLIPSE E800-Nikon with a capture camera DXM1200F-Nikon were carried out on both sides of the cast samples. A 40· times objective was used to examine the samples.

Laser Raman Spectrophotometer

Raman images were taken with a Jasco NRS-3100 Confocal Micro-Raman spectrophotometer, which provides high laser spot lateral and depth sample resolutions, i.e. measured samples areas are smaller than 2 microns when the optimum confocal instrumental setup is selected and by using a 100x microscope objective. The laser source used was a red light tuned at 632,8 nm and powered at 12,4 mW. Raman imaging was carried out in the point by point mode by rationing the area of two Raman bands arising from the different phases of the composites, and were constructed by taken 15x15 spectra equally spaced across the selected sample area.

DSC measurements

Differential scanning calorimetry (DSC) of PHBV, PLA, PCL and its biocomposites were performed on a Perkin-Elmer DSC 7 thermal analysis system on typically 7 mg of dry material at a scanning speed of 10 ºC/min from room temperature to the melting point using N_2 as the purging gas. Before evaluation, the thermal runs were subtracted similar runs of an empty pan. The DSC equipment was calibrated using indium as a standard and typically only one measurement was carried out on the samples.

Gravimetric measurements

Direct permeability to D(+)-limonene of 95% purity (Panreac Química, Spain) and direct permeability to water were determined from the slope of weight loss vs. Time experiments at 24 └C and 40%RH. The films were sandwiched between the aluminium top (open O-ring) and bottom (deposit for the permeant) parts of aluminium permeability cells. A Viton rubber O-ring was placed between the film and the bottom part of the cell to enhance sealability. Then the bottom part of the cell was filled with the permeant and the pinhole secured with a rubber O-ring and a screw. Finally, the cell was placed in the desired environment and the solvent weight loss through a film area of 0.001 m^2 was monitored and plotted as a function of time. The samples were preconditioned at the desired testing conditions for 24 h, and to estimate permeability we used only the liner part of the weight loss data to ensure sample steady-state conditions. Cells with aluminum films (with thickness of ca. 100 microns) were used as control samples to estimate solvent loss through the sealing. The

permeability sensibility of the permeation cells was determined to be of ca. $0.01 \cdot 10^{-13}$ kg m/s m^2 Pa based on the weight loss measurements of the aluminium cells. Cells clamping polymer films but with no solvent were used as blank samples to monitor water uptake. Solvent permeation rates were estimated from the steady-state permeation slopes. Organic vapor weight loss was calculated as the total cell loss minus the loss through the sealing and plus the water weight gain.
The tests were done in duplicate. The diffusion coefficient of D-limonene was estimated during desorption experiments at 24ºC and 40%RH by means of weight loss experiments using an analytical balance Voyager V11140. Thus, at saturation conditions, checked by observing no changes in successive weight uptake measurements of the specimens dipped in the compound, the samples were thoroughly bottled with a tissue to remove the excess of aroma vapor condensed over the film surface (this step is considered as time zero) and were periodically weighted until they yielded constant weight. D values were obtained from fitting the experimental data vs. time to the first six sum terms of the corresponding solution of Fick's second law (1) during desorption experiments (Crank, 1975).

$$\frac{M_t}{M_e} = \frac{8}{\pi^2} \sum_{n=0}^{\infty} \frac{1}{(2n+1)^2} \exp\left\{ \frac{-D(2n+1)^2 \pi^2 t}{l^2} \right\} \qquad \text{Equation 1}$$

Results and discussion
Biocomposites morphology

Simple naked eye examination of the films obtained by the solvent cast method applied indicated that good filler dispersion was achieved in the low fiber content materials, since optical properties such as transparency of the composites remained virtually unmodified compared to the neat biopolymers. On the other hand, cast films with fiber contents beyond 5% showed fiber agglomeration in the matrix as fiber white agglomerates could easily be spotted in the films. To observe the morphology at the micron and submicron level, SEM observations were initially carried out in the biocomposites. SEM experiments usually allow a clear observation of the phase morphology in composite materials and do additionally provide information about interfacial adhesion. The SEM results showed that observation of the biofiller strongly depended on the loading levels for all biopolymers. Fig. 1 shows the fracture morphology of some of the films prepared with low, medium and high fiber contents. The SEM examination reveals that a homogeneous distribution of the fibers in the PHBV and PCL matrixes and a continuous phase morphology must have been achieved at low fiber contents (1 wt%) since the presence of the fibers cannot be unambiguously discerned from the matrix (see Fig. 1A and C). On the contrary, films prepared by casting with 10 wt% fiber content in the PHBV matrix easily revealed the presence of long fibers, fiber agglomerates and phase discontinuity likely as a result of insufficient dispersion caused by self-association of excess filler (Fig. 1B). Fig. 1D indicates that for a 5 wt% fiber addiction to the PCL matrix, long fibers can be seen aligned along the facture surface. It is evident that given the relatively large size of the fibers, the difficult observation of these must be attributed to a limitation of the SEM technique to resolve between the two components, filler and matrix, particularly when the dispersion of the filler and phase continuity seems high.

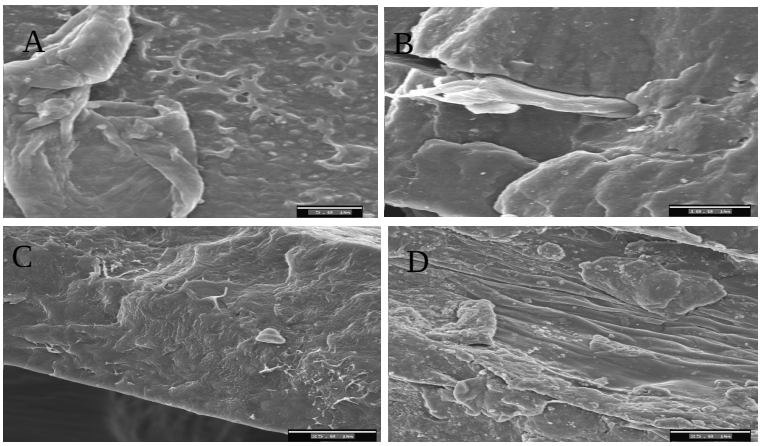

Figure 1. Scanning electron micrographs of the cross section of: (A) A film prepared by casting of PHBV with 1 wt.-% fiber content (scale marker is 5 microns), (B) a film prepared by casting of PHBV with 10 wt.-% fiber content (scale marker is 10 microns), (C) a film prepared by casting of PCL with 1 wt.-% fiber content (scale marker is 25 microns) and (D) a film prepared by casting of PCL with 5 wt.-% fiber content (scale marker is 25 microns).

AFM is a very powerful technique for the observation of materials morphology and it also provides a feasible route to investigate the topography of films containing micro- and nanofibers (Kirby, Ng, & Waldron, 2006). AFM and transmission electron microscopy (TEM) replicate techniques have previously been used to study the nanoscale surface chemistry and the morphology of biodegradable materials containing fibers when SEM observations were not successful (Kirby et al., 2006; Lopez-Rubio et al., 2007). Consequently, additional observation of the samples was carried out by AFM at the top surface and cryofractured surfaces. Even with this technique it was not very easy to detect the fibers at the samples surface. Nevertheless, Fig. 2 shows, as an example, that the surface roughness of the composites can be well resolved by the AFM tip. This figure shows the presence on the top surface of a fiber in the 1 wt% fiber-PHBV sample prepared by casting. The picture reveals the presence of what appears to be a fiber of 50 µm in length and a width of approximately ca. 8.5 µm, which seems strongly attached to matrix. Since the typical fiber thickness of the starting filler is around 20 microns, the detected thinner fiber could suggest (see later) that fibers could split in the cross section dimension during the homogenization step in the preparation.

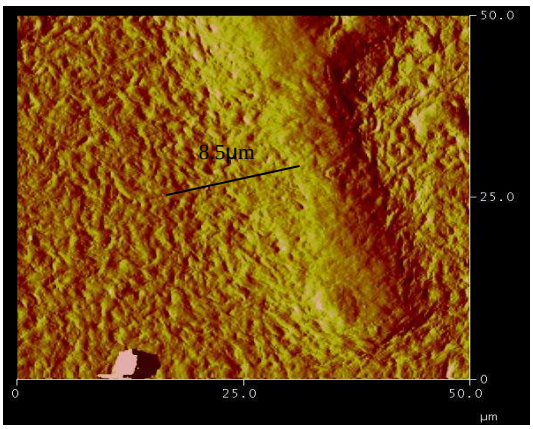

Figure 2. AFM phase image of the PHBV with 1 wt.-% fiber content sample.

However, the best techniques to resolve the morphology of the fibers in the biopolymer matrixes turned out to be in this study polarized optical microscopy (Colomb et al., 2005) and Raman imaging. Polarized optical light microscopy photographs allowed to take clear images of the cellulose fibers embedded in the biodegradable matrixes. The biocomposites showed no apparent differences in fiber homogeneity across the thickness and top and bottom sides of the biocomposites showed similar morphologies. However, some of the samples, particularly higher filler content biocomposites, showed the presence of larger fiber aggregates, probably deposited by gravity, at the bottom of the cast films. Observation of the fibers was, however, easier in the PLA samples because these particular samples were totally transparent. Fig. 3A and B clearly shows the presence of highly dispersed fibers in the 1 and 5 wt% fiber-PLA sample prepared by casting. The Fig. 3A indicates that the dimensions of the fibers in the biocomposites are not homogeneous but vary from 10 to 25 microns in thickness and between 50 and 100 microns in length. In the 5 wt% fiber-PLA sample (see Fig. 3B) it can be easily observed that the excess of fibers results in a tendency of these to crowd together and
entangle. The identification of the filler in the other two biomaterials was feasible but due to a lack of transparency in the cast films, the phase structure could not be so well resolved as for the PLA case. Fig. 3C and D shows the presence of dispersed fibers in the 1 and 5 wt% fiber-PCL samples. The Figs. 3C (PCL+1 wt% fiber) and 3E (PHBV+1 wt% fiber) suggest that the cross-sectional dimensions of the fibers in these biocomposites are finer than in PLA, i.e. the observed fibers are smaller than 5 microns in thickness and with lengths around 60 microns. The reason for the latter observation is uncertain but it could be due to the specific rheological properties or interactions between the different materials and the fibers during the homogenization step. To check for the latter observation In Fig. 3D, the PCL biocomposite containing 5 wt% of fiber shows that the filler begin to collide and agglomerate, albeit this event is not as clear as was seen for PLA.

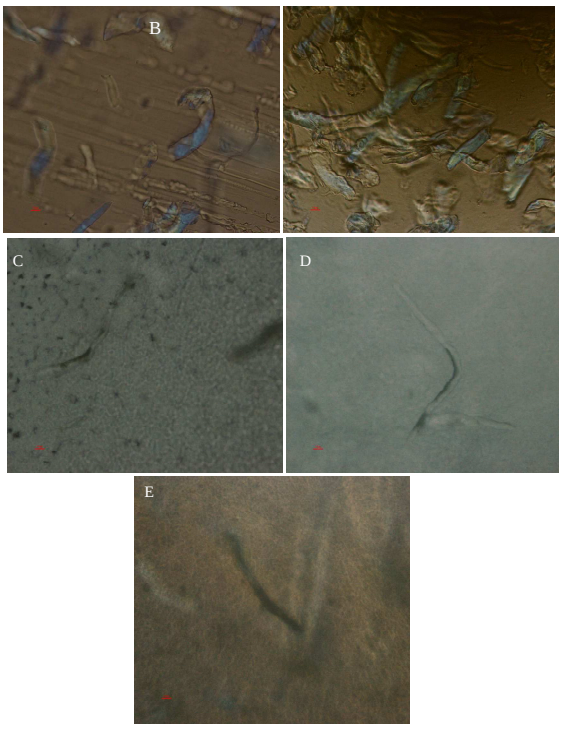

Figure 3. Optic micrographs of: (A) A film prepared by casting of PLA with 1 wt.-% fiber content (scale marker is 10 microns), (B) a film prepared by casting of PLA with 5 wt.-% fiber content (scale marker is 10 microns). (C) A film prepared by casting of PCL with 1 wt.-% fiber content (scale marker is 10 microns), (D) a film prepared by casting of PCL with 5 wt.-% fiber content (scale marker is 10 microns). (E) A film prepared by casting of PHBV with 1 wt.-% fiber content (scale marker is 10 microns).

A definitive proof of the above mentioned good fiber phase dispersion and phase morphology for the 1 wt% fiber content composites was provided by the Raman chemical compositional image depicted in Fig. 4 for the case of the PLA composite. Fig. 4 highlights the various parts where signal from the fibers is stronger in the composites (green-yellowed areas). A curious observation is that, despite the fact that the confocal laser spot was much smaller (ca. 1 micron in axial resolution and 2 microns in depth) than the width of most fibers, no single spectrum of the Raman image showed the neat spectrum of the fibers within the biocomposites, whereas this was often the case when the matrix was targeted with the laser spot. This observation suggests that the fibers are well embedded in the matrix or even intercalated by the matrix.

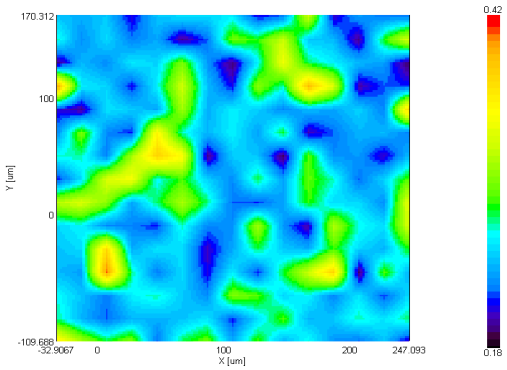

Figure 4. Raman imaging of a peak height ratio ($Peak_{fiber}/Peak_{matrix}$) of a specimen of PLA with 1 wt.-% fiber content. The selected matrix peak is at 1122.3 cm^{-1} and fiber peak is at 1090.3 cm^{-1}.

Thermal properties

Melting temperature (Tm) and Heat of fusion (DHm) corrected for biopolymer content in the biocomposites were determined from the DSC first heating runs of the samples. These are summarized in Table 1 for cast films with different fiber contents. The PHBV copolymer shows a multiple melting endotherm with two peaks, reflect of the heterogeneity in the crystalline structure of this copolymer. Table 1 shows the variation of the two thermal parameters as a function of fiber content for the PCL and PHBV composites. From this Table 1, the heat of fusion of the latter two biomaterials is seen to drop in the composites, however, this drop, and also the melting point drop in PHBV, is larger for the samples with lower fiber contents, i.e. for the samples exhibiting more dispersed filler morphologies. Higher filler dispersion and interfacial adhesion is thought to hinder to some extent polymer chains lateral rearrangements and hence crystallization in these two materials.

Table 1. DSC melting point and melting enthalpy of the neat films of PHBV and PCL and of their biocomposites with 1, 2, 4, 5 and 10 wt.-% fiber content prepared by solving casting**.**

Sample	T_m (ºC)	ΔH_m (J/g)
PHBV	145-157	47
PHBV+1 wt.-%fiber	139-154	28
PHBV+5 wt.-%fiber	137-153	23
PHBV+10 wt.-%fiber	140-155	37
PCL	62	96
PCL+1 wt.-%fiber	63	62
PCL+5 wt.-%fiber	64	69
PCL+10 wt.-%fiber	62	79

The thermal behavior of PLA is different and more complex than that of the other two biomaterials, because PLA exhibits (see Fig. 5) a cold crystallization process (Mathew, Oskman, & Sain, 2006) similar to that typically observed for the petroleum-based polyester polyethylene terephthalate (PET). Fig. 4 indicates that the cold crystallization peak occurs at a lower temperature in the biocomposites and it seems to spread over a wider temperature range in composites with 10 wt% fiber. This observation points that, in an opposite effect to that reported above for PCL and PHVB, the fibers can facilitate the crystallization process of the PLA biopolymer. In fact, it has been broadly reported in polypropylene (Quillin, Caulfield, & Koutsky, 1993; Zafeiropoulos, Baillie, & Matthews, 2001; Son, Lee, & Im, 2000; Houshyar & Shanks, 2003; Lenes & Gregersen, 2006) but also in PLA (Mathew et al., 2006) composites, that unmodified cellulose fibers can induce crystal nucleation of these polymers at the fiber surface, i.e. the so-called transcrystallinity effect. The transcrystallinity event is not observable in the optical micrographs here, possibly because the crystallinity of the cast PLA samples is very low (see Table 2). However, the broad single melting peak of PLA is seen to become multiple in the biocomposites, which show two melting peaks with one of them having higher melting point than the neat biopolymer. This latter effect strongly reveals the nucleating role of the fibers, which are able to promote a more robust crystalline morphology for this particular biopolymer during the heating run.

Table 2. DSC melting point and melting enthalpy of solvent cast PLA and its biocomposites with 1, 5 and 10% wt of filler.

Sample	T_m (°C)	T_c (°C)	ΔH_m (J/g)	T_g (°C)
PLA	151	119	3	57
PLA+1 wt.-%fiber	151-156	112	4	59
PLA+5 wt.-%fiber	149-154	112	4	56
PLA+10 wt.-%fiber	150	110	1	55

The PLA crystallinity, defined as the area of the melting peak minus the area of the cold crystallization peak, seems somewhat larger, except in the 10 wt% fiber content sample, for the biocomposites than for the neat material indicating that, as mentioned above, the fibers tend to favour some crystallization of the biopolymer (see Table 2). In principle, filler-induced crystallization of the biopolymers is positive from a barrier perspective, since crystals are typically impermeable systems, but crystallization may promote, as a downside, additional rigidity and hence fragility for the biopolymer mechanical performance. Nevertheless, the heat of fusion (crystallinity) is very small for the current cast PLA-based samples compared to the other
two biopolymers, indicating that the crystallization process of PLA is extremely metastable. Finally, the polymer Tg was also observed to increase but only in the 1 wt% fiber- PLA biocomposites, highlighting the reinforcing synergetic role of the fibers for this particular composition. The reason for not observing a Tg rise for samples with higher fiber loads could be due to fiber segregation and agglomeration.
In conclusion, the cellulose filler does not have a generic role in the biocomposites thermal properties. Thus, depending on the biomaterial, it has been found to act as impairment to crystal development, as for PCL and PHBV,or as a nucleating agent, as for PLA.

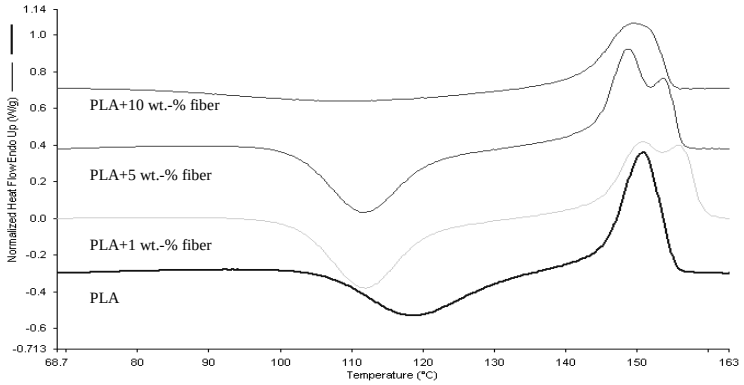

Figure 5. DSC curves of samples of neat PLA and of their nanobiocomposites with 1, 5 and 10 wt.-% of the filler.

Mass transport properties

Table 3 gathers all the barrier data (direct permeability, diffusion coefficient and solvent uptake) that has been measured in the neat biopolymers and in their biocomposites and also gathers permeability values reported in the literature for the neat biopolymers. A curious first observation from Table 3 and regarding PCL is that the water permeability coefficient of 0.4 x 10^{-13} kg m/s m^2 Pa is much higher than that of 0.0023 x 10^{-13} kg m/s m^2 Pa previously reported for toluene cast PCL (Messersmith & Giannelis, 1995). The reason for the large disagreement could be related to the different origins of the two samples (lab scale material vs. Industrial scale material production) and the fact that molecular weight, the solvent used and the differences in relative humidity gradient used for testing were totally different. Direct permeability for limonene in PLA was not reported, because the measurements yielded values below the sensibility of the permeation cells; a previous study reported that the limonene permeability for PLA is of ca. 0.000002 x 10^{-13}kg m/s m^2 Pa when measured at 45 ºC and 258 Pa of vapor partial pressure gradient (Auras, Harte, & Selke, 2005).

Table 3. D-Limonene and water permeability, d-limonene diffusion coefficient and d-limonene %uptake for PHBV and PCL films with 1, 2, 4, 5 and 10 wt.-%fiber content. Values between brackets represent uptake values corrected for the heat of fusion (crystallinity) values in Table 1.

	P limonene (Kg m/s m^2 Pa)	**P water (Kg m/s m^2 Pa)**	**D limonene (m^2/s)**	**Limonene uptake (%)**
PHBV	$1.99\pm1.01e^{-13}$	$0.127\pm0.001e^{-13}$	$2.21\pm0.0e^{-13}$	12.7%
PHBV+1 wt.-% fiber	$1.27\pm0.08e^{-13}$	$0.038\pm0.0002e^{-13}$	$1.34\pm0.09e^{-13}$	13.3% (8.1%)
PHBV+2 wt.-% fiber	$1.67\pm0.12e^{-13}$	$0.049\pm0.010e^{-13}$	$1.97\pm0.73e^{-13}$	12.5%
PHBV+4 wt.-% fiber	$1.44\pm0.12e^{-13}$	$0.093\pm0.009e^{-13}$	$2.41\pm0.63e^{-13}$	12.2%
PHBV+5 wt.-% fiber	$1.76\pm0.21e^{-13}$	$0.053\pm0.01e^{-13}$	$2.31\pm0.1e^{-13}$	16.2% (8.1%)
PHBV+10 wt.-% fiber	$2.15\pm0.16e^{-13}$	$0.067\pm0.0005e^{-13}$	$2.71\pm0.1e^{-13}$	15.7% (12.3%)
PCL	$5.51\pm0.25e^{-13}$	$0.339\pm0.061e^{-13}$	$5.48\pm0.0e^{-13}$	9.8%
PCL+1 wt.-% fiber	$2.58\pm0.56e^{-13}$	$0.198\pm0.025e^{-13}$	$2.86\pm0.24e^{-13}$	15.3% (9.9%)
PCL+2 wt.-% fiber	$4.96\pm0.29e^{-13}$	$0.208\pm0.005e^{-13}$	$4.77\pm0.47e^{-13}$	14.0%
PCL+4 wt.-% fiber	$3.89\pm0.29e^{-13}$	$0.252\pm0.015e^{-13}$	$5.23\pm0.82e^{-13}$	13.2%
PCL+5 wt.-% fiber	$4.61\pm0.16e^{-13}$	$0.286\pm0.027e^{-13}$	$7.30\pm0.32e^{-13}$	13.2% (9.4%)
PCL+10 wt.-% fiber	$5.28\pm0.21e^{-13}$	$0.430\pm0.013e^{-13}$	$7.59\pm0.38e^{-13}$	14.1% (11.6%)
Literature value PCL		**[§]$0.0023e^{-13}$**		

In the case of the PHBV biopolymer, Table 3 and Fig. 6A teach that the limonene and water permeability show minimum values for specimens with 1 wt% fiber content. Further increase in fiber content results in increased permeability to values, as for the case of limonene, even higher than that of the neat component. Films of PHBV with 1 wt% fiber content have a water permeability decrease of 71% compared to the unfilled material, whereas films of PHBV with 10 wt% fiber content show a water permeability reduction of ca. 52%. Increasing fiber content was seen to result in fiber agglomeration and this is thought to cause a reduction in matrix homogeneity and cohesion and lead to preferential penetrant paths and to detrimental effects in barrier properties. A reduction in limonene permeability of ca. 64% and in the diffusion coefficient of ca. 58% is observed in the biocomposite of PHBV with 1 wt% fiber content. Interestingly, limonene uptake appears to remain unmodified, or to increase very slightly, in the biocomposites of this material. However, when the uptake values are corrected for the crystallinity drop of the matrix in the biocomposites (only the amorphous phase is thought to uptake the penetrant), the actual uptake decreases (see corrected uptake values between brackets in Table 3) indicating that the fibers do actually sorb less aroma component than the biopolymer matrix. Thus, the above results suggest that the reduction in permeability for this vapor is both strongly related to a reduction in the diffusion coefficient imposed by the presence of the fibers but also to a decrease in solubility of the penetrant. It is remarkable to observe that even when the crystallinity of the matrix goes down by the influence of the fibers and, therefore, the matrix should become more permeable, the overall blocking effect of

the fiber crystals, well dispersed and embedded in the matrix, overrides this negative effect and drives the biocomposite to become more impermeable. Fig. 6B and Table 3 show direct limonene and water permeability and limonene diffusion coefficients for films of
PCL reinforced with different fiber contents. From the results, a reduction in limonene permeability of ca. 53%, a reduction in water permeability of ca. 58% and in the limonene diffusion coefficient of 52% is observed in the biocomposite with 1 wt% fiber content compared with the unfilled biopolymer. Limonene permeability and diffusion appear to match very well for this material suggesting that
the permeability drop could be primarily related to the more tortuous path imposed by the fibers. Limonene uptake (see Table 3) is for the case of neat PCL somewhat lower than for neat PHBV, but the uptake of limonene is higher in the PCL biocomposites. Nevertheless, if a correction for the crystallinity drop of the matrix is carried out the uptake values remain constant pointing that the fibers sorb equally as the matrix. The overall permeability trend is again in agreement with the behavior observed earlier for the PHBV biocomposites. A curious general observation from Fig. 6 is that while the samples with 1 wt% fiber content show as already mentioned the lowest permeability values, the samples with 2 wt% fiber content tend to increase permeability to values higher than samples with for instance 5 wt% fiber content. This observation may indicate that there must be a balance in the biocomposites between increasing the amount of fiber used, which has in itself barrier capacity, and the permeability deterioration apparently caused by fibber agglomeration. This balance could become less favorable, in the low filler range, for biocomposites with 2 wt% fiber content. The crystallinity drop being higher at low additions of fiber can also add as an effect to account for this observation.

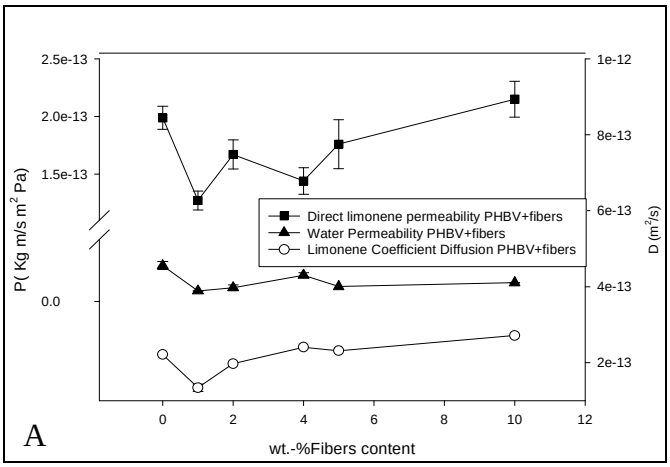

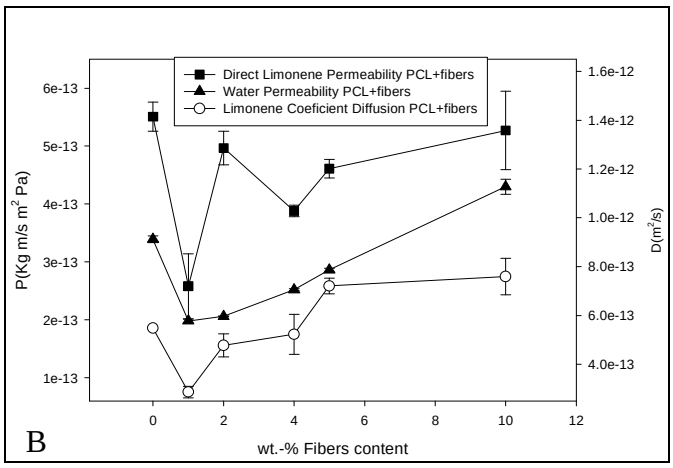

Figure 6. D-limonene and water direct permeability and limonene diffusion coefficient as determined by gravimetry for (A) the films of PHBV with 1, 2, 4, 5 and 10 wt.-% fiber contents and (B) the films of PCL with 1, 2, 4, 5 and 10 wt.-% fiber contents.

Finally, Table 4 gathers the water permeability of PLA as a function of filler content. These samples indicate that the barrier properties to water of PLA biocomposites is only reduced (by 10%) in the sample containing 1 wt% of fibers. The other composite samples show no barrier improvements and for the case of the 10 wt% fiber content the permeability was seen to increase by ca. 80%. Curiously enough, even when crystallinity (which is for all samples very small) has a potentially favorable impact in most of the biocomposites, except for the case of the 10 wt% sample, the barrier improvement of the very low content biocomposites is smaller than that seen for the other two biomaterials. The reason for this behavior could be attributed to the fact that thicker fiber morphologies where generally observed for the composites of PLA. Thicker fibers imply less dispersed morphologies in the cast material and hence lower tortuosity factors and lower impact in barrier properties.

Table 4. Water permeability for PLA films with 1, 4, 5 and 10 wt.-%fiber contents.

	P water (Kg m/s m^2 Pa)
PLA	$0.230\pm0.007e^{-13}$
PLA+1 wt.-% fiber	$0.208\pm0.009e^{-13}$
PLA+4 wt.-% fiber	$0.293\pm0.019e^{-13}$
PLA+5 wt.-% fiber	$0.332\pm0.027e^{-13}$
PLA+10 wt.-% fiber	$0.414\pm0.032e^{-13}$

References

Auras, R., Kale, G., & Singh, S. P. (2006). Degradation of commercial
biodegradable packages under real composting and ambient exposure conditions. Journal of Polymers and the Environment, 14(3), 317–334.

Auras, R., Harte, B., & Selke, S. (2005). Sorption of ethyl acetate and Dlimonene in poly(lactide) polymers. Society of Chemical Industry. Journal of the Science of Food and Agriculture, 0022–5142.

Bodros, E., Pillin, I., Montrelay, N., & Baley, C. (2007). Could biopolymers reinforced by randomly scattered flax fibre be used in structural applications?. Composite Science Technological 67(3–4), 462–470.

Colomb, T., Durr, F., Cuche, E., et al. (2005). Polarization microscopy by use of digital holography: application to optical-fiber birefringence
measurements. Applied Optics, 44(21), 4461–4469. Crank, J. (1975). The mathematics of diffusion (2nd ed.). Oxford: Oxford Science Publications.

Dufresne, A., Dupeyre, D., & Paillet, M. (2003). Lignocellulosic flourreinforced poly(hydroxybutyrate-co-valerate) composites. Journal of Applied polymer Science, 87(8), 1302–1315.

Gross, R. A., & Kalra, B. (2002). Biodegradable polymers for the environment. Science, 297, 803–807.

Haugaard, V.K., Udsen, A.M., Mortensen, G., Hoegh, L., Petersen, K. & Monahan, F. (2001). Food biopackaging, in Biobased Packaging
Materials for the Food Industry – Status and Perspectives, Ed. C.J. Weber, Copenhagen.

Houshyar, S., & Shanks, R. A. (2003). Morphology, thermal and mechanical properties of Poly(propylene) fibre–matrix composites. Macromolecular Materials and Engineering, 288, 599–606.

Huang, Z. M., Zhang, Y. Z., & Kotaki, M. (2003). A review on polymer nanofibers by electrospinning and their applications in nanocomposites. Composites Science and Technology, 63(15), 2223–2253.

Iannace, S., Luca, N., & Nicolais, L. (1990). Physical characterization of incompatible blends of polymethylmethacrylate and polycaprolactone. Journal Applied Polymer Science, 41, 269–2704.

Ichazo, M. N., Albano, C., Gonzalez, J., Perera, R., & Candal, M. V.
(2001). Polypropylene/wood flour composites: Treatments and properties. Composites Structures, 54, 207–214.

Khalil, H. P. S. A., Shahnaz, S. B. S., Ratnam, M. M., Ahmad, F., &
Fuaad, N. (2006). Recycle polypropylene (RPP) wood saw dust (WSD) composites – Part 1: The effect of different filler size and filler loading on mechanical and water absorption properties. Journal of reinforced plastics and composites, 25(12), 1291–1303.

Kijchavengkul, T., Auras, R., Rubino, M., Ngouajio, M., & Fernandez,
R. T. (2006). Development of an automatic laboratory-scale respirometric system to measure polymer biodegradability. Polymer Testing, 25(8), 1006–1016.

Kirby, A. R., Ng, A., Waldron, K. W., et al. (2006). AFM investigations of cellulose fibers in Bintje potato (Solanum tuberosum L.) cell wall fragments. Food Biophysics, 1(3), 163–167.

Lagaron, J.M., Catala´, R., & Gavara, R. (2004). Structural characteristics defining high barrier polymeric materials. Materials Science and Technology, 20, 1–7.

Lenes, M., & Gregersen, W. (2006). Effect of surface chemistry and topography of sulphite fibres on the crystallinity of polypropylene. Cellulose, 13, 345–355.

Lopez-Rubio, A., Lagaron, J. M., Ankerfors, M., Lindstrom, T., Nordqvist, D., Mattozzi, A., et al. (2007). Enhanced film forming and film properties of amylopectin using micro-fibrillated cellulose. Carbohydrate Polymers, 68(4), 718–727.

Malainine, M. E., Mahrouz, M., & Dufresne, A. (2004). Lignocellulosic flour from cladodes of Opuntia ficus-indica reinforced poly(propylene) composites. Macromolecular Material and Engineering, 289, 855–863.

Mathew, A., Oskman, K., & Sain, M. (2006). The effect of morphology and chemical characteristics of cellulose reinforcements on the crystallinity of polylactic acid. Journal of Applied Polymer Science, 101, 300–310.

Messersmith, Pb., & Giannelis, Ep. (1995). Synthesis and barrier properties of poly(-caprolactone)-layered silicate nanocomposite. Journal Polymer Science Polymer Chemical, 33(7), 1047–1057.

Mutje, P., Girones, J., & Lopez, A. (2006). Hemp strands: PP composites by injection molding: Effect of low cost physico-chemical treatments. Journal Reinforced Plastics Composites, 25(3), 313–327.

Nabi Sahed, D., & Jog, J. P. (1999). Natural fiber polymer composites: A review. Advances in Polymer Technology, 18, 351.

Najafi, S. K., Tajvidi, M., & Chaharmahli, M. (2006). Long-term water uptake behavior of lignocellulosic-high density polyethylene composites. Journal of Applied Polymer Science, 102(4), 3907–3911.

Nitz, H., Semke, H., Landers, R., & Mulhaupt, R. (2001). Reactive extrusion of polycaprolactone compounds containing wood flour and lignin. Journal Applied Polymer Science, 81, 1972–1984.

Orts, W. J., Shey, J., Imam, S. H., Glenn, G. M., Guttman, M. E., & Revol, J. F. (2005). Application of cellulose microfibrils in polymer nanocomposites. Journal Polymer Environment, 13(4), 301–306.

Peoples, O.P. & Sinskey, A.J. (1990). Polyhydroxybutyrate (PHB): a model system for biopolymer engineering: II. Novel Biodegradable Microbial Polymers (pp. 191–202). Dordrecht: Kluwer Academic Publishers.

Petersen, K., Nielsen, P. K., Bertelsen, G., Lawther, M., Olsen, M. B., Nilsson, N. H., et al. (1999). Potential of biobased materials for food packaging. Trends in Food Science and Technology, 10, 52–68.

Petersson, L., & Oksman, K. (2006). Preparation and properties of biopolymer-based nanocomposite films using microcrystalline cellulose. American Chemical Society Symposium Series, 938, 132–150.

PigŁowski, J., & Kiersnowski, A. (2006). Preparation, structure and useful properties of poly(e-caprolactone)/layered silicates nanocomposites. Polymers, 51(10), 704–715.

Quillin, D. T., Caulfield, D. F., & Koutsky, J. A. (1993). Crystallinity in the polypropylene/cellulose system. I. nucleation and crystalline morphology. Journal of Applied Polymer Science, 50, 1187–1194.

Rana, A. K., Basak, R. K., Mitra, B. C., Lawther, M., & Banerjee, A. N. (1997). Studies of acetylation, of jute using simplified procedure and its characterization. Journal Applied Polymer Science, 64, 1517–1523.

Rosa, D. S., Lotto, N. T., Lopes, D. R., & Guedes, C. G. F. (2004). The use of roughness for evaluating of poly-b-(hidroxybutyrate) and polyb-(hidroxybutyrate-co-b-valerate). Polymer Testing, 23, 3–8.

Son, S.-J., Lee, Y.-M., & Im, S.-S. (2000). Transcrystalline morphology and mechanical properties in polypropylene composites containing cellulose treated with sodium hydroxide and cellulose. Journal of Materials Science, 35(22), 5767–5778.

Tserki, V., Matzinos, P., Zafeiropoulos, N. E., & Panayiotou, C. (2006). Development of biodegradable composites with treated and compatibilized lignocellulosic fibers. Journal of Applied Polymer Science, 100, 4471–4703.

Zafeiropoulos, N. E., Baillie, C. A., & Matthews, F. L. (2001). Study of transcrystallinity and its effect on the interface in flax fibre reinforced composite materials. Composites Part A: Applied Science and Manufacturing, 32(3–4), 525–543.

PAPER VII: On the use of plant Cellulose Nanowhiskers to enhance the barrier properties of Polylactic Acid

Abstract

Polylactic acid (PLA) nanocomposites were prepared using cellulose nanowhiskers (CNW) as a reinforcing element in order to asses the value of this filler to reduce the gas and vapour permeability of the biopolyester matrix. The nanocomposites were prepared by incorporating 1, 2, 3 and 5 wt.-% of the CNW into the PLA matrix by a chloroform solution casting method. The morphology, thermal and mechanical behaviour and permeability of the films were investigated. The CNW prepared by acid hydrolysis of highly purified alpha cellulose microfibers, resulted in nanofibers of 60-160 nm in length and of 10-20 nm in thickness. The results indicated that the nanofiller was well dispersed in the PLA matrix, did not impair the thermal stability of this but induced the formation of some crystallinity, most likely transcrystallinity. CNW prepared by freeze drying exhibited in the nanocomposites better morphology and properties than their solvent exchanged counterparts. Interestingly, the water permeability of nanocomposites of PLA decreased with the addition of CNW by up to 82% and the oxygen permeability by up to 90%. Optimum barrier enhancement was found for composites containing loadings of CNW below 3 wt.-%. Typical modelling of barrier and mechanical properties failed to describe the behaviour of the composites and appropriate discussion regarding this aspect was also carried out. From the results, CNW exhibit novel significant potential in coatings, membranes and food agrobased packaging applications.

Keywords: Cellulose, Nanobiocomposites, Mass transport properties, PLA.

Introduction

Production of 'green materials' based on raw materials derived from natural sources of plant or animal origin are of great interest both in the academic and industrial fields. The most widely researched thermoplastic sustainable biopolymers for food agrobased packaging applications are starch, PLA and PHA's. From these, starch and PLA biopolymers are without doubt the most interesting families of biodegradable materials because they have become commercially available, are produced in a large industrial scale and also because they present an interesting balance of properties. Yet, the main drawbacks of this new family of polymers regarding performance are still associated to low thermal resistance, excessive brittleness and insufficient barrier to oxygen and/or to water compared to for instance other benchmark packaging polymers such as polyolefins and PET. It is, therefore, of great general interest to identify means of enhancing the barrier properties of these materials while maintaining their inherently good properties such as transparency and biodegradability (Koening, Huang, 1195; Bastiolo et al. 1992; Park et al. 2002; Tsuji, Yamada, 2003). A feasible route to do so is by means of the use of various nanoparticles.

Some studies based on bio-nanocomposites using nanoclays as reinforcement for polylactic acid (PLA) have been reported by scientists in recent years (Sanchez-Garcia et al. 2008a; Sanchez-Garcia et al. 2008b; Sanchez-Garcia et al. 2007). Poly(lactic acid) (PLA) is a biodegradable thermoplastic polyester produced from L- and D-lactic acid, which is derived from the fermentation of corn starch. Currently, PLA is being commercialized and used as a food packaging polymer for relatively short shelf-life products with common applications such as containers, drinking cups, sundae and salad cups, overwrap and lamination films, and blister packages (Auras et al. 2006).

More recently, there is an increased use of cellulose nanowhiskers or nanocrystals as the load-bearing constituent in developing new and inexpensive biodegradable materials due to their high aspect ratio, good mechanical properties (Sturcova et al. 2005; Helbert et al. 1996) and fully degradable and renewable character.

As compared to other inorganic reinforcing fillers, cellulose nanowhiskers have many additional advantages, including wide availability of sources, low-energy consumption, ease of recycling by combustion, high sound attenuation and comparatively easy processability due to their nonabrasive nature, which allows high filling levels, in turn resulting in significant cost savings (Podsiadlo et al. 2005; Azizi Samir et al. 2005).

Cellulose nanowhiskers or nanocrystals are prepared by treating native microfibrillated cellulose with high strong acids such as sulfuric acid, where small amounts of sulphate ester groups are introduced to the surfaces (Marchessault et al. 1959). This treatment is, however, hydrolytic and thus results in dramatic decreases in both the yield and fibril length down to 100-150 nm. The use of cellulose nanowhiskers as nanoreinforcement is a relatively new field in nanotechnology and as a result there are still many issues to be resolved and understood. Firstly, the production of CNW is time consuming and is still associated with low yields. Secondly, they are difficult to use in systems that are not water based due to their

strong hydrogen self-association and potential compatibility issues. This affects directly the formulation of nanocomposites of PLA which are not water soluble. In this case, a solvent exchange process is a procedure that has been used before (Petersson et al. 2007; Ayuk et al. 2009). Petersson et al. (Petersson et al. 2007) reported a solvent exchange treatment of the CNW with tert-butanol, which was added to PLA and Ayuk et al. (Ayuk et al. 2009) reported the properties of cellulose acetate butyrate (CAB) nanocomposites based also on solvent exchange CNW. The dynamic mechanical properties and thermal stability were found to increase with increasing the content of solvent exchanged CNW in both polymers.

Kvien et al. (Kvien et al. 2005) reported a comparative study of the morphology of PLA/CNW composites as determined by AFM, SEM and TEM. CNW were obtained by acid hydrolysis of microcrystalline cellulose from wood. A good morphology of the PLA/CNW composites was claimed, i.e. by using TEM the authors identified individual whiskers, which enabled determination of their sizes and shape. However, the SEM resolution was deemed insufficient to add morphological insight.

Oksman et al. studied other processing routes for the preparation of cellulose based nanocomposites, using N,N-dimethylacetamide with 0.5 wt.-% of LiCl as swelling/separation agent, and they reported an improvement on the mechanical properties (Oksman et al. 2006). Aizizi Samir et al. (Aizizi Samir et al. 2005) reviewed works detailing the effect of the various parameters that influence the mechanical properties of these nanocomposites, such as the geometrical aspect ratio (L/W) of the nanowhiskers, where the fillers with a high aspect ratio give the best reinforcing effect (Favier 1995); the processing methods, where evaporation seems to give the highest mechanical performance materials compared to hot pressing and evaporation (Morin, Dufresne. 2002; Hajji et al. 1996) the matrix structure and the resulting competition between matrix/filler and filler/filler interactions; where the higher the affinity between the cellulosic filler and the host matrix the lower the mechanical performance (Dufresne et al. 1999; Angles et al. 2001).

Angle's et al. (Angles et al. 2001) reported the mechanical behaviour of plasticized starch/tunicin whisker composites, in which they observed a comparatively very low reinforcing effect with the addition of tunicin whiskers. This observation was explained on the bases of competitive interactions between the components and the accumulation of plasticizer in the cellulose/amylopectin interfacial zone. This plasticizer accumulation phenomenon was attributed to interfere with the hydrogen-bonding forces that hold the percolating cellulose whiskers network within the matrix.

Lopez et al. reported that the addition of microfibrillated cellulose (MFC) to amylopectine films, resulted in stiff and strong films but not brittle. They attributed this counterintuitive but remarkable reinforcing-plasticizing effect to the moisture retention properties provided by the MFC (López-Rubio et al. 2007).

Despite all of the above, very little is known about the effect of the CNW in the gas and vapour transport properties, often termed barrier properties, of nanocomposites in general and of PLA in particular. Petersson et al. studied the barrier properties of composites of PLA with microcrystalline cellulose (MCC), but they reported an increase in the oxygen permeability, due to the not efficient shape, loading and

dispersion of the MCC in blocking the gas molecules path in the matrix (Petersson, Oksman. 2006). More recently however, Sánchez-García et al. (Sanchez-Garcia et al. 2008b) reported an improvement in the barrier properties of biocomposites of PCL, PLA and PHBV with alpha purified cellulose microfibers. Although, in accordance with the morphology data, water and d-limonene direct permeability were seen to decrease to a significant extent in the biocomposites with low fiber contents, i.e. for 1 wt.-% filler loading, higher fiber contents led to filler agglomeration and detrimental effects on permeability.

The aim of the current work is to study the impact of cellulose nanowhiskers derived from highly purified alpha cellulose fibers in the general properties, but with special unprecedented focus in the barrier properties of their nanobiocomposites with PLA. The study covers the effect of freeze-drying versus direct chloroform solvent exchange processing method and details morphological, thermal, mechanical and, of course, mass transport properties. A comparison of the barrier performance of the nanowhiskers vs. that of their original microfibers published earlier (Sanchez-Garcia et al. 2008b) is also carried out.

Experimental

Materials

The semicrystalline Poly(lactic acid) (PLA) used was a film extrusion grade produced by Natureworks (with a D-isomer content of approximately 2%). The molecular weight had a number-average molecular weight (M_n) of ca. 130,000 g/mol, and the weight-average molecular weight (M_w) was ca. 150,000 g/mol as reported by the manufacturer.

A purified cellulose microfiber grade from CreaFill Fibers Corp. (US), having an average fiber length of 60 µm and an average fiber width of 20 µm was used. According to the manufacturer specifications, these fibers had an alfa-cellulose content in excess of 99.5 %.

Sulphuric acid 95–97% from Sigma Aldrich, Germany was used during the CNW production. Sodium Hydroxide from Fluka, was used during neutralization of the CNW. Acetone 99.5% from Panreac Quimica (Spain), was also used during the solvent exchange of the CNW.

Preparation of nanocomposites

CNW production

Microcrystalline Cellulose (MCC), 10 g/100 ml, was hydrolyzed in 9.1 mol/l sulphuric acid at 44ºC for 130 min. The procedure is in accordance with previous works (Petersson et al. 2007; Jiang et al. 2008). Nevertheless, different hydrolysis times where trial and it was observed that higher digestion times led to carbonization and darkening of the product. The excess of sulphuric acid was removed by repeated

cycles of centrifugation, 10 min at 13,000 rpm. The supernatant was removed from the sediment and was replaced by deionized water. The centrifugation continued until the supernatant became turbid. After centrifugation the suspension containing cellulose nanowhiskers had a pH of 3.5 and the solution was drop by drop neutralized with sodium hydroxide until a pH of 7, following a procedure described elsewhere (Petersson et al. 2007). The CNW after acid hydrolysis was checked for composition consistency by FTIR spectroscopy (see later) and the yielding was estimated to be ca. 4 wt.-%.

CNW dispersion and film preparation

The suspensions containing whiskers were freeze-dried in a VirTus Genesis 35 EL. After freeze-drying, chloroform was directly added to the solid whiskers forming 1, 2, 3 and 5 wt.-% suspensions. CNW dispersion in chloroform were mixed in a homogenizer (Ultraturrax T25 basic, Ika-Werke, Germany) for two minutes, sonicated for 30 seconds and were then stirred with the PLA at 40ºC during 30 min. The solutions were subsequently cast to generate films of ca. 100 μm after removal of the solvent as checked by FTIR spectroscopy.

In another procedure the cellulose whiskers still in the neutralized dispersion were solvent exchanged into chloroform. This process was carried out after centrifugation and removal of the supernatant, which was replaced by a solution of acetone. Two cleaning cycles were carried out using this procedure. After solvent exchange, PLA was directly added to the whiskers forming 1, 2, 3 and 5 wt.-% suspensions. Solution-cast film samples of the PLA materials with 1, 2, 3 and 5 wt.-% CNW contents were prepared as described above.

Optical light polarized microscopy

Polarized light microscopy (PLM) examinations using an ECLIPSE E800-Nikon with a capture camera DXM1200F- Nikon were carried out on both sides of the cast samples.

SEM measurements

For scanning electron microscopy (SEM) observation, the samples were criofractured after immersion in liquid nitrogen, mounted on bevel sample holders and sputtered with Au/Pd in a vacuum. The SEM pictures (Hitachi S4100) were taken with an accelerating voltage of 10 keV on the sample thickness.

AFM measurements

AFM measurements were performed on CNW after chloroform solvent evaporation using a NanoScope IIIa (Digital Instruments Inc.). The images were scanned in tapping mode in air using commercial Si cantilevers with a resonance frequency of 320 kHz.

TEM measurements

Transmission electron microscopy (TEM) was performed using a JEOL 1010 equipped with a digital Bioscan (Gatan) image acquisition system. TEM observations were performed on ultra-thin sections of microtomed thin biocomposite sheets. The samples were then stained by allowing the grids to float in a 2 wt.-% solution of uranyl acetate for 3 min.

DSC measurements

Differential scanning calorimetry (DSC) of PLA and of its nanobiocomposites was performed on a Perkin-Elmer DSC 7 thermal analysis system on typically 7 mg of dry material at a scanning speed of 10ºC/min from room temperature to the melting point using N2 as the purging gas. The first and second melting endotherms after controlled crystallization at 10oC/min from the melt, were analysed. Before evaluation, the thermal runs were subtracted similar runs of an empty pan. The DSC equipment was calibrated using indium as a standard.

The crystallinity(%) of the PLA was estimated from the corrected enthalpy for biopolymer content in the PLA nanocomposites, using the ratio between the heat of fusion of the studied material and the heat of fusion of an infinity crystal of same material, i.e. %Xc = , where ΔHf is the enthalpy of fusion of the studied specimen and ΔHfº is the enthalpy of fusion of a totally crystalline material. The ΔHfº fed to the equation was 93 J/g for PLA (Liu et al. 1997).

TGA measurements

The thermal stability of both freeze dried whiskers and cellulose microfibers and of the nanocomposites was investigated using a TGA Q500 from TA Instruments USA. The samples were heated from room temperature up to 500ºC with a heating rate of 10ºC/ min and a nitrogen flow of 100 ml/min.

FTIR analysis

Pellets containing 2 mg of cellulosic material were prepared by mixing with 200 mg of spectroscopic KBr grade. The mixture was blended for 5 min in an agate mortar before pressing. The infrared spectroscopic measurements were carried out in the transmission mode using a Tensor FTIR spectrometer from Bruker, Germany. The spectra were recorded in the range 2000–500 cm−1 with a resolution of 2 cm−1. The crystallinity index (CI) was estimated from the ratios of absorption bands such as A1430/A894, A1278,1282/A1263, and A1372/A894 in accordance with a previous work (Oh et al. 2005). As internal standards, the bands at 2901 (2892), 1373 (1376), 897 (894), 1263, 668 cm-1 were selected.

Gravimetric measurements

Direct permeability to water was determined from the slope of the weight gain–time curves at 24°C. The films were sandwiched between the aluminium top (open O-ring) and bottom (deposit for the silica gel that provides 0%RH) parts of a specifically designed permeability cell with screws and placed inside a desiccator at 75%RH. A Viton rubber O-ring was placed between the film and the bottom part of the cell to

enhance sealability. The solvent weight gain through the film was monitored and plotted as a function of time. The samples were preconditioned at the desired testing conditions for 24 hours, and to estimate permeability we used only the linear part of the weight gain data to ensure sample steady state conditions. Cells with aluminium films (with thickness of ca. 100 microns) were used as control samples to estimate solvent gain through the sealing. The permeability sensibility of the permeation cells was determined to be of ca. 0.01 10^{-13} Kg m/s m^2 Pa based on the weight gain measurements of the aluminium films. Solvent permeation rates were estimated from the steady-state permeation slopes. Water vapour weight gain was calculated as the total cell weight gain minus the gain through the sealing. The tests were done in duplicate.

Oxygen transmission rate

The oxygen permeability coefficient was derived from oxygen transmission rate (OTR) measurements recorded using an Oxtran 100 equipment (Modern Control Inc., Minneapolis, MN, US). During all experiments temperature and relative humidity were held at 24ºC and 80%RH humidity. 80% relative humidity was generated by a built-in gas bubbler and was checked with a hygrometer placed at the exit of the detector. The experiments were done in duplicate. The samples were purged with nitrogen for a minimum of 20 h in the previously relative humidity equilibrated samples, prior to exposure to an oxygen flow of 10 ml/min. A 5 cm2 sample area was measured by using an in-house developed mask.

Tensile test

Tensile tests were carried out at ambient conditions typically at 21ºC and 60%RH on an Instron 4400 Universal Tester. Preconditioned dumb-bell shaped specimens with initial gauge length of 25 mm and 5 mm in width were die-stamped from the sheets in the machine direction according to the ASTM D638. A fixed crosshead rate of 10 mm/min was utilized in all cases and results were taken as the average of four tests.

Results and Discussion

Morphological characterization

Figure 1 shows typical photographs taken in the cast PLA films containing 1 wt.-% freeze dried or solvent exchange CNW. Samples with 1 wt.-% showed the best optical properties being the samples with 3 wt.-% but specially the sample with 5 wt.-% filler loading less transparent (see crystallinity data later in text for further insight). Both, contact transparency (see Figure 1a) and transparency against a background (see Figure 1b) were evaluated. In the contact transparency, both films show apparently similar performance. However, in transparency against a background the films containing freeze dried CNW show better performance suggesting that a better dispersion has been achieved by this method.

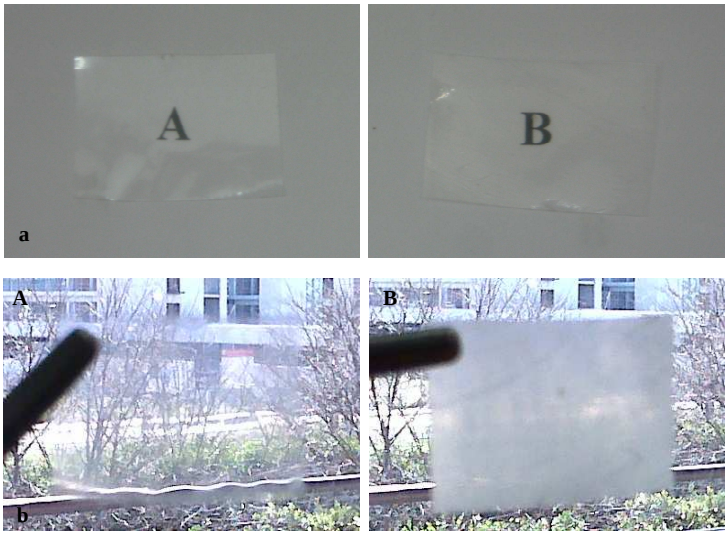

Figure 1. Typical photographs of 100 microns thickness films of A) PLA containing 1wt.-% of CNW-freeze dried and B) PLA containing 1wt.-% of CNW-solvent exchange.

Polarized optical microscopy permits to zoom up the morphology in order to observe the PLA microcomposites (Sanchez-Garcia et al. 2008b) and to potentially check the efficiency of the hydrolysis and separation processes in the nanocomposites (see Figure 2). From this Figure, it can be seen that some microfibers can still be detected in the separated and dried CNW fraction. In spite of this, the scarce remaining fiber particles are of course much thinner in comparison with the original microfibers. Figure 2A indicates that the dimensions of the cellulose microfibers in the biocomposites are not homogeneous but vary from 10 to 25 microns in thickness and between 50 and 100 microns in length in the polymer matrix.

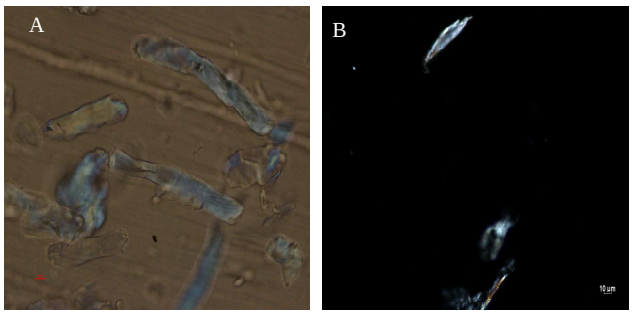

Figure 2. Optic micrographs of: (A) A film prepared by casting of PLA with 1 wt.-% cellulose microfiber content (scale marker is 10 microns), (B) a film prepared by casting of PLA with 1wt.-% CNW-freeze dried content (scale marker is 10 microns).

To observe the morphology at the micron and submicron level, SEM observations were subsequently carried out in the original cellulose microfibers and in the freeze-dried CNW. Figure 3A presents typical pictures taken in cellulose microfibers and Figure 3B presents typical images taken in the freeze-dried CNW. The comparative observation of this Figure clearly shows how the size of the CNW is much smaller and how these are agglomerated into bigger structures in the solid state. The nanocomposites were also observed by SEM. Figure 3C shows the fracture morphology of the films of PLA prepared with low CNW contents. The SEM examination revealed that a homogeneous morphology with potentially good interfacial adhesion seems to have been achieved for the composites studied, since the presence of the fibers cannot be unambiguously discerned. Nevertheless, it has also been suggested that to study the morphology of PLA with CNW by SEM may not provide adequate insight, since the resolution of the technique is considered insufficient for detailed information (Kvien et al. 2005).

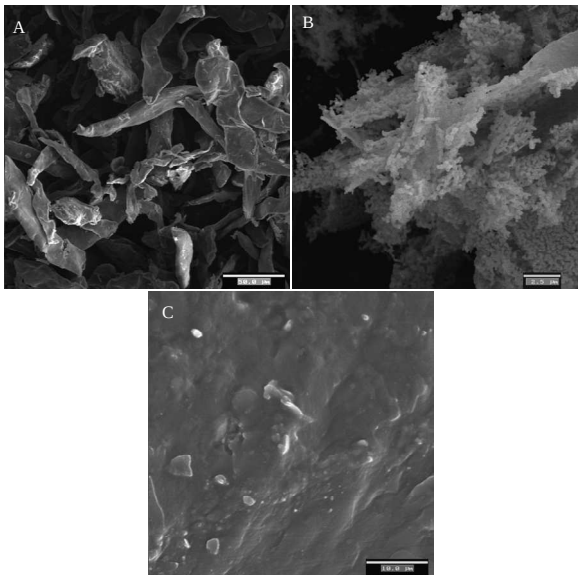

Figure 3. SEM micrographs of: (A) Original purified cellulose microfibers (scale marker is 50 microns), (B) Cellulose Nanowhiskers (scale marker is 2.5 microns). (C) A film prepared by casting of PLA with 1 wt.-% nanowhiskers content (scale marker is 10 microns)

In this context, TEM and AFM are considered more powerful tools for the characterization of cellulose whiskers. AFM analysis of the cellulose whiskers showed to be a good alternative to SEM. The shape of the whiskers by AFM was seen, however, different from that observed by TEM and SEM (see Figure 4). The whiskers in the AFM images appear to have a rounded shape, most likely due to the fact that the images may be in practice a convolution of the whiskers and the tip geometry in the measuring contact mode (Kvien et al. 2005). Figure 4 indicates rounded whiskers measuring between 25 and 75 nm in length.

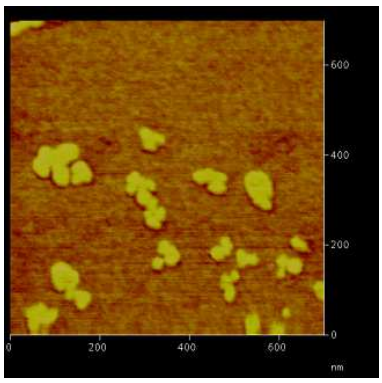

Figure 4. AFM phase image of cellulose nanowhiskers after chloroform solvent evaporation.

On the other hand, the TEM analysis of the nanocomposites show very clear pictures of the nanowhiskers within the matrix in the stained samples (see Figure 3). From this Figure 5A, the CNW obtained via freeze-drying appear nicely dispersed across the biopolymer matrix. The size of the CNW ranges from 60 to 160 nm in length and between 10-20 nm in thickness. The length is similar to that measured by AFM. From these pictures, it becomes clear that a considerable reduction in fiber size has been accomplished by the acid hydrolysis in agreement with previous findings by other authors. Figure 5C shows that a more agglomerated morphology appears in the chloroform solvent exchanged CNW in the PLA matrix, maybe due to higher agglomeration during the solvent exchange process. During the production of the CNW from solvent exchange some water may still be retained and/or agglomeration can take place during the centrifugation process that may not revert in the organic solvent before the casting process. This may explain the above differences in the macroscopic optical properties of the biocomposites of Figure 1. Perhaps stronger mixing such as sonication or homegenization after the solvent exchange step can lead to a better morphology.

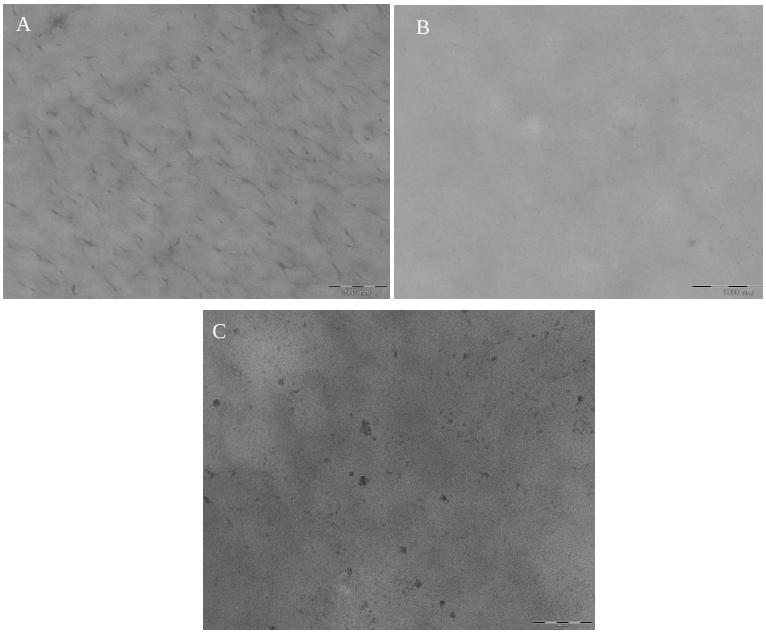

Figure 3. SEM micrographs of: (A) Original purified cellulose microfibers (scale marker is 50 microns), (B) Cellulose Nanowhiskers (scale marker is 2.5 microns). (C) A film prepared by casting of PLA with 1 wt.-% nanowhiskers content (scale marker is 10 microns)

FTIR Analysis

FTIR analysis was carried out on both the original microfibers and the CNW powder to asses the purity and the crystalline morphology of the filler. Thus, Figure 6 shows the FTIR spectra of the freeze-dried CNW after acid digestion and of the original highly purified alfa cellulose microfibers for comparative purposes. From the Figure, it can be seen that the conformationally sensitive spectral bands of the cellulose reduce band width to become sharper, effect usually associated with higher molecular conformational order, which is in turn usually associated to higher crystallinity in crystalline systems. Moreover, the peak at 1245 cm^{-1} assigned to methyl ester groups appears to reduce intensity in the spectra, hence suggesting removal of hemicellulose by the acid digestion (Wang et al. 2007).

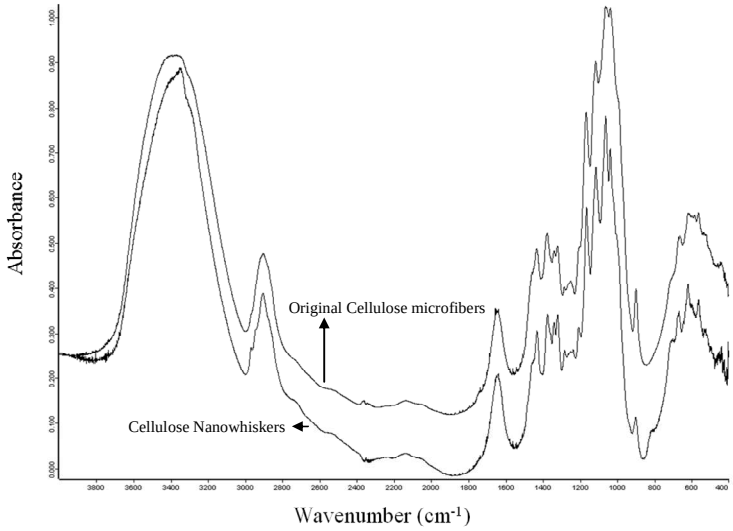

Figure 6. FTIR spectra of cellulose nanowhiskers (CNW) and the original purified cellulose microfibers.

The FTIR crystallinity Index (CI) (see Table 1) was also calculated from the spectra in accordance with ref. (Oh et al. 2005), by taking the ratio of the absorbance of different cellulose bands. In the so-called CI (1); the band at 1430 cm-1 is divided by the absorbance at 894 cm-1. For the CI (2); the band at ca. 1282 cm-1 is divided by the absorbance at 1263 cm-1 and for the CI (3); the bands used are the absorbance at 1372 cm-1 divided by the band at 894 cm-1. It should be noted that the FTIR CI is not a direct crystallinity measurement but an empirical method which provides a fast comparative protocol to determine the level of molecular order in cellulose samples.

Table 1. FTIR crystallinity index of CNW and original purified cellulose microfibers

	$CI(1)=\frac{A_{1430}}{A_{894}}$	$CI(2)=\frac{A_{1278,1282}}{A_{1263}}$	$CI(3)=\frac{A_{1372}}{A_{894}}$
CNW	3.11	1.01	3.03
Original cellulose microfibers	1.23	0.97	1.31

Table 1 shows the estimated CI values for the original cellulose microfibers and for the CNW. From this, it can be seen than all of the CI´s are higher in the cellulose nanowhiskers than in the original cellulose microfibers, indeed suggesting that the

acid digestion has led to a significantly purified and crystalline material as expected. Oh et al. (Oh et al. 2005) reported correlation curves between the (CI(1)) and the cellulose type I crystallinity content as determined by wide-angle X-Ray diffraction (CI(X-Ray)). From the correlation established by these authors between CI (1) (A1430/A894) and CI (X-Ray), it is estimated that the crystallinity fraction of cellulose I for the CNW could be of ca. 0.86. On the other hand, the estimated crystallinity of the cellulose I for the original microfibers using this methodology is estimated to be of ca. 0.36.

Thermal properties

Melting temperature (T_m), cold crystallization temperature (T_c) and heat of fusion (ΔH_m) corrected for biopolymer content in the PLA nanocomposites were determined from the DSC first and second heating runs (see Tables 2 and 3) of the samples and the glass transition temperature (Tg) only from the second heating run (see Table 3). The Tg could not be unambiguously determined in the first run. A first run of the biocomposites (but not for the pure PLA) showed noticeable sorbed moisture (results not shown) and hence the samples had to the dried to be properly analyzed by DSC. From a recent work on solvent cast PLA nanobiocomposites containing microfibrilated cellulose, sorption of moisture occurs in the biocomposites very fast within the first 24 hours (Tingaut et al. 2010). Nevertheless, the drying process impeded the observation during the first run of the Tg. The thermal behaviour of PLA exhibits a cold crystallization process (Oksman et al. 2006) similar to that typically observed for the petroleum-based polyester polyethylene terephthalate (PET).

Table 2. DSC melting point, melting enthalpy, cold crystallization temperature and degree of crystallinity of solvent cast PLA and its nanobiocomposites with 1, 3 and 5%.-wt of CNW during the first heating run.

Sample	T_m (ºC)	ΔH_m (J/g)	T_{cc} (ºC)	$\%X_c$
PLA	152.5±0.2	8.5±1.6	110.9±1.3	9.1
PLA+1 wt.% CNW freeze dried	151.9±0.1	14.2±4.7	111.0±1.4	15.3
PLA+3 wt.-% CNW freeze dried	154.5±0.7	17.2±1.3	110.9±1.5	18.5
PLA+5 wt.-% CNW freeze dried	154.7	21.3	109.5	22.9
PLA+1 wt.-% CNW solvent exchanged	153.6±0.8	12.8±3.1	106.6±0.1	13.7
PLA+3 wt.-% CNW solvent exchanged	152.0	9.9	105.3	10.7
PLA+5 wt.-% CNW solvent exchanged	152.7	10.0	108.5	10.8

Table 3. DSC melting point, melting enthalpy, cold crystallization temperature and glass transition temperature of solvent cast PLA and its nanobiocomposites with 1, 3 and 5%.-wt of CNW during the second heating run.

Sample	T_m (ºC)	ΔH_m (J/g)	T_{cc} (ºC)	T_g (ºC)
PLA	151.4±0.1	-	-	59.1±0.3
PLA+1 wt.% CNW freeze dried	150.5±0.0	-	-	59.4±0.4
PLA+3 wt.-% CNW freeze dried	(149.5-155.2) ± (0.0-0.5)	-	119.6±0.1	57.6±0.3
PLA+5 wt.-% CNW freeze dried	153.5	13.8	117.9	57.8
PLA+1 wt.-% CNW solvent exchanged	152.9±1.4	-	-	60.1±0.7
PLA+3 wt.-% CNW solvent exchanged	149.0	-	-	58.5
PLA+5 wt.-% CNW solvent exchanged	153.2±0.9	-	-	59.5

During the first heating run the heat of fusion, defined as the area of the melting peak to which the area of the cold crystallization peak has been subtracted, seems somewhat larger for the biocomposites than for the neat material indicating that the CNW tend to favour the crystallization, perhaps transcrystallinity formation (Dufresne et al. 1999; Angles, Dufresne. 2001), of the biopolymer (see Table 2).

The same behavior was observed in a previous work for cellulose microfibers in the same PLA (Sanchez-Garcia et al.2008b). It was also reported that the nanowhiskers can induce crystal nucleation in a PHBV matrix (Jiang et al. 2008). However, Roohani et al. reported that both the melting point and the degree of crystallinity of the matrix material tended to remain roughly constant or to slightly decrease as the whiskers content increased in polyvinyl alcohol (PVA) copolymers (Roohani et al. 2008) and Petersson et al. reported the same in PLA (Petersson, Oksman. 2006). Roohani et al. (Roohani et al. 2008) attributed this behaviour to positive interactions between the cellulosic surface and polymeric matrix for the latter. These interactions were most probably claimed to restrict the capability of the matrix chains to grow bigger crystalline domains.

Table 2 also shows the actual PLA crystallinity content in the composites. This parameter is of course seen to increase with the addition of CNW in agreement with the increase in the heat of fusion. This behaviour is in contrast to the work by Peterson but agrees with a previous work in PHBV (Jiang et al. 2008). The crystallinity increase with the addition of CNW has been explained by the assumption that the CNW act as efficient nucleating agents, which enhance the crystallization rate of the matrix molecules (Zhang et al. 2003). In principle, filler-induced crystallization of the biopolymers, particularly transcrystallinity that blocks the filler matrix interface, is positive from a barrier perspective, since crystals are typically impermeable systems.

On the other hand, this feature typically brings in as a downside some opacity and additional stiffness in the biopolymer mechanical performance (see later that this is not the case here).

The incorporation of nanowhiskers increased slightly the melting temperature, indicating bigger and/or denser PLA crystals in accordance with the higher crystallinity and a potential nucleation effect. From the DSC curves (results not shown) it can be seen that the melting peak broadens in the composites suggesting a more heterogeneous crystalline morphology.

Finally, the polymer Tg was seen in the second heating run (see Table 3) to remain unmodified or increase very slightly in the 1 wt.-% CNW-PLA biocomposites, but decreased slightly in the other nanocomposites. It should be noted that this parameter could only be unambiguously detected in the second heating run after melting, and hence any issues with sorbed moisture and the corresponding plasticization cannot be discussed on the bases of this analysis. In any case, neither in the cellulose microfibers (Sanchez-Garcia et al. 2008b) nor in CNW the SEM experiments indicated interfacial debonding, preferential paths or any other suggestion for lack of adhesion at the interphase at low filler loadings. However, in the case of the microfibers the higher filler loadings led to filler agglomeration and interphase debonding observed by the SEM technique hence reducing interfacial interactions. In the case of the solvent exchange CNW-based composites the Tg increased marginally for the 1 wt.-% loaded sample, remaining unmodified at higher filler loadings. Jiang et al. also reported some increase in the Tg of the samples of PHBV with the addition of CNW (Jiang et al. 2008). From the DSC curves (dates not shown) it can be seen that during the second heating run, i.e. after controlled cooling from the melt, the cold crystallization process is rather suppressed in the pure and in the related 1 wt.-% freeze dried CNW loaded sample. On the other hand, the Tcc is seen at higher temperature (see Table 3), compared to first heating run, for the 3 wt.-% sample but with no crystallinity development and also for the 5 wt.-% but with crystallinity development. This again suggests that with increasing the CNW content crystallinity development becomes feasible in the biopolymer matrix.

In the case of the nanocomposites containing CNW obtained from a solvent exchange process the thermal properties presented the same behaviour as the freeze-dried CNW nanocomposites. Nevertheless, in these nanocomposites the crystallinity increase was seen smaller in the first melting run (see Table 2); being the overall effect in thermal properties also smaller than that of freeze-dried CNW most likely due to higher agglomeration. As a result, the differences in transparency observed in Figure 1 between CNW samples with same filler loading but different processing must arise from the effect of the filler dispersion as hypothesised earlier.

Finally, thermal degradation of PLA and of PLA/nanocomposites was also studied by TGA. Table 4 summarizes the decomposition temperature (peak maximum for the first derivative) and the residue (%) of all samples. From Table 4, the temperature at which the PLA decomposition rate is higher is at 371.5ºC. The first derivative maximum for the neat CNW is at 331.4ºC, i.e. 30ºC lower than for the original cellulose microfibers, so the cellulose nanowhiskers are more sensitive to thermal decomposition. The CNW are thus influenced by the swelling/separation treatment with the acid hydrolysis and seem to degrade faster compared to the starting purified

cellulose microfibers. In spite of this, with addition of low contents of nanowhiskers, the decomposition temperature of the PLA remained unmodified. However, with the addition of 3 wt.-% and 5 wt.-% CNW, the decomposition temperature seemed to decrease slightly, i.e. by ca. 2ºC. This decrease may not be significant.

For the pure PLA, the residue at 410ºC was found to be of ca. 3%, however with the addition of nanowhiskers the residue increased to ca. 6%, regardless of filler content. Table 4 also indicates that the CNW have lower residual weight at 410ºC than the original cellulose microfibers. This may be explained by purification of the fibers by the acid hydrolysis.

Table 4. TGA decomposition temperature and % residue at 410ºC of solvent cast PLA and its nanobiocomposites with 1, 2, 3 and 5%.-wt of nanowhiskers, CNW and original purified cellulose microfibers.

Sample	**T_d (ºC)**	**Residue % at 410ºC**
PLA	371.5	2.9
PLA+1 wt.-% CNW	371.5	6.7
PLA+2 wt.-% CNW	371.5	6.7
PLA+3 wt.-% CNW	370.0	6.1
PLA+5 wt.-% CNW	370.8	6.5
CNW	331.4	80.3
Alpha purified cellulose microfibers	363.9	89.6

Mass transport properties

Table 5 gathers the water and oxygen permeability coefficients of the PLA and of their nanocomposites. From this Table 5, the previously reported direct water permeability of chloroform cast PLA films at 1.80 10^{-14} Kg m / s m^2 Pa using chloroform as a solvent, is seen to be very similar to the one measured in this study, due to the similar processing conditions.

Table 5. Water and Oxygen permeability coefficients for PLA films with 1, 2, 3 and 5 wt.-% CNW content.

	P water (kg m/s m^2 Pa)	Reduction in water permeability	P oxygen (m^3 m/s m^2 Pa)	Reduction in oxygen permeability
PLA	$2.303\pm0.065e^{-14}$		$1.37\pm0.006e^{-17}$	
PLA+1 wt.-% CNW freeze dried	$0.819\pm0.160e^{-14}$	64%	$0.23\pm0.02e^{-17}$	83%
PLA+2 wt.-% CNW freeze dried	$0.505\pm0.053e^{-14}$	78%	$0.14\pm0.005e^{-17}$	90%
PLA+3 wt.-% CNW freeze dried	$0.422\pm0.147e^{-14}$	82%	$0.15\pm0.013e^{-17}$	90%
PLA+5 wt.-% CNW freeze dried	$0.439\pm0.123e^{-14}$	81%	$0.16\pm0.005e^{-17}$	88%
Literature value PLA	(Luo. Daniel. 2003) $1.26\ e^{-14}$		(Petersen et al. 2001)[a] $1.75e^{-18}$	
Literature value PLA	(Rhim et al. 2009) $1.80e^{-14}$			
PLA+1 wt.-% CNW solvent exchanged	$1.294\pm0.060e^{-14}$	44%		
PLA+3 wt.-% CNW solvent exchanged	$1.186\pm0.061e^{-14}$	49%		
PLA+3 wt.-% CNW solvent exchanged	$1.821\pm0.031e^{-14}$	21%		

[a]At 75%RH (commercial biobased material)

Figure 7 shows the plot of the water permeability of the neat PLA and of their nanocomposites with different contents of nanowhiskers. Reductions of water permeability of ca. 64%, 78%, 82% and 81% were obtained for the cast films containing 1, 2, 3 and 5 wt.-% of nanowhiskers, respectively. For the films of PLA with CNW prepared by solvent exchange with chloroform we obtained reductions of ca. 44%, 49% and 21% for the films containing 1, 3 and 5 wt.-% of CNW, respectively. Thus, the best results in water permeability are found for the films containing freeze-dried CNW in accordance with morphology data.

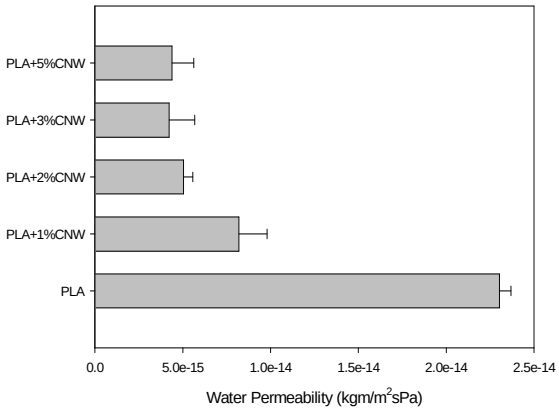

Figure 7. Water Permeability of PLA and their nanocomposite with 1, 2, 3 and 5 wt.-%CNW-freeze dried content.

From previous work (Sanchez-Garcia et al. 2008b), the barrier properties to water of PLA biocomposites containing cellulose microfibers were seen to be only reduced (by ca. 10%) in the sample containing 1 wt.-% of the filler. The biocomposite samples with 4 or 5 wt.-% microfibers content showed no barrier improvements and for the case of the 10 wt.-% microfibers content the permeability was even seen to increase by ca. 80%. By nanofabrication, the same material is dispersed to a higher extent and possesses higher levels of crystallinity, thus yielding a more efficient barrier effect. The transport properties are known to be strongly influenced by tortuous path altering factors including shape and aspect ratio of the filler, degree of exfoliation or dispersion, filler loading and orientation, adhesion to the matrix, moisture activity, filler-induced crystallinity, polymer chain inmobilization, filler-induce solvent retention, degree of purity, porosity and size of the permeant (Sanchez-Garcia et al. 2008a, Sanchez-Garcia et al. 2008b).

Table 5 gathers the oxygen permeability value measured at 75%RH and reported in the literature for PLA (extruded film) of $1.75e^{-18}$ m^3m/sm^2Pa (Petersen et al. 2001), which is somewhat lower than the value of $1.37e^{-17}m^3m/sm^2Pa$ measured in our lab at 80%RH. The reason for the disagreement could be related to the different origins of the samples. For the PLA composites containing 1, 2, 3 and 5 wt.-% of the filler oxygen permeability reductions of 83%, 90%, 90% and 88% were observed, respectively (see Figure 8).

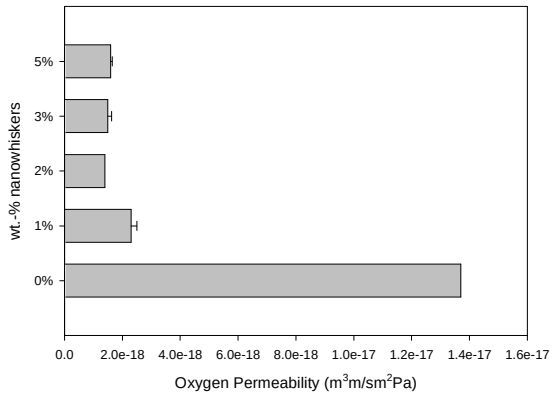

Figure 8. Oxygen Permeability of PLA and their nanocomposite with 1, 2, 3 and 5 wt.-%CNW content.

It is a general observation that composites containing between 2 and 3 wt.-% of the nanowhiskers exhibit the highest water and oxygen barrier. The barrier results are in good accordance in relative terms with the water permeability and with the thermal data discussed above, i.e. crystallinity rise due to filler-induced nucleation. Another general observation is that the barrier properties are significantly enhanced with the addition of cellulose nanowhiskers compared to the cellulose microfibers for same filler content in the PLA.

Nielsen (Nielsen. 1967) developed an expression to model the permeability of a two-phase film in which impermeable square plates are dispersed in a continuous conducting matrix. The plates are oriented so that the two edges of equal length, L, are perpendicular to the direction of transport: and the third edge, of width W, is parallel to the direction of transport. This is expressed as follows:

$$P = P_m\left(1-\phi_d\right)/\left[1+\left(L/2W\right)\phi_d\right]$$

where P is the permeability of the composite, Pm, is the permeability of the matrix, and Φd is the volume fraction of the impermeable filler. The (1 - Φd) term accounts for volume exclusion and the (1 + (L/2W) Φd) term for the tortuosity factor. In the following, this model will be called the tortuosity model. Note that this model does not account for permeation through the dispersed phase.

A more realistic system to consider is one in which a discontinuous low-permeability phase is present in a high-permeability matrix. Maxwell (Maxwell. 1891) developed a model to describe the conductivity of a two-phase system in which permeable spheres are dispersed in a continuous permeable matrix. Fricke (Fricke. 1924) extended Maxwell's model to describe the conductivity of a two-phase system in which permeable ellipsoids are dispersed in a more permeable continuous matrix.

Figure 9 shows the experimental permeability values, these corrected by crystallinity alterations and the modelling results using the Nielsen and Fricke

extended Maxwell´s models. The latter model describes the conductivity of a two-phase system in which lower permeability elongated ellipsoids (Pd) are dispersed in a more permeable continuous matrix (Pm). According to this model, the permeability of a composite system consisting of a blend of the two materials in which the dispersed phase (Φ2 is the volume fraction of the dispersed phase) is distributed as ellipsoids can be expressed as follows (Paul, Bucknall. 2000):

$$P = (Pm + PdF)/(1+F)$$

where

$$F = [\Phi 2/1 - \Phi 2][1/(1+(1-M)(Pd/Pm-1))]$$

$$M = \cos\theta / \sin 3\theta\,[\theta - 1/2 \sin 2\theta]$$

and

$$\cos\theta = W/L$$

Where ρcellulose nanowhiskers = 1.6 g/ml (Jeffrey et al. 2009), Pd ≈ 0 , Pm=100 and L/W of 8 and 50.

W is the dimension of the axis of the ellipsoid parallel to, and L the dimension perpendicular to, the direction of transport, and θ in radians.

The whiskers observed by TEM in the PLA film suggested experimental L/W (particle length/width ratio) values ranging from 6 to 16. From the results, the permeability drop with increasing filler volume is actually higher than predicted by the modelling even for aspect ratios which seem bigger than the actual experimental aspect ratios. Only the permeability to water corrected for crystallinity changes and at low filler contents appears to resemble the modelling but of ellipsoids with higher aspect ratio. It is also observed that the experimental data is closer to the Fricke model than to the Nielsen model. The reason for the disagreement could be the role of sorbed moisture. It has been reported before that there are regimens in hydrophilic polymers such as in ethylene vinyl alcohol copolymers (EVOH) in which gas permeability is actually lower at medium low relative humidity conditions than in dry conditions due to the fact that sorbed moisture is thought to fill in the existing free volume without breaking the polymer chain self-association (Lagaron et al. 2003; Lagaron et al. 2004). It is possible that moisture sorbed by the filler could act as a plasticizer for the polymer (see later) but at the same time could fill in the available free volume hence exhibiting a blocking effect and subsequent reduction in permeability beyond what is expected by the modeling.

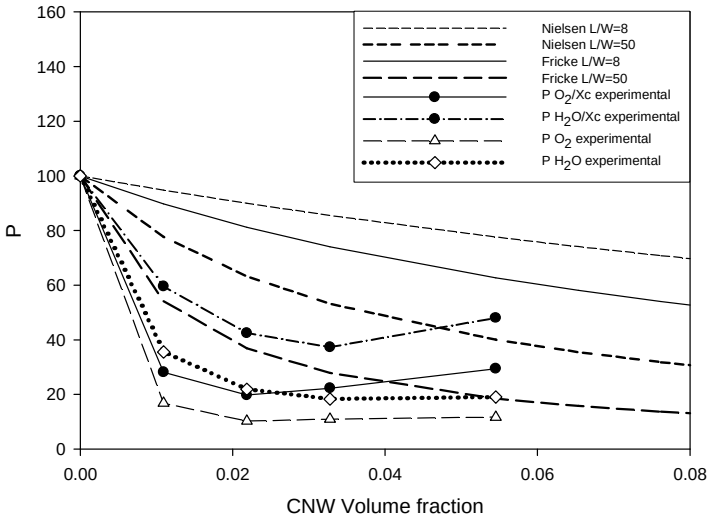

Figure 9. Permeability modelling of a hypothetical blend vs. vol% of the dispersed phase with different aspect ratio L/W compared with the experimental relative permeability values and these corrected for the crystallinity increase.

Mechanical properties

Specimens of the PLA films and of their nanocomposites were evaluated by tensile testing, in order to ascertain the effect of the cellulose nanowhiskers on the mechanical properties of this biopolymer. Mechanical properties such as tensile strength, tensile modulus and elongation at break vs. filler content tested at room temperature are plotted in Figure 10.

Table 6. **Mechanical properties for PLA films and their nanocomposites**

	E Modulus (MPa)	Tensile Strength (MPa)	Elongation at Break (%)
PLA	1886.44±9.11	58.22±0.31	6.03±1.26
PLA+1%CNW freeze dried	1197±3.50	30.42±0.15	6.87±0.25
PLA+2%CNW freeze dried	990.5±174.65	26.84±0.79	7.64±2.04
PLA+3%CNW freeze dried	1070±362.03	36.48±6.97	12.57±3.78
PLA+5%CNW freeze dried	1225±208.79	37.23±3.35	8.19±0.65
PLA+1%CNW solvent exchanged	271.5±74.82	16.65±3.40	2.02±0.59
PLA+3%CNW solvent exchanged	298.84±85.32	12.66±1.21	1.99±0.31
PLA+5%CNW solvent exchanged	911.33±289.43	35.74±12.74	5.75±1.23

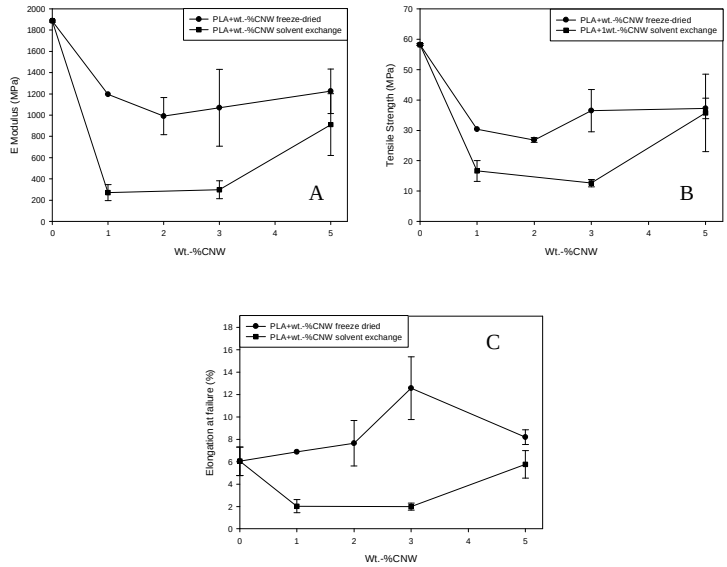

Figure 10. A) Young Modulus E (MPa) as a function of PLA containing freeze dried CNW and solvent exchange CNW. B) Tensile strength as a function of CNW content and C) Elongation at failure (%) as a function of the CNW content.

From the results, the mechanical properties did not show improvement when compared to the pure PLA. From Table 6 and Figure 10, it can be seen a reduction in tensile modulus and tensile strength and an increase in the elongation at break. Curiously, with increasing filler loading a reinforcing effect is displayed compared to lower filler loadings but in the range screened the mechanical rigidity is always below that of neat PLA. Thus, a reduction in tensile modulus of ca. 37%, 47%, 43% and 35% for PLA films containing 1, 2, 3 and 5 wt.-% freeze-dried CNW were obtained. Films of PLA with CNW obtained by solvent exchange with chloroform presented a reduction in Young Modulus of ca. 86%, 84% and 52% for related composites containing 1, 3 and 5 wt.-% of the filler. This indicates a stronger softening effect of the CNW obtained by the latter method.

In the case of tensile strength, reductions of 48%, 54%, 37% and 36% in the property value with the addition of 1, 2, 3 and 5 wt.-% of freeze-dried CNW were measured. For films of PLA with 1, 3 and 5 wt.-% of solvent exchanged CNW again a greater reduction in the property of ca. 71%, 78% and 38% was seen.

For the elongation at break, an increase of ca. 14%, 27%, 108% and 35% in the property with the addition of 1, 2, 3 and 5 wt.-% of freeze-dried CNW was observed. As opposed to the plasticizing behaviour of the latter CNW, in the case of the nanocomposites with 1, 3 and 5 wt.-% of solvent exchanged CNW a significant

reduction in the elongation at break of ca. 66%, 67% and 5% was observed, suggesting a lower interfacial interaction effect and/or lack of optimum dispersion.

Petersson et al. reported earlier a decrease in mechanical properties in PLA films containing microfibrillated cellulose and attribute these results to an agglomerated morphology and lack of good interaction between the matrix and the cellulose microfibers (Petersson, Oksman. 2006). However, this does not seem to be case here, where a nice CNW dispersion and excellent barrier properties were obtained.

Siqueira et al. (Siqueira et al. 2009) also reported that the addition of raw sisal whiskers to PCL resulted in a global decrease of the tensile mechanical behaviour of the material. This result was again ascribed to the poor interfacial adhesion between the cellulosic nanoparticles (hydrophilic) and the PCL matrix (hydrophobic). However, other previous studies have indicated that not only the filler-matrix adhesion but also the filler-filler interactions are important when considering the reinforcing capability of cellulose whiskers (Siqueira et al. 2009; Oksman et al. 2006). Thus, it has been reported that the mechanical properties of cellulosic whiskers are far from simple and strongly depend on the matrix system and processing conditions. Thus, in whisker based composite materials, in fact a curious counterintuitive trend has often been reported, i.e. the higher the affinity between the cellulosic filler and the host matrix, the lower is the mechanical performance. Achieving the so-called percolation threshold, where the whiskers attained are strongly interconnected by a 3D network, has also being claimed as a necessary condition to achieve strong mechanical reinforcement in these systems and interference of this by structural, compositional or environmental factors is thought to be fatal for strong reinforcement. By making use of the following equation where the percolation threshold can be easily anticipated on the bases of the aspect ratio (Oksman et al. 2006),

it is determined that for our system with a maximum experimental aspect ratio of ca. 16, the percolation threshold should lay around 4 v.-% of CNW. In fact we begin to see the recovery in the mechanical properties at the higher filler loading studied of ca. 5.5 v.-% of CNW. In addition, a recent work also explained the potential plasticization effect that the reinforcing hydrophilic filler microfibrilated cellulose can bring to a matrix (López-Rubio et al. 2007). This counterintuitive effect was ascribed to filler-induced sorbed moisture.

Modelling of the mechanical properties using the below Halpin-Tsai equation was also carried out to determine the theoretical expectations (Petersson, Oksman. 2006):

$$E = \frac{E_m(1+\xi\eta\phi)}{1-\eta\phi}, \quad \eta = \frac{E_r/E_m - 1}{E_r/E_m + \xi},$$

$$\xi = \frac{2xLength}{Thickness}, \ \phi = \text{volume fraction}$$

The Halpin-Tsai equation is normally used to predict the modulus for aligned fiber composites, but it has been used before to predict the modulus of nanocomposites (Petersson, Oksman. 2006; Wu et al. 2004).

The following data were used in the calculations: E_{PLA}=1.7GPa (Wu et al. 2004), $E_{cellulose}$=167.5GPa (Tsahiro, Kobayaski. 1991), ρ_{PLA}=1.25 g/cm^3 (Ganster et al. 1999), $\rho_{cellulose}$=1.6 g/cm^3 (Fricke. 1924), $Dimensions_{CNW}$ 160 x 10 nm. The volume fraction of the nanoreinforcement was calculating using the following equation (Luo, Daniel. 2003):

$$V_r = \frac{w_r / \rho_r}{w_r / \rho_r + (1 - w_r) / \rho_m}$$

A comparison between the theoretical and experimental results is presented in Figure 11. The theoretical calculations are based on fully dispersed systems where the filler is aligned in the longitudinal direction and has perfect interfacial adhesion to the matrix. The experimental results are clearly not aligned with the expected results. This is most likely due to the combination of many factors but potentially two could play greater role: Water-induced plasticization and being below the percolation threshold.

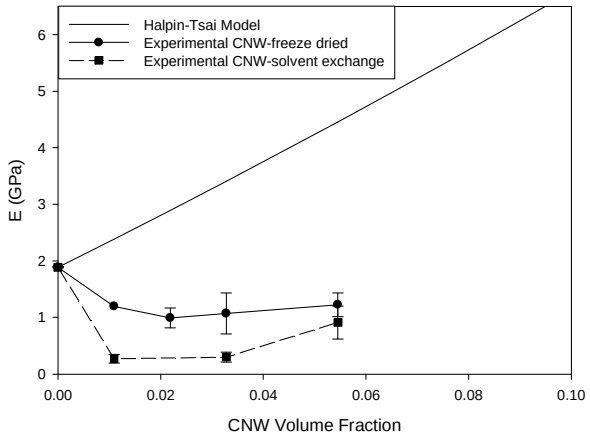

Figure 11. Experimentally measured tensile E modulus compared to theoretical predictions by Halpin-Tsai.

Conclusions

Cellulose nanowhiskers, with lengths ranging from 60-160 nm and thicknesses ranging from 10-20 nm, were prepared from highly purified alpha-cellulose microfibers (with 50-100 μm length and 10-20 μm thickness) by acid hydrolysis and were used to reinforce a PLA matrix with contents ranging from 1 to 5 wt.-% by a solvent casting method. Two methods were used to disperse the whiskers in the PLA

matrix namely, freeze dried CNW and CNW obtained after solvent exchange with chloroform.

The TEM results indicated that the freeze dried CNW were better dispersed in the PLA matrix. The solvent exchanged CNW showed less dispersion and transparency. From the DSC results, melting point and crystallinity increased with increasing CNW loading hence suggesting a filler-induced crystallinity development. From TGA results, it was concluded that the addition of low fractions of CNW in the PLA do not alter the thermal degradation of the matrix.

Interestingly, the CNW were able to reduce the water permeability by up to 82% and the oxygen permeability by up to 90% with only 3 wt.-% of nanofiller content. This barrier enhancement was higher than expected by applying the most widely used models. The presence of highly crystalline cellulose nanoshields, PLA crystallinity development (e.j. transcrystallinity) and sorbed moisture filling the free volume were put forward as the most likely factors behind this behaviour. Contrarily, the mechanical performance was seen lower than that of neat PLA and than expected by typical modelling work. This observation was ascribed to both the filler ranged screened being below the percolation threshold and most importantly to filler-induced plasticization by sorbed moisture.

In spite of the above, the main conclusion from this work is that purified cellulose nanowhiskers were shown for the first time, to be adequate for significant improvement in the barrier properties to gases and vapours of polylactic acid, hence resulting in fully renewable biocomposites of interest in biopackaging, membrane and coating applications.

References

Angle`s MN, Dufresne A. Plasticized starch/tunicin whiskers nanocomposites: 2. Mechanical behavior. Macromolecules 2001, 34 (9), 2921-2931.

Auras R, Kale G, Singh SP. Degradation of commercial biodegradable packages under real composting and ambient exposure conditions. Journal of Polymers and the Environment 2006,14, 3, 317-334.

Ayuk JE, Mathew AP, Oksman K. The Effect of Plasticizer and Cellulose Nanowhisker Content on the Dispersion and Properties of Cellulose Acetate Butyrate Nanocomposites. Journal of Applied Polymer Science 2009, 114, 2723–2730.

Azizi Samir MAS, Alloin F, Dufresne A. Review of Recent Research into Cellulosic Whiskers, Their Properties and Their Application in Nanocomposite Field. Biomacromolecules 2005, 6, 612-626.

Bastiolo C, Bellotti V, Del Tredici GF, Lombi R, Montino A, Ponti. R. Int. Pat. Appl. 1992, WO92/19680.

Cava D, Gimenez E, Gavara R, Lagaron JM. Comparative performance and barrier properties of biodegradable thermoplastics and nanobiocomposites vs. PET for food packaging applicationsJournal of Plastics films and sheeting, 2006, 22, 265.

Dufresne A, Kellerhals MB, Witholt B. Transcrystallization in mcl-PHAs/cellulose whiskers composites. Macromolecules 1999, 32 (22), 7396-7401.

Favier V. Ph.D. Thesis, Joseph Fourier University, Grenoble, France, 1995.

Fricke H. Phys. Rev. 1924, 24, 575.

Ganster J, Fink HP, In: Brandrup J, Immergut EH, Grulke EA, editors. Polymer handbook, Fourth ed.,volume 1. Usa: John Wiley and Sons, Inc.; 1999.

Hajji P, Cavaille´ JY, Favier V, Gauthier C, Vigier G. Tensile behavior of nanocomposites from latex and cellulose whiskers. Polym Compos. 1996, 17 (4), 612-619

Helbert W, Cavaille JY, Dufresne A. Thermoplastic nanocomposites filled with wheat straw cellulose whiskers. Part I: Processing and mechanical behaviour. Polym. Compos. 1996, 17, 604-611.

Jeffrey R, Capadona KS, Trittschuh S, Scott S, Stuart JR,Weder C. Polymer Nanocomposites with Nanowhiskers Isolated from Microcrystalline Cellulose. Biomacromolecules 2009, 10, 712–716.

Jiang L, Morelius E, Zhang J, Wolcott M. Study of the Poly(3-hydroxybutyrate-co-3-hydroxyvalerate)/Cellulose Nanowhisker Composites Prepared by Solution Casting and Melt Processing .Journal of Composite Materials, 2008, 42, 24.

Koening MF, Huang SJ. Biodegradable blends and composites of polycaprolactone and starch derivatives. Polymer 1995, 36, 1877.

Kvien I, Tanem BS, Oksman K. Characterization of Cellulose Whiskers and Their Nanocomposites by Atomic Force and Electron Microscopy. Biomacromolecules 2005, 6, 3160-3165.

Lagaron JM, Gimenez E, Catala R, Gavara R. Mechanisms of moisture sorption in barrier polymers used in food packaging: amorphous polyamide vs. high barrier ethylene-vinyl alcohol copolymer studied by vibrational spectroscopy.
Macromolecular Chemistry and Physics 2003, 204, (4), 704-713.

Lagaron JM, Catalá R, Gavara R. Structural characteristics defining high barrier polymeric materials. Materials Science and Technology 2004, 20 (1), 1-7.

Liu X, Dever M, Fair N, Benson RS. Thermal and Mechanical Properties of Poly(lactic Acid) and Poly(ethylene/butylene Succinate) Blends. Journal of Environmental Polymer Degradation 1997, 5, 4.

López-Rubio A, Lagaron JM, Ankerfors M, Lindström T, Nordqvist D, Mattozzi A, Hedenqvist MS. Enhanced film forming and film properties of amylopectin using micro-fibrillated cellulose. Carbohydrate Polymers, 2007, 68, 718–727.

Luo JJ, Daniel IM. Characterization and modelling of mechanical behaviour of polymer/clay nanocomposites. Compos Sci Technol 2003, 63: 1607-16.

Marchessault RH, Morehead FF, Walter NM. Liquid Crystal Systems from Fibrillar Polysaccharides. Nature 1959,184, 632-633.

Maxwell JC.; Electricity and Magnetism, 1891,1, 3rd., Dover. New York.

Morin A, Dufresne A. Nanocomposites of chitin whiskers from Riftia tubes and poly(caprolactone). Macromolecules 2002, 35 (6), 2190-2199.

Nielsen LW. J. Macromol Sci. 1967, 929.

Oh SY, Yoo DI, Shin Y, Kim HC, Kim HY, Chung YS, Park WH, Youk JH. Crystalline structure analysis of cellulose treated with sodium hydroxide and carbon dioxide by means of X-ray diffraction and FTIR spectroscopy. Carbohydrate Research 2005, 340, 2376–2391.

Oksman K, Mathew AP, Bondeson D, Kvien I. Manufacturing process of cellulose whiskers/polylactic acid nanocomposites. Composites Science and Technology, 2006, 66, 2776–2784.

Park ES, Kim MN, Yoon JSJ. Grafting of polycaprolactone onto poly(ethylene-co-vinyl alcohol) and application to polyethylene-based bioerodable blends Polym. Sci.: Part B Polym. Phys. 2002, 40, 2561.

Paul DR, Bucknall CB. Polymer Blends Volume 2: Performance. 2000

Petersen L, Nielsen PV, Olsen MB. Physical and mechanical properties of biobased materials. Starch, 2001, 53, 8, 356.

Petersson L, Kvien I, Oksman K. Structure and thermal properties of poly(lactic acid)/cellulose whiskers nanocomposite materials. Composites Science and Technology 2007, 67, 2535–2544.

Petersson L, Oksman K. Biopolymer based nanocomposites: Comparing layered silicates and microcrystalline cellulose as nanoreinforcement. Composites Science and Technology, 2006, 66, 2187–2196.

Podsiadlo P, Choi S, Shim B, Lee J, Cussihy M, Kotov N. Molecularly Engineered Nanocomposites: Layer-by-Layer Assembly of Cellulose Nanocrystals. Biomacromolecules 2005, 6, 2914-2918.

Rhim JW, Hong SI, Ha, C. S. Tensile, water vapor barrier and antimicrobial properties of PLA/nanoclay composite films. Food Science and Technology, 2009, 42, 612–617.

Roohani M, Habibi Y, Belgacem NM, Ebrahim G, Karimi AN, Dufresne A. Cellulose whiskers reinforced polyvinyl alcohol copolymers nanocomposites.European Polymer Journal 2008, 44, 2489–2498.

Sanchez-Garcia MD, Gimenez E, Lagaron JM. Comparative Barrier Performance of Novel PET Nanocomposites With Biopolyester Nanocomposites of Interest in Packaging Food Applications. Journal of Plastic Film and Sheeting 2007;23 133-148.

Sanchez-Garcia MD, Gimenez E, Lagaron JM. Development and Characterization of Novel Nanobiocomposites of Bacterial Poly(3-hydroxybutirate), Layered silicates and Poly(ε-caprolactone).Journal of Applied Polymer Science. 2008a, 108, 2787–2801.

Sanchez-Garcia MD, Gimenez E, Lagaron JM. Mophology and Barrier Properties of Solvent Cast Composites of Thermoplastic Biopolymers and Purified Cellulose Fibers. Carbohydrate Polymers, 2008b, 71, 235–244.

Siqueira G, Bras J, Dufresne A. Cellulose Whiskers versus Microfibrils: Influence of the Nature of the Nanoparticle and its Surface Functionalization on the Thermal and Mechanical Properties of Nanocomposites. Biomacromolecules 2009, 10, 425–432.

Sturcova A, Davies GR, Eichhorn SJ. Elastic modulus and stress-transfer properties of tunicate cellulose whiskers. Biomacromolecules 2005, 6, 1055-1061.

Tingaut P, Zimmermann T, Lopez-Suevos F. Synthesis and Characterization of Bionanocomposites with Tunable Properties from Poly(lactic acid) and Acetylated Microfibrillated Cellulose. Biomacromolecules 2010, 11, 454-464.

Tsahiro K, Kobayaski M. Theorical evaluation of three-dimesional elastic constant of native and regenerated celluloses: role of hydrogen bonds. Polymer 1991; 32: 1516-26.

Tsuji H, Yamada TJ. Blends of aliphatic polyesters. VIII. Effects of poly(L-lactide-co-ε-caprolactone) on enzymatic hydrolysis of poly(L-lactide), poly(ε - caprolactone), and their blend films. Appl. Polym. Sci. 2003. 87, 412.

Wang B, Sain M, Oksman K. Study of Structural Morphology of Hemp Fiber from the Micro to the Nanoscale. Appl. Compos. Mater. 2007,14:89–103.

Wu YP, Jia QX, Yu DS, Zhang LQ. Modelling young´s modulus of rubber-clay nanocomposites using composites theories. Polymer Testing 2004; 23:903-9.

Zhang G, Yan DJ. Crystallization kinetics and melting behavior of nylon 10,10 in nylon 10,10-montmorillonite nanocomposites. Appl Polym Sci 2003, 88, 2181–2188.

<u>PAPER VIII:</u> Morphology and Barrier Properties of Solvent Cast Nanobiocomposites of κ/ι--carrageenan and Cellulose Nanowhiskers.

Abstract

The current study presents the development and characterization of novel carrageenan nanobiocomposites showing enhanced water barrier due to incorporation of cellulose nanowhiskers (CNW). CNW, prepared by acid hydrolysis of highly purified alpha cellulose microfibers, were seen to have a length of around 25-50 nm and a cross-section of ca. 5 nm when dispersed in the matrix. The nanobiocomposites were prepared by incorporating 1, 3 and 5.-wt% of the CNW into a carrageenan matrix using a solution casting method. Morphological data (TEM and optical microscopy) of the nanocomposites containing CNW were compared with the morphology of the corresponding biocomposites containing the original cellulose microfibers and differences discussed. The main conclusion arising from the analysis of the results is that the nanobiocomposites containing 3 wt.-% of CNW exhibited the lowest reduction in water permeability, i.e. ca. 71%, and that this reduction was largely attributed to a filler-induced water solubility reduction. This fully biobased nanoreinforced carrageenan can open new opportunities for the application of this biopolymer in food packaging and coating applications.

Keywords: Carrageenan, Food packaging, Food coating, Biocomposites, Cellulose

1. Introduction

Biopolymer films have been the focus of worldwide attention for the past few decades because they offer favorable environmental advantages in terms of biodegradability compared to conventional synthetic polymeric films. Edible and biodegradable natural polymer films offer alternative packagings and coatings with lower environmental costs. The search for new renewable resources for the production of edible and biodegradable materials has steadily increased in recent years. In particular, nonconventional sources of carbohydrates have been extensively studied. There are various unique carbohydrates that are found in marine organisms that represent a largely unexplored source of valuable materials. These nonconventional and underexploited renewable materials can be used as an interesting alternative to produce edible films and coatings (4).

The biopolymers studied in this work to produce edible films and coatings were κ/ι-hybrid carrageenan extracted from Mastocarpus stellatus, an underexploited red algae present in the Portuguese marine coast (1-4). Carrageenans are water-soluble polymers with a linear chain of partially sulfated galactans,which present high potentiality as film-formingmaterials. Carrageenans are structural polysaccharides from red seaweed and have beenused extensively in foods, cosmetics, and pharmaceuticals (5). Carrageenan biopolymer extracted from M. stellatus seaweeds was shown to be a κ/ι-hybrid carrageenan with gel properties comparable to those of commercial κ-carrageenan gel formers. The use of carrageenan as edible films and coatings already covers various fields of the food industry such as application on fresh and frozen meat, poultry, and fish to prevent superficial dehydration (6), hamor sausage casings (7), granulation-coated powders, dry solids foods, oily foods (8), etc., and also the manufacture of soft capsules (9, 10) and especially nongelatin capsules (11). Polysaccharide and protein film materials are characterized by high moisture permeability, low oxygen and lipid permeability at lower relative humidities, and compromised barrier and mechanical properties at high relative humidities (12).

To tailor the properties and improve the water resistance of these biopolymers, it is often desirable to blend them with more waterresistant biopolymers orwith nanoadditives. In the case of the addition of nanoclays, the nanocomposite films have been seen to substantially reduce water-vapor permeability, solving one of the long-standing problems in the production of biopolymer films and coatings (13).

More recently, cellulose nanowhiskers (CNW), also termed cellulose nanocrystals, are increasingly used as load-bearing constituents in developing new and inexpensive biodegradable materials due to their high aspect ratio, good mechanical properties (14), and fully degradable and renewable character.

As compared to other inorganic reinforcing fillers, CNW have many additional advantages, including a positive ecological footprint, wide variety of fillers available throughout the world, low density, low energy consumption in manufacturing, ease of recycling by combustion, high sound attenuation, and comparatively easy processability due to their nonabrasive nature (15,16).

Cellulose nanowhiskers are prepared by treating native cellulosic products with acid reagents, most typically sulfuric acid, where small amounts of sulfate ester groups are introduced to the surfaces (17). This treatment is, however, hydrolytic and thus results in dramatic decreases in both the yield and fibril length attained down to 100-150 nm. The use of cellulose nanowhiskers as nanoreinforcement is a new field in nanotechnology, and as a result there are stillmany obstacles remaining regarding their use. Their production is time-consuming and is still associated with low yields. They are difficult to use in systems that are not water based due to

their strong self-association by hydrogen bonding. Here, the cellulose nanowhiskers are added to the carrageenan, which is water-soluble. Because cellulose nanowhiskers allow a quite stable dispersion in water, composites are generally obtained with matrices that can be dissolved/suspended in water such as latex (18-20), starch (21, 22), poly(ethylene oxide) (PEO) (23, 24), chitosan (25), and soy protein (26). A previous study showed for the first time the capacity of this natural nanoreinforcing element to develop nanobiocomposites of solvent cast PLA by various methods, which resulted in enhanced barrier properties to gases and vapors (31).

However, very little is known about the development and characterization of carrageenan nanocomposites. Daniel-Da-Silva et al. reported the use of ι-carrageenan polysaccharide for the production of macroporous composites containing nanosized hydroxyapatite, with application in bone tissue engineering (27). Gan et al. developed a new injectable biomaterial, carrageenan/ nanohydroxyapatite/collagen, for bone surgery (28). In a previous work, Sanchez-Garcia et al. reported the development and barrier properties of new nanocomposites of carrageenan based on nanoclays (13). However, to the best of our knowledge, the addition of cellulose nanowhiskers to carrageenan and the study of the resulting barrier properties of these novel nanobiocomposites have not been reported before.

Thus, the objective of this work is to develop new fully renewable and biodegradable edible films for food-packaging applications with better barrier properties, especially better water resistance. A top-down nanotechnology approach is used to reach this objective, which consists of the incorporation via solution casting of plant -derived cellulose nanowhiskers previously hydrolyzed from the corresponding microfibers.

2. Experimental

2.1 Materials

Details about the recovery of κ/ι-hybrid carrageenan biopolymers from M. stellatus seaweeds can be found elsewhere (1, 2, 29). The polysaccharide used in the present study was obtained through a hot extraction process performed during 2 h at 95ºC and a pH of 8 on alkalitreated M. stellatus seaweeds. The resulting powder was then purified by mixing 1 g of isolated product with 50mL of hot distilled water during 1 h and subsequent centrifugation performed at sequence cycles at 104 rpm (13.7 g) and 40ºC during 40 min. The supernatant was finally recovered and used for film forming by casting.

A highly purified R-cellulose microfiber grade from CreaFill Fibers Corp. (USA), having an average fiber length of 60 μmand an average fiber width of 20 μm, was used. According to the manufacturer's specifications, these fibers had an R-cellulose content in excess of 99.5%.

Sulfuric acid (95-97%) from Sigma Aldrich, Germany, was used during the CNW production. Sodium hydroxide from Fluka was also used during neutralization of the CNW. Glycerol was used as plasticizer and was supplied by Panreac Quimica S.A. (Spain).

2.2 Preparation of nanocomposites

2.2.1. CNW production

Highly purified R-cellulose microfibers, 10 g/100 mL, were hydrolyzed in 9.1 mol/L sulfuric acid at 44ºC for 130 min. The excess of sulfuric acid was removed by repeated cycles of centrifugation, 10 min at 13000 rpm (20.4g). The supernatant was removed from the sediment and was replaced by deionized water. The centrifugation continued until the supernatant became turbid, which suggested that the nanowhiskers became largely released into the solution in

accordance with a previous work (30). After centrifugation, the suspension containing cellulose nanowhiskers had a pH of 3.5, and the solution was drop by drop neutralized with sodium hydroxide to pH 7 and subjected to dialysis, following a procedure described elsewhere (33). The nanofiller was used suspended in water to make the various nanobioblends to avoid potential agglomeration during drying.

2.2.2. CNW dispersion and film preparation

Solution-cast film samples of carrageenan containing 1, 3, and 5 wt % of CNW were prepared, using water as a solvent. CNW solutions were mixed in a homogenizer (Ultraturrax T25 basic, Ika-Werke, Germany) for 2 min and were then stirred with the carrageenan at ambient temperature during 30 min and, subsequently, cast onto Petri dishes to generate films of around 50 μm thickness after solvent evaporation at room temperature conditions. In the case of carrageenan films with glycerol, 10 wt%of glycerol was added to the solution before casting. Similar blends were obtained with 1, 3, and 5 wt % contents of the original cellulose microfibers for comparative purposes.

2.3 Optical light polarized microscopy

Polarized light microscopy (PLM) examinations using an ECLIPSE E800-Nikon with a capture camera DXM1200F- Nikon were carried out on both sides of the cast samples.

2.4 TEM measurements

TEM was performed using a JEOL 1010 equipped with a digital Bioscan (Gatan) image acquisition system. TEM observations were very difficult to perform due towater absorption and difficult handling of the films. However, some pictures were taken onmicrodrops of the film-forming solutions cast directly onto the TEM observation grids. The solutions were stained before casting by adding a 2 wt%solution of uranyl acetate for 3min. The pure cellulose nanowhiskers were also observed by direct casting of water suspensions over the TEM grids followed by solvent evaporation.

2.5 TGA measurements

The thermal stability of both freeze-dried CNW and cellulose microfibers and of the nanocomposites was investigated using a TGA Q500 from TA InstrumentsUSA. The samples were heated from room temperature to 600ºC at a heating rate of 10ºC/min and a nitrogen flow of 100 mL/min.

2.6 Gravimetric measurements

Direct water vapor permeability was determined from the slope of the weight gain versus time curves at 24ºC. The films were sandwiched between the aluminum top (open O-ring) and bottom parts of a specifically designed permeability cell with screws containing silica gel to generate 0% relative humidity (RH). A Viton rubber O-ring was placed between the film and the bottom part of the cell to enhance sealability. Then, the cells were placed in the desired environment, namely, a desiccator conditioned at 75%RH generated by a saturated salt solution, and the solvent weight gain through the film was monitored as a function of time. Cells with aluminum films were used as control samples to estimate solvent gain through the sealing. Solvent permeation rateswere estimated from the steady-state linear permeation slopes. Water weight gain was calculated as the total cell weight gainminus the gain through the sealing. The tests were done in duplicate.

For the percent water uptake, samples were dried in a desiccator at 0% RH until constant weight to obtain the so-called dry weight. They were then allowed to saturate in moisture inside desiccators at 11, 54, and 75% RH and monitored during sorption until constant weight (indicating water uptake). The experiments were done in triplicate and averaged. The water uptake was calculated as the water gain at the desired RH divided by the dry weight and multiplied by 100.

3. Results and Discussion

3.1 Morphological characterization

Figure 1 shows typical photographs taken in the cast carrageenan film and its nanocomposite containing 5 wt % CNW and its microcomposite containing 5 wt%cellulose microfiber. Samples with CNWshowed the best optical properties, the samples with cellulose microfibers being less transparent. Both contact transparency (see Figure 1a) and transparency against light (see Figure 1b) were evaluated. In the contact transparency, the samples appear to exhibit similar behaviors. However, in transparency against light the film containing CNW shows better performance, suggesting that the cellulose nanowhiskers must be well dispersed in contrast to large cellulose microfibers, which scatter light to a significant extent. In any case, unfilled carrageenan films do still show the highest transparency.

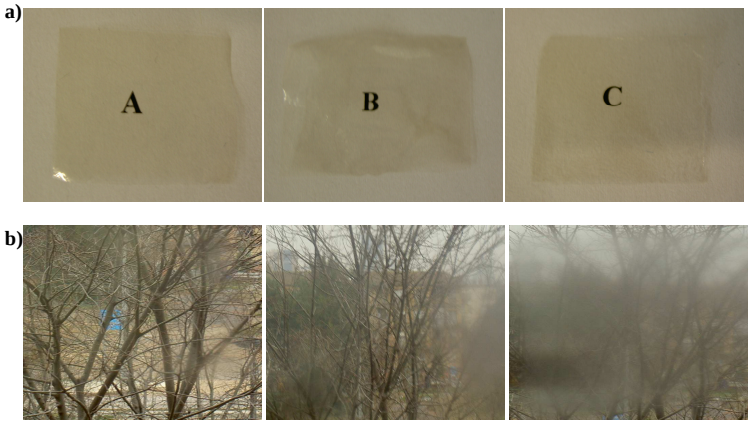

Figure 1. Typical photographs of 30 microns thickness films of A) Carrageenan, B) Carrageenan film containing 5wt.-% of CNW and B) Carrageenan film containing 5wt.-% of cellulose microfibers.

Polarized optical microscopy permits one to zoom up the morphology at the micrometer level to observe the carrageenan composites and to potentially assess the efficiency of the hydrolysis and separation processes in the nanocomposites (see Figure 2). From this figure, it can be seen that some remaining microfibers can still be detected in the separated CNW fractions. Despite this, the scarce remaining microfiber particles are of course much thinner in comparison with the original microfibers.

Optical microscopy was not often utilized when nanofabrication of cellulose was carried out in the previous literature and, hence, it is difficult to assess whether this is the result of our process or if it is a general effect during the hydrolysis of microfibers. The optimization of the hydrolysis time and the effect of using different acidswill be reported elsewhere.

Figure 2A indicates that the dimensions of the cellulose microfibers in the biocomposites are not homogeneous but vary from 10 to 30 μm in the cross section and between 50 and 150 μm in length across the polymer matrix. For biocomposites with higher filler contents, larger fiber aggregates and agglomeration of the microfibers in the matrix are observed (see Figure 2E), as reported by Sanchez-Garcia and Lagaron in previous works (31, 32).

Thus, from this figure, it can be seen that although the hydrolysis was not able to break down completely the fibers, the larger fibers are much thinner and relatively scarce in comparison with the originalmicrofibers also shown for comparison purposes. The films were observed on both sides by opticalmicroscopy andwere found to provide similar results, indicating that the observations are not the result of detectable uneven dispersion across the film thickness.

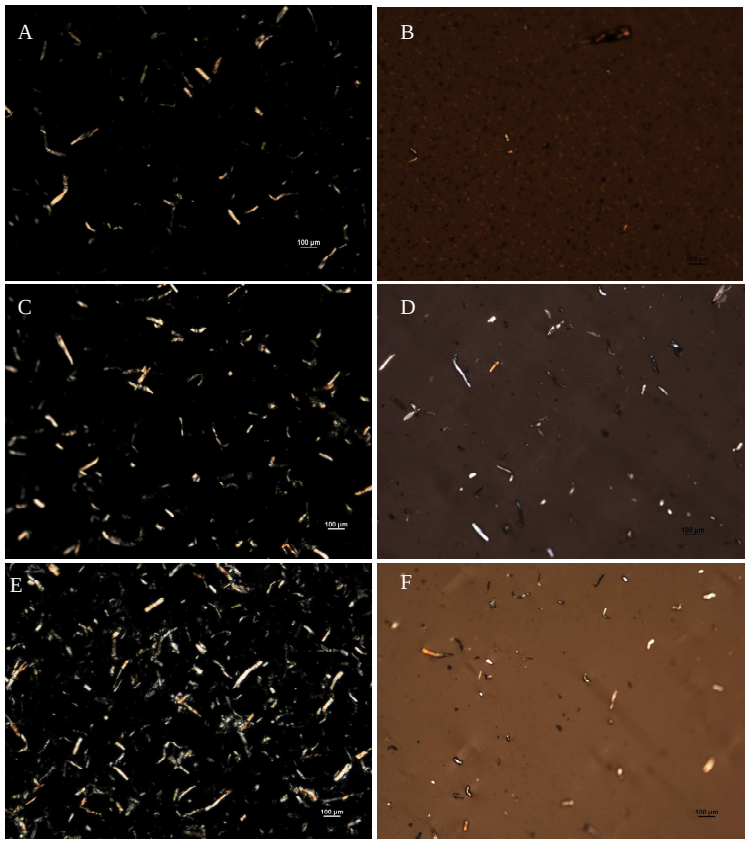

Figure 2. Optical micrographs of carrageenan based films prepared by casting containing: (A) 1 wt.-% cellulose microfibers, (B) 1 wt.-% CNW, (C) 3 wt.-% cellulose microfibers, (D) 3 wt.-% CNW, (E) 5 wt.-% cellulose microfibers, (F) 5 wt.-% CNW. The scale marker is 100 microns.

When glycerol was added to the biopolymer, some interesting observations were made. On the one hand, glycerol was seen to form inhomogeneous but rather large segregated domains in the absence of filler (see Figure 3B). This is in accordance with previous

observations by the authors in the biopolymer amylopeptine plasticized with glycerol (47). More interestingly, however, is the observation that in the presence of the microcomposites, the cellulose microfibers do not seemto be homogeneously dispersed and appear to be rather segregated to the matrix fraction (see Figure 3C-F). Indeed, when polarized light was used, the microfibers appeared to set aside and to preferentially locate within the matrix fraction. Panels E and F of Figure 3 (see arrows) also support the latter observations by suggesting that glycerol domains seem to form boundaries around the fibers. Even more interesting is the fact that when CNW were used, it was much more difficult to spot in the composite the otherwise large glycerol domains, and observation of Figure 3H suggests that the glycerol domains become smaller and more homogeneously dispersed across the matrix in the presence of the nanofiller. This could be related to the nanosize of the cellulose whiskers, which makes difficult the aggregation of glycerol in the matrix providing a more homogeneous composite. This observation may also help to explain the completely different water barrier performance of plasticized micro- and nanocomposites (see later).

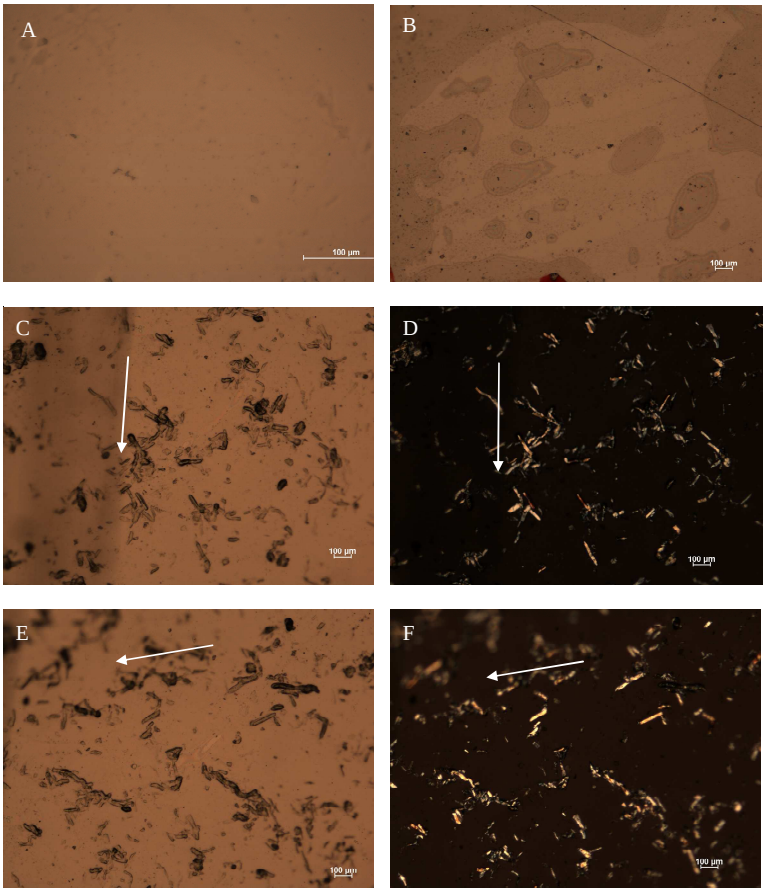

Figure 3. Optical micrographs of carrageenan based films containing: (A) Pure carrageenan, (B) 10 wt.-% glycerol, (C)(D)(E)(F) 3 wt.-% of microfibers and 10 wt.-% glycerol, (G)(H) 1 wt.-% of microfibers and 10 wt.-% glycerol, (I) 3 wt.-% of CNW and (H) 3 wt.-% of CNW and 10 wt.-% glycerol.

TEM is a powerful tool for the analysis of cellulose whiskers and nanoparticles dispersion in general. In any case, TEM analysis of the nanocomposite structure was challenging for several reasons: The major problem is the impossibility of microtoming the biocomposite films, because the cuts are usually collected on liquids, which either dissolve the polymer or lead to rolled pieces very difficult to handle and observe.However, by direct casting of polymer solution drops over the TEM grid, relatively good images of the nanobiocomposites were obtained. Figure 4 shows pictures of the pure carrageenan, pure nanowhiskers, and the corresponding nanobiocomposites. From Figure 4B a good dispersion of the nanowhiskers in the matrix becomes apparent; however, increasing the nanofiller content in the matrix (Figure 4C) results in an increase in the number of agglomerates,most likely due to the well-reported natural trend of the cellulosic fillers to selfassociate via hydrogen bonding as the concentration builds up in composites.

The typical size of the cellulose nanowhiskers as determined by TEM was found to be around 25-50 nm in length and around 5 nm in the cross section within the polymeric matrix. Thus, by comparing the size of the attained CNWwith that of the original cellulose microfibers, it becomes evident that a considerable (by ca. 3 orders of magnitude) reduction in fiber size has been accomplished by the acid hydrolysis. These results are in agreement with previous findings by these authors using this type of microfibers (31) and also with previous results by other authors using different cellulosic materials (30, 31). Direct TEM observation of the pure cellulose nanowhiskers after solvent evaporation indicates that a very intricate network of aggregated whiskers is formed with cross sections in the thinnest fibers below 10 nm. By drying, the cellulosic material tends to agglomerate and, therefore, it is likely that the presence of the biopolymer molecules in the composites helps to better retain the dispersibility expected to exist in the solution form.

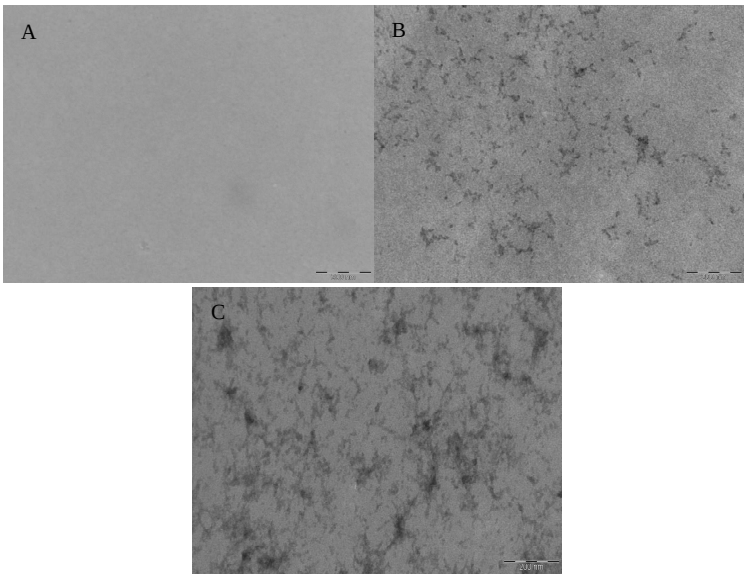

Figure 4. TEM images of: (A) carrageenan film, (scale market is 200nm); (B) carrageenan containing 1 wt.-% CNW content, (scale market is 200nm); (C) carrageenan containing 5 wt.-% of CNW (scale market is 200nm).

3.2 Thermal stability

Thermal degradation of carrageenan and its nanocomposites containing both CNW and the original microfibers was studied by determining the corresponding mass loss during heating by TGA. Table 1 summarizes the decomposition thermograms (maximum of the weight loss first derivate) for all samples. From Table 1, the temperature atwhich the carrageenan decomposition rate is the highest is 219.78ºC. On the other hand, the weight loss first-derivative maximum for the neat CNW is located at 331.55ºC. This is ca. 32ºC lower than that for the original cellulose microfibers, indicating that the CNW are less thermally stable than the original microfibers, in agreement with previous works (48), due tomost likely the hydrolysis process that promotes the presence of sulfate groups on the fiber surface. At low contents of CNW (1 and 3 wt %), the decomposition temperature of the biocomposites without glycerol decreases; however, further incorporation of CNW (5 wt %) results in a slightly increased thermal stability.

Table 1. TGA Maximum of the Weight Loss First Derivative (Td) and the Corresponding Peak Onset and Endset Values for the Carrageenan-Based Materials.

sample	onset (°C)	T_d (°C)	endset (°C)	sample	onset (°C)	T_d (°C)	endset (°C)
carrageenan	211.9	219.8	226.4	carrageenan + 10% Gly	213.2	223.3	233.0
carrageenan + 1% CNW	196.8	201.9	207.0	carrageenan + 1% CNW + 10% Gly	221.7	227.5	233.3
carrageenan + 3% CNW	204.9	210.0	215.7	carrageenan + 3% CNW + 10% Gly	226.0	231.1	236.3
carrageenan + 5% CNW	218.7	222.5	227.9	carrageenan + 5% CNW + 10% Gly	227.0	231.7	237.2
carrageenan + 1% fiber	206.9	211.7	216.9	carrageenan + 1% fiber + 10% Gly	211.8	227.1	233.4
carrageenan + 3% fiber	191.6	196.4	201.7	carrageenan + 3% fiber + 10% Gly	224.4	229.2	234.3
carrageenan + 5% fiber[a]				carrageenan + 5% fiber + 10% Gly	222.4	228.1	233.3
CNW	312.6	331.5	349.0	CNW	312.6	331.5	349.0
purified cellulose microfibers	309.8	363.9	384.2	purified cellulose microfibers	309.8	363.9	384.2

[a] TGA of carragenan containing 5 wt % of fiber was not measured.

For the films of carrageenan containing glycerol, the decomposition temperature increased by 4ºC, suggesting that the plasticizer stabilizes the polymer to some extent. In the case of the nanocomposite samples containing glycerol, the decomposition temperature also increased by ca. 8ºC, suggesting that glycerol can also act as a stabilizer for the blend. This increase was arrested for the composites containing CNW in excess of 3 wt%. Pandey et al. reported a decrease in thermal stability with the addition of cellulose nanowhiskers to a PLA matrix(34). The authors discussed that there are conflicting reports about the thermal stability of esterified lignocellulosic materials, the behavior of which was seen to depend on the reagents used for modification. Esterification with maleic and succinic anhydrides was also reported to lead to a decrease in thermal stability, whereas treatment with fatty acids, acrylonitrile, methyl methacrylate, did enhance thermal stability (34). Chen et al. also showed a reduction in decomposition temperature with the addition of pea hull fiber (PHF)-derived nanowhiskers to pea starch ascribed to the longer interaction with the acid media (35). Ayuk et al. reported that an improvement in thermal degradation temperatures, even at high whisker contents, is considered to be an indication for efficient dispersion of the filler (36). On the other hand, Li et al. reported that the decomposition temperature of chitosan films containing CNWderived from cotton linter pulp hardly changed with an increase in nanofiller content in the matrix. The latter authors suggested that the addition of CNWretained the thermal stability of the films because of the strong interactions between the whiskers and chitosan (37).

Addition of cellulose microfibers to unplasticized carrageenan resulted in a continuous decrease in the decomposition temperature for microfiller loadings of up to 3 wt %. Thus, whereas 1 wt% of CNW dropped the most the thermal stability and further nanofiller loading resulted in increased stability, for the microfibers the maximum drop was for 3wt%loading. On the other hand, the behavior of adding cellulose microfibers to the carrageenan containing glycerol was found to be rather similar to that of CNW.

Previous studies reported that glycerol can help increase dispersion and interaction with fillers and, hence, the higher stability of the blends with glycerol could be ascribed to this phenomenon (13, 36, 37). Nevertheless, although it is possible that a better interaction can occur in the composites containing glycerol, a better dispersion was in fact not observed in the current experiments in the cellulosemicrofibers. This also points out that, in fact, glycerol is a stabilizing agent on its own because it also stabilizes the pure matrix. With regard to the losses in thermal stability for unplasticized nanocomposites with low contents of cellulosic materials, it is feasible that because dispersion is higher at low loadings but the reinforcing effect is higher in terms of water resistance (see later), higher influence in the performance of the composites compared to the matrix could be detrimental to the stability. Therefore, the results here suggest that higher dispersion leads to earlier matrix degradation due to enhanced interaction between filler and matrix and/or the corresponding property alterations.

On the overall, the TGA data indicate that the nanobicomposites are thermally stable in the temperature range in which carrageenan is typically processed, i.e. below 190ºC.

3.3 Mass transport properties

Table 2 gathers the direct water vapor permeability coefficients of carrageenan and its nanobiocomposites. These values are in good agreement with the values previously reported by the authors in similarly produced films (4). From Table 2, it can also be seen that a water vapor permeability decrease of ca. 32% is observed with the addition of 10 wt % of glycerol. This is expected as Talja et al. reported that the water vapor permeability for potato starch-based films without plasticizer was higher compared to that of starch-based films plasticized with 20 wt % of glycerol at various RH conditions (39). However, as opposed to this, the films plasticized with 30 and 40 wt%of glycerol increased the water vapor permeability (38,39,). In the current study, a similar behavior of a water vapor permeability reduction at low additions of glycerol was observed in carrageenan films. Visible cracks in the carrageenan film without plasticizer were not seen before testing. However, the increase in water vapor permeability of carrageenan in the absence of glycerol could be hypothesized as being caused by microcracks in the film. Alternatively, Guo et al. reported that cellulose acetate films at plasticizer contents of 5-10% (w/w, solids) had lower water vapor permeability than filmswithout plasticizer because of the decreased molecular mobility of the cellulose acetate promoted by the plasticizer (40).

Table 2. Water permeability for the carrageenan based materials[a].

sample	P (kg m/s m^2 Pa)	% reduction	sample	P (kg m/s m^2 Pa)	% reduction
carrageenan	$^{AB}6.86 \pm 0.041E^{-14}$		carrageenan + 10% Gly	$^{ABC}4.65 \pm 0.542E^{-14}$	
carrageenan + 1% CNW	$^{C}2.16 \pm 0.23E^{-14}$	68	carrageenan + 1% CNW + 10% Gly	$^{C}2.32 \pm 0.15E^{-14}$	50
carrageenan + 3% CNW	$^{C}2.01 \pm 0.37E^{-14}$	71	carrageenan + 3% CNW + 10% Gly	$^{C}1.87 \pm 0.14E^{-14}$	60
carrageenan + 5% CNW	$^{BC}2.89 \pm 0.57E^{-14}$	58	carrageenan + 5% CNW + 10% Gly	$^{C}1.74 \pm 0.78E^{-14}$	63
carrageenan + 1% fiber	$^{AB}4.15 \pm 0.12E^{-14}$	40	carrageenan + 1% fiber + 10% Gly	$^{ABC}4.62 \pm 0.53E^{-14}$	
carrageenan + 3% fiber	$^{BC}3.00 \pm 0.69E^{-14}$	56	carrageenan + 3% fiber + 10% Gly	$^{A}7.11 \pm 1.52E^{-14}$	
carrageenan + 5% fiber	$^{AB}6.31 \pm 0.54E^{-14}$	8	carrageenan + 5% fiber + 10% Gly	$^{A}7.32 \pm 0.51E^{-14}$	
[4,38] *k*/*ι*-carrageenan literature value	$6.7E^{-14}$				

[a] Statistical analysis by Tukey test is indicated by A, B, and C.

Figure 5 shows a plot summarizing the water vapor permeability of neat carrageenan and its nanocomposites with CNW and of the corresponding biocomposites with the original cellulose microfibers for various filler contents with and without glycerol. Fromthe results, in the case of the films without glycerol (Figure 5A), reductions of water vapor permeability of ca. 68, 70, and 58% were obtained in films containing 1, 3, and 5 wt % of CNW, respectively, compared with unfilled carrageenan. In the case of the composites of carrageenan with the original microfibers, decreases inwater vapor permeability of ca. 40, 56, and 8% with the addition of 1, 3, and 5 wt%of microfibers compared to neat carrageenan were obtained. Thus, at highermicrofiber contents, the water vapor permeability reduction is most likely decreased

due to filler agglomeration as observed by optical microscopy (see Figure 1E). This result is consistent with a previous study on the addition of similar cellulosemicrofibers to PLA, in which filler agglomeration as observed by SEM occurred with increasing filler loading and resulted in increased permeability due to the creation of preferential paths for diffusion (32). Interestingly, for similar filler contents, the CNW are more efficient in reducing water vapor permeability compared to the microfibers due to chiefly nanodispersion versus microdispersion of the filler.

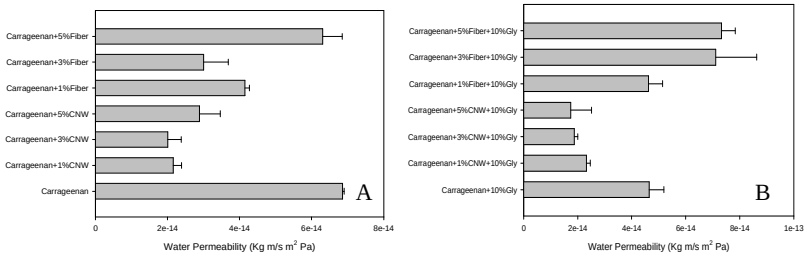

Figure 5. (A) Permeability to water of carrageenan and of its nanocomposites containing 1, 3 and 5 wt.-% of CNW and of cellulose microfibers. (B) Permeability to water of carrageenan with 10 wt.-% of glycerol and of its nanocomposites containing 1, 3 and 5 wt.-% of CNW and of cellulose microfibers.

When nanocomposites with glycerol were formulated, a reduction in water vapor permeability was also observed (see Table 2 and Figure 5B); that is, reductions of ca. 50, 60, and 63% were obtained for 1, 3, and 5 wt%of nanofiller contents, respectively, with regard to the matrix containing glycerol. In principle, the barrier reinforcement was not seen higher than for the samples without glycerol, a fact that perhaps rules out the hypothesis of higher dispersion between the filler and the matrix assisted by glycerol. This may also suggest that the observation of glycerol increasing the thermal stability of the blend may be regarded as the plasticizer increasing interaction between the filler and the matrix and/or acting as a stabilizer during the thermal runs. The facts that the glycerol is not miscible with the carrageenan (31) and that the cellulosic material may not be as well dispersed in the glycerol phase can lead to a more unhomogeneous dispersion of the nanofiller in the glycerol-containing composites, which in turn can promote higher overall thermal stability for the blends. In sharp contrast to the behavior of the CNW, the addition of 1 wt % ofmicrofibers did not result in enhanced barrier performance, and but adding 3 and 5 wt%of the originalmicrofibers increased water vapor permeability by ca. 53 and 57% compared to pure carrageenan containing glycerol. This behavior in barrier performance is unexpected here but was already reported before in PLA(32); cellulosemicrofiber loadings beyond 1 wt% resulted in barrier deterioration due to sudden microfiber agglomeration and lack of adhesion at the polymer-filler interphase as characterized by SEM. In the current experiments, if the microfiller was not homogeneously dispersed but rather segregated to the matrix phase as the morphology study suggested, this could detrimentally affect the barrier performance. It is also relevant to point out that higher thermal stability seems to be actually promoted in the current experiments by filler agglomeration.

In summary, the best water barrier performance was found for CNW loadings of ca. 3 wt %. This suggests that higher CNW contents lead to nanofiller agglomerations that no longer enhance dispersion and which are detrimental in terms of barrier enhancement. Surprisingly, microfibers become inefficient as barrier elements in the presence of glycerol, due tomost likely segregation and agglomeration of the microfibers outside glycerol domains.

To better assess the barrier performance, some typical models were applied to compare the experimental results with widely used simple models. Nielsen (41) developed an expression to model the permeability of a two-phase composite sheet in which impermeable square plates are dispersed in a continuous conducting matrix. The plates are oriented so that the two edges of equal length, L, are perpendicular to the direction of transport and the third edge, of width W, is parallel to the direction of transport. This expression is:

$$P = P_m(1-\phi_d)/[1+(L/2W)\phi_d] \quad (1)$$

where P is the permeability of the composite, Pm, is the permeability of the matrix, and Φd is the volume fraction of the impermeable filler. The (1 - Φd) term accounts for volume exclusion and the (1 + (L/2W) Φd) term for tortuosity. In the following, this model will be called the tortuosity model. Note that this model does not account for permeation through the dispersed phase.

A more realistic system to consider is one in which a discontinuous low-permeability phase is present in a high-permeability matrix. Maxwell (42) developed a model to describe the conductivity of a two-phase system in which permeable spheres are dispersed in a continuous permeable matrix. Fricke (43) extended Maxwell's model to describe the conductivity of a two-phase system in which ellipsoids with permeability Pd are dispersed in a more permeable continuous matrix. According to this model, the permeability of the composite system with Φ2 the volume fraction of the dispersed phase, is (44):

$$P = (P_m + P_d F)/(1+F) \quad (2)$$

where

$$F = [\Phi 2/1 - \Phi 2][1/(1+(1-M)(Pd/Pm-1))]$$

$$M = \cos\theta / \sin 3\theta\,[\theta - 1/2 \sin 2\theta]$$

and

$$\cos\theta = W/L$$

W is the dimension of the axis of the ellipsoid parallel to, and L the dimension perpendicular to, the direction of transport, and θ in radians.

Figure 6 plots the experimental permeability values and modeling results using eqs 1 and 2. TEM characterization of CNW in the carrageenan films suggested experimental L/W(particle length/ width ratio) values ranging from 5 to 10 and in the cellulose microfibers from 2 to 15. Therefore, in fact, the main relevant factor in reducing permeability in these models for a given filler loading is to have higher L/W for the filler. Curiously enough, the L/W factors achieved as a result of the top-bottom nanofabrication approach do not change to a significant extent and, hence, the two models for a start cannot really pick up the overall downsizing differentiating effect. Another factor not involved in themodeling is the different permeability blocking capacity for a given filler loading, which for the case of the CNW is hypothesized to be higher because the overall crystallinity of the filler is increased during nanofabrication.

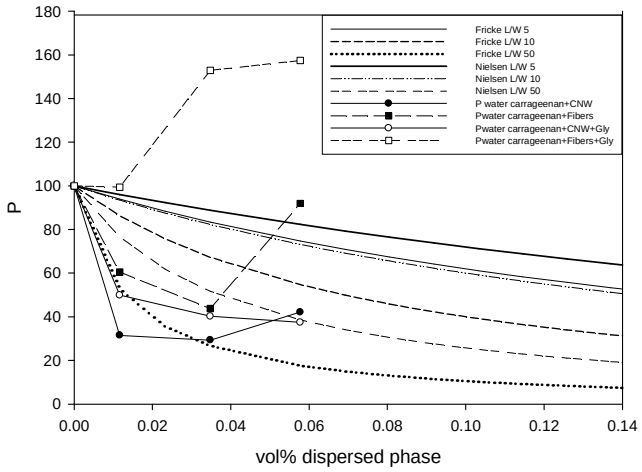

Figure 6. Permeability modelling vs. vol.-% of a dispersed phase with different aspect ratios L/W and the normalized experimental permeability values.

The following set of parameters were used in equations (1) and (2): ρcellulose nanowhiskers = 1.6 g/ml (45), Pd ≈ 0 , Pm=100 and L/W of 5, 10 and 50. The results displayed in Figure 7 suggest that the permeability drop in nanobiocomposites containing 1 and 3 wt.-% of CNW, does not follow the expected trend in permeability drop, i.e. they arrest earlier, and is actually much higher than predicted for aspect ratios between 5 and 10. However for aspect ratios of 50, which seem larger than the actual experimental aspect ratios, a better fit to the experimental data is achieved (see Figure 6), especially at both 1 wt.-% of CNW with glycerol and of microfibers without glycerol. It is also observed that the Fricke model better describes the experimental data at low contents of CNW when considering L/W=50. This indicates that a nanodispersion factor should be implemented in the modeling when the filler does not change the L/W ratio to account for overall size reduction. Data for the carrageenan film with 5 wt % of CNW, as the filler seems to more strongly agglomerate, deviate from the modeling expected trend as filler content builds up. This again suggests that filler agglomeration has to be taken into account in the modeling as it reduces the expected barrier enhancement. In the case of the films with cellulose microfibers and glycerol, the water vapor permeability was seen to increase and shows a completely different behavior from themodel predictions. We conjecture that the agglomerated morphology of the cellulose microfibers in the carrageenan films and the lack of homogeneity in dispersion could be at the origin of the discrepancy between experimental data for cellulose microfibers and the models.

Nevertheless, the applied simple models largely underpin their barrier responses on the bases of the so-called morphological tortuosity effect at low filler loadings, which is mostly related to diffusion, so they conjecture that a diffusion reduction by a fillerassisted blocking of the permeants is the chief phenomenon accounting for the permeability reductions. To gain more knowledge in this respect, evaluation of water solubility by measuring water uptake was also carried out in the samples.

3.4. Water uptake

Table 3 summarizes the water uptake at 11, 54, and 75% RH in carrageenan with and without glycerol and in the nanobiocomposites with CNW and cellulose microfibers. A general observation is that water uptake in all films increased with increasing RH, as expected (39).

However, for the case of the microfiber-based composites, this increase in water uptake is smaller in the low- and medium-humidity range. In Table 3, the water uptake at 11%RHis surprisingly reduced by asmuch as 77, 91, and 91% with the addition of 1, 3, and 5 wt % of CNW, respectively. At higher relative humidity, namely, at 54 and 75% RH, a similar strong reduction in water uptake is observed as CNW are added to the carrageenan matrix. In the case of the composites with fibers, the water uptake at 11% RH shows a similar uptake value as for the pure carrageenan, but at 54 and 75% RH the water uptake is clearly smaller than in carrageenan and rather similar to that in the corresponding CNW-based composites. Thus, the good morphology and dispersion of the highly crystalline CNW (as determined and reported elsewhere (31)) in the carrageenan films produced this significant reduction in water uptake. The microfibers also reduce to a significant extent the water uptake but only atmedium-high relative humidity conditions.

Table 3. Percent Water Uptake at 11, 54, and 75% Relative Humidity (RH) for the Carrageenan-Based Materials[a].

	water uptake at 11% RH	water uptake at 54% RH	water uptake at 75% RH
carrageenan	$^{AB}5.12 \pm 0.08$	$^{A}10.90 \pm 0.29$	$^{B}17.02 \pm 0.34$
carrageenan + 1 wt % CNW	$^{DE}1.18 \pm 0.01$	$^{D}3.49 \pm 0.52$	$^{C}4.93 \pm 1.29$
carrageenan + 3 wt % CNW	$^{E}0.45 \pm 0.28$	$^{CD}4.20 \pm 0.19$	$^{C}7.54 \pm 0.45$
carrageenan + 5 wt % CNW	$^{E}0.41 \pm 0.09$	$^{CD}4.18 \pm 0.19$	$^{A}7.54 \pm 0.38$
carrageenan + 10% Gly	$^{ABCDE}3.62 \pm 0.32$	$^{A}12.41 \pm 0.21$	$^{C}6.03 \pm 0.62$
carrageenan + 1 wt % CNW + 10% Gly	$^{CDE}1.46 \pm 0.04$	$^{BC}6.13 \pm 0.012$	$^{C}8.89 \pm 0.62$
carrageenan + 3 wt % CNW + 10% Gly	$^{E}0.85 \pm 0.10$	$^{CD}4.77 \pm 0.39$	$^{BC}9.19 \pm 2.38$
carrageenan + 5 wt % CNW + 10% Gly	$^{A}1.93 \pm 0.89$	$^{BCD}5.05 \pm 0.93$	$^{C}6.38 \pm 0.84$
carrageenan + 1 wt % fiber	$^{ABCD}4.71 \pm 0.25$	$^{CD}4.57 \pm 0.28$	$^{C}6.05 \pm 0.57$
carrageenan + 3 wt % fiber	$^{ABC}4.74 \pm 0.42$	$^{BCD}5.24 \pm 0.15$	$^{C}6.49 \pm 0.02$
carrageenan + 5 wt % fiber	$^{AB}5.19 \pm 0.07$	$^{BCD}5.31 \pm 0.44$	$^{C}7.48 \pm 0.82$
carrageenan + 1 wt % fiber + 10% Gly	$^{A}5.87 \pm 0.50$	$^{BC}5.87 \pm 0.10$	$^{C}8.23 \pm 2.13$
carrageenan + 3 wt % fiber + 10% Gly	$^{A}5.61 \pm 1.85$	$^{B}6.97 \pm 0.05$	$^{C}8.65 \pm 0.80$
carrageenan + 5 wt % fiber + 10% Gly	$^{AB}5.45 \pm 0.35$	$^{BC}6.23 \pm 0.08$	$^{C}9.70 \pm 1.88$

[a] Statistical analysis by Tukey test is indicated by A, B, C, D, and E.

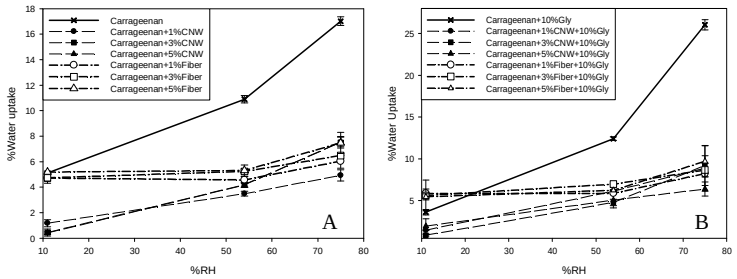

Figure 7. Water uptake (wt.-%) at 11%, 54% and 75%RH for: (A) Carrageenan and its nanocomposites with different contents of CNW and microfibers; (B) carrageenan with 10% of glycerol and its nanocomposites with different contents of CNW and microfibers.

The impact of adding glycerol to the carrageenan films on water uptake was also determined at different humidity levels. The water uptake of pure carrageenan was seen to decrease with the addition of glycerol at low relative humidity, but increased at higher relative humidity. The same behavior was reported by Zeppa et al. (46). Thus, glycerol was also reported to decrease water uptake at low water activity and to increase this at high water activity. In particular, at low water activity, the decrease in solvent uptake was attributed to a decrease of available sorption sites in the presence of the plasticizer. The rationale for this is that in plasticized films there are interactions between the hydroxyl groups of the polysaccharide and these of glycerol, and so there are fewer sorption sites for water binding (39, 46). When CNW are added, the available free volume is also thought to be filled in by the highly crystalline nanofiller, hence resulting in reduced uptakes. That effect seems less efficient with microfibers at low water

activity. At medium-high relative humidity conditions, water-clustering phenomena resulting in plasticization are thought to occur, thus increasing the overall water uptake as observed here (46). This phenomenon is thought to be more favored in the glycerol plasticized films due to enhanced molecular mobility of the polymer chains in the presence of the plasticizer and also to the hydrophilicity of the plasticizer.

Table 3 also shows that films of carrageenan with 10 wt % of glycerol and with 1, 3, and 5 wt%of CNWpresent a decrease in the water uptake at 11%RHof ca. 60, 76, and 47%, respectively, compared with the plasticized carrageenan containing glycerol. In the case of the water uptake at 54%RH, reductions of 50, 61, and 59% were observed for the films of carrageenan with 1, 3, and 5 wt%of CNW. Water uptakes measured at 75%RH were also seen to present decreases of ca. 66, 65, and 75% for the glycerol plasticized films containing 1, 3, and 5 wt% of CNW. At low and medium water activity, the water uptake reductions are clearly smaller in the presence of glycerol than in the absence of the plasticizer. In the case of the composites of carrageenan with cellulose microfibers, an increase inwater uptake at 11%RH was seen. On the other hand, at higher humidity conditions, the microfibers exhibit significantly reduced water uptake, which becomes similar as this observed for the CNW. The behavior in water uptake at low humidity conditions does single out the behavior of the microcomposites containing glycerol, but curiously this is not the case at high humidity and, therefore, the reproducible barrier performance of the microcomposites in the presence of glycerol must be related to diffusion.

As expected, the addition of cellulose nanowhiskers was generally seen to be more efficient in reducing water sorption across relative humidity in the presence and in the absence of glycerol due to both the higher crystallinity present in the CNW and the higher dispersion in the matrix due to the nanosize. Interestingly, the exhibited water uptake drops are generally similar to the corresponding water vapor permeability reductions and, hence, a surprisingly strong contribution to permeability is anticipated from this solubility indicative factor.

To further study the impact of solubility orwater uptake on the observed permeability, Figure 7 shows the ratio of water vapor permeability measured at 75% RH divided by water uptake at 75% RH for the carrageenan films and the nanocomposites containing CNW and cellulose microfibers with and without glycerol. This ratio can tell us something about the water diffusion (D=P/S) in the materials at this high relative humidity condition. From the results, it is surprising to see that in fact diffusion seems to be rather constant or to decrease in unplasticized CNW based-biocomposites and to slightly increase in plasticized CNW based-composites, suggesting that the water solubility reduction is a strong factor behind the reduction in moisture permeability in the nanobiocomposites. A higher water diffusion seems clearer in the microcomposites and especially for the samples containing glycerol, a fact that again supports the lower dispersion and/or interfacial interaction and agglomeration of the microfiller in the glycerol-containing samples. These observations are very relevant because they may provide a better understanding of the barrier effect of the CNW as based on the presence of crystalline blocks, which reduce solubility to a significant extent and, hence, permeability.

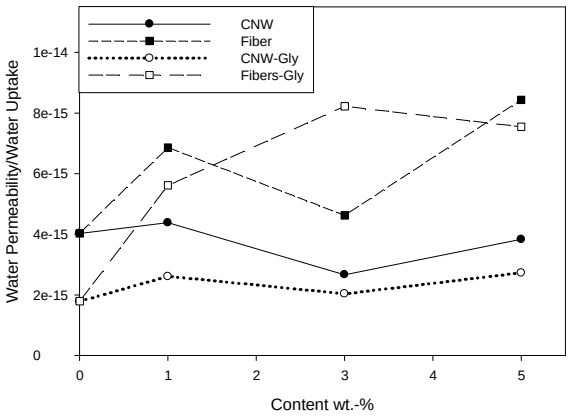

Figure 8. Water permeability/Water uptake (%) ratio at 75%RH for the various samples with and without glycerol.

3.5 Conclusions.

As a summary, cellulose nanowhiskers, with lengths ranging from 25 to 50 nm and cross sections around 5 nm, were prepared from highly purified R-cellulose microfibers (of 50-100 μm length and 10-20 μm cross section) by acid hydrolysis and were used to reinforce the water barrier of a carrageenan matrix with contents ranging from1 to 5 wt% using a solvent casting method. From TGA results, the addition of low contents of nanowhiskers in the carrageenan films was seen to reduce to some extent the overall thermal stability of the biopolymer, which was reversed by filler agglomeration at higher loadings and with the addition of the plasticizer glycerol. Addition of cellulose nanowhiskers to carrageenan resulted in good dispersion of the nanofiller in the matrix, especially at low filler contents. However, increasing the nanofiller loading in excess of 3 wt % TEM and water vapor permeability data suggested that agglomeration of these CNW takes place due to hydrogenbonding- induced self-association. Optimum performance in terms of barrier, that is, a ca. 70%water vapor permeability drop, was seen to occur at around 3 wt%of CNW. The permeability drop was chiefly ascribed to a strong reduction in water uptake rather than a diffusion-driven tortuosity effect. On the other hand, the addition of the parent cellulose microfibers did also result in reductions in permeability at low filler loadings, but these were smaller per filler volume compared to the CNW and were seen only in the absence of the plasticizer glycerol. The optical properties of themicrocompositeswere detrimentally affected compared to both CNW-based composites and pure carrageenan. Surprisingly, the addition of glycerol resulted in increased permeability for the microcomposites due to most likely segregation of the cellulosic material to the matrix fraction as suggested by optical microscopy and subsequent agglomeration and creation of preferential paths for diffusion.

Overall, the main conclusion arising from this study is that cellulose nanowhiskers obtained by acid hydrolysis can be used to enhance the water barrier and resistance of carrageenan and hence can have significant potential in food-packaging and -coating applications.

4. Acknowledgements

The authors would like to thank the MICINN projects MAT2009-14533-C02-01, EUI2008-00182, the projects POCTI/ EQU/45595/2002 and POCI/EQU/58064/2004 and

the EU FP7 project EcoBioCap for financial support. Finally, M.DSGwould like to thank the FPI program of the GV associated to the MEC project MAT2003-08480-C3 for the research grant.

5. References

(1) Hilliou, L.; Larotonda, F.D.S.; Abreu, P.; Ramos, A.M; Sereno, A.M; Gonçalves M.P. Effect of extraction parameters on the chemical structure and gel properties of kappa/iota-hybrid carrageenans obtained from Mastocarpus stellatus. Biomolecular Engineering, 2006, 23: 201-208.

(2) Hilliou, L.; Larotonda, F.D.S.; Sereno, A.M.; Gonçalves, M.P. Thermal and viscoelastic properties of κ/ι-hybrid carrageenan gels obtained from the Portuguese seaweed Mastocarpus stellatus. Journal of Agricultural and Food Chemistry. 2006, 54 (20), pp. 7870-7878. ANTIGUO 24

(3) Hilliou, L.; Gonçalves, M.P.. Gelling properties of a kappa/iota-hybrid carrageenan: effect of concentration and steady shear. International Journal of Food Science & Technology, 2007, 42: 678-685.

(4) Larontonda, F. D. S.; Hilliou, L.; Goncalves, M. P.; Sereno, A. M. – From Low Value renewable Resources to green Biomaterials for Edible Coating Applications. In Recent Advances In Research on Biodegradable Polymers and Sustainable Composites (vol. 3); A. Jiménez, G. E. Zaikoz (Eds.), 2008, p. 19. ISBN 978-1-60692-155-5.

(5) De Ruiter, G. A.; Rudolph, B. Carrageenan biotechnology Trends Food Sci. Technol. 1997, 8, 389-395

(6) Shaw, C.; Secrist, J.; Tuomy, J. Method of extending the storage life in the frozen state of precooked foods and product produced. U.S. Patent 4,196,219, 1980

(7) Macquarrie, R. Edible film formulation. U.S. Patent 0155200 A1, 2002.

(8) Ninomiya, H.; Suzuki, S.; Ishii, K. Edible film and method of making same. U.S. Patent 5,620,757, 1997

(9) Tanner, K.; Getz, J.; Burnett, S.; Youngblood, E.; Draper, P. Film forming compositions comprising modified starches and iota-carrageenan and methods for manufacturing soft capsules using same. U.S. Patent 0081331 A1, 2002.

(10) Bartkowiak, A.; Hunkeler, D. Carrageenan–oligochitosan microcapsules: optimization of the formation process. Colloids Surf. B: Biointerfaces 2001, 21, 285-298.

(11) Fonkwe, L.; Archibald, D.; Gennadios, A. Nongelatin capsule shell formulation. U.S. Patent 0138482 A1, 2003

(12) A.L. Brody, Edible packaging. Food Technol. 2005, 59, 65

(13) Sanchez-Garcia, M.D. Hilliou, Loic and Lagaron, J.M. Nanobiocomposites of Carrageenan, Zein and Mica of Interest in Food Packaging and Coating Applications. Journal of Agricultural and Food Chemistry, Accepted 2010.

(14)Sturcova, A.; Davies, G. R.; Eichhorn, S. J. The Elastic Modulus and Stress-Transfer Properties of Tunicate Cellulose Whiskers. Biomacromolecules 2005, 6, 1055-1061;

(15)Podsiadlo, P.; Choi, S.; Shim, B.; Lee, J.; Cussihy, M.; Kotov, N. Molecularly Engineered Nanocomposites: Layer-by-Layer Assembly of Cellulose Nanocrystals. Biomacromolecules 2005, 6, 2914-2918. (21);

(16) Azizi Samir, M. A. S.; Alloin, F.; Dufresne, A. A review of recent research into cellulosic whiskers, their properties and their application in nanocomposite field. Biomacromolecules 2005, 6, 612-626

(17) Marchessault, R. H.; Morehead, F. F.; Walter, N. M. Liquid crystal systems from fibrillar polysaccharides Nature 1959,184, 632-633

(18) Alain Dufresne, Michele B. Kellerhals, and Bernard Witholt. Transcrystallization in Mcl-PHAs/Cellulose Whiskers Composites. Macromolecules 1999, 32, 7396-7401;

(19) Favier V, Canova GR, Shrivastava SC, Cavaille JY (1997). Mechanical Percolation in Cellulose Whisker Nanocomposites. Polym Eng Sci 37:1732;

(20)Dufresne A, Cavaille JY, Helbert W (1997) Thermoplastic Nanocomposites Filled With Wheat Straw Cellulose Whiskers. Part II: Effect of Processing and Modeling. Polym Compos 18:198

(21)Yun Chen, Changhua Liu, Peter R. Chang, Xiaodong Cao, Debbie P. Anderson. Bionanocomposites based on pea starch and cellulose nanowhiskers hydrolyzed from pea hull fibre: Effect of hydrolysis time. Carbohydrate Polymers 76 (2009) 607–615;

(22) Ingvild Kvien, Junji Sugiyama, Martin Votrubec, Kristiina Oksman. Characterization of starch based nanocomposites. J Mater Sci (2007) 42:8163–8171;

(23)Samir M, Alloin F, Sanchez JY, Dufresne A (2004). Cellulose nanocrystals reinforced poly(oxyethylene)Polymer 45:4149,

(24)Samir M, Mateos AM, Alloin F, Sanchez JY, Dufresne A (2004). Plasticized nanocomposite polymer electrolytes based on poly(oxyethylene) and cellulose whiskers. Electrochim Acta 49:4667

(25)Qian Li, Jinping Zhou, Lina Zhang. Structure and Properties of the Nanocomposite Films of Chitosan Reinforced with Cellulose Whiskers. Journal of Polymer Science: Part B: Polymer Physics, Vol. 47, 1069–1077 (2009)

(26)Yixiang Wang, Xiaodong Cao, Lina Zhang. Effects of Cellulose Whiskers on Properties of Soy Protein Thermoplastics. Macromol. Biosci. 2006, 6, 524–531

(27)Daniel-Da-Silva, A.L., Lopes, A.B., Gil, A.M., Correia, R.N. Synthesis and characterization of porous κ-carrageenan/calcium phosphate nanocomposite scaffolds. J Mater Sci (2007) 42:8581–8591

(28)Gan, S.-L., Feng, Q.-L. Preparation and characterization of a new injectable bone substitute-carrageenan/nano-hydroxyapatite/collagen. Acta Academiae Medicinae Sinicae 2006, 28 (5), pp. 710-71

(29)L. Hilliou, F.D.S. Larotonda, P. Abreu, A.M. Ramos, A.M. Sereno a, M.P. Gonc¸alves. Effect of extraction parameters on the chemical structure and gel properties of k/i-hybrid

carrageenans obtained from Mastocarpus stellatus. Biomolecular Engineering 23 (2006) 201–208

(30) L. Petersson , I. Kvien , K. Oksman. Structure and thermal properties of poly(lactic acid)/cellulose whiskers nanocomposite materials. Composites Science and Technology 67 (2007) 2535–2544

(31)Sanchez-Garcia, M. D. and Lagaron, J.M. On the use of plant cellulose nanowhiskers to enhance the barrier properties of polylactic acid. Cellulose, 2010

(32)Sanchez-Garcia, M. D.; Gimenez E.; Lagaron, J. M. Mophology and Barrier Properties of Solvent Cast Composites of Thermoplastic Biopolymers and Purified Cellulose Fibers. Carbohydrate Polymers, 2008, 71, 235–244

(33)Oh, S. Y.; Yoo, D. I.; Shin, Y.; Kim, H. C.; Kim, H. Y.; Chung, Y. S; Park, W. H.; Youk, J.H. Crystalline structure analysis of cellulose treated with sodium hydroxide and carbon dioxide by means of X-ray diffraction and FTIR spectroscopy. Carbohydrate Research 2005, 340, 2376–2391)

(34) J.K. Pandey, W.S. Chu, C.S. Kim, C.S. Lee, S.H. Ahn. Bio-nano reinforcement of environmentally degradable polymer matrix by cellulose whiskers from grass. Composites: Part B 40 (2009) 676–680).

(35) Yun Chen, Changhua Liu, Peter R. Chang, Xiaodong Cao, Debbie P. Anderson. Bionanocomposites based on pea starch and cellulose nanowhiskers hydrolyzed from pea hull fibre: Effect of hydrolysis time. Carbohydrate Polymers 76 (2009) 607–615

(36) Jackson Etang Ayuk, Aji P. Mathew, Kristiina Oksman. The Effect of Plasticizer and Cellulose Nanowhisker Content on the Dispersion and Properties of Cellulose Acetate Butyrate Nanocomposites. Journal ofAppliedPolymer Science,Vol. 114, 2723–2730 (2009)

(37) Li, Q., Zhou, J. and Zhang, L. Structure and Properties of the Nanocomposite Films of Chitosan Reinforced with Cellulose Whiskers. Journal of Polymer Science: Part B: Polymer Physics, Vol. 47, 1069–1077 (2009)

(38) F.D.S. Larotonda, L.Hilliou, M.P. Goncalves, A.M. Sereno. Film properties of κ/ι-hybrid carrageenan natural polymer. The Polymer Processing Society 23rd Annual Meeting

(39) Riku A. Talja, Harry Helen, Yrjo H. Roos, Kirsi Jouppila. Effect of various polyols and polyol contents on physical and mechanical properties of potato starch-based films. Carbohydrate Polymers 67 (2007) 288–295

(40) Guo, J. H. (1993). Effects of plasticizers on water permeation and mechanical properties of cellulose acetate: antiplasticization in slightly plasticized polymer film. Drug Development and Industrial Pharmacy, 19(13), 1541–1555.

(41) Nielsen, L. W. J. Macromol Sci. 1967, Al, 929.

(42) Maxwell, J. C. Electricity and Magnetism, 3rd ed.; Dover: New York, 1891; Vol. 1.

(43) Fricke, H. Phys. Rev. 1924, 24, 575.

(44) Paul, D. R.; Bucknall, C. B. Polymer Blends; 2000; Wiley InterScience: NY, Vol. 2: Performance.

(45)Jeffrey R. Capadona, Kadhiravan Shanmuganathan, Stephanie Trittschuh, Scott Seidel, Stuart J. Rowan and Christoph Weder. Biomacromolecules 2009, 10, 712–716

(46)C. Zeppa, F. Gouanve´, E. Espuche. Effect of a Plasticizer on the Structure of Biodegradable Starch/Clay Nanocomposites: Thermal, Water-Sorption, and Oxygen-Barrier Properties. Journal of Applied Polymer Science,Vol. 112, 2044–2056 (2009)

(47) López-Rubio, A.; Lagaron J. M.; Ankerfors, M.; Lindström, T.; Nordqvist, D.; Mattozzi, A.; Hedenqvist, M. S.; Carbohydrate Polymers, 2007, 68, 718–727.

(48) Roman Maren and Winter William, Effect of Sulfate Groups from Sulfuric-Acid Hydrolysis on the Thermal Degradation Behavior of Bacterial Cellulose. Biomacromolecules 2004, 5, 1671-1677

Chapter III.

Nanobiocomposites based on Carbon nanotubes and Carbon Nanofibers.

PAPER IX: Effect of addition of carbon nanofibers and carbon nanotubes on properties of thermoplastic biopolymers

Abstract

This paper presents the properties of nano-bio-composites of solvent cast polyhydroxybutyrate-co-valerate (PHBV) and polycaprolactone (PCL) containing carbon nanofiber or carbon nanotubes as a function of filler content. It is found that carbon nanotubes and nanofibers can be used to enhance the conductivity, thermal, mechanical and to enhance gas barrier properties of thermoplastic biopolyesters.

Keywords: Carbon nanotubes, Carbon nanofibers, Nanocomposites, Biodegradable polymers, Barrier properties

Introduction

Biodegradable polymers have received considerable attention due to their potential application in fields related to environmental protection and ecology in the last two decades. Most biodegradable polymers have excellent properties comparable to manypetroleumbased plastics. They possess a number of excellent and promising properties that can be used in a number of applications, including packaging, automotive and biomedical sectors. Thermoplastic biodegradable polymers, such as polyhydroxyalkanoate (PHA) and polycaprolactones (PCL), are processable using conventional plastics machinery. For the polyhydroxyalkanoates (PHAs) family, the most widely used material is the polyhydroxybutyrate (PHB) and its copolymers with valerate. These microbial biopolymers are storage materials produced by a variety of bacteria in response to particular environmental stresses [1]. Polyhydroxybutyrate (PHB) is a naturally occurring b-hydroxyacid (a linear polyester). The homopolymer, poly(hydroxybutyrate) PHB, and its copolymer with hydroxyvalerate, PHBV, are biodegradable engineering thermoplastic polymers with important properties that make them suitable for many applications for which petroleum-based synthetic polymers are currently used. PHB polymers are already used in small disposable products and in packaging materials [2]. PCL is a thermoplastic biodegradable polyester synthesized by chemical conversion of crude oil. PCL has good water, oil, solvent, and chlorine resistance, low melting point, low viscosity, and is easily processed using conventional melt blending technologies [3]. PCL is being investigated for use in biomedical utensils, pharmaceutical controlled release systems, and in biodegradable packaging [4]. Biodegradable polymers have strong commercial potential for bio-plastics. However, they exhibit low toughness, low heat distortion temperature, relatively high gas permeability compared to oil based polyesters such as PET, low melt viscosity, low thermal and electrical conductivity. These shortcomings restrict their use. Reinforcement of these materials using nanoparticles may be an effective way to improve these properties [5–7]. There are research studies showing property improvements in biodegradable materials with the addition of carbon nanotubes. Reinforcement of PCL with carbon nanotubes has been carried out with the overall aim of increasing its biodegradation rate and to enhance mechanical properties, i.e. this route led to considerable improvements in the composites tensile strength [8]. Other authors reported that the addition of small amount of MWCNT into PCL matrix can improve its thermal stability, and the loading of MWCNT into PCL matrix induced heterogeneous nucleation during crystallization processes as studied by DSC [9]. Saeed and Park reported that the conductivity of the nanocomposite of PCL increases with the increase of CNT content [10]. Lai et al. found that addition of carbon nanotubes into PHBV enhanced its thermal stability studied by TGA. The thermal properties and the crystallization behaviour of the composites were characterized by differential scanning calorimetry and wide-angle X-ray diffraction and the nucleant effect of MWNTs on the crystallization of PHBV was confirmed [11]. However, to the best of our knowledge there is no prior work on the use of carbon nanotubes and carbon nanofibers to simultaneously enhance various properties of the materials including barrier properties against the absorption of gases and water vapour. In this study, the morphology, thermal, conductivity, mechanical and solvent barrier properties as a function of filler content of bio-composites of PCL and PHBV

containing carbon nanotubes or nanofibers as reinforcing elements are presented and discussed.

Materials and methods

Materials

The bacterial polyhydroxyalkanoate grade was purchased from Goodfellow Cambridge Limited, UK, in pellet form. The supplied material was a melt-processable semicrystalline thermoplastic PHBV (polyhydroxybutyrate with 12 mol% of valerate) copolymer made by biological fermentation from renewable carbohydrate feedstocks. The PCL grade FB100 was supplied in pellet form by Solvay Chemicals, Belgium. This grade has a density of 1.1 g/cm^3 and a mean molecular weight of 100,000 g/mol. Carbon nanotubes used are agglomerate of Multi-Wall Carbon Nanotubes, with commercial name Baytubes^R C 150 P supplied by Bayer Material Science. Baytubes^R are agglomerates of multi-wall carbon nanotubes with low outer diameter, narrow diameter distribution and an ultra-high aspect ratio (length-to-diameter ratio). Baytubes^R show excellent tensile strength and E-modulus, as well as exceptional thermal and electrical conductivity. Size of carbon nanotubes are 1 to 10 μm of length and around 5–20 nm in diameter. Carbon nanofibers are supplied by Pyrograf^R-III, with diameters ranging from 70 to 200 nm and a length estimated to be 50–100 μm.

Preparation of blends

Solution-cast film samples of the biodegradables materials with 1, 3, 5, and 10 wt.% carbon nanofiber, and the same for the carbon nanotubes contents were prepared with a dry film thickness of around 100 μm, using chloroform as a solvent. Fiber solutions in chloroform were mixed in a homogenizer (Ultraturrax T25 basic, Ika-Werke, Germany) for 4 min and then stirred with the polymer at 40ºC for 24 h. Subsequently, the material was cast onto Petri dishes to generate films after solvent evaporation at room temperature.

Optical light polarized microscopy

Polarized light microscopy (PLM) examinations using Leitz Ergolux with a capture camera moticam 2000 with 2.0 MPixel were carried out on both sides of the cast samples. A 40X objective was used to examine the samples.

SEM measurements

For SEM observation, the samples were cryo-fractured by hand after immersion in liquid nitrogen, mounted on bevel sample holders and sputtered with Au/Pd in a vacuum. SEM pictures (Hitachi S4100) were taken with an accelerating voltage of 10 keV.

TEM measurements

Transmission electron microscopy (TEM) was performed using a JEOL 1010 equipped with a digital Bioscan (Gatan) image acquisition system. TEM observations were performed on ultra-thin sections of microtomed thin bio-composite sheets.

AFM measurements

AFM measurements were performed using a Nanoscope III Atomic Force Microscope, Veeco (IMS) (Veeco Instruments) to investigate the morphology on the top of the cast films in the bio-composites. The images were scanned in tapping mode in air using commercial Si cantilevers (Veeco Instruments) with a resonance frequency of 165 kHz.

DSC measurements

Differential scanning calorimetry (DSC) of PHBV, PCL and their composites were performed on a DSC Q10 thermal analysis system on typically 7 mg of dry material at a scanning speed of 10 ºC/min from room temperature to the melting point using N2 as the purging gas. Before evaluation, the thermal runs were subtracted from similar runs of an empty pan. The DSC equipment was calibrated using indium as a standard and typically two measurements were carried out on the samples.

TGA measurements

Thermogravimetric analysis was carried out with a TGA Q50. Samples were heated from ambient temperature to 700 ºC in a flow of N_2 and a heating rate of 20 ºC/min.

Thermal and electrical diffusivity

Electrical conductivity was measured by van der Pauw method [16]. Being a four probe method the contact resistance is eliminated and only one accurate dimension (thickness) is needed to calculate the volume resistivity of the sample. Basically, a current (I_{12}) is forced through two adjacent corners of the sample and the voltage drop (V_{43}) is recorded on the other two corners. The conductivity is calculated using the following equation:

$$\exp(-\pi \cdot t \cdot \sigma \cdot R_A) + \exp(-\pi \cdot t \cdot \sigma \cdot R_B) = 1 \quad (1)$$

where t is the sample thickness (m) and r is the conductivity (S/m).

$$R_A = (V_{34}/I_{12} + V_{12}/I_{34})/2 \ (\Omega) \quad \text{and} \quad R_B = (V_{41}/I_{23} + V_{23}/I_{41})/2 \ (\Omega) \quad (2)$$

The sample thickness was averaged over nine measurements. Prior to the measurement, the corners of the sample were coated with silver paste. The current source (Keithley 6220 DC) and the nanovoltmeter (Keithley 218A) were linked

together and the measurements were done in delta mode, when the current source alternates the signal polarity and triggers the nanovoltmeter to read at each polarity. This current reversal technique cancels out any constant thermoelectric offsets. Depending on the sample conductivity, the current levels were determined such that the measured voltage ranged from 10 mV to 1 V. The accuracy of the measurement setup was verified by a resistivity standard of 111.1 S/m (VLSI Standards Inc.).

Thermal diffusivity was measured by a Flash Diffusivity Instrument (Nanoflash LFA 447, Burlington, MA, USA) in nanocomposite samples of 12.7 mm wide and 1 mm thick. Nanocomposite test samples were prepared by compression molding. Measurements were done at different temperatures 25, 35 and 45 ºC. The illumination was a Xenon flash lamp and the wavelength was in broadband visible and near IR.

Mechanical properties

Tensile relaxation properties were measured using an SER-HVP01 Universal Testing Platform for the Anton Paar Physica MCR300/301/500/501 rotational rheometer host system (Xpansion Instruments, LLC). Tensile test was done at the melting point of the material. As such, for the PCL the test was done at 65 ºC and for the PHBV at 165 ºC. The following generalized equation can be used to calculate the tensile relaxation modulus for polymers in step extension on the sentmanat extensional rheometer (SER).

$$E(t) = \frac{\sigma_t}{\varepsilon_H} = \frac{\left(T - T_{offset}\right)}{2R\varepsilon_H A_o \left(\rho_S / \rho_M\right)^{2/3} \exp\left(-\varepsilon_H\right)} \qquad (3)$$

where E(t) is the calculated tensile stress relaxation modulus; rt the true stress in extension; εH = 0.1 applied step Hencky strain

$$\varepsilon_H = \frac{2\Omega R}{L_o}$$

where 2R = 1.031 cm (diameter of the equal dimension drums) and L_o is fixed at 1.272 cm, and X is the Hencky strain rate; T the torque; Toffset the torque offset value (if needed); R the drum radius = 5.156 mm; A_0 the initial specimen cross-sectional area (width x thickness); ρ_S is the solid state polymer density; ρ_M the polymer melt density (for elastomers $\rho_S = \rho_M$).
The following generalized equation can be used to calculate the engineering tensile stress, r, for tensile specimens in extension on the SER:

$$\sigma = \frac{\left(T - T_{offset}\right)}{2RA_o} \qquad (4)$$

where σ is the engineering tensile stress; T the torque; Toffset the torque offset value (if needed); R the drum radius = 5.156 mm; A_0 is the initial specimen cross-sectional area (width ┐ thickness).

Water uptake

Samples were allowed to dry in a dessicator at 0%RH for one week until constant weight is reach. They were then placed in a dessicator at 100%RH and allowed to

absorb water until constant weight (indicating equilibrium) was reached. The water uptake was estimated during the sorption experiments of water using an analytical balance Voyager V11140. Thus, saturation condition was checked by observing no changes in successive weight uptake measurements of the specimen. Tests were done in quadruplicate and average values and standard errors are provided.

Oxygen permeability

The oxygen permeability coefficient was derived from oxygen transmission rate (OTR) measurements recorded using an Oxtran 100 equipment (Modern Control Inc., Minneapolis, MN, US). During all experiments temperature and relative humidity were held at 24 ºC and 80% relative humidity. Eighty percentage of the relative humidity was generated by a built-in gas bubbler and was checked with a hygrometer placed at the exit of the detector. To facilitate sample humidity equilibration during the actual oxygen transmission rate test at 80%RH and to avoid potential fluctuations on barrier during the test, the samples were preconditioned at 80%RH by storage in a dessicator set up at this RH by appropriate salt solution. The experiments were done in duplicate. The samples were purged with nitrogen for a minimum of 20 h, prior to exposure to a 100% oxygen flow of 10 ml/min, and a 5 cm^2 sample area was measured by using an in-house developed mask.

Results and discussion

Bio-composites morphology

Polarized optical light microscopy photographs allowed to take clear images of the carbon nanotubes embedded in the biodegradable matrixes. Fig. 1 shows the morphology of the PCL films prepared with low, medium and high carbon nanotubes contents. Fig. 1A and B shows the presence of well dispersed carbon nanotubes in the 1 wt.% and 3 wt.% fiber–PCL sample prepared by casting. It can be seen the increase of carbon nanotubes and the agglomeration of the carbon nanotubes in the 5 and 10 wt.% carbon nanotubes (Fig. 1C and D).

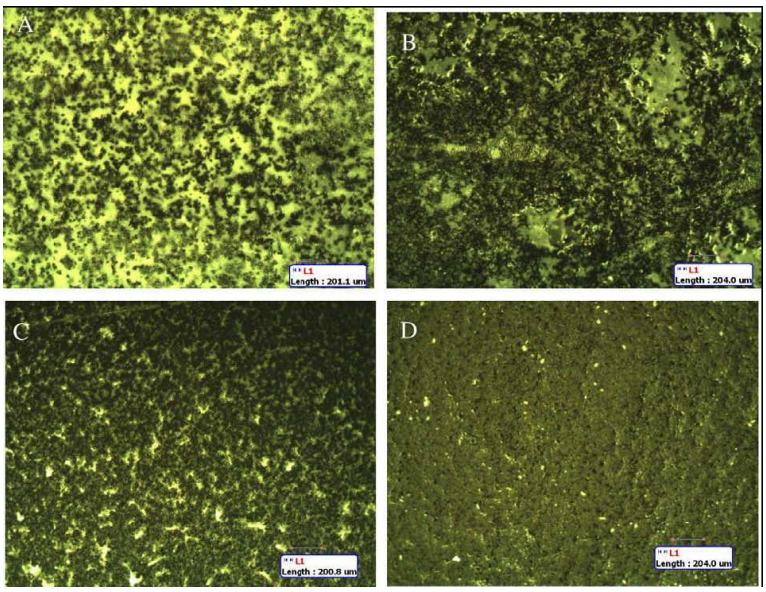

Fig. 1. Optical micrographs of: (A) a film prepared by casting of PCL with 1 wt.% carbon nanotubes content (scale marker is 201.1 μm), (B) a film prepared by casting of PCL with 3 wt.% carbon nanotubes content (scale marker is 204.0 μm), (C) a film prepared by casting of PCL with 5 wt.% carbon nanotubes content (scale marker is 204.0 μm), (D) a film prepared by casting of PCL with 10 wt.% carbon nanotubes content (scale marker is 204.0 μm). Magnification of the optical micrographs is 500x.

Fig. 2 shows the carbon nanofibers in the PCL castings. Fig. 2A clearly shows the presence of highly dispersed fibers in the 1 wt.% carbon nanofiber–PCL sample prepared by casting. In the 10 wt.% carbon nanofiber–PCL sample (see Fig. 2B) it can be observed that the excess of fibers results in a tendency for crowding and entangling.

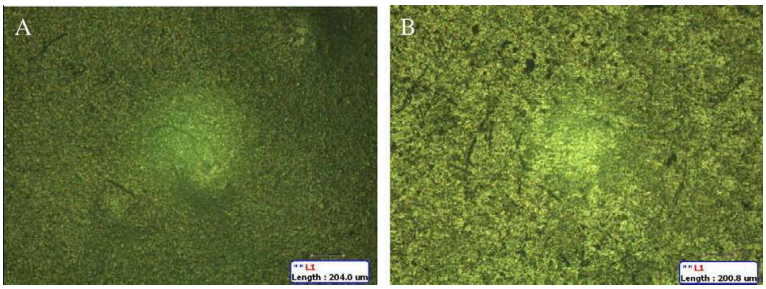

Fig. 2. Optical micrographs of: (A) a film prepared by casting of PCL with 1 wt.% carbon nanofibers content (scale marker is 204.0 μm), (B) a film prepared by casting of PCL with 10 wt.% carbon nanofibers content (scale marker is 200.8 μm). Magnification of the optical micrographs is 500x.

To observe the morphology at the micron and submicron level, SEM observations were initially carried out in the bio-composites. Fig. 3 shows the fracture morphology

of some of the films prepared by casting with low and high content of carbon nanofibers and carbon nanotubes. Fig. 3A shows a film of PCL with 1%CNF. It can be seen that the carbon nanofibers are embedded in the matrix. There is good adhesion and good dispersion of the carbon nanofiber in the PCL matrix. However, with the increase of carbon nanofibers contents (Fig. 3B) the carbon nanofibers exhibit agglomeration morphology. Fig. 3C and D shows the morphology of carbon nanotubes in the PCL. In Fig. 3C, film of PCL with 1%CNT shows the dispersion and intercalation of the carbon nanotubes in the matrix. Nevertheless, in Fig. 3D, film with 10%CNT shows agglomeration of the carbon nanotubes, the same behaviour for the carbon nanofibers.

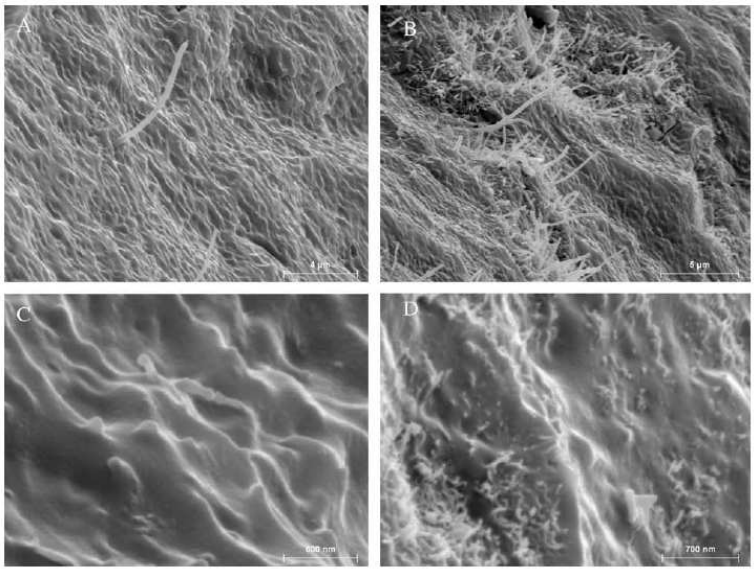

Fig. 3. Scanning electron micrographs of the cross section of: (A) a film prepared by casting of PCL with 1 wt.% carbon nanofibers content (scale marker is 4 μm), (B) a film prepared by casting of PCL with 10 wt.% carbon nanofibers content (scale marker is 5 μm), (C) a film prepared by casting of PCL with 1 wt.% carbon nanotubes content (scale marker is 600 nm), (D) a film prepared by casting of PCL with 10 wt.% carbon nanotubes content (scale marker is 700 nm).

Fig. 4 shows TEM results taken on specimens of the PCL with carbon nanotubes and carbon nanofibers in different contents. The dispersion and intercalation of low contents of carbon nanotubes and nanofibers in the matrix is clear. However, with the increase of the content of carbon nanotubes and carbon nanofibers, there is an agglomeration of the nanoparticles in the PCL, the same observation as by SEM. The picture reveals clearly the size of the carbon nanotubes of around 175–200 nm in length and a width of approximately 15 nm. The size of the carbon nanofibers is around 280 nm in length and 64 nm in width. The size of carbon nanotubes and carbon nanofibers observed by TEM is similar to the size indicated by specifications of the materials. AFM is a very powerful technique for the observation of materials morphology. It also provides a feasible route to investigate the topography of films containing micro- and nanofibers [17]. The observation of the samples was carried out

by AFM at the top surface. Fig. 5 shows the presence on the top surface of carbon nanotubes in the 5 wt.% carbon nanotube–PCL sample prepared by casting. The picture reveals the size of the carbon nanotube of about 670 nm in length and a width of approximately 75 nm (similar size observed in the SEM micrographs), which seems strongly attached to the matrix.

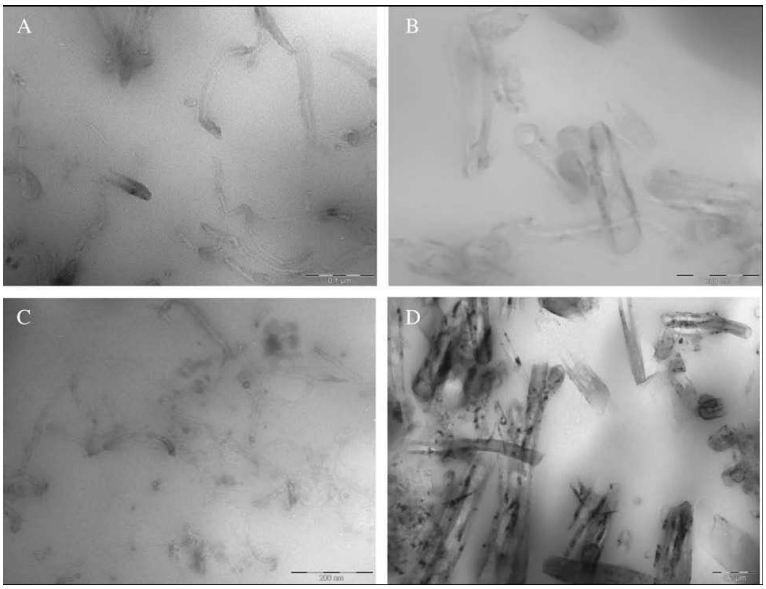

Fig. 4. Transmission electron micrographs of the cross section of: (A) a film prepared by casting of PCL with 1 wt.% carbon nanotubes content (scale marker is 0.1 μm), (B) a film prepared by casting of PCL with 1 wt.% carbon nanofibers content (scale marker is 200 nm), (C) a film prepared by casting of PCL with 10 wt.% carbon nanotubes content (scale marker is 200 nm), (D) a film prepared by casting of PCL with 10 wt.% carbon nanofibers content (scale marker is 0.2 μm).

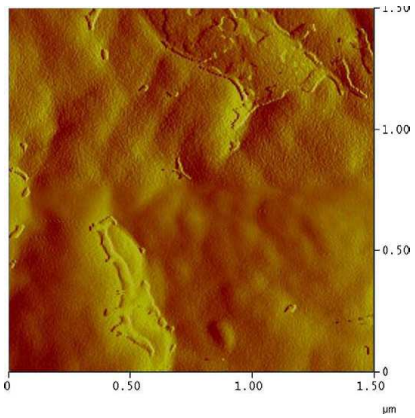

Fig. 5. Atomic force microscopy phase typical image of the top surface of a cast sample of PCL containing 5 wt.% of carbon nanotubes in an area of 1.50 lm.

Thermal properties

Melting temperature (T_m) and heat of fusion (ΔH_m) corrected for biopolymer content in the bio-composites were determined from the DSC second heating runs of the samples. Crystallization temperature (T_c) and heat of crystallization (ΔH_c) were determined from the DSC cooling runs of these samples. These are shown in Table 1 for PCL cast films with different carbon nanotubes and carbon nanofibers contents. From literature, it was known that nanofiber/ nanotube acts either as nucleating agents or as obstacles to crystallization depending on the types of matrices [18–21]. Table 1 shows the variation of thermal parameters as functions of the carbon nanotubes and carbon nanofiber content for the PCL composites. For the case of the carbon nanotubes, there is a multiple crystallization with two peaks. This reflects the induction of the heterogeneous crystallinity structure and a decrease of the crystallization due to the addition of carbon nanotubes.
The crystalline temperature and heat of crystallinity are seen to drop with the increase of the carbon nanotubes contents. There are two peaks of the crystalline temperature with 1, 3 and 5 wt.% of carbon nanotubes. With 10 wt.% carbon nanotubes the crystalline temperature is approximately 10º higher than the pure PCL (see Fig. 6A). The heat of fusion of these biomaterials with carbon nanotubes is seen to increase a little with the addition of 1% carbon nanotubes (see Fig. 6B). From Table 1, in the case of carbon nanofibers, the heat of fusion, and heat of crystallization of the carbon nanofibers biomaterials are seen to drop. This drop is larger for samples with higher fiber contents, similar to the materials with carbon nanotubes, however there are not multiple crystallizations in these cases due to the fact that carbon nanofibers produce less modification in the crystallinity of these PCL material than the carbon nanotubes. Table 2 summarizes the thermal parameters for the PHBV composites with different carbon nanotubes and carbon nanofibers contents. From these results, the same behaviour as in the PCL biomaterial can be seen. From Table 2, the glass transition temperature (Tg) of the PHBV increases with the addition of CNT and CNF, a higher increase with low content of filler can be observed, due to the better dispersion of the carbon nanotubes and nanofibers in the matrixes, corroborating the morphology results.
In summary, carbon nanofibers and nanotubes hindered the crystallization process of these biodegradable materials. Filler dispersion and interfacial adhesion is thought to hinder to some extent
polymer chains lateral re-arrangements and hence crystallization in these biomaterials. Thermal degradation of PCL and PCL/nanocomposites was studied by determining their mass loss during heating by TGA.

Table 1. DSC melting point and melting enthalpy of the neat film of PCL and of their biocomposites with 1, 3, 5 and 10 wt.-% carbon nanotubes and with 1, 3, 5 and 10 wt.-% carbon nanofiber content prepared by solving casting.

	Tm (ºC)	AHm (J/g)	Tc (ºC)	AHc (J/g)
PCL	55.34 ± 0.41	63.07 ± 0.18	34.31 ± 0.04	59.90 ± 0.55
PCL+1%CNT	55.71 ± 0.25	63.59 ± 1.89	(34.31-43.22) ± (0.02-0.007)	57.93 ± 0.38
PCL+3%CNT	55.66 ± 0.37	61.73 ± 4.28	(35.10-43.25) ± (0.02-0.04)	54.70 ± 3.58
PCL+5%CNT	55.46 ± 0.03	58.48 ± 2.67	(36.11-44.66) ± (0.28-1.79)	54.35 ± 2.34
PCL+10%CNT	55.44 ± 0.29	58.10 ± 1.14	43.00 ± 0.14	51.96 ± 0.62
PCL+1%CNF	56.56 ± 0.73	57.12 ± 2.75	35.61 ± 0.41	47.78 ± 5.42
PCL+3%CNF	56.07 ± 0.04	58.26 ± 1.35	36.03 ± 0.03	51.24 ± 1.75
PCL+5%CNF	55.81 ± 0.13	57.38 ± 6.21	35.65 ± 0.007	48.17 ± 3.77
PCL+10%CNF	55.59 ± 1.53	55.40 ± 1.53	36.18 ± 0.09	46.56 ± 2.39

Table 2. DSC melting point and melting enthalpy of the neat film of PHBV and of their biocomposites with 1, 3, 5 and 10 wt.-% carbon nanotubes and with 1, 3, 5 and 10 wt.-% carbon nanofiber content prepared by solving casting

	Tm (ºC)	AHm (J/g)	Tc (ºC)	AHc (J/g)	Tg (ºC)
PHBV	(145.45-156.15) ± (0.54-0.61)	58.46 ± 2.47	96.95 ± 0.29	56.19 ± 2.93	55.3
PHBV+1%CNT	(145.66-156.08) ± (0.23-0.13)	57.83 ± 1.99	98.93 ± 0.50	55.45 ± 1.18	58.63 ± 0.11
PHBV+3%CNT	(147.48-156.79) ± (0.23-0.17)	56.74 ± 2.97	102.09 ± 0.08	45.66 ± 1.09	56.12 ± 0.03
PHBV+5%CNT	(147.23-156.68) ± (0.12-0.13)	55.54 ± 1.13	103.20 ± 0.02	34.27 ± 1.02	58.21 ± 0.09
PHBV+10%CNT	(146.97-156.40) ± (0.31-0.40)	49.64 ± 2.43	102.05 ± 0.11	40.88 ± 4.05	57.63 ± 0.16
PHBV+1%CNF	(145.48-156.11) ± (0.05-0)	66.94 ± 2.68	98.32 ± 0.25	63.13 ± 2.12	60.73 ± 3.46
PHBV+3%CNF	(146.58-156.71) ± (0.19-0.2)	58.85 ± 3.09	100.18 ± 1.20	54.29 ± 3.43	58.62
PHBV+5%CNF	(146.65-156.83) ± (0.12-0.13)	50.18 ± 2.45	100.03 ± 0.23	47.45 ± 2.48	59.31 ± 2.04
PHBV+10%CNF	(147.73-157.11) ± (0.11-0.21)	51.38 ± 0.67	103.71 ± 0.17	47.71 ± 0.81	58.35 ± 2.07

Table 3. TGA decomposition point of the neat film of neat PCL and of their nanobiocomposites with 1, 3, 5 and 10 wt.-% of the carbon nanotubes and carbon

nanofibers and for the PHBV and of their biocomposites with 1, 3, 5 and 10 wt.-% carbon nanotubes and carbon nanofiber prepared by solving casting

	$T_{decomposition}$ (ºC)		$T_{decomposition}$ (ºC)
PCL	413.36 ± 1.14	PHBV	286.01 ± 1.92
PCL+1%CNT	417.68 ± 3.21	PHBV+1%CNT	291.21 ± 1.92
PCL+3%CNT	417.17 ± 0.43	PHBV+3%CNT	288.79 ± 4.35
PCL+5%CNT	416.19	PHBV+5%CNT	286.31 ± 1.45
PCL+10%CNT	415.89 ± 0.04	PHBV+10%CNT	288.73 ± 1.91
PCL+1%CNF	406.02 ± 3.29	PHBV+1%CNF	278.36 ± 3.51
PCL+3%CNF	404.75 ± 1.60	PHBV+3%CNF	280.46 ± 3.26
PCL+5%CNF	411.37 ± 3.52	PHBV+5%CNF	284.33 ± 2.88
PCL+10%CNF	412.02 ± 4.33	PHBV+10%CNF	293.72 ± 1.08

Table 3 summarizes the decomposition temperature of all samples. As an example, Fig. 7 shows the weight loss and Fig. 8 shows the derivative mass loss curves of PCL and of their nano-bio-composites with 1, 3, 5 and 10 wt.% of the carbon nanotubes and carbon nanofibers, at a heating rate of 20 ºC/min. From the thermogravimetric curves it can be seen that PCL and samples with different contents of carbon nanotubes and nanofibers present a relatively good thermostability since no remarkable weight loss occurred until 290 ºC. As it can be observed from the peak of the first derivative, the temperature for highest PCL decomposition rate is T = 413.36 ± 1.14 ºC, for a heating rate of 20 ºC/min. Similar decomposition temperature was reported [8]. In the case of the addition of carbon nanotubes to the PCL, the decomposition temperature increased by 4 ºC. However, for the carbon nanofiber the decomposition temperature decreases by 8 ºC. The carbon nanotubes reduce the thermal degradation and the best increase in the decomposition temperature is for low additions of carbon nanotubes (1% and 3%), probably due to the fact that films with low nanotubes contents have better morphology and dispersion, though increasing carbon nanotubes contents do result in filler agglomeration. From Fig. 7A, the remaining residue at 550 ºC is for pure PCL 0.67%, and with the addition of 1, 3, 5 and 10 wt.% carbon nanotubes the remaining residue is between 0.67%, 1.64%, 3.11%, 4.55% and 8.12%. As can be seen, the additional residue is close to the added nanoparticles amount. However, the remaining residue at 550 ºC for the PCL films with 1, 3, 5 and 10 wt.% carbon nanofibers is between 3.65%. 6.67%, 10.26% and 17.90% (see Fig. 7B). These residues are higher than the added nanotubes content. This may be due to the shielding effect of the large nanofibers that prevents the evaporation of the polymer. From Table 3, the temperature at which the PHBV decomposition rate is highest is T = 286.01 ± 1.92 ºC, for a heating rate of 20 ºC/min. This decomposition temperature is lower than the PCL. PHBV and the samples with different contents of carbon nanotubes and nanofibers present a relatively good thermostability
since no remarkable weight loss occurred until 190 ºC. For the PHBV films it has similar behaviour as PCL. With the addition of carbon nanotubes the decomposition temperature increases until 5 ºC with low content of carbon nanotubes and with the

addition of carbon nanofibers the decomposition temperature increases until 7 ºC. Remaining residue at 400 ºC for the pure PHBV is 5.99%. With the addition of 1, 3, 5 and 10 wt.% carbon nanotubes the remaining residue is between 6.00%, 7.90%, 12.68%, and 16.88%. Pure PHBV has a higher residue and with the additional residue it is close to the added nanoparticles amount. In the case of increasing the content of carbon nanofibers, the remaining residue is between 14.48%, 14.53%, 20.72% and 14.52%. As it can be seen, this is similar behaviour to the PCL films, the addition of carbon nanofibers produces higher remaining residue than the carbon nanotubes. From these experimental results, it can be observed that the presence of CNT and CNF in these biodegradable polymers induced better thermal stability and therefore the onset of degradation clearly shifted to higher temperatures.

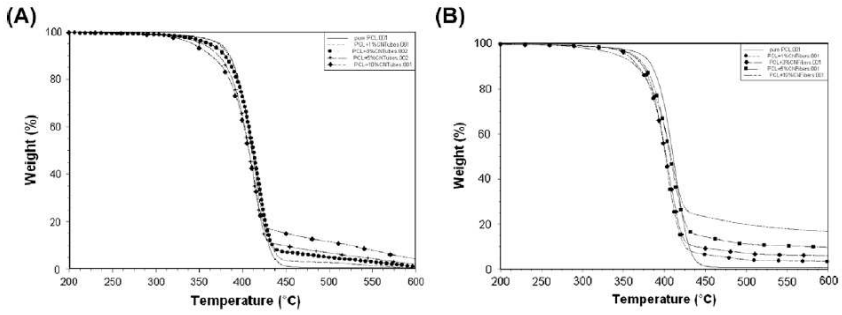

Fig. 7. (A) TGA curves of samples of neat PCL and of their nano-bio-composites with 1, 3, 5 and 10 wt.% of the carbon nanotubes. (B) TGA curves of samples of neat PCL and of their nano-bio-composites with 1, 3, 5 and 10 wt.% of the carbon nanofibers.

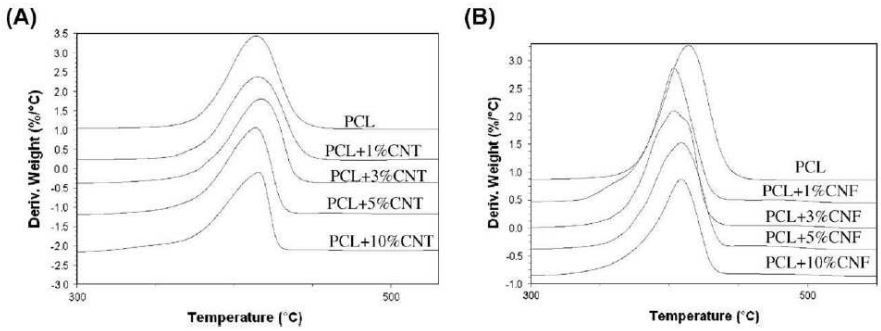

Fig. 8. (A) TGA derivative mass loss versus temperature of samples of neat PCL and of their nano-bio-composites with 1, 3, 5 and 10 wt.% of the carbon nanotubes. (B) TGA derivative mass loss versus temperature of samples of neat PCL and of their nano-bio-composites with 1, 3, 5 and 10 wt.% of the carbon nanofibers.

Electrical and thermal conductivity

The electrical conductivities of the biodegradable materials with carbon nanotubes and carbon nanofibers were tested, and the results are shown in Fig. 9. With the increase in CNT and CNF loading, the electrical conductivity of the PCL and PHBV nanocomposite increases, which is attributed to the high electrical conductivity and good dispersion of the CNT and CNF. The electrical conductivity of the nanocomposites of carbon nanotubes is higher than the nanocomposite with carbon nanofiber. The electrical conductivity of the nanocomposites increased from 2.4 x 10^{-6} S/cm for PCL with 1 wt.% CNT to 0.33 S/cm for PCL with 10 wt.% CNT. In the case of carbon nanofibers the electrical conductivity increases with the increase of carbon nanofiber up to 0.10 S/cm for PCL with 10 wt.% CNF. A similar behavior is observed for PHBV nanocomposites, the carbon nanotubes produce higher increase in the electrical conductivity than the carbon nanofibers. As expected, there is a significantly increase in the conductivity as a function of the increasing content of carbon nanotubes and nanofibers in the nanocomposites. The electrical conductivity increases sharply after 5% of filler. This can be attributed to the percolation threshold for electrical conductivity. The thermal conductivity of carbon materials is dominated by atomic vibrations or phonons. The thermal diffusion was calculated by the Radiant Method and the Cowan Method for all the samples (see Fig. 10). In the case of the PCL nanocomposites, Fig. 10A, thermal diffusion of the pure PCL it can not be calculated, possibly due to the low value. There is an increase of the thermal diffusivity of around 160% in the PCL with 10%CNT compared to the PCL + 1%CNT. In the case of the nanocomposite with carbon nanofibers, there is an increase of around 165% in the film PCL + 10%CNF compared with the film PCL + 1%CNF. Fig. 10B shows the thermal diffusion (ratio of thermal conductivity to volumetric heat capacity) of the carbon nanotubes and carbon nanofibers of PHBV. For both samples with carbon nanotubes and carbon nanofibers, an increase of the thermal diffusion of ca. 235% for the PHBV with 10% content compared with the unfilled material was observed. The thermal transport in the CNT and CNF nanocomposites includes phonon diffusion in the matrix and ballistic transportation in the filler, for that reason increasing the carbon fillers increase the thermal transport in these nanocomposites.

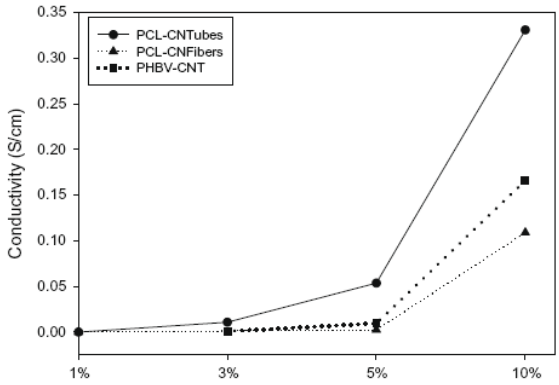

Fig. 9. Conductivity measurements of the neat film of neat PCL and of their nanobiocomposites with 1, 3, 5 and 10 wt.% of the carbon nanotubes and

carbonnanofibers and for the PHBV and of their bio-composites with 1, 3, 5 and 10 wt.%carbon nanotubes prepared by solvent casting.

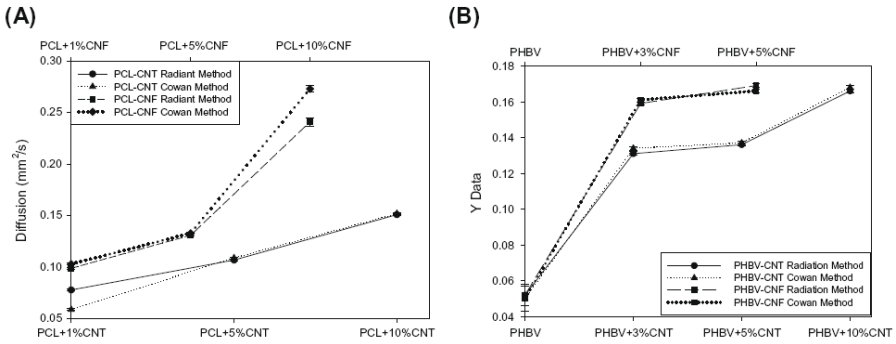

Fig. 10. (A) Thermal diffusion coefficient (mm2/s) of samples of neat PCL and of their nano-bio-composites with 1, 5 and 10 wt.% of the carbon nanotubes and carbon nanofibers measured by Radiation and Cowan Method. (B) Thermal diffusion coefficient (mm2/s) of samples of neat PHBV and of their nano-bio-composites with 1, 3, 5 and 10 wt.% of the carbon nanotubes and carbon nanofibers measured by Radiation and Cowan Method.

Water uptake

Water uptakes of PCL and PHBV and their nanocomposite were tested. The results of the water uptake are shown in Fig. 11. From the results (Fig. 11A), in the case of PCL containing carbon nanotubes, a reduction in water uptake of 45% is observed in the PCL with 1 wt.% carbon nanotube content as compared with the pure biopolymer. There is a reduction in water uptake up to 50% in the case of the PCL + 3%CNT. However with the increase of CNT content the reduction in the water uptake decreases slowly. There is a reduction in water uptake of ca. 40% and 41% for the PCL with 5 and 10%CNT, respectively. For the PCL with carbon nanofibers, Fig. 11A shows the same behavior of the PCL with carbon nanotubes. Fig. 11A shows that water uptake has minimum values for specimens with 1 and 3 wt.% carbon nanofiber content. Further increase in fiber content results in slightly improved water uptake. Films of PCL with 1 and 3 wt.% carbon nanofiber content have a water uptake decrease of 62% and 67% compared to the unfilled material, whereas films of PCL with 10 wt.% carbon nanofiber content show a water uptake reduction of 57%. Fig. 11B shows water uptake for films of PHBV reinforced with different carbon nanotubes and carbon nanofibers contents. In the case of PHBV with carbon nanotubes there is a reduction in the water uptake of 23% for the film of PHBV + 1%CNT compared to the unfilled material, however with the increase of carbon nanotubes content the water uptake increases, to reach values even higher than that of the neat component.

For the PHBV with carbon nanofibers, a reduction of 49% is observed in the film of PHBV + 1%CNT. However, with the increase of carbon nanofiber content, the water uptake increased, to become even 52% higher than the pure PHBV in the case of

PHBV + 10%CNF. Increasing carbon nanotubes or carbon nanofibers content was seen to result in fiber agglomeration and this is thought to cause a reduction in matrix homogeneity and cohesion which leads to preferential penetrant paths and to detrimental effects in the water solubility. This is specially the case of PHBV.

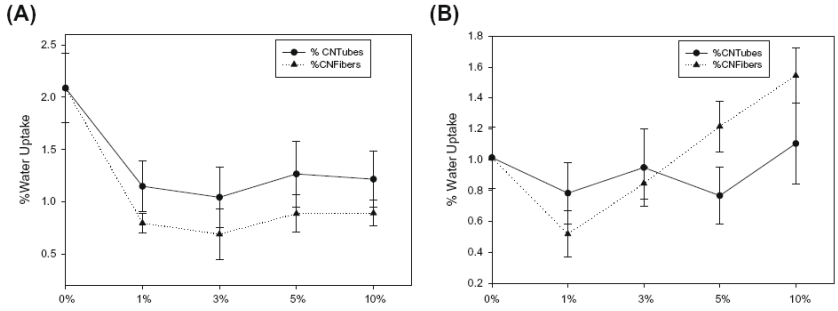

Fig. 11. (A) Water uptake of neat PCL and of their nano-bio-composites with 1, 3, 5 and 10 wt.% of the carbon nanotubes and carbon nanofibers. (B) Water uptake of neat PHBV and of their nano-bio-composites with 1, 3, 5 and 10 wt.% of the carbon nanotubes and carbon nanofibers.

Oxygen permeability

Table 4 shows the oxygen permeability of the biodegradables PCL, PHBV and their nanocomposites with carbon nanotubes and carbon nanofibers measured at 80%RH. From Table 4, the reported value of oxygen permeability for the PCL is 1.9 x 10^{-18} m^3 m/s m^2 Pa measured at 0%RH [22]. This is somewhat lower than the value of 7.06 x 10^{-18} m^3 m/s m^2 Pa measured at 80%RH in our laboratory, the difference could be related to the different material origins and history and testing conditions. For the films of PCL, there is a reduction of oxygen permeability of 52%, 38%, 8% and 10% for the films with 1%, 3%, 5% and 10% of carbon nanotubes, respectively, compared with the unfilled material (see Fig. 12A). Increasing carbon nanotubes contents results in reduction in the oxygen barrier. This is due to carbon nanotubes agglomeration. This observation is similar to the water uptake results and is corroborated by morphological observations.

In the case of carbon nanofibers, films of PCL with 1%, 3%, 5% and 10 wt.% of carbon nanofibers the oxygen permeability is reduced by 26%, 29%, 25% and 25%, respectively, compared with the unfilled material (see Fig. 12A). In the case of the PHBV, the reported value 5.10 x 10-18 m^3 m/s m^2 Pa measured at 75%RH [23] is somewhat higher than the value of 1.44 x 10^{-18} m^3 m/s m^2 Pa measured at our laboratory at 80%RH. This may result from the different origins of the two samples and testing conditions. Reductions in oxygen permeability of 14%, 5%, 21% and 58% for the filmof PHBVwith 1%, 3%, 5% and 10 wt.% of carbon nanofibers, compared with the unfilled material were observed (see Fig. 12B). In this case, with increasing carbon nanofibers content, the oxygen permeability decreases. These observations are in good agreement with the water uptake. Films of PHBV with 1%, 5% and 10 wt.% carbon nanotubes reduce the oxygen permeability 62%, 10% and 33%, respectively,

compared with the pure PHBV (see Fig. 12B). It can be observed that the best reduction in the oxygen permeability occurs at low content of carbon nanotubes.

Table 4. Oxygen permeability for PCL, PHBV and their nanocomposites

	P O_2 (m^3 m/s m^2 Pa) at 80%RH		**P O_2 (m^3 m/s m^2 Pa) at 80%RH**
PCL	7.06 e^{-18}	PHBV	1.78 e^{-18}
PCL+1%CNT	3.39 e^{-18}	PHBV+1%CNT	0.67 e^{-18}
PCL+3%CNT	4.41 e^{-18}		
PCL+5%CNT	6.51 e^{-18}	PHBV+5%CNT	1.61 e^{-18}
PCL+10%CNT	6.36 e^{-18}	PHBV+10%CNT	1.18 e^{-18}
PCL+1%CNF	5.23 e^{-18}	PHBV+1%CNF	1.53 e^{-18}
PCL+3%CNF	5.03 e^{-18}	PHBV+3%CNF	1.70 e^{-18}
PCL+5%CNF	5.27 e^{-18}	PHBV+5%CNF	1.40 e^{-18}
PCL+10%CNF	5.33e^{-18}	PHBV+10%CNF	0.75 e^{-18}
Literature value [24]PCL	[a]1.9e^{-18}	**Literature value [25]PHB**	[b]5.10e^{-18}

[a]At 0%RH (solvent casting)
[b]At 75%RH (commercial biobased materials)

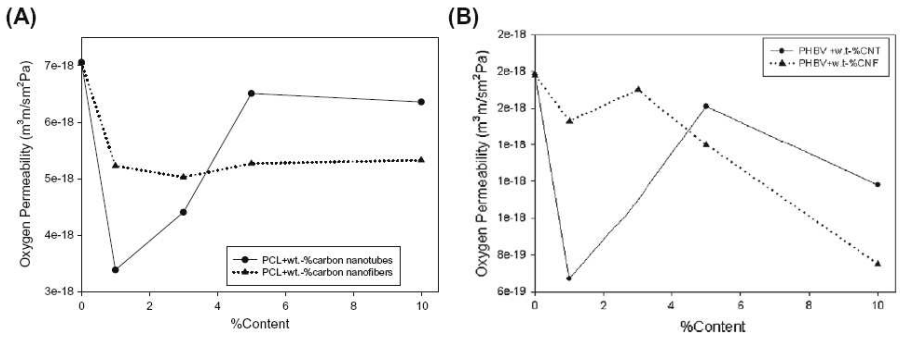

Fig. 12. (A) Oxygen permeability of neat PCL and of their nano-bio-composites with 1, 3, 5 and 10 wt.% of the carbon nanotubes and carbon nanofibers measured at 80%RH. (B) Oxygen permeability of neat PHBV and of their nano-bio-composites with 1, 3, 5 and 10 wt.% of the carbon nanotubes and carbon nanofibers.

Mechanical properties

Specimens of the PCL with CNT and CNF nanocomposites were tested in tensile relaxation experiments, in order to evaluate the effect of CNTs and CNFs contents on the mechanical properties of the nanocomposites (see Fig. 13).
From Fig. 13, E was seen to increase with increasing the CNT content. This implies that CNT enhances the rigidity of the nanocomposites as expected and widely reported. Increases in Young modulus of 49%, 103%, 114% and 166% for the films of PCL with 1%, 3%, 5% and 10% CNT respectively compared to the unfilled material are observed. Yield stress σ (MPa) does also increase with increasing the CNT

contents, attaining enhancements of 53%, 110%, 120% and 170% for the films of PCL with 1, 3, 5 and 10 wt.% of carbon nanotubes. For films of PCL with carbon nanofibers, it can be seen the same behavior of the carbon nanotubes. A remarkable increase in Young modulus of 321% and in yield stress of 330% is seen for the film of PCL + 10%CNF. Increases in Young modulus and yield stress which result from CNT [24–26] and CNF [27,28] incorporation have also been reported earlier.

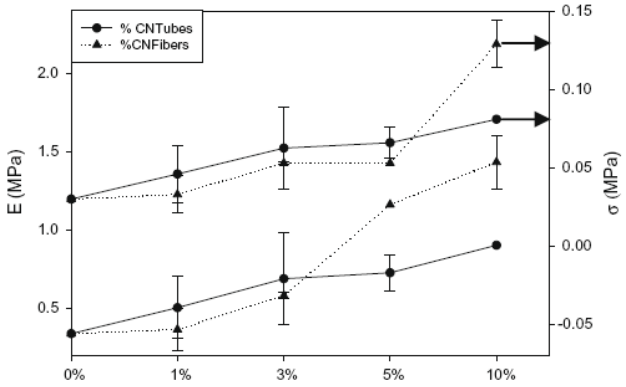

Fig. 13. Young modulus E (MPa) and tensile stress σ(MPa) at 65 _C of PCL and of their nano-bio-composites with 1, 3, 5 and 10 wt.% of the carbon nanotubes and carbon nanofibers.

Conclusions

The objective of this work was to study the morphology, thermal, conductivity, mechanical and barrier properties of nanocomposites of two biodegradable materials reinforced with carbon nanotubes and carbon nanofibers. Biodegradable nanocomposites of PCL and PHBV with different contents of CNT and CNF were prepared by the solvent casting method. The results from optical microscopy, SEM, TEM and AFM showed that CNF and CNT are well embedded in the matrix and exhibit a good dispersion of the nanofillers in the matrixes at low filler contents. However, with increasing the nanofiller content the CNT and CNF fillers agglomerate to some extent. From the DSC measurements, the carbon nanofibers and nanotubes hindered the crystallization transformation of these biodegradable materials. Filler dispersion and interfacial adhesion are thought to hinder to some extent polymer chains lateral re-arrangements and hence crystallization in these biomaterials. From the TGA results, it can be seen that the presence of
CNT and CNF in these biodegradable polymers induced better thermal stability as the onset of degradation clearly shifted to higher temperatures. Electrical conductivity of PCL and PHBV nanocomposites increased with increasing the CNT and CNF loading, effect attributed to the high electrical conductivity and good dispersion
of the CNT and CNF fillers. The electrical conductivity of the nanocomposites of carbon nanotubes was seen to be higher than the nanocomposites with carbon nanofibers. Thermal diffusion increased with increasing CNT and CNF, i.e. an increase in thermal diffusion of up to 165% in the PCL and up to 235% in the nanocomposites of PHBV was observed. In the case of barrier properties, clear

improvements in water uptake with the addition of low contents of CNT and CNF were seen. For the PCL, reductions in water uptake of ca. 50% with CNT and of 67% with CNF were seen. In the case of PHBV, reductions 23% and 49%, with CNT and CNF, respectively were observed. Improvements in oxygen permeability of ca. 52% and 26% for PCL and of ca. 58% and 62% for PHBV with CNT and CNF were also obtained. Increasing carbon nanotubes or carbon nanofibers content was seen to result in fiber agglomeration and this is thought to cause a reduction in matrix homogeneity and cohesion which leads to preferential penetrant paths and to detrimental effects in barrier properties. Moreover, a significant increase in Young modulus and yield stress which result from CNT and CNF incorporation in the biodegradable materials was also obtained.

In summary, the increased barrier properties, water and oxygen transmission, and conductivity and mechanical properties, suggests a great potential of the biodegradables PHBV and PCL with 1 wt.% carbon nanotubes and nanofibers composite films, in the applications including medicine, aerospace engineering, public transportation, home appliances, and food and beverage packaging.

References

[1] Peoples OP, Sinskey AJ. Polyhydroxybutyrate (PHB): a model system for biopolymer engineering: II. Novel Biodegrad Microbial Polym 1990:191–202.
[2] Rosa DS, Lotto NT, Lopes DR, Guedes CGF. The use of roughness for evaluating of poly-b-(hydroxybutyrate) and polyb-(hydroxybutyrate-co-b-valerate). Polym Test 2004;23:3–8.
[3] Gross RA, Kalra B. Biodegradable polymers for the environment. Science 2002;297:803–7.
[4] PigŁowski J, Kiersnowski A. Preparation, structure and useful properties of poly(e-caprolactone)/layered silicates nanocomposites. Polymers 2006;51(10): 704–15.
[5] Sinha Ray S, Okamoto M. Polymer/layered silicate nanocomposites: a review from preparation to processing. Prog Polym Sci 2003;28:1539–641.
[6] Sanchez-Garcia MD, Gimenez E, Lagaron JM. Comparative barrier performance of novel PET nanocomposites with biopolyester nanocomposites of interest in packaging food applications. J Plast Film Sheet 2007;23:133–48.
[7] Sanchez-Garcia MD, Gimenez E, Lagaron JM. Development and characterization of novel nanobiocomposites of bacterial poly(3-hydroxybutyrate), layered silicates and poly(e-caprolactone). J Appl Polym Sci 2008;108:2787–801.
[8] Chrissafis K, Antoniadis G, Paraskevopoulos KM, Vassiliou A, Bikiaris DN. Comparative study of the effect of different nanoparticles on the mechanical properties and thermal degradation mechanism of in situ prepared poly(ecaprolactone) nanocomposites. Compos Sci Technol 2007;67:2165–74.
[9] Chen Erh-Chiang, Wu Tzong-Ming. Isothermal crystallization kinetics and thermal behavior of poly(3-caprolactone)/multi-walled carbon nanotube composites. Polym Degrad Stabil 2007;92:1009–15.
[10] Saeed Khalid, Park Soo-Young. Preparation and properties of multiwalled carbon nanotube/polycaprolactone nanocomposites. J Appl Polym Sci 2007;104: 1957–63.
[11] Lai Mingfang, Li Jing, Yang Jun, Liu Jingjiang, Tong Xin, Cheng Huiming. The morphology and thermal properties of multi-walled carbon nanotube and poly(hydroxybutyrate-co-hydroxyvalerate). Compos Polym Int 2004;53:
1479–84.
[16] van der Pauw LJ. A method of measuring the resistivity and Hall coefficient on lamellae of arbitrary shape. Philos Technol Rev 1958;20:220–4.
[17] Kirby AR, Ng A, Waldron KW, et al. AFM investigations of cellulose fibers in Bintje potato (Solanum tuberosum L.) cell wall fragments. Food Biophys 2006;1(3):163–7.

[18] Yang S, Castilleja J, Barrera EV, Lozano K. Thermal analysis of an acrylonitrile–butadiene–styrene/SWNT composite. Polym Degrad Stabil 2004;83:383–8.
[19] Yang S, Lozano K, Jones R, Espinoza L, Lomeli A. Thermal and electrical analysis of vapor grown carbon nanofiber/polyoxymethylene (VGCNF/POM) composites. In: ANTEC2004, Chicago (IL), May 16–20, 2004.
[20] Yang S, Lomeli A, Borrego M, Jones R, Lozano K. Thermal and electrical analysis of vapor grown carbon nanofiber (VGCNF)/LCP composites. In: 35th International SAMPE technical conference, Dayton, OH, September 28–October 2, 2003.
[21] Dutra RCL, Soares BG, Campos EA, Silva JLG. Hybrid composites based on polypropylene and carbon fiber and epoxy matrix. Polymer 2000;41: 3841–9.
[22] Olabarrieta I, Forsström D, Gedde UW, Hedenqvist MS. Transport properties of chitosan and whey blended with poly(e-caprolactone) assessed by standard permeability measurements and microcalorimetry. Polymer 2001; 42:4401–8.
[23] Petersen K, Nielsen PV, Olsen MB. Physical and mechanical properties of biobased materials. Starch 2001;53(8):356.
[24] Shih YF, Chen LS, Jeng RJ. Preparation and properties of biodegradable PBS/ multi-walled carbon nanotube nanocomposites. Polymer 2008;49:4602–11.
[25] Kim Hun-Sik, Park Byung Hyun, Yoon Jin-San, Jin Hyoung-Joon. Thermal and electrical properties of poly(L-lactide)-graft-multiwalled carbon nanotube composites. Eur Polym J 2007;43:1729–35.
[26] Bikiaris D, Vassiliou A, Chrissafis K, Paraskevopoulos KM, Jannakoudakis A, Docoslis A. Effect of acid treated multi-walled carbon nanotubes on the mechanical, permeability thermal properties and thermo-oxidative stability of isotactic polypropylene. Polym Degrad Stabil 2008;93:952–967).
[27] Zeng Jijun, Saltysiak Bethany, Johnson WS, Schiraldi David A. Satish Kumar. Processing and properties of poly(methyl methacrylate)/carbon nanofiber composites. Composites: Part B 2004;35:245–9.
[28] Kumar S, Rath T, Mahaling RN, Reddy CS, Das CK, Pandey KN, et al. Study on mechanical, morphological and electrical properties of carbon nanofiber/ polyetherimide composites. Mater Sci Eng B 2007;141:61–70.

Chapter IV. Blends of biobased materials.

PAPER X: Incorporating Amylopectin in Poly(lactic Acid) by Melt Blending Using Poly(ethylene-co-vinyl Alcohol) as a Thermoplastic Carrier. (I) Morphological Characterization

Abstract

In this study, the possibility of using a biodegradable grade of thermoplastic poly(ethylene-co-vinyl alcohol) with high (71 mol %) vinyl alcohol (EVOH-29), as a carrier to incorporate the renewable and biodegradable component amylopectin (AP) into poly(lactic acid) (PLA) through melt blending, was investigated. The effect of using a plasticizer/compatibilizer (glycerol) in the blend systems was also investigated. In a first step, the EVOH/AP blends were produced and thereafter, in a second step, these were mixed with PLA. In this first study, the blend morphology was investigated using optical microscopy, scanning electron microscopy and Raman imaging spectroscopy and the thermal properties were measured by differential scanning calorimetry. Despite the fact that EVOH and AP are both highly polar, their blends were immiscible. Still, the blends exhibited an excellent phase dispersion on a micron level, which was enhanced further by the addition of glycerol. A good phase dispersion was finally observed by incorporation of the latter blends in the PLA matrix, suggesting that the proposed blending route can be successfully applied for these systems. Finally, the Differential scanning calorimetry (DSC) data showed that the melting point of EVOH dropped in the EVOH/AP blends, but the properties of the PLA phase was still relatively unaffected as a result of blending with the above components.

Keywords: polymer blends; biopolymers; EVOH copolymers; amylopeptine; PLA; packaging applications; biomedical applications; morphology; raman imaging

Introduction

Poly(lactic acid) (PLA) is a biodegradable linear aliphatic thermoplastic polyester that has received significant attention among researchers as an alternative material for packaging applications. Today, PLA is one of the most important biodegradable/renewable plastic materials on the market; to a great extent due to its interesting mechanical, optical, and processing properties, and, of course, to its renewability and biodegradability aspects.[1,2] In attempt to improve desired properties or lower the processing costs both blends and composites have been produced. Several studies have been carried out on PLA blends, both with non-biodegradable and biodegradable materials.[3–6] By blending PLA with other, less expensive, biodegradable polymers, the ‘‘green’’ factor can be retained at the same time as properties are improved and cost lowered. A possible candidate is starch, due to its biobased origin, low price, good availability, and high performance. Starch consists of a mixture of amylose (30%) and amylopectin (AP) (~70%), both based on chains of 1,4- linked a-D-glucose.7 Amylose is linear whereas AP is highly branched and forms transparent films, a very attractive feature when it comes to the packaging industry.[8] Martin and Averous[9] previously studied melt-blended PLA/starch systems. The observation of two glass transition temperatures (Tg), and a twophase morphology, indicated a low compatibility between the two polymers. The use of adequate compatibilizers was, therefore, suggested. Poly(ethylene-co-vinyl alcohol) (EVOH) polymers are a family of semicrystalline random co-polymers with excellent barrier properties to gases and hydrocarbons, and with outstanding chemical resistance.[10] EVOH copolymers are commonly produced via a saponification reaction of a parent ethylene-co-vinyl acetate copolymer, whereby the acetoxy group is converted into a secondary alcohol. These materials have been, increasingly, implemented in many pipe and packaging applications where high demands on chemical resistance and gas, aroma, and hydrocarbon permeation have to be met. In particular, copolymers with low contents of ethylene (below 38 mol % ethylene)
have outstanding barrier properties under dry conditions compared with other polymeric materials. In spite of the low gas permeation, EVOH copolymers generally show a high hydrophilic character that can be tuned by composition. A higher vinyl alcohol content gives a more water sensitive polymer. The EVOH properties can be designed for different applications by controlling the ethylene/vinyl alcohol ratio. Even though the EVOH family is not made from renewable resources, some grades of the poly (vinyl alcohol) homopolymer (PVOH) are water soluble and classified as biodegradable. Moreover, EVOH grades with high vinyl alcohol content (i.e., higher than 71 mol %) are highly hygroscopic and can biodegrade under certain conditions.[11,12] The similarities to biopolymers exhibited by EVOH in properties have also led to studies and trials where blends with biodegradable materials have been produced.[13,14] This highly transparent and excellent barrier material is thought to improve some properties for PLA and serve as an adequate melt blending carrier for highly polar polymers, e.g., many proteins and polysaccharides, which otherwise are not so readily melt blendable with PLA. In spite of the above, only limited work on pure blends of PLA and EVOH have been performed.[15] Lee at al.[16] used reactive blending to induce a reaction between the two components in blends with different concentrations, the material obtained was compared with EVOH/PLA simple blends. The mechanical properties were far better when a reactive blending component was

used, also the morphology studies indicated that this route resulted in better compatibility. Recently, Orts et al.[17] studied blends of EVOH and thermoplastic starch with water/glycerol as a plasticizer. They found that the most important factor altering the mechanical properties and the change in morphology was the relative humidity (RH) at which the samples were stored because this affected the degree of crystallinity of the materials. Also in the case of AP films, the RH affects the crystallization process and the degree of crystallinity.[18,19] Therefore, the films produced in this study were stored at the same RH before testing. The present study reports on the feasibility of using EVOH-29 (containing 29 mol % of ethylene in the copolymer) to implement AP into PLA via melt compounding. Also the different properties of these binary and ternary systems are investigated. This first article discusses the morphology obtained using several different microscopy techniques and Raman imaging spectroscopy as well as thermal property data of the blends. In a subsequent study, the mechanical, oxygen, and moisture transport properties as well as biodegradability tests will be presented and discussed.

Experimental

Materials

An extrusion grade of semicrystalline (PLA) manufactured by Natureworks (with a D-isomer content of approximately 2%) was used in this study. The material was disclosed to have a molecular weight (Mn) of ca. 130,000 g/mol and a weight-average molecular weight (Mw) of 150,000 g/mol. Soarnol^{R} standard grade (EVOH2903) of ethylene-vinyl alcohol copolymers with 29 mol % of ethylene in the composition was supplied by Nippon Synthetic Chemical Industry Co. (Nippon Goshei, Osaka, Japan). A very low ethylene-content EVOH grade was selected to promote both higher compatibility with the starch component and biodegradability. Even lower ethylene content EVOH grades exist, such as the one with 26 mol % ethylene (EVOH26); however, these have higher melting points and, therefore, require processing temperatures that may degrade the starch component. AP from maize [CAS: 9037–22-3] was purchased from Sigma-Aldrich (Sweden) and glycerol was obtained from Panreac Quimica S.A. (Spain).

Film preparation

Several different routes were investigated to find the best dispersion. In the first trials, the intention was to disperse AP in EVOH using a solution (isopropanol/ water), which could be melt mixed with PLA in a following step, this because AP, in contrast to EVOH, is not a thermoplastic polymer. The route involving solvent casting of EVOH/AP films, followed by grinding and melt mixing with PLA,
resulted in poor dispersion and was abandoned at an early stage. Consequently, the study was focused on using a direct melt-mixing step. EVOH/AP at different relative concentrations, with and without
glycerol, were first melt mixed in a Brabender Plastograph mixer (16 cm^3) during 4 min at 195¬ C. The mixing temperature was just above the melting point of EVOH but low enough to avoid excessive thermal exposure for AP. Higher mixing temperatures led to browning of the mixture and degradation that was later observed

as tiny dark spots in the PLA matrix after subsequent blending. On the other hand, lower
temperatures did not melt the EVOH phase sufficiently. Trials in which AP was added to the molten EVOH, either as granules or in a water solution, were performed. From the preliminary dispersion results, the latter procedure yielded the best films and was, therefore, selected throughout this study. After mixing, the batches were allowed to cooldown at room temperature and after drying the resulting EVOH/AP blends were mixed with PLA in a second melt-blending step. The sample codes used throughout the article are 45/45/10 and refer to the content (in wt %) of EVOH/AP/glycerol, respectively. The samples containing PLA were coded throughout the article as follows: PLAx% (45/45/10), where x% corresponds to the content of the EVOH/AP/glycerol blend in the PLA matrix. Mixing was finally performed during 5 min at 40 rpm followed by 1 min at 60 rpm (190ºC). After removal, the batches were allowed to cool-down at room temperature, and subsequently compression molded into films using a hot-plate hydraulic press (190ºC and 2 MPa for 4 min). The thicknesses of the films were between 80 and 110 lm as measured with a Mitutoyo micrometer by averaging four measurements on each sample.

Optical light polarized microscopy

Polarized light microscopy (PLM) examinations were carried out using an ECLIPSE E800-Nikon with a capture camera DXM1200F-Nikon. A minimum of four different pictures were taken from the examined samples.

Scanning electron microscopy

A Hitachi S-4100 Scanning Electron Microscope (SEM) was used to take SEM pictures on cryofractured samples. Prior to SEM examination, the cryofractured specimens were mounted on bevel sample holders and sputtered with Au/Pd under vacuum. An accelerating voltage of 10 kV was used.

Differential scanning calorimetry

DSC of EVOH, PLA and their blends were performed on a Perkin-Elmer DSC 7 thermal analysis system on typically 4 mg of dry material at a heating rate of 10ºC/min from 40ºC to 200ºC, followed by a cooling step (at 10ºC/min) back to 50ºC, where it was kept isothermally for 5 min. The second heating started at 50ºC and ended at 210ºC, using a 10ºC/ min heating rate. N_2 was used as the purge gas. Before evaluation, the thermograms were subtracted with similar thermograms using an empty pan. The DSC parameters presented in the article were evaluated from the cooling and the second heating runs. The DSC equipment was calibrated using indium as standard and the results presented were based on the average of two measurements.

Raman spectroscopy

Raman images were taken with a Jasco NRS-3100 Confocal Micro-Raman spectrophotometer (Jasco, Easton, MD) using a short working distance 100x objective, which under high confocal conditions provides according to the manufacturer, a lateral resolution of ca. 1 to 2 µm and a depth resolution of 2 to 3 µm.

An NIR excitation laser source, tuned at 785 nm to avoid excessive fluorescence in the Raman
signal, was used. Raman imaging was carried out in the point by point mode by rationing the area of typical Raman bands (Fig. 1—Raman spectra of the three components used) of the compounds, i.e. 865
cm^{-1} for PLA, 472 cm^{-1} for AP, and 1443 cm^{-1} for EVOH, arising from the different phases of the composites, and were constructed by taken 15 x 15 spectra equally spaced across the selected sample area.

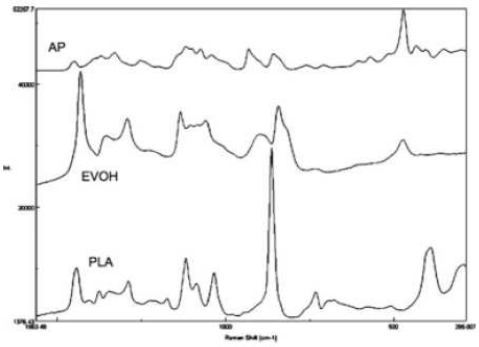

Figure 1. Raman spectra of the three components used. Higher intensity Raman bands can here be seen at ~865 cm^{-1} for PLA, ~472 cm^{-1} for AP, and ~1443 cm^{-1} for EVOH.

Results and Discussion

The first objective of this work was to generate blends of EVOH/AP with the highest possible content of AP to keep the final blends as ‘‘renewable’’ as possible. After trying several different relative mass concentrations of EVOH and AP, the 35/65 and 50/50 blends were found to have the ‘‘most promising’’ morphologies. A visually good blending was also observed at higher AP contents, but only when glycerol was present (31.5/58.5/10). Complementary information about the blends was obtained by analyzing fracture surfaces using SEM [Fig. 2(a– e)]. From this figure, some level of porosity or voids were seen when starch was present in the blend, with or without glycerol. Weak cohesion between the different blend constituents could explain the observed voiding (which could be thought as arising from detached phase separated particles and not as
porosity). However, a clear pattern of phase separation is not unambiguously discerned.[13] The glycerol containing samples can be differentiated because they give rise to surfaces that have smoother and more cohesive areas, hence indicating glycerol richer parts. The samples containing higher amounts of AP (without glycerol) show a considerably rougher fracture surface indicating a lower affinity between the two phases. However, when glycerol is also added to the AP-rich samples, the fracture surface becomes more homogenous suggesting that the glycerol can help the blending of the two polymers by promoting stronger phase adhesion and/or by reducing the EVOH polymer melting point and, therefore, reducing the blend viscosity at the mixing temperature (vide infra). This behavior has also been reported for PLA/starch

blends elsewhere.[3] Furthermore, studies on the rheological properties of extruded starch/ EVOH blends have shown similar results.[20]

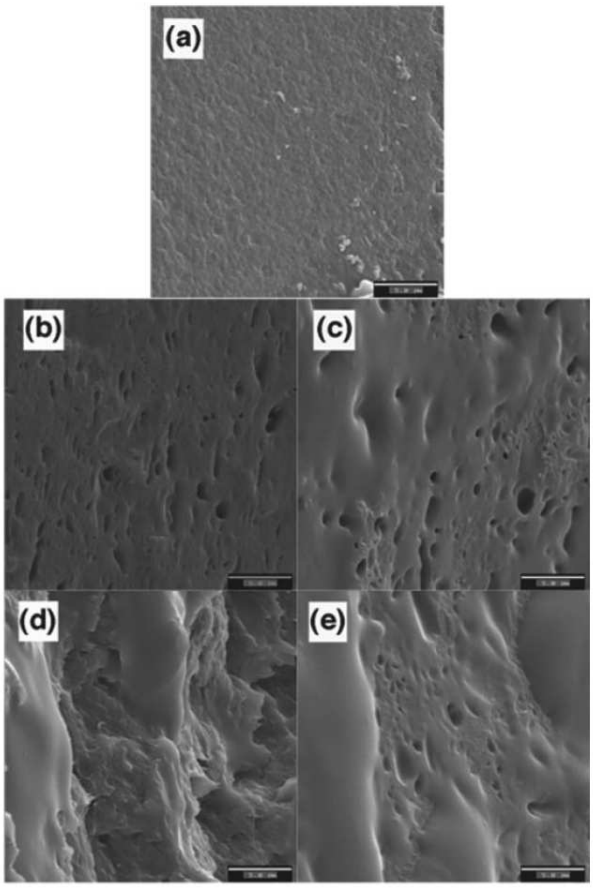

Figure 2. SEM micrographs showing fracture surfaces of (EVOH/AP/glycerol) films: a) (100/0/0), b) (50/50/0), c) (45/ 45/10), d), (35/65/0), and e) (31.5/58.5/10). The scale bars correspond to 5 µm.

Raman imaging (Fig. 3) provides unique chemical images with spatial resolutions down to the micron level. In Figure 3, the Raman image of (50/50/0) is shown. From the analysis of individual spectra at contrasting points in the image, it was observed that there were areas in the sample where one component was more dominent. Complete phase separation was not observed at the present spatial resolution level, suggesting a good intermix between the two components. Some extreme band ratio points in the image, that might indicate phases filled with one component, were in fact often areas of high fluorescence (spectrum at point b in Fig. 3a). Still the more narrow intensity spectrum in Figure 3(b) as compared to Figure 3(a) suggested that a more homogeneous mixing occurred in the presence of glycerol. The reason for this might be that the glycerol increases the distances between the AP molecules and makes them more flexible and hence improve the miscibility between the components. It is well

known that EVOH is strongly self associated and does not mix well with other polymers whether of polar or non-polar character.[21] Despite this, the present blends showed a morphology indicative of a well-dispersed multi-component system. To conclude, the Raman technique was very useful in determining the phase morphology beyond the ambiguous phase structure provided by the SEM observations. Thus, the combination of SEM and Raman chemical imaging gives a more complete understanding of the phase morphology in the blends. In this case, the techniques yielded information on the beneficial effects of glycerol on providing a more homogeneous distribution of the blend components/ polymers; a result that has also been shown elsewhere
for starch/EVOH systems.[22] In a second mixing step, the EVOH/AP blends were mixed with PLA at contents of 1, 5, and 10%, and compression molded into films. The films containing EVOH/AP, with or without glycerol, retain transparency and when compared with the unfilled material they were not discernible to the naked eye.

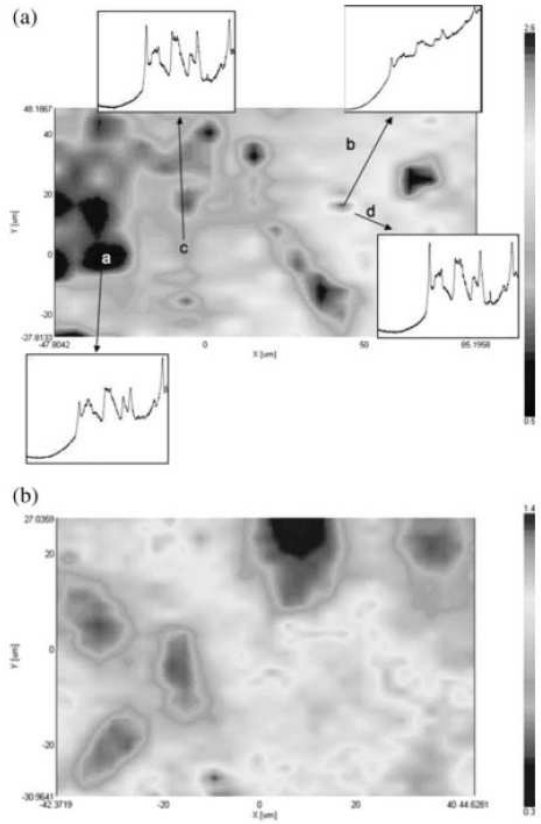

Figure 3. Raman imaging picture of EVOH/AP (50/50) at 100x magnification. The image displays the band intensity ratio E-29 (1443 cm^{-1})/AP (472 cm^{-1}). The intensity ratio scale runs from 0.5 to 2.6 and the size of the picture is ca. 75 x132 µm. Raman imaging map of EVOH/AP/glycerol (45/45/10) at 100x magnification. The image displays the band intensity ratio E-29 (1,443 cm^{-1})/AP (472 cm^{-1}). The intensity ratio scale runs from 0.3 to 1.4 and the size of the picture is ca. 75 x132 µm.

Figure 4 shows the optical microscopy pictures of these blends. No significant difference could be observed between the morphologies of the pure EVOH samples and those of the blends containing AP (not shown here). In the EVOH/AP/glycerol, glycerol could be easily discerned as well dispersed droplets throughout the matrix (Fig. 4). Apart from glycerol, no other differences in the constituent concentrations could be differentiated in Figure 4 between the various samples. SEM observations did, however, reveal the presence of a fine and well-dispersed EVOH phase within the PLA matrix in all samples (Fig. 5).

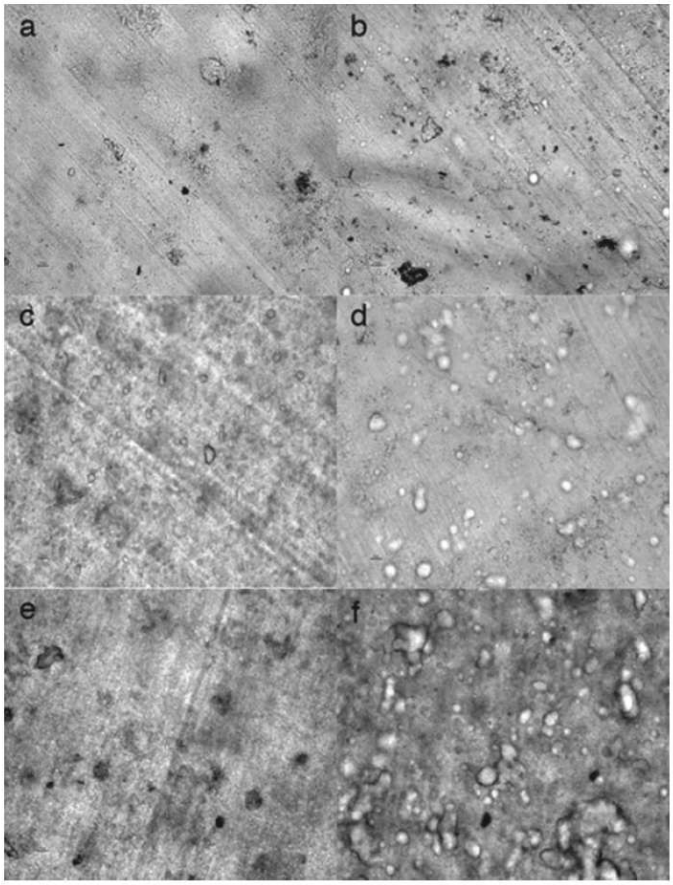

Figure 4. Optical microscopy pictures of a) PLA1% (100/0/0), b) PLA1% (45/45/10), c) PLA5% (100/0/0), d) PLA5% (45/45/10), e) PLA10% (100/0/0), f) PLA10% (45/45/10). The glycerol rich regions can easily be seen on the pictures to the right. Scale bars are 10 µm in the pictures.

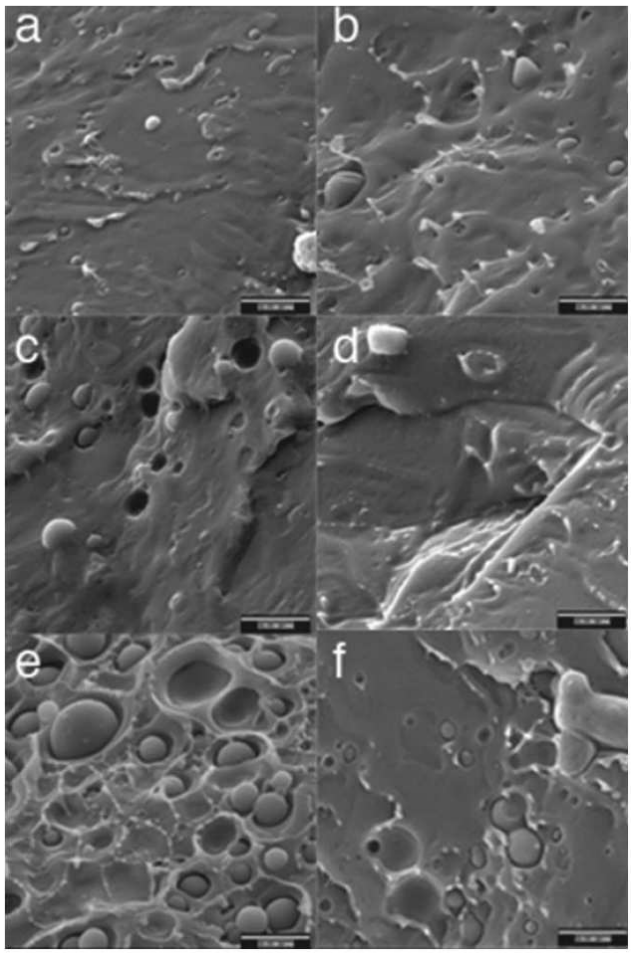

Figure 5. SEM pictures of fracture surfaces of the following films; a) PLA1% (100/0/0), b) PLA1% (50/50/0), c) PLA5% (100/0/0), d) PLA5% (50/50/0), e) PLA10% (100/0/0), f) PLA10% (50/50/0). The scale bars correspond to 5 µm.

The pictures indicate some positive interactions at the interphase, albeit adhesion is not deemed to be very strong because some particle pull-outs leaving voids are clearly observed. Pull-outs were not as obvious in the samples with lower contents of EVOH/AP but they could still, to some extent, be observed. For the blend with 10% EVOH, the phase separation was more evident. When AP was introduced into the formulation of the segregated phase, the material became more homogenous than with neat EVOH. In this case, the interface between PLA and EVOH were not as distinct; indicating that a higher interface adhesion was obtained for the three-component systems. Also, one should note that as the AP was introduced, the EVOH content was lowered. It is probable that, by tuning/adjusting the process parameters and the

quantity of AP in the blend formulation, the interfacial adhesion can, perhaps, be improved even further.[23]

Raman imaging was also finally used to assess the chemical composition of the discrete phase in the PLA matrix. Figure 6 presents images (obtained from plotting the band ratio of EVOH/PLA as explained in the experimental part) of samples containing 5 wt % of EVOH, EVOH/AP (50/50), and EVOH/AP/glycerol (45/45/10). From the images, a micron level phase dispersion was observed for the added element with little variations across the image in the ratio of the two band intensities at contrasting regions. As the SEM experiments suggested, a fine dispersion of the discrete phase was observed. A slightly better distribution of the minor phase in the PLA matrix was seen for the two latter systems, particularly for the AP, as the spectra of the contrasting phases was more even. This might suggest that the presence of AP and also of glycerol slightly increased the dispersion of the discrete phase although the recorded variations between the three systems were small.

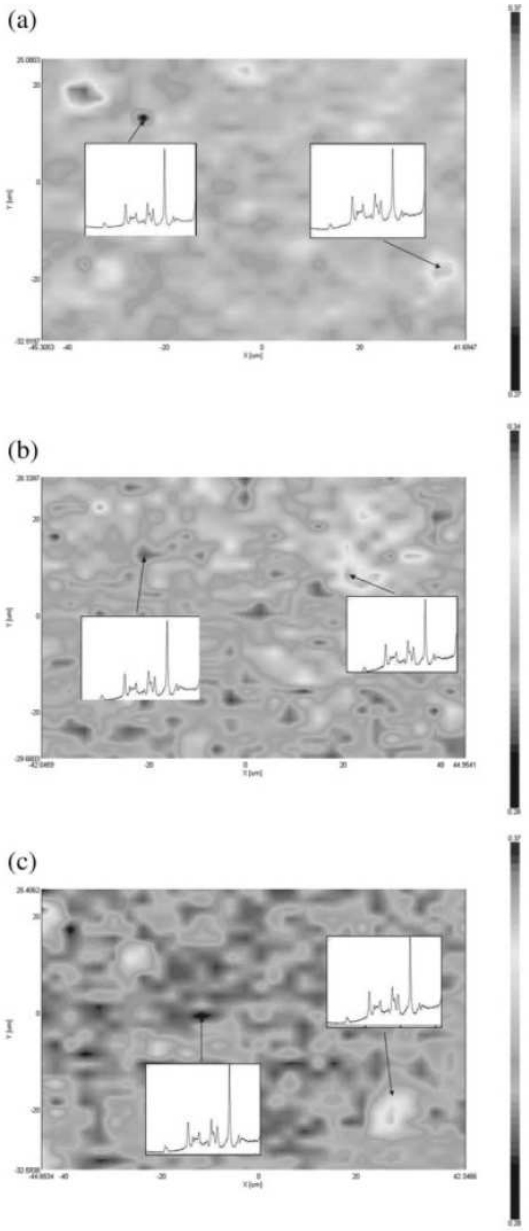

Figure 6. Raman imaging map of PLA5% (100/0/0) at 100x magnification. Peak height E-29 (1443 cm^{-1})/PLA (865 cm^{-1}). Scale from 0.27 to 0.37 and the size of the picture is ca. 57 x 86 µm. Raman imaging picture of PLA5% (50/50/0) at 100x magnification. Peak height E-29 (1443 cm^{-1})/PLA (865 cm^{-1}). Scale from 0.29 to 0.34 and the size of the picture is ca. 57 x 87 lm. Raman imaging picture of PLA5% (45/45/10) at 100x magnification. Peak height E-29 (1443 cm^{-1})/PLA (865 cm^{-1}). Scale from 0.29 to 0.37 and the size of the picture is ca. 57 x 86 µm.

Thermal properties of the blends

Tables I to III summarize the melting enthalpy and temperature of EVOH based and PLA/EVOH based blends. The values for the melting enthalpy (ΔH) have all been normalized to the PLA or EVOH contents in the blends. The first observation in EVOH and its blends (Table I) was that the melting temperature (T_m) was not significantly affected by the addition of AP. However, when glycerol was also present, the T_m clearly dropped by ca. 10ºC, illustrating the ''solvent''-induced melting point depression.[24] Previous reports show that an increase in moisture level in starch-based materials decreases the melting point.[17,25] Furthermore, in these studies ΔH_m and ΔH_c appeared to decrease somewhat when starch was introduced in the blend, this reduction was also observed in the presence of glycerol; the lower melting enthalpy is related to a decrease in crystallinity. [21] Interestingly, the crystallization temperature of EVOH was not significantly affected by the presence of AP, albeit it may seem slightly reduced suggesting some sort of phase interaction. On the other hand, the presence of glycerol clearly reduced the crystallization temperature demonstrating its strong interacting effect with EVOH. Orts et al.[17] studied starch/EVOH blends and found a very similar T_c (153.4ºC) for the same composition (45/45/10). The DSC data was in accordance with the morphology data, which suggested that phase separation between the blended components was clear, particularly from the Raman images, but that the presence of glycerol helped to enhance dispersion and interaction between the constituents. It is also interesting to note that the presence of glycerol (Table II) did not decrease the melting point of the EVOH in the PLA blends to the same levels as in the EVOH blends, perhaps, indicating that it goes into the PLA matrix during mixing. Table II indicates that the melting point of EVOH in the PLA blends was about 5 degrees lower than in the neat component. This regardless of whether it had AP or glycerol in the formulation. Interestingly, this effect was not observed in the EVOH/AP blends and, therefore, it must be a result of the interaction between the EVOH and PLA. The crystallinity also seemed to be reduced in the blends, suggesting again interactions and crystal formation interference between the blend components. The reason why EVOH and AP were not seen to interact so strongly in the DSC data in Table I compared with PLA, could lie in the fact that the samples selected were very close to the phase inversion and blends can often behave differently in compositions close to 50/50. Table III shows the thermal data corresponding to the PLA phase. From this, it can be observed that the PLA melting and crystallization points were not significantly altered, albeit they tended to decrease in the blends again suggesting interfacial interactions. The Tg of the PLA was also seen to decrease slightly and perhaps more in the blends with glycerol, although the differences were small. The melting enthalpy, calculated by subtracting the cold crystallization exothermal peak from the endothermal fusion peak, was also lower in the case of EVOH but was somewhat higher for the case of AP and glycerol as blending components, although the differences were again small. Perhaps, the latter components could affect the PLA crystallization process, which is relatively slow, and lead to a somewhat less crystalline material. All these observations supported the phase-separated structure depicted by the morphology study presented above but also indicated that some level of interaction at the interphase between the components took place. Also moisture probably had some effects. This factor has been studied for wheat starch/PLA blends containing

methylenediphenyl diisocyanate by Wang et al.,[26] reporting a negative effect on the interfacial binding at moisture levels of 10–20%. However, Ke and Sun[27] reported that the thermal, including the crystallization, properties
of PLA, in a PLA/cornstarch blend, were not affected by the moisture content. Another study concluded that the degree of mixing between PLA and glycerol plasticized starch was relatively poor.[28] The role of glycerol in the PLA blends was not so clearly discerned by the DSC data albeit the Tg of the PLA seemed to be lowest in its presence. Indicating that the molecular mobility might increase due to the presence of the plastisizer (glycerol). The PLA blends showed that the crystallization was induced when EVOH was added (Table III). The melting endotherm shifted to lower temperatures as more EVOH (with or without AP and glycerol) was added. The same effect was previously observed when plasticizers were added to PLA.[29] The explanation here was more likely to be that there were less crystalline areas in the blends leading to a lower melting point.[30] Something that could be a consequence of that glycerol contributed to prevent
re-agglomeration as the plasticizer remained between the AP polymer chains.[31]

Table 1. DSC melting and crystallization points and melting and crystallization enthalpies for EVOH and its blends corresponding to the EVOH phase. The sample names refer to wt.% content of EVOH/AP/glycerol

Sample	T_m [°C] $_{EVOH}$	T_c [°C] $_{EVOH}$	ΔH_m [J/g] $_{EVOH}$	ΔH_c [J/g] $_{EVOH}$
100/0/0	190.0±0.8	165.6±0.6	63.6±5.2	78.4±5.7
50/50/0	189.7±0.6	163.5±0.1	46.2±2.3	55.5±6.2
35/65	191.2±0.3	164.3±0.2	56.5±1.2	48.7±0.8
45/45/10	179.7±0.7	154.5±0.1	52.7±2.8	65.9±0.1
31.5/58.5/10	180.2±0.2	153.1±0.2	53.1±0.2	64.9±5.4

Table 2. DSC melting point and enthalpy for PLA blends corresponding to the EVOH phase.

Sample	T_m [°C]$_{EVOH}$	ΔH_m [J/g]$_{EVOH}$
EVOH29	190.0±0.8	63.6±5.2
PLA10%(100/0/0)	185.0±0.7	34.4±1.3
PLA10% (50/50/0)	184.1±1.5	50.9±1.8
PLA10%(45/45/10)	185.2±1.7	31.6±1.6

Table 3. DSC melting point and enthalpy for the PLA blends corresponding to the PLA phase.

Sample	T_m [ºC]$_{PLA}$	T_c [ºC] $_{PLA}$	ΔH_m [J/g] $_{PLA}$	T_g [ºC] $_{PLA}$
PLA	150.2	119.5	15.7	61.9
PLA1%(100/0/0)	150.1±1.1	119.0±1.1	14.0±3.1	60.5±3.1
PLA5%(100/0/0)	149.2±1.0	116.0±1.1	12.1±0.4	58.6±0.4
PLA10%(100/0/0)	149.7±1.2	117.7±1.0	13.9±0.1	58.0±0.4
PLA1%(50/50/0)	148.8±0.4	117.2±2.1	15.4±3.4	57.7±0.4
PLA5%(50/50/0)	149.4±0.5	118.5±0.2	13.1±0.3	58.1±0.1
PLA10%(50/50/0)	148.5±0	114.8±0.1	18.2±2.7	58.7±0.4
PLA1%(45/45/10)	149.0±0.1	116.5±0.0	17.2±2.5	57.6±0.1
PLA5%(45/45/10)	148.3±0.1	115.3±0.1	15.2±6.2	57.2±0.8
PLA10%(45/45/10)	149.5±1.3	118.5±0.6	17.2±1.2	56.8±0.0

Conclusions

In this study, AP was melt blended with PLA by using a thermoplastic EVOH carrier with and without glycerol as plasticizer/compatibilizer. The inclusion of AP in PLA seeks to enhance the properties of the latter, mainly gas barrier and biodegradability characteristics. The rationale behind using EVOH as carrier is double, on the one hand, EVOH is a highly polar polymer with very high gas barrier properties and potentially good interaction with the starch component; and on the other hand, the EVOH material can be melt compounded and, therefore, could serve as a vehicle to incorporate AP into PLA by melt blending. SEM and Raman imaging spectroscopy were applied to show that AP and EVOH were indeed well mixed up to 50 wt % of AP, albeit not miscible. At higher AP contents (65 wt %), the addition of glycerol was needed to obtain a more homogenous system. In a second step, this material was blended with PLA. The presence of AP, with or without glycerol, was found to lead to a somewhat better dispersion in the PLA blends, although the variations were very small. DSC data showed that EVOH and its blends were not essentially affected by the addition of AP. When glycerol was added the T_m, however, dropped by ca. 10ºC. Minor effects on the thermal blends of PLA were also noticed and the Tg decreased slightly with the addition of AP, with or without glycerol.

References

1. Auras, R.;Harte, B.; Selke, S. Macromol Biosci 2004, 4, 835.
2. Fang, Q.; Hanna, M. A. Ind Crop Prod 1999, 10, 47.
3. Sarazin, P.; Li, G.; Orts, W. J.; Favis, B. D. Polymer 2008, 49, 599.
4. Nijenhuis, A. J.; et al. Polymer 1996, 37, 5849.

5. Wang, L.; et al. Polym Degrad Stab 1998, 59, 161.
6. Ma, X. F.; Yu, J. G. Carbohydr Polym 2004, 57, 197.
7. Ritzl, A.; Regev, O.; Yerushalmi-Rozen, R. Acta Polym 1998, 49, 566.
8. Rindlav-Westling, A.; Stading, M.; Gatenholm, P. Biomacromolecules 2002, 3, 84.
9. Martin, O.; Averous, L. Polymer 2001, 42, 6209.
10. Lagaron, J. M.; Powell, A. K.; Bonner, G. Polym Test 2001,20, 569.
11. Tomita, K.; Kojoh, K.; Suzuki, A. J Ferment Bioeng 1997, 84, 400.
12. Mejia, A. I.; Lopez, B. L.; Sierra, L. Mater Res Innovat 2001, 4,148.
13. Stenhouse, P. J.; Ratto, J. A.; Schneider, N. S. J Appl Polym Sci 1997, 64, 2613.
14. Jiang, T.; et al. Eur Polym J 2005, 41, 459.
15. Jacobsen, S.; Fritz, H. G. Polym Eng Sci 1996, 36, 2799.
16. Lee, C. M.; Kim, E. S.; Yoon, J. S. J Appl Polym Sci 2005, 98, 886.
17. Orts, W. J.; et al. Polym Adv Technol 2007, 18, 629.
18. Myllarinen, P.; et al. Carbohydr Polym 2002, 48, 41.
19. Rindlav-Westling, A.; et al. Carbohydr Polym 1998, 36, 217.
20. Villar, M. A.; Thomas, E. L.; Armstrong, R. C. Polymer 1995, 36, 1869.
21. Lagaron, J. M.; et al. Polymer 2001, 42, 7381.
22. Jiang, W. B.; Qiao, X. Y.; Sun, K. Carbohydr Polym 2006, 65, 139.
23. Huneault, M. A.; Li, H. B. Polymer 2007, 48, 270.
24. Hedenqvist, M.; et al. Polym Eng Sci 1996, 36, 271.
25. Dell, P. A.; Kohlman, W. G. J Appl Polym Sci 1994, 52, 353.
26. Wang, H.; Sun, X. Z.; Seib, P. J Polym Environ 2002, 10, 133.
27. Ke, T. Y.; Sun, X. Z. J Appl Polym Sci 2001, 81, 3069.
28. Wang, N.; et al. Carbohydr Polym 2008, 71, 109.
29. Pillin, I.; Montrelay, N.; Grohens, Y. Polymer 2006, 47, 4676.
30. Younes, H.; Cohn, D. Eur Polym J 1988, 24, 765.
31. Park, J. W.; Im, S. S.; Kim, S. H.; Kim, Y. H. Polym Eng Sci 2000, 40, 2539.

PAPER XI: Incorporating Amylopectin in Poly(lactic Acid) by Melt Blending Using Poly(ethylene-co-vinyl Alcohol) as a Thermoplastic Carrier. (II) Physical Properties

Abstract

This study adds to a previous morphological work (paper I) with further characterization of the developed PLA blends containing amylopectin, which made use of an ethylene-vinyl alcohol copolymer (EVOH) as a melt-compoundable carrier for the polysaccharide in the biopolyester. The effect of using glycerol as compatibilizer was also characterized. Water and oxygen transport parameters, mechanical properties and comparative biodegradability tests were evaluated for the blends. From the results, the barrier properties to oxygen were only seen to improve at 0%RH and mostly for the PLA-EVOH blends, which furthermore showed a positive deviation from the rule of mixtures. At high relative humidity the blends showed somewhat poorer barrier performance due to the comparatively higher improvement in barrier of the neat PLA at 80%RH. Interestingly, room temperature biodegradability testing suggested that low additions of the blending elements seemed to facilitate the biodegradability of the biopolyester. Despite the fact that properties were not so dramatically improved, incorporating renewable resources within PLA seems as a potentially viable route to reduce PLA supply dependency, retain good optical properties as well as to overcome some drawbacks associated to the use of this biopolyester.

Keywords: polylactic acid, renewable resources, packaging, bioplastis, amylopeptine

Introduction

Poly (lactic acid) (PLA) is today one of the most important renewable/biodegradable plastic materials. Hence, this linear aliphatic thermoplastic polyester is receiving a lot of attention from researchers all over the world as an alternative material for packaging applications. Besides being renewable and biodegradable, its transparency, mechanical properties, and processability make PLA an attractive and interesting material from an application point of view [1,2]. A problem with PLA is, as with many other environmentally friendly materials, the fact that the biopolymer and processing costs are too high compared to its petroleum-based polymers. The properties of this biodegradable polymer are still considered to be insufficient for some applications and demand continuous efforts to exceed production capacity. Therefore, several studies have been carried out where PLA has been mixed with other biodegradable and nonbiodegradable materials. [3–6] By choosing a less expensive, biodegradable polymer as blending material for PLA the production costs and inaccessibilitycould be potentially lowered at the same time as the "eco" factor is retained.

Several materials can be considered as a blending component for PLA. The low price, good availability and performance along with its biobased origin make starch an attractive and promising candidate for renewable applications. Starch consists of a mixture of amylose (~30%) and amylopectin (~70%), both based on chains of 1,4-linked α-D-glucose [7]. Amylose is linear whereas amylopectin (AP) is highly branched and forms transparent films, a very attractive feature when it comes to the packaging area [8]. Martin et al. [9] previously studied melt blended PLA/starch systems. The results showed a relatively low level of compatibility between the two systems, reported after observation of two glass transition temperatures (T_g). Also their SEM studies indicated a low degree of compatibility and the use of adequate compatibilizers was suggested as the right way forward.

Ethylene-vinyl alcohol (EVOH) copolymers are a family of semicrystalline materials with excellent barrier properties to gases and hydrocarbons (in drier conditions), and with outstanding chemical resistance [10]. These materials have been increasingly implemented in many pipe and packaging applications where stringent criteria in terms of chemical resistance and gas, water, aroma and hydrocarbon permeation are to be met. In particular, the copolymers with low contents of ethylene (below 38 mol% ethylene) have outstanding barrier properties under dry conditions compared to most other polymeric materials. In spite of the low gas permeation, EVOH copolymers generally show a high hydrophilic character that can be tuned by composition. The hydrophilicity results in high water uptake in high relative humidity environments. The EVOH end properties can be designed for different applications by controlling the ethylene/vinyl alcohol composition ratio. Even when the EVOH family comprises no sustainable polymers, some grades of the homopolymer PVOH are water soluble and are classified as biodegradable. Moreover, EVOH grades with high vinyl contents (i.e. higher that 71 mol% of vinyl alcohol) are highly hygroscopic and can biodegrade under certain conditions [11,12]. The similarities to biopolymers exhibited by EVOH in properties have also led to studies and trials where blends with biodegradable materials have been produced [13,14]. By using this material the biodegradation time

could be shortened, prices lowered and at the same time hopefully the properties kept at an acceptable level.

In spite of the above, limited work on pure blends of PLA and EVOH has been performed, even if the topic has been under investigation for some years [15]. Lee at al. [16] used reactive blending to induce a reaction between the two components and the material obtained was compared with EVOH/PLA simple blends. The mechanical properties were far better when a reactive blending component was used, also the morphology studies indicated that this route resulted in better compatibility. Orts et al. [17] recently studied blends of EVOH and thermoplastic starch with water/glycerol as a plasticizer. They found that the most important factor altering the mechanical properties and the change in morphology was the relative humidity (RH) at which the samples were stored since this affects the degree of crystallinity in the materials. The crystallinity of amylopectin films has been studied before and showed that the level of humidity at film forming can affect the crystallization process [18, 19]. The produced films in this study were, therefore, handled in the same way and stored at the same RH before testing.

In this study, the feasibility of using EVOH-29 (containing 29 mol% of ethylene in the copolymer) to implement AP into PLA via melt compounding is presented. In this first study, the blend morphology was investigated using optical microscopy, scanning electron microscopy and Raman imaging spectroscopy and the thermal properties were measured by differential scanning calorimetry. Despite the fact that EVOH and amylopectin are both highly polar, their blends were immiscible. Still, the blends exhibited an excellent phase dispersion on a micron level, which was enhanced further by the addition of glycerol. A good phase dispersion was finally observed by incorporation of the latter blends in the PLA matrix, suggesting that the proposed blending route can be successfully applied for these systems. Finally, the DSC data showed that the melting point of EVOH dropped in the EVOH/amylopectin blends, but the properties of the PLA phase was still relatively unaffected as a result of blending with the above components [30].

In this second study of the materials, the barrier properties against oxygen and water as well as the mechanical properties are investigated. Furthermore, room temperature simple comparative biodegradability tests between the different systems are presented.

Material and Methods

Materials

A semicrystalline extrusion grade of poly(lactid acid) (PLA) (Natureworks) with a D-isomer content of approximately 2% was used in this study. It had a weight-average molecular weight (Mw) of 150,000 g/mol and a molecular weight (Mn) of ca. 130,000 g/mol. Soarnol® standard grades (EVOH2903) of ethylene-vinyl alcohol copolymer with 29 mol% ethylene was supplied by Nippon Synthetic Chemical Industry Co. Ltd. (Nippon Goshei, Osaka, Japan). Amylopectin (AP) (α-1,4-glucan with α-1,6-cross-linking; one terminal group per 25 glucose units) from maize [CAS: 9037-22-3] was

purchased from Sigma-Aldrich Inc. (Sweden) and glycerol was purchased from Panreac Quimica S.A. (Spain).

Preparation of blends

To get the highest degree of dispersion, several different routes were investigated. These are described more thoroughly in part I of this study.[20] The preparation process selected in the end was a direct melt mixing step. Different concentrations of EVOH/AP with and without glycerol were first melt-mixed in a Brabender Plastograph mixer (16 cm^3) for 4 min at 195ºC. The mixing temperature was chosen low enough to avoid excessive thermal exposure to the AP but high enough to melt EVOH. The AP was added in a water solution as that resulted in better films than simply adding AP in its granular form. Subsequent to the mixing, the batches were left at room temperature to cool-down. After drying the resulting EVOH/AP blends, in a second melt-blending step, were mixed with PLA. The sample codes used throughout the paper are 45/45/10 and refer to the content (in wt %) of EVOH/AP/glycerol, respectively. The samples containing PLA were coded throughout the paper as follows: PLAx% (45/ 45/10), where x% corresponds to the content of the EVOH/AP/glycerol blend in the polymer matrix. Mixing times were finally selected to 5 min at 40 RPM followed by 1 min at 60 RPM at 190ºC. The batches were allowed to cool-down to room temperature after removal and were after this pressed into films using a hot-plate hydraulic press (190ºC and 2 MPa for 4 min). By averaging four independent measurements for each sample using a Mitutoyo micrometer, the thicknesses of the films were determined to be between 80 and 110 µm. Figure 1 shows typical optical pictures of PLA and of PLA-blend films containing 5 wt % of EVOH, of (EVOH29/AP) and of (EVOH29/AP/Gly). From these pictures, it can be seen that all samples remain transparent at 100 µm thickness. The biocomposites exhibit good optical properties and clarity, even with the addition of EVOH, amylopectin or with the addition of glycerol. The samples after pressing were conditioned at 54% RH and tested within 2 weeks of preparation.

Gravimetric measurements

Direct permeability to water was determined from the slope of weight loss vs. time experiments at 24°C and 40%RH. The films were sandwiched between the aluminium top (open O-ring) and bottom (deposit for the permeant) parts of aluminium permeability cells. A Viton rubber O-ring was placed between the film and the bottom part of the cell to enhance sealability. Then the bottom part of the cell was filled with the permeant and the pinhole was secured with a rubber O-ring and a screw. Finally, the cell was placed in the desired environment and the solvent weight loss through a film area of 0.001 m^2 was monitored and plotted as a function of time. The samples were preconditioned at the desired testing conditions for 24 hours, and to estimate permeability we used only the linear part of the weight loss data to ensure sample steady state conditions. Cells with aluminium films (with thickness of ca. 100 microns) were used as control samples to estimate solvent loss through the sealing. The permeability sensitivity of the permeation cells was determined to be of ca. 0.01 10-13 kg m/s m^2 Pa based on the weight loss measurements of the aluminium cells. Cells clamping polymer films but with no solvent were used as blank samples to monitor water uptake. Solvent permeation rates were estimated from the steady-state

permeation slopes. Water vapour weight loss was calculated as the total cell loss minus the loss through the sealing and plus the water weight gain. The tests were done in duplicate and one-way analysis of the variance (ANOVA) was performed using XLSTAT-Pro (Win) 7.5.3 (Addinsoft, NY) software package. Comparisons between samples were evaluated using the Tukey test.

Water uptake

The water uptake was estimated during the sorption experiments at 24ºC and 100%RH by means of weight gain using an analytical balance Voyager^{R} V11140. Thus, at saturation conditions, no changes in successive weight uptake were observed during the measurements of the specimens.

Oxygen transmission rate

The oxygen permeability coefficient (P) was derived from oxygen transmission rate (OTR) measurements recorded using an Oxtran 100 equipment (Modern Control Inc., Minneapolis, MN, US). The temperature was kept at 24ºC while experiments were performed at two different relative humidities, 0%RH and 80%RH. The reason for the latter is that such conditions are closer to real applications. 80% relative humidity was generated by a built-in gas bubbler and was checked with a hygrometer placed at the exit of the detector. Experiments were done in duplicate. Diffusion and solubility coefficients were also estimated at 0% and at 80%RH. The samples were purged with nitrogen for a minimum of 20 h, prior to exposure to a 100% oxygen flow of 10 ml/min, and a 5 cm2 sample area was measured by using an in-house developed mask. The Diffusion (D) coefficient was estimated from fitting the OTR-time curve to the first six sum terms of the following solution of the Fick's second law [21,22]:

$$OTR(t) = \frac{Pp}{l}\left[1 + 2\sum_{n=1}^{\infty}(-1)^n \exp(-\frac{D\pi^2 n^2 t}{l^2})\right] \quad \text{Equation 1}$$

In Equation 1, p is the oxygen partial pressure and l is the film thickness.

The solubility coefficient was calculated by solving for S in the following equation [20]:

$$P = D \times S \quad \text{Equation 2}$$

Mechanical properties

Tensile tests were carried out at 24ºC and 50% RH on an Instron 4400 Universal Tester. Dumb-bell shaped specimens with initial gauge length of 25 mm and 5 mm in width were die-stamped from the sheets in the machine direction according to ASTM D638. The thickness of all specimens was approximately 100 µm. A fixed crosshead rate of 10 mm/ min was utilized in all cases, and results were taken as the average of four tests. The samples were preconditioned at 54% RH before testing and were assayed within 2 weeks after preparation ofthe films.

Biodegradability

Biodegradability may be tested by various methods. For simplicity in experimental setup, we chose a comparative method. Polycaprolactone (PCL), known to be readily biodegradable, was chosen as a reference material [23]. Biodegradability of the films was tested in a composting plant, filled with fresh compost, and ''fed'' regularly with apple slices. The temperature of the compost was around 25ºC at all times, while the relative humidity was around 60–70%. The samples were sandwiched between wire nets, placed in the composting plant and covered with the fresh compost. Photographs were taken regularly during a period of 60 days to monitor the biopolymer degradation.

Results and Discussion

Mass transport properties

Table 1 summarizes measured direct permeability of water and water uptake for the PLA film and their blends together with permeability values reported in the literature for EVOH29 [24].

Table 1. Water permeability and water uptake for PLA films and their blends. The a, b, c and d letters correspond to the ANOVA statistical analysis and Tukey test of the data that indicate that with a 95% level of confidence the values are significantly different.

Sample	*P* water (kg m/s m^2 Pa)	Water uptake 100% RH (%)
PLA	[a]1.18 ± 0 e^{-14}	Literature value[33] 0.85
PLA + 1% EVOH29	[b]1.38 ± 0.04 e^{-14}	1.05
PLA + 5% EVOH29	[b]1.33 ± 0.03 e^{-14}	1.42
PLA + 10% EVOH29	[b]1.30 ± 0.10 e^{-14}	1.43
PLA + 1% (E29 + 50% AP)	[c]1.40 ± 0.04 e^{-14}	0.81
PLA + 5% (E29 + 50% AP)	[c]1.40 ± 0.03 e^{-14}	1.06
PLA + 10% (E29 + 50% AP)	[c]1.49 ± 0.04 e^{-14}	2.22
PLA + 1% (E29 + 50% AP + 10%Gly)	[d]1.79 ± 0.03 e^{-14}	1.14
PLA + 5% (E29 + 50% AP + 10% Gly)	[d]1.71 ± 0.009 e^{-14}	2.15
PLA + 10% (E29 + 50% AP + 10% Gly)	[d] 1.87 ± 0.05 e^{-14}	3.19
PLA + 5% (E29 + 65% AP + 10% Gly)	[d] 1.79 ± 0.03 e^{-14}	2.82
EVOH29		9.33
Literature value[24] EVOH29	1.70 e^{-14}	
EVOH29 + 50% AP		19.01
EVOH29 + 65% AP		28.04
Literature value[25] amylopectin	1.15 e^{-14}	21[28]

The a, b, c, and d letters correspond to the ANOVA statistical analysis and Tukey test of the data that indicate that with a 95% level of confidence the values are significantly different.

EVOH films have, as expected, poorer water barrier than PLA films, hence the addition of EVOH29 to PLA leads to higher water permeability when compared to pure PLA. Thus, the blends of PLA with an EVOH29 content of 1, 5, and 10 wt % have a water permeability increase of 17, 13, and 10%, respectively, compared to the unfilled material. The statistical analysis indicates that the variations on permeability between the different EVOH sample contents are not significant. The water uptake was also seen to increase and was found to be for these samples of 1.1, 1.4, and 1.4%, respectively, whereas was of 0.85% for the pure PLA.

In a similar fashion, the addition of amylopectin to these blends led to a further increase in water permeability. Blends of PLA with 1, 5 and 10 wt.-% (EVOH29+50%AP) content exhibited a water permeability increase of 19%, 19% and 26%, respectively, compared to the unfilled material. This is not surprising since the water uptake of amylopectin is also much higher than that of PLA [25]. Amylopectin is a hydrophilic material which also leads to slightly higher water uptake when present in the blend. The water uptake for the different amylopectin blends was found to be 0.8%, 1.1% and 2.2%, respectively.

Glycerol is a very hydrophilic material and, therefore, the addition of it to the different blends leads to additional increases in the water permeability. PLA-blends with 1, 5 and 10 wt.-% (EVOH29+50%AP+10%Glycerol) content showed water permeability increases of 52%, 50% and 58%, respectively, compared to the unfilled material. The water uptake increases further until 1.1%, 2.2% and 3.2% respectively in these blends. This is expected and a normal behaviour due to the hydrophilic character of glycerol [26].

Table 2 shows the measured oxygen permeability and also oxygen diffusion and solubility coefficients for the films. The table also gathers permeability values reported in the literature for PLA [24-27]. The oxygen permeability coefficients reported from different authors for pure PLA, measured at dry and wet conditions, provide similar values as those measured in our laboratory and suggest that %RH has a minor effect on the permeability for the biopolymer. In this context, Auras et al. [1] also reported a reduction in the oxygen permeability coefficient for the pure PLA with increasing water activity (at a constant temperature).

From Table 2, it is observed that EVOH29 is at 0%RH and at 80%RH a much better barrier than PLA. Therefore, the rationale behind the current blending work was that the addition of EVOH29 to the PLA should result in enhanced oxygen permeability compared to the unfilled PLA, and that this enhancement should be greater at 0%RH, due to the better permeability of the EVOH29 at low humidity.

Table 2. Oxygen permeability and standard deviation, oxygen diffusion coefficient at 80%RH and 0%RH, and at 24C for these blends.

	P oxygen 80%RH, 24C (m^3 m/s m^2 Pa)	**P oxygen 0%RH, 24C (m^3 m/s m^2 Pa)**	**D oxygen 80%RH, 24ºC (m^2/s)**	**D oxygen 0%RH, 24ºC (m^2/s)**	**S oxygen 80%RH, 24ºC (g/gPa)**	**S oxygen 0%RH, 24ºC (g/gPa)**
PLA	$1.64\pm0.27\ e^{-18}$	$2.26\pm0.01e^{-18}$	$1.97e^{-12}$	$1.53e^{-12}$	$9.28e^{-7}$	$14.80e^{-7}$
Literature Value [24]PLA	**$2.21e^{-18}$**	**$2.25e^{-18}$**				
Literature Value [27]PLA	**$1.75e^{-18}$**					
PLA+1%EVOH29	$2.03\pm0.46\ e^{-18}$	$2.21\pm0.02e^{-18}$	$1.82e^{-12}$	$1.72e^{-12}$	$9.34e^{-7}$	$12.88e^{-7}$
PLA+5%EVOH29	$1.81\pm0.15\ e^{-18}$		$2.08e^{-12}$		$8.20e^{-7}$	
PLA+10%EVOH29	$1.72\pm0.07e^{-18}$	$1.67\pm0.08e^{-18}$	$1.83e^{-12}$	$0.95e^{-12}$	$9.12e^{-7}$	$17.64e^{-7}$
PLA+1%(E29+50%AP)	$2.42\pm0.36\ e^{-18}$		$1.85e^{-12}$		$11.70e^{-7}$	
PLA+5%(E29+50%AP)	$2.18\pm0.17\ e^{-18}$	$2.24\pm0.05e^{-18}$	$2.31e^{-12}$	$1.54e^{-12}$	$8.65e^{-7}$	$14.50e^{-7}$
PLA+10%(E29+50%AP)	$2.19\pm0.10\ e^{-18}$		$1.94e^{-12}$		$10.91e^{-7}$	
PLA+1%(E29+50%AP+10%Gly)	$2.12\pm0.06\ e^{-18}$		$1.68e^{-12}$		$12.32e^{-7}$	
PLA+5%(E29+50%AP+10%Gly)	$1.69\pm0.19\ e^{-18}$		$1.97e^{-12}$		$7.89e^{-7}$	
PLA+10%(E29+50%AP+10%Gly)	$2.13\pm0.17\ e^{-18}$		$1.80e^{-12}$		$11.13e^{-7}$	
PLA+5%(E29+65%AP+10%Gly)	$1.99e^{-18}$		$2.18e^{-12}$		$9.10e^{-7}$	
Literature valueEVOH29 20ºC	**$0.0023e^{-18}$**	**$0.00084\ e^{-18}$**				
Literature Value [28]Amylopectin 50%RH, 20ºC	**$0.004e^{-18}$**					
Literature Value [28]Amylopectin+10%Gly 50%RH, 20ºC	**$0.006e^{-18}$**					

The results measured at 0%RH and 24ºC indicate that blends of PLA with EVOH29 have a lower average oxygen permeability compared to the unfilled material. This decrease is higher, particularly for the 10 wt.-% loading, than expected by the simple rule of mixtures as seen in Figure 2. The rule of mixtures predicts a permeability drop of 10% for 10 wt.-% loading, but the experimental value shows a decrease of ca. 26%. A reduction in the oxygen diffusion coefficient of ca. 38% can also be seen and as a result a corresponding increase in oxygen solubility of around 20%. Curiously, the previous work indicated that the crystallinity of the PLA phase, but also the Tg, decreased to a small extent by blending with EVOH [20]. Hence, the increase of the oxygen solubility may be attributed to the different phase structures in the blend suggested by the crystallinity alterations reported in the previous work [20].

Unfortunately, at 80%RH the oxygen permeability provided no apparent improvement with the addition of EVOH. The oxygen diffusion coefficient and the oxygen solubility coefficient measured at 80%RH showed no improvement compared to the pure PLA. The reason for this behaviour must then be attributed to the interaction of the blends with water, which seems to be detrimental for the blends. Table 2 shows

that while pure PLA reduces somewhat permeability with increasing humidity, the blends reduce to a much lesser extent and in some cases remain unmodified.

The addition of amylopectin to these blends results in a slight decrease in the oxygen permeability measured at 0%RH. However, in the case of the measurements in moist conditions, the oxygen permeability measured at 80%RH increases and remains almost unmodified compared to the permeability at 0%RH case, while for pure PLA the permeability decreases at high humidity. Blends of PLA with 1, 5 and 10 wt.-% (EVOH29+50%AP) show an increase in oxygen permeability of, respectively, 47%, 32% and 34%, compared to the unfilled material measured at 80%RH and 24ºC. From the results, the oxygen diffusion coefficient tends to decrease slightly, however the oxygen solubility coefficient increases [20]. As it can be seen in the previous study of the thermal properties, data on the PLA blends showed that crystallization was reduced to some extent when EVOH and amylopectin was added, so this could be affecting the solubility and the role of humidity in the blends.

Blends of PLA with 1 and 10 wt.-% (EVOH29+50%AP+10Gly) filler content have an oxygen permeability increase of 29% and 30%, respectively, again compared to the unfilled material measured at 80%RH and 24ºC. However, the oxygen diffusion coefficient decreases. The reason for the increase in the oxygen permeability is in fact attributed to an increased solubility [20]. Nevertheless, the sample of PLA with 5 wt.-% (45/45/10) content has the lowest oxygen permeability increase, i.e. only 3%. Hence, the better barrier performance may be attributed to the presence of a fine dispersion of the EVOH phase in the blend, which establishes a positive interaction with the PLA as suggested from the previous work. The results indicate, in conclusion, that this amylopectin based blend has the best morphology (as shown by Nordqivst et al. in the former study [20]) and least impact in oxygen barrier properties.

Mechanical properties

Table 3 summarizes the mechanical properties of the PLA films and of their blends. With the addition of EVOH29 the Young's Modulus decreases slightly. With the addition of AP and glycerol to the blend this change is also very small suggesting that stiffness is rather unchanged in the polymer since the three polymers have relatively similar E modulus, being smallest for amylopectin.

Table 3. Youngs´s Modulus, Stress at Break and Elongation at Break for the different samples. *)Unpublished data by Nordqvist et al.

Sample	E [GPa]	Strength [Mpa]	E_b [%]
PLA	2.01±0.04	54.16±5.22	9.20±0.09
PLA+1%EVOH29	1.97±0.13	57.05±5.00	8.84±5.46
PLA+5%EVOH29	1.83±0.17	51.15±2.20	8.10±2.85
PLA+1%(E29+50%AP)	1.98±0.09	53.91±4.71	6.59±1.17
PLA+5%(E29+50%AP)	2.01±0.03	52.19±1.80	4.37±0.84
PLA+5%(E29+50%AP+10%Gly)	1.81±0.06	45.25±7.25	4.66±1.28
PLA+10%(E29+50%AP)	2.00±0.02	49.52±1.75	3.59±0.30
Literature Value [29]EVOH29, dried films conditions	**2.398**		**46.16**
Amylopectin*	**1.93 ± 0.07**	**40.0 ± 1.3**	**2.3 ± 0.3**

Also the tensile strength of the films does not significantly change with the addition of EVOH29. The strength was not affected greatly by the addition of AP at lower levels. However, for the sample containing 10 %(EVOH/AP) or when glycerol was present the strength decreased. The reason for this is that AP is naturally weaker than PLA and EVOH, and to the plasticizing effect of glycerol. From Table 3, it can be seen that pure amylopectin has lower tensile strength, so as expected with the addition of AP the tensile strength of the blends decreases.

Finally, the elongation at break decreases slightly with the addition of EVOH, but with the addition of amylopectin the elongation at break decreases considerably. This result is not surprising since amylopectin as a very brittle material and hence is expected to translate this effect into the blend. Another result that might seem surprising is that when glycerol is added this does not increase the strain at break. At low glycerol content the plasticizing effect is not noticeable, something that has been shown for the AP system earlier [26, 30].

Biodegradability

A significant drawback of using PLA as a biodegradable material is the slow rate of degradation when compared to other biodegradable materials. The biodegradation of PLA in a composting environment has two steps. In the first step, the high-molecular-weight PLA chains hydrolyze into low-molecular-weight oligomers. This step is catalyzed by temperature and moisture. The second step is the conversion of the oligomeric components into CO_2, water, and humus by means of the action of microorganisms. Therefore, any factors that increase the hydrolysis tendency can promote the degradation of PLA. Other factors affecting the biodegradation of polymers are the molecular weight and the degree of crystallinity. Lower molecular weight PLA materials do show higher rates of enzymatic degradation due to the higher concentration of accessible chain-end groups. It is also known that the amorphous phase is easier to biodegrade compared to the crystalline phase [31-32].

Figure 3 shows the degradation patterns of a polycaprolactone (PCL) film. PCL is often used as reference material in biodegradability tests, and accordingly the PCL films degraded within 60 days.

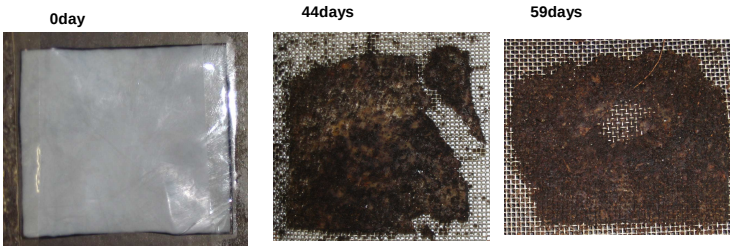

Figure 3. Degradation of PCL Films – Reference Material for Biodegradability

Figure 4 shows the time dependence of the biodegradation study for the pure PLA. In this case, the PLA samples did not degrade within 60 days as did the PCL. After 90 days the PLA films had still not degraded. This further confirmed that PLA presents very slow rate of degradation compared to polycaprolactone [32].

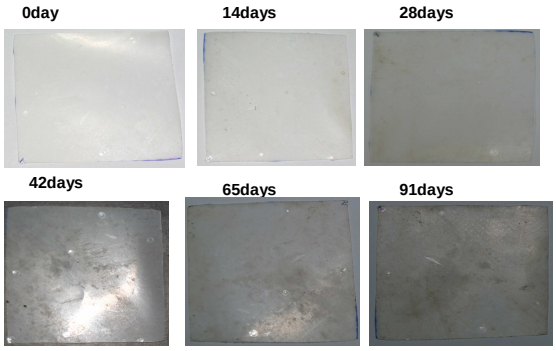

Figure 4. Degradation of pure PLA Films

Curiously, Figure 5 shows that the films of PLA with low contents of EVOH and amylopectin and with added glycerol became extremely fragile and developed biofilm layer during the composting period suggesting that the biodegradability of PLA in the blends containing EVOH, amylopectin and glycerol seemed to be enhanced. Similar results were found for the blend without glycerol (results not shown) The biodegradability of PLA has elsewhere also been found to increase considerably with the addition of a cellulosic component [33].

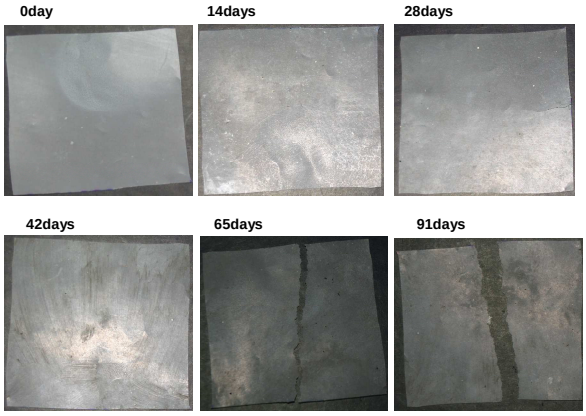

Figure 5. Degradation of pure PLA + 5% (E-29 + 65% AP + 10% gly)

In summary, the biodegradability tests indicated that while the blends did not biodegrade in the time of the evaluation, they showed better availability to do so in comparison with the neat PLA. The more favourable tendency towards biodegradability could be related to the addition of the biodegradable amylopectin component and perhaps also to the somewhat lower crystallinity of the blends [20].

Conclusions

In this study, amylopectin was melt blended with PLA by using a thermoplastic EVOH carrier with and without glycerol as plasticizer/compatibilizer. The rationale behind using EVOH as carrier is double, on the one hand, EVOH is a highly polar polymer with very high gas barrier properties and potentially good interaction with the starch component; and on the other hand the EVOH material can be melt-compounded and, therefore, could serve as a vehicle to incorporate amylopectin into PLA by melt blending. From the results, barrier properties to oxygen were only seen to improve at 0%RH. At 80%RH the blend of PLA with 5 wt.-% of (45/45/10) content showed the lowest oxygen permeability increase, due to the presence of glycerol promoting the best blend morphology, as shown by the previous work (Paper I). Despite the fact that properties were not dramatically improved, incorporating renewable resources within PLA seems to be a potentially viable route to obtain new cost effective biocomposites with good optical properties and clarity, and also with enhanced biodegradability properties.

References

1. Auras, R.; Harte, B.; Selke, S. Macromol Biosci 2004, 4, 835.
2. Fang, Q.; Hanna, M. A. Ind Crops Prod 1999, 10, 47.
3. Sarazin, P.; Li, G.; Orts, W.;Fauis, B. O. Polymer 2008, 49,

599.
4. Nijenhuis, A. J.; Colstec, E.; Czejpma, D. W.; Penning, A. J.Polymer 1996, 37, 5849.
5. Wang, L.; Ma, W.; Gzors, R. A.; Mc Carthy, S. P. Polym Degrad Stab 1998, 59, 161.
6. Ma, X. F.; Yu, J. G. Carbohyd Polym 2004, 57, 197.
7. Ritzl, A.; Regev, O.; Yerushalmi-Rozen, R. Acta Polym 1998, 49, 566.
8. Rindlav-Westling, A.; Stading, M.; Gatenholm, P. Biomacromolecules 2002, 3, 84–91.
9. Martin, O.; Averous, L. Polymer 2001, 42, 6209.
10. Lagaron, J. M.; Powell, A. K.; Bonner, G. Polym Test 2001, 20, 569.
11. Tomita, K.; Kojoh, K.; Suzuki, A. J Ferment Bioeng 1997, 84, 400.
12. Mejia, A. I.; Lopez, B. L.; Sierra, L. Mater Res Innovations 2001, 4, 148.
13. Stenhouse, P. J.; Ratto, J. A.; Schneider, N. S. J Appl Polym Sci 1997, 64, 2613.
14. Jiang, T.; et al. Eur Polym J 2005, 41, 459.
15. Jacobsen, S.; Fritz, H. G. Polym Eng Sci 1996, 36, 2799.
16. Lee, C. M.; Kim, E. S.; Yoon, J. S. J Appl Polym Sci 2005, 98, 886.
17. Orts, W. J.; et al. Polym Adv Technol 2007, 18, 629.
18. Myllarinen, P.; et al. Carbohydr Polym 2002, 48, 41.
19. Rindlav-Westling, A.; et al. Carbohydr Polym 1998, 36, 217.20. Crank, J. Second ed, Oxford Science Publications, Oxford, 1975
20. Nordqvist, D.; Dolores Sanchez, M.; Hedenqvist, M. S.; Lagaron, J. M. J Appl Polym Sci Febrero 2010, 15, 1315.
21. Crank, J. Mathematics of Diffusion, 2nd ed.; Oxford Science Publications: Oxford, 1975.
22. Hiltner, A.; Liu, R. Y. F.; Hu, Y. S.; Baer, E. J Polym Sci Part B: Polym Phys 2005, 43, 1047.
23. Yang, H. S.; Yoon, J. S.; Kim, M. N. Polym Degrad Stab 2005, 87, 131.
24. Cava, D.; Gimenez, E.; Gavara, R.; Lagaron, J. M. J Plast Films Sheeting 2006, 22, 265.
25. Rindlav-Westling, A.; Stadingb, M.; Anne-Marie, H.; Paul, G. Carbohydr Polym 1998, 36, 217.
26. Mylla¨rinen, P.; Partanen, R.; Seppa¨la, J.; Forsell, P. Carbohydr Polym 2002, 50, 355.
27. Petersen, K.; Nielsen, P. V.; Olsen, M. B. Starch 2001, 53, 356.
28. Forsell, P.; et al. Carbohydr Polym 2002, 47, 125.
29. Russo, P.; Acierno, D.; Di Maio, L.; Demma, G. Eur Polym J
1999, 35, 1261.
30. Nordqvist, et al. J Biobased Mater Bioenergy 2009, 3, 1.
31. Guralp, O.; Sebnem, K. J Appl Sci 2009, 114, 2481.
32. Ray, S. S.; Okamoto, M. Macromol Rapid Commun 2003, 24, 815.
33. Levit, M. R.; Farrel, R. E.; Gross, R. A.; McCarthy, S. P. ANTEC ’96: Plastics - Racing Into the Future 1996, 42, 1387.

6. Conclusiones

La presente tesis doctoral ha contribuido al desarrollo de nuevos biocompuestos, mediante la adición de micro y nanopartículas tales como fibras de celulosa, nanocristales de celulosa, nanotubos de carbono, nanofibras de carbono, amilopectina y nanoarcillas permitidas para contacto alimentario en matrices poliméricas de biopoliésteres y polisacáridos. La aplicación de la nanotecnología al refuerzo de biomateriales es un área de gran interés en la ciencia y tecnología de materiales de envase y recubrimiento.

De este trabajo de tesis se derivan las siguientes conclusiones:

1. En el caso de los nanobiocompuestos con nanoarcillas laminares preparados por mezclado en fundido:

   1.1. La adición de organoarcillas de tipo caolinita al PHB permitió obtener nanocompuestos con buena morfología y propiedades barrera mejoradas. La adición de organoarcillas comerciales del tipo montmorillonita condujo a una degradación acelerada del polímero y a materiales sin consistencia mecánica inadecuados para su aplicación en envases alimentarios.

   1.2. La adición del PCL al PHB condujo a un compuesto no miscible pero con buena adhesión en la interfase, redujo la excesiva rigidez e inestabilidad térmica del PHB y actúo de agente compatibilizante con las nanoarcillas.

   1.3. De manera específica los nanocompuestos con caolinita de mezclas de PHB/PCL permitieron mejorar las propiedades térmicas y consiguieron reducir el transporte de los permeantes estudiados entre un 40-70%.

2. En el caso de los nanocompuestos de PET con arcillas laminares:

   2.1. La adición de contenidos iguales o menores de un 5% en peso de una nanoarcilla apta para contacto alimentario basado en MMT permitió mejorar significativamente la barrera a oxígeno, limoneno y agua del PET.

   2.3 Sin embargo en un estudio comparativo con biopoliesteres, los nanocompuestos de PHB y de las mezclas de PHB/PCL mostraron mejor barrera a agua, componentes de aroma (limoneno) y a oxígeno que el PET puro. En cualquier caso, los nanocompuestos base arcilla de PET obtenidos mostraron la mejor barrera de todos los poliesteres estudiados.

3. En el caso de los nanobiocompuestos de PHB, PHBV y PCL con nanoarcillas laminares basadas en mica y procesados por casting:

   3.1. Se observó un aumento en la cristalinidad con el contenido de nanoarcilla y los coeficientes de permeabilidad a oxígeno, pero especialmente a agua y limoneno disminuyeron significativamente,

encontrándose un balance óptimo de propiedades para cargas de un 5% en peso para los tres biopolímeros.

3.2. Al aumentar el contenido en nanoarcilla, la transmisión de luz a través del material compuesto disminuyó hasta en un 90% en la región del UV, debido al bloqueo natural en el UV de la nanoarcilla desarrollada. Así, estos nuevos biocompuestos presentan un gran potencial para el desarrollo de envases, recubrimientos y membranas con mejores propiedades a gases y vapores y con bloqueo a la radiación UV. De los resultados de este trabajo se derivó una patente internacional.

4. En el caso de los nanobiocompuestos de carragenatos derivados de un alga recogida en la costa de Portugal con nanoarcillas laminares basadas en mica y procesadas por casting:

4.1. Se obtuvieron con éxito films de mezclas de carragenatos, zeina y nanoarcilla usando glicerol como agente plastificante. La adición de un 10% en peso de glicerol a los nanocompuestos de carragenatos permitió mejorar la dispersión de la arcilla y por tanto se obtuvieron las mejores propiedades en propiedades mecánicas, barrera, así como de bloqueo de la radiación UV.

4.2. Los nanocompuestos obtenidos presentan una cierta coloración ocre en espesores elevados pero son transparentes y con gran capacidad de bloqueo de la radiación UV, incluso en contenidos de nanoarcilla inferiores a un 5 % en peso.

4.3. La principal conclusión de este trabajo es que la adición de bajos contenidos de nanoarcilla (1 o 5 % en peso) a los carragenatos plastificados permite reducir significativamente la permeabilidad al agua (entre un 86 y 83 % respectivamente) y la sorción de ésta se reduce en más de un 90% a humedades relativas altas.

4.4. La nanoarcilla utilizada es más eficiente en aportar resistencia al agua que la zeina (prolamina) resistente a la humedad. Así, estos nuevos nanobiocompuestos basados en carragenatos presentan un gran potencial para el desarrollo de films de envases y recubrimientos para alargar la vida útil de alimentos.

5. En el caso de los nanobiocompuestos de PCL conteniendo un antimicrobiano y antioxidante natural, timol, y nanoarcillas base mica y procesados por casting se encontró, que la nanoarcilla permite, además de mejorar las propiedades físicas, incrementar la solubilidad y reducir la difusión del elemento activo. Estos nanocompuestos presentan por tanto un gran valor en la liberación controlada de agentes naturales para el desarrollo de nuevos envases activos y bioactivos.

6. - En el caso de biocompuestos de PCL, PLA y PHBV con microfibras de celulosa purificadas

6.1. Se observó una gran dispersión e interacción del refuerzo con las matrices por varias técnicas incluyendo microespectroscopia Raman confocal, para bajos contenidos de fibra. Sin embargo, para contenidos superiores a un 5% en peso se observá la aglomeración de las fibras en la matriz y la consiguiente perdida de propiedades.

6.3. En consonancia con los resultados morfológicos los biocompuestos de PLA, PCL y PHBV con microfibras de celulosa mejoraron las propiedades barrera a agua y a limoneno entre un 50-75% pero sólo para contenidos bajos de fibra.

6.4. Como resultado del trabajo, la incorporación de microfibras de celulosa alfa altamente purificada a biopoliesteres genera un importante impacto en las propiedades barrera sin la necesidad de la adición de compatibilizadores o de otros agentes interfaciales, y permite probar por primera vez que las fibras también reducen permeabilidad mas allá de mejorar las propiedades mecánicas.

7. En nanobiocompuestos basados en nanowhiskers de celulosa (CNW) y PLA

7.1. Se prepararon nanocompuestos incorporando 1, 2, 3 y 5 en peso de CNW en la matriz de celulosa procesado por casting. Los CNW se prepararon por hidrólisis ácida de la microfibra de celulosa alfa purificada, obteniendose nanofibras de 60-160 nm de longitud y de 10-20 nm de espesor.

7.2. Los resultados indican que los nanowhiskers se dispersaron bien en la matriz de PLA, sin afectar a la estabilidad térmica, pero induciendo algo de cristalinidad que muy posiblemente será transcristalinidad. CNW preparados por liofilización en los nanocompuestos exhiben mejor morfología que los preparados por intercambio del disolvente.

7.3. La permeabilidad a agua de los nanocompuestos de PLA disminuye con la adición de CNW preparados por liofilización hasta en un 82% y la permeabilidad a oxígeno se reduce hasta en un 90%. Las mejoras óptimas de las propiedades barrera se encontraron para los nanocompuestos conteniendo cargas de CNW menores del 3 % en peso, mostrando un gran potencial para la aplicación de estos CNW en recubrimientos, membranas y envases de alimentos.

8. Nanobiocompuestos basados en nanowhiskers de celulosa (CNW) y carragenatos

8.1. CNW se prepararon también por hidrólisis ácida de las microfibras de celulosa alfa purificada, obteniendose nanofibras con una longitud entre 25-50 nm y un diámetro de alrededor 5 nm. Se prepararon nanocompuestos incorporando 1, 3 y 5 % en peso de CNW en los carragenatos mediante el método de casting.

8.2. Nanobiocompuestos que contenían un 3 % en peso de CNW presentaron una reducción significativa de la permeabilidad al agua del orden del 71%, atribuido en parte a la alta reducción en la sorción de agua observada.

9. Nanobiocompuestos basados en nanotubos y nanofibras de carbono en biopolímeros (PHBV y PCL).

9.1. Se prepararon con éxito nanocompuestos de PHBV y PCL incorporando 1, 3, 5 y 10 % en peso de CNT y CNF mediante el método de casting. El mejor balance de propiedades se obtuvo con la adición de bajos contenidos de los aditivos, ya que al aumentar el contenido de estos se observo aglomeración y empeoramiento de la morfología y de las propiedades barrera.

9.2. El aumento de las propiedades barrera a agua y oxígeno, de la conductividad eléctrica y térmica así como de las propiedades mecánicas hace que estos materiales puedan tener interés en aplicaciones de envasado microhorneable o antiestático.

10. Mezclas de biomateriales: refuerzo de PLA con amilopeptina mediante mezclado en fundido

10.1 Se consiguió incorporar el componente renovable y biodegradable de alta barrera a oxígeno en seco amilopectina en una matriz de PLA mediante mezclado en fundido utilizando un grado biodegradable de EVOH como vehículo. Las mezclas presentaron una mejor dispersión de fases con la adición de glicerol.

10.2 Aunque se observó una mejora en la barrera a oxígeno en seco, en general ni las propiedades barrera, ni las propiedades mecánicas se incrementaron significativamente. Aun así se desarrolló un método de incorporación por mezclado en fundido de un polisacárido no procesable altamente biodegradable y renovable que reteniendo la transparencia del PLA mejoró la biodegradación de este.

Novel PET Nanocomposites of Interest in Food Packaging Applications and Comparative Barrier Performance with Biopolyester Nanocomposites*

M.D. Sanchez-Garcia,[1] E. Gimenez[2] and J.M. Lagaron[1,†]

[1]*Novel Materials and Nanotechnology, IATA, CSIC, Burjassot, Spain*

[2]*Area of Materials, Department of Industrial Systems Engineering and Design, University Jaume I, Castellon, Spain*

ABSTRACT: Poly(ethylene terephthalate) (PET) is one of the polymers most widely used in the packaging industry. However, it is highly desirable to enhance its barrier properties for applications, such as carbonated drinks and other rigid and flexible packaging applications. The nanocomposites route offers unique possibilities to enhance the properties of this material, provided that adequate thermally resistant and legislation complying nano-additives are used. This study presents novel PET nanocomposites with enhanced barrier properties to oxygen, water, and limonene based on a new specifically developed food-contact-complying highly swollen montmorillonite grade, and, furthermore, presents and discusses morphological data. Moreover, given the current interest in the packaging industry to replace this material by other biopolyesters, a comparative barrier performance of PET nanocomposites versus that of biopolymers, such as poly(lactic acid) (PLA), polyhydroxyalkanoates (PHB, PHBV), and polycaprolactones (PCL) and their corresponding nanocomposites is also reported.

KEY WORDS: PET, food packaging, composites, barrier properties, biopolyesters.

*This is an expansion of a paper presented at the Society of Plastics Engineers' *ANTEC 2007* conference held in Cincinnati, USA on May 6–10, 2007. Copyright SPE.

†Author to whom correspondence should be addressed. E-mail: lagaron@iata.csic.es

Figure 3 appears in color on line: http://jpf.sagepub.com

8756-0879/07/02 0133–16 $10.00/0 DOI: 10.1177/8756087907083590

Morphology and Barrier Properties of Nanobiocomposites of Poly(3-hydroxybutyrate) and Layered Silicates

M. D. Sanchez-Garcia,[1] E. Gimenez,[2] J. M. Lagaron[1]

[1]*Novel Materials and Nanotechnology, IATA, CSIC, Apdo Correos 73, Burjassot 46100, Spain*
[2]*Area of Materials, Department of Industrial Systems Engineering and Design, University Jaume I, Castellô 12071, Spain*

Received 28 May 2007; accepted 2 October 2007
DOI 10.1002/app.27622
Published online 25 February 2008 in Wiley InterScience (www.interscience.wiley.com).

ABSTRACT: Polyhydroxybutyrate (PHB) is generally considered to be a very uneasy biopolymer to handle because of significant instability during melt processing and some excessive brittleness. This work studied the morphological, thermal, and barrier properties of novel melt-mixed nanobiocomposites of PHB, poly(ε-caprolactones) (PCL), and layered phyllosilicates based on commercial organomodified kaolinite and montmorillonite clay additives. The addition of PCL component to the blend was seen to reduce oxygen permeability but it was also found to lead to a finer dispersion of the clay. The addition of highly intergallery swollen organomodified montmorillonite clays to the PHB blend led to a highly dispersed morphology of the filler, but this simultaneously increased to a significant extend the melt instability of the biopolymer. Nevertheless, the organomodified kaolinite clay, despite the fact that it was found to both lead to less dispersed and irregular morphology, particularly for higher clay loadings, it led to enhanced barrier properties to oxygen, D-limonene, and water. D-limonene and specially water molecules were, however, found to sorb in both hydrophobic and hydrophilic sites of the filler, respectively, hence diminishing the positive barrier effect of an enlarged tortuosity factor in the permeability. Mass transport properties were found to depend on the type of penetrant and modeling of the permeability data to most commonly applied formalisms was not found to be satisfactory because of factors such as morphological alterations, heterogeneity in the clay dispersion, and penetrant solubility in the filler.
 J Appl Polym Sci 108: 2787–2801, 2008

Key words: biopolymers; packaging applications; barrier properties; nanocomposites; polyhydroxybutyrate

INTRODUCTION

In the last decades, there has been a significant increase in the amount of plastics being used in packaging applications. In fact, the largest application for plastics today is packaging, and within the packaging niche, food packaging amounts has the largest plastics demanding application. This substantial increase in use has also raised a number of environmental concerns from a waste management point of view.[1–3] As a result, there is a strong research interest, pushed by authorities at national and international levels, and a parallel industrial growing demand in the development and use of materials which can disintegrate and biodegrade through processes such as composting into carbon dioxide and water.

Correspondence to: J. M. Lagaron (lagaron@iata.csic.es).
Contract grant sponsor: EU integrated project SUSTAINPACK.
Contract grant sponsor: CYCIT project; contract grant numbers: MAT2006-10261-C03-01, MAT2003-08480-C3.

Journal of Applied Polymer Science, Vol. 108, 2787–2801 (2008)

Among biodegradable materials, three families[1–4] are usually considered: polymers directly extracted from biomass such as the polysaccharides starch, chitosan, and cellulose and proteins such as gluten, soy protein, and zein. A second family comprises oil based monomers or biomass derived monomers, but uses classical chemical synthetic routes to obtain the final biodegradable material, this is the case of for instance poly(ε-caprolactones) (PCL), polyvinyl-alcohol (PVOH) and for the case of sustainable monomers polylactic acid (PLA). The third family comprises polymers produced by natural or genetically modified microorganisms such as polyhydroxylalcanoates and polypeptides.[5]

Recently, surface modified clays have been studied as advanced additives to improve or balance thermal, mechanical, fire resistance, surface, or conductivity properties of nanocomposites because of its high surface to volume ratios and the subsequent intimate contact that they promote with the matrix at low filler additions.[5] Aside from the enhancement in these properties, these clay platelets with very few nanometers (ideally one nanometer in fully exfoliated systems) in thickness have the potential to uniquely reduce the matrix permeability to gases and vapors,

Available online at www.sciencedirect.com
ScienceDirect
Carbohydrate Polymers 71 (2008) 235–244
Carbohydrate Polymers
www.elsevier.com/locate/carbpol

Morphology and barrier properties of solvent cast composites of thermoplastic biopolymers and purified cellulose fibers

M.D. Sanchez-Garcia [a], E. Gimenez [b], J.M. Lagaron [a,*]

[a] Novel Materials and Nanotechnology, IATA, CSIC, Apdo. Correos 73, 46100 Burjassot, Spain
[b] Area of Materials, Department of Industrial Systems Engineering and Design, University Jaume I, 12071 Castellón, Spain

Received 12 March 2007; received in revised form 23 May 2007; accepted 24 May 2007
Available online 12 June 2007

Abstract

This paper shows and discusses the morphology, thermal and transport properties of solvent cast biocomposites of poly(lactic acid) (PLA), polyhydroxybutyrate-co-valerate (PHBV) and polycaprolactones (PCL) containing purified alfa micro-cellulose fibers as a function of filler content. The SEM, optical microscopy and Raman imaging results indicate that a good dispersion of the fibers in the matrix was achieved for the three biopolymers. However, detrimental fiber agglomeration was clearly observed to take place for samples with fiber contents in excess of 5 wt%. The heat of fusion (related to crystallinity) of the semicrystalline PCL and PHBV biopolymers was seen to decrease, particularly in low fiber content biocomposites, but it seemed to increase slightly in the highly amorphous PLA biocomposites. In accordance with the morphology data, water and D-limonene direct permeability were seen to decrease to a significant extent in the biocomposites with low fiber contents. The permeability reduction was mostly related to a decrease in diffusivity but solubility was also found to be favorable. The main conclusion from this work is that purified cellulose fibers can also be used to enhance the barrier properties of thermoplastic biopolyesters of interest in, for instance, packaging and membrane applications.

Keywords: Cellulose fibers; Composites; Barrier properties; PLA; PCL and PHBV

1. Introduction

There is a growing worldwide interest pushed by governments and societies to increment the responsible use of renewable resources in commodity plastic products in order to reduce the waste associated to their use, particularly in packaging applications (Petersen et al., 1999; Haugaard et al., 2001). The use of biodegradable plastics and resources are seen as one of the many strategies to minimise the environmental impact of petroleum-based plastics. The biological base of these new biopolymers provides a unique opportunity to incorporate a highly demanded property of these materials, i.e. the compostability. It must be considered that among the plastic waste there are products with a high degree of contamination and recycling requires a high energy cost. Therefore, compostability is a very interesting property that guarantees that these new biomaterials will degrade mostly into carbon dioxide and water after disposal (Kijchavengkul, Auras, Rubino, Ngouajio, & Fernandez, 2006). These biodegradable materials present a number of excellent and promising properties in a number of applications, including packaging, automotive and biomedical sectors. Thus, thermoplastic biodegradable polymers, such as poly(lactic acid) (PLA), polyhydroxyalkanoate (PHA) and polycaprolactones (PCL), exhibit an excellent equilibrium of properties, i.e. they are processable using conventional plastics machinery and, for the case of the first two, they arise from renewable resources. PLA is a thermoplastic biopolyester produced from L-lactid acid, which typically comes from the fermentation of corn starch. Currently, PLA is being commercialized and being used as a food packaging polymer for short shelf-life products with common applications such as containers,

* Corresponding author.
E-mail address: lagaron@iata.csic.es (J.M. Lagaron).

0144-8617/$ - see front matter © 2007 Elsevier Ltd. All rights reserved.
doi:10.1016/j.carbpol.2007.05.041

Novel Polycaprolactone Nanocomposites Containing Thymol of Interest in Antimicrobial Film and Coating Applications*

M.D. Sanchez-Garcia,[1] M.J. Ocio,[1,2] E. Gimenez[3] and J.M. Lagaron[1,†]

[1]*Novel Materials and Nanotechnology Lab., IATA, CSIC Apdo Correos 73, 46100 Burjassot, Spain*

[2]*Departmento Medicina Preventiva, Faculty of Pharmacy, University of Valencia, 46100 Burjassot, Spain*

[3]*Area of Materials, Department of Industrial Systems Engineering and Design, University Jaume I, 12071 Castelló, Spain*

ABSTRACT: It is well-known that the nanocomposites technology can significantly enhance, among others, the thermal, mechanical, and barrier properties of plastics. It is also known that most bioplastics, including the thermoplastic biopolymers, have lower than desired levels for certain properties which makes their use in certain packaging applications problematic. The combination of active technologies such as antimicrobials and nanotechnologies such as nanocomposites can synergistically lead to bioplastic formulations with balanced properties and functionalities for their implementation in packaging applications. The present work presents the development and characterization of novel nanocomposites of polycaprolactone with enhanced barrier properties and with controlled-release of the biocide natural extract thymol. The antimicrobial nanocomposites of biodegradable materials were prepared in solution by a casting method. The morphology of the biocomposites was visualized by transmission electron microscopy and by atomic force microscopy, the thermal properties were investigated by differential scanning calorimetry and the relative uptake (solubility) and kinetics (diffusion) of the released biocide were determined by Attenuated Total Reflection Fourier Transformed Infrared spectroscopy. Water, oxygen, and limonene barrier properties were also enhanced in the biocomposites.

*This is an expansion of a paper presented at ANTEC 2008, the annual technical meeting of the Society of Plastics Engineers, held in Milwaukee, Wisconsin on 4–8 May 2008.

†Author to whom all correspondence should be addressed. E-mail: lagaron@iata.csic.es

Figure 1 appears in color online: http://jpf.sagepub.com

8756-0879/08/3-4 0239–13 $10.00/0 DOI: 10.1177/8756087908101539

Los Angeles, London, New Delhi and Singapore

Effects of Ionizing Radiation in Ethylene-Vinyl Alcohol Copolymers and in Composites Containing Microfibrillated Cellulose

Avelina Fernández,[1] M. Dolores Sánchez,[1] Mikael Ankerfors,[2] Jose M. Lagaron[1]

[1]*Institute of Agrochemistry and Food Technology (IATA), CSIC, 46100 Burjassot, Valencia, Spain*
[2]*STFI-Packforsk AB, Box 5604, SE-114 86 Stockholm, Sweden*

Received 24 August 2007; accepted 30 October 2007
DOI 10.1002/app.27709
Published online 20 March 2008 in Wiley InterScience (www.interscience.wiley.com).

ABSTRACT: This study reports on the effect of gamma radiation on morphological, thermal, and water barrier properties of pure ethylene vinyl alcohol copolymers (EVOH29 and EVOH44) and its biocomposites with the nanofiller microfibrillated cellulose (2 wt %). Added microfibrillated cellulose (MFC) preserved the transparency of EVOH films but led to a decrease in water barrier properties. Gamma irradiation at low (30 kGy) and high doses (60 kGy) caused some irreversible changes in the phase morphology of EVOH29 and EVOH44 copolymers that could be associated to crosslinking and other chemical alterations. Additionally, the EVOH copolymers and the EVOH composites reduced the number of hygroscopic hydroxyl functionalities during the irradiation processing and novel carbonyl based chemistry was, in turn, detected. As a result of the above alterations, the water barrier properties of both neat materials and composites irradiated at low doses were notably enhanced, counteracting the detrimental effect on water barrier of adding MFC to the EVOH matrix. © 2008 Wiley Periodicals, Inc. J Appl Polym Sci 109: 126–134, 2008

Key words: EVOH; EVOH composites; irradiation; water barrier; microfibrillated cellulose

INTRODUCTION

Ethylene vinyl alcohol copolymers (EVOH) are random semicrystalline materials with excellent barrier properties to gases and food aroma compounds. They are produced via saponification of ethylene-*co*-vinyl acetate copolymers where the acetoxy group is converted into a secondary alcohol. These materials are increasingly used in the food packaging industry, especially in multilayer packaging. However, barrier and mechanical properties of EVOH suffer from water contact due to water uptake and the associated swelling ratio.[1] EVOH crystallinity and performances have been conveniently enhanced by adding, for example, low amounts of organoclays.[2,3] Microfibrillated cellulose (MFC) from wood pulp is a reinforcing filler with excellent potential to be used in polymer composites. The MFC material consists of long nanoscale bundles of microfibrills, which form entangled networks. MFC is normally prepared by the delamination of delignified wood fibers in high-pressure homogenizers; the diameter of the MFC from Scandinavian softwood pulp is ~ 17–30 nm.[4] This filler is being currently studied to increase the amount of sustainable components in the formulation of plastics, and to provide additional benefits related to the mechanical and barrier properties of the films. Thus, MFC has been reported to have an acceptably high aspect ratio and, in general, the composites with cellulose derived materials have been observed to improve the mechanical properties of polymer films.[4–7] However, its hydrophilic nature may diminish the composites performances in contact with moisture, and therefore have to be carefully investigated.

Gamma irradiation is not only used for material sterilization but also to improve the properties of polymers and in aseptic packaging technologies.[8] Typical effects of irradiation in polymers are chain scission associated to the formation of free radicals and low molecular weight radiolysis compounds, and finally crosslinking[9]. Changes in permeation and mechanical properties due to crosslinking might improve the performances of plastics for instance storage of packaged food at low doses,[10,11] and usually mechanical properties are only affected by high radiation doses.[11] The formation of free radicals and low-molecular-weight compounds might generate undesirable off-flavors or discolorations in the plastics, which could impair the use of this treatment during processing of packaged foods.

Correspondence to: J. M. Lagaron (lagaron@iata.csic.es).
Contract grant sponsor: CYCIT project; contract grant number: MAT2003-08,480-C3.
Contract grant sponsor: EU integrated project SUSTAINPACK.
Contract grant sponsor: MEC; contract grant number: MAT2006-10261-C03.

Journal of Applied Polymer Science, Vol. 109, 126–134 (2008)

Composites Science and Technology 70 (2010) 1095–1105

Contents lists available at ScienceDirect

Composites Science and Technology

journal homepage: www.elsevier.com/locate/compscitech

Effect of addition of carbon nanofibers and carbon nanotubes on properties of thermoplastic biopolymers

M.D. Sanchez-Garcia [a], J.M. Lagaron [a], S.V. Hoa [b,*]

[a] Novel Materials and Nanotechnology Group, IATA, CSIC, Apdo. Correos 73, 46100 Burjassot, Spain
[b] Concordia Centre for Composites, Department of Mechanical and Industrial Engineering, Concordia University, Montreal, Quebec, Canada H3G 1M8

ARTICLE INFO

Article history:
Received 24 July 2009
Received in revised form 10 February 2010
Accepted 16 February 2010
Available online 20 February 2010

Keywords:
A. Carbon nanotubes
Carbon nanofibers
A. Nanocomposites
Biodegradable polymers
Barrier properties

ABSTRACT

This paper presents the properties of nano-bio-composites of solvent cast polyhydroxybutyrate-co-valerate (PHBV) and polycaprolactone (PCL) containing carbon nanofiber or carbon nanotubes as a function of filler content. It is found that carbon nanotubes and nanofibers can be used to enhance the conductivity, thermal, mechanical and to enhance gas barrier properties of thermoplastic biopolyesters.

1. Introduction

Biodegradable polymers have received considerable attention due to their potential application in fields related to environmental protection and ecology in the last two decades. Most biodegradable polymers have excellent properties comparable to many petroleum-based plastics. They possess a number of excellent and promising properties that can be used in a number of applications, including packaging, automotive and biomedical sectors. Thermoplastic biodegradable polymers, such as polyhydroxyalkanoate (PHA) and polycaprolactones (PCL), are processable using conventional plastics machinery. For the polyhydroxyalkanoates (PHAs) family, the most widely used material is the polyhydroxybutyrate (PHB) and its copolymers with valerate. These microbial biopolymers are storage materials produced by a variety of bacteria in response to particular environmental stresses [1]. Polyhydroxybutyrate (PHB) is a naturally occurring b-hydroxyacid (a linear polyester). The homopolymer, poly(hydroxybutyrate) PHB, and its copolymer with hydroxyvalerate, PHBV, are biodegradable engineering thermoplastic polymers with important properties that make them suitable for many applications for which petroleum-based synthetic polymers are currently used. PHB polymers are already used in small disposable products and in packaging materials [2]. PCL is a thermoplastic biodegradable polyester synthesized by chemical conversion of crude oil. PCL has good water, oil, solvent, and chlorine resistance, low melting point, low viscosity, and is easily processed using conventional melt blending technologies [3]. PCL is being investigated for use in biomedical utensils, pharmaceutical controlled release systems, and in biodegradable packaging [4].

Biodegradable polymers have strong commercial potential for bio-plastics. However, they exhibit low toughness, low heat distortion temperature, relatively high gas permeability compared to oil based polyesters such as PET, low melt viscosity, low thermal and electrical conductivity. These shortcomings restrict their use. Reinforcement of these materials using nanoparticles may be an effective way to improve these properties [5–7].

There are research studies showing property improvements in biodegradable materials with the addition of carbon nanotubes. Reinforcement of PCL with carbon nanotubes has been carried out with the overall aim of increasing its biodegradation rate and to enhance mechanical properties, i.e. this route led to considerable improvements in the composites tensile strength [8]. Other authors reported that the addition of small amount of MWCNT into PCL matrix can improve its thermal stability, and the loading of MWCNT into PCL matrix induced heterogeneous nucleation during crystallization processes as studied by DSC [9]. Saeed and Park reported that the conductivity of the nanocomposite of PCL increases with the increase of CNT content [10]. Lai et al. found that addition of carbon nanotubes into PHBV enhanced its thermal stability studied by TGA. The thermal properties and the crystallization behaviour of the composites were characterized by differential

* Corresponding author. Tel.: +1 514 848 2424; fax: +1 514 848 3175.
E-mail address: hoasuon@vax2.concordia.ca (S.V. Hoa).

0266-3538/$ - see front matter © 2010 Elsevier Ltd. All rights reserved.
doi:10.1016/j.compscitech.2010.02.015

Incorporating Amylopectin in Poly(lactic Acid) by Melt Blending Using Poly(ethylene-*co*-vinyl Alcohol) as a Thermoplastic Carrier. (I) Morphological Characterization

D. Nordqvist,[1] Maria D. Sanchez-García,[2] Mikael S. Hedenqvist,[1] Jose M. Lagaron[2]

[1]*Department of Fiber and Polymer Technology, Royal Institute of Technology, Stockholm, Sweden*
[2]*Novel Materials and Nanotechnology Lab, Institute of Agrochemistry and Food Technology (IATA), CSIC, Burjassot, Valencia, Spain*

Received 18 November 2008; accepted 11 February 2009
DOI 10.1002/app.31290
Published online 7 October 2009 in Wiley InterScience (www.interscience.wiley.com).

ABSTRACT: In this study, the possibility of using a biodegradable grade of thermoplastic poly(ethylene-*co*-vinyl alcohol) with high (71 mol %) vinyl alcohol (EVOH-29), as a carrier to incorporate the renewable and biodegradable component amylopectin (AP) into poly(lactic acid) (PLA) through melt blending, was investigated. The effect of using a plasticizer/compatibilizer (glycerol) in the blend systems was also investigated. In a first step, the EVOH/AP blends were produced and thereafter, in a second step, these were mixed with PLA. In this first study, the blend morphology was investigated using optical microscopy, scanning electron microscopy and Raman imaging spectroscopy and the thermal properties were measured by differential scanning calorimetry. Despite the fact that EVOH and AP are both highly polar, their blends were immiscible. Still, the blends exhibited an excellent phase dispersion on a micron level, which was enhanced further by the addition of glycerol. A good phase dispersion was finally observed by incorporation of the latter blends in the PLA matrix, suggesting that the proposed blending route can be successfully applied for these systems. Finally, the Differential scanning calorimetry (DSC) data showed that the melting point of EVOH dropped in the EVOH/AP blends, but the properties of the PLA phase was still relatively unaffected as a result of blending with the above components. © 2009 Wiley Periodicals, Inc. J Appl Polym Sci 115: 1315–1324, 2010

Key words: polymer blends; biopolymers; EVOH copolymers; amylopeptine; PLA; packaging applications; biomedical applications; morphology; raman imaging

INTRODUCTION

Poly(lactic acid) (PLA) is a biodegradable linear aliphatic thermoplastic polyester that has received significant attention among researchers as an alternative material for packaging applications. Today, PLA is one of the most important biodegradable/renewable plastic materials on the market; to a great extent due to its interesting mechanical, optical, and processing properties, and, of course, to its renewability and biodegradability aspects.[1,2] In attempt to improve desired properties or lower the processing costs both blends and composites have been produced. Several studies have been carried out on PLA blends, both with non-biodegradable and biodegradable materials.[3–6] By blending PLA with other, less expensive, biodegradable polymers, the "green" factor can be retained at the same time as properties are improved and cost lowered. A possible candidate is starch, due to its biobased origin, low price, good availability, and high performance. Starch consists of a mixture of amylose (~30%) and amylopectin (AP) (70%), both based on chains of 1,4-linked α-D-glucose.[7] Amylose is linear whereas AP is highly branched and forms transparent films, a very attractive feature when it comes to the packaging industry.[8] Martin and Averous[9] previously studied melt-blended PLA/starch systems. The observation of two glass transition temperatures (T_g), and a two-phase morphology, indicated a low compatibility between the two polymers. The use of adequate compatibilizers was, therefore, suggested.

Poly(ethylene-*co*-vinyl alcohol) (EVOH) polymers are a family of semicrystalline random co-polymers with excellent barrier properties to gases and hydrocarbons, and with outstanding chemical resistance.[10] EVOH copolymers are commonly produced via a saponification reaction of a parent ethylene-*co*-vinyl acetate copolymer, whereby the acetoxy group is converted into a secondary alcohol. These materials have been, increasingly, implemented in many pipe and packaging applications where high demands on chemical resistance and gas, aroma, and hydrocarbon

Correspondence to: J. M. Lagaron (lagaron@iata.csic.es).

Journal of Applied Polymer Science, Vol. 115, 1315–1324 (2010)

Incorporating Amylopectin in Poly(lactic acid) by Melt Blending Using Poly(ethylene-*co*-vinyl alcohol) as a Thermoplastic Carrier. II. Physical Properties

M. D. Sanchez-Garcia,[1] D. Nordqvist,[2] M. Hedenqvist,[2] J. M. Lagaron[1]

[1]*Novel Materials and Nanotechnology Group, IATA-CSIC, Apdo Correos 73, Burjassot 46100, Spain*
[2]*Royal Institute of Technology, Department of Fibre and Polymer Technology, Stockholm SE-100 44, Sweden*

Received 30 October 2009; accepted 25 May 2010
DOI 10.1002/app.32891
Published online 6 October 2010 in Wiley Online Library (wileyonlinelibrary.com).

ABSTRACT: This study adds to a previous morphological work (paper I) with further characterization of the developed poly(lactic acid) (PLA) blends containing amylopectin, which made use of an ethylene-vinyl alcohol copolymer (EVOH) as a melt-compoundable carrier for the polysaccharide in the biopolyester. The effect of using glycerol as compatibilizer was also characterized. Water and oxygen transport parameters, mechanical properties, and comparative biodegradability tests were evaluated for the blends. From the results, the barrier properties to oxygen were only seen to improve at 0%RH and mostly for the PLA-EVOH blends, which furthermore showed a positive deviation from the rule of mixtures. At high relative humidity, the blends showed somewhat poorer barrier performance due to the comparatively higher improvement in barrier of the neat PLA at 80% RH. Interestingly, room temperature biodegradability testing suggested that low additions of the blending elements seemed to facilitate the biodegradability of the biopolyester. Despite the fact that properties were not so dramatically improved, incorporating renewable resources within PLA seems as a potentially viable route to reduce PLA supply dependency, retain good optical properties and to overcome some drawbacks associated to the use of this biopolyester.
 J Appl Polym Sci 119: 3708–3716, 2011

Key words: polylactic acid; renewable resources; packaging; bioplastis; amylopeptine

INTRODUCTION

Poly (lactic acid) (PLA) is today one of the most important renewable/biodegradable plastic materials. Hence, this linear aliphatic thermoplastic polyester is receiving a lot of attention from researchers all over the world as an alternative material for packaging applications. Besides being renewable and biodegradable, its transparency, mechanical properties, and processability make PLA an attractive and interesting material from an application point of view.[1,2] A problem with PLA is, as with many other environmentally friendly materials, the fact that the biopolymer and processing costs are too high compared to its petroleum-based polymers. The properties of this biodegradable polymer are still considered to be insufficient for some applications and demand continuous efforts to exceed production capacity. Therefore, several studies have been carried out where PLA has been mixed with other biodegradable and nonbiodegradable materials.[3–6] By choosing a less expensive, biodegradable polymer as blending material for PLA the production costs and inaccessibility could be potentially lowered at the same time as the "eco" factor is retained.

Several materials can be considered as a blending component for PLA. The low price, good availability, and performance along with its biobased origin make starch an attractive and promising candidate for renewable applications. Starch consists of a mixture of amylose (~ 30%) and amylopectin (~ 70%), both based on chains of 1,4-linked α-D-glucose.[7] Amylose is linear, whereas amylopectin (AP) is highly branched and forms transparent films, a very attractive feature when it comes to the packaging area.[8] Martin and Averous[9] previously studied melt-blended PLA/starch systems. The results showed a relatively low level of compatibility between the two systems, reported after observation of two glass transition temperatures (T_g). Also their SEM studies indicated a low degree of compatibility and the use of adequate compatibilizers was suggested as the right way forward.

Ethylene-vinyl alcohol (EVOH) copolymers are a family of semicrystalline materials with excellent barrier properties to gases and hydrocarbons (in drier conditions), and with outstanding chemical resistance.[10] These materials have been increasingly implemented in many pipe and packaging applications where stringent criteria in terms of chemical resistance and gas, water, aroma, and hydrocarbon

Correspondence to: J. M. Lagaron (lagaron@iata.csic.es).

Journal of Applied Polymer Science, Vol. 119, 3708–3716 (2011)

Novel Clay-Based Nanobiocomposites of Biopolyesters with Synergistic Barrier to UV Light, Gas, and Vapour

M. D. Sanchez-Garcia, J. M. Lagaron

Novel Materials and Nanotechnology Lab., IATA, CSIC, Burjassot 46100, Spain

Received 6 August 2009; accepted 16 December 2009
DOI 10.1002/app.31986
Published online 19 May 2010 in Wiley InterScience (www.interscience.wiley.com).

ABSTRACT: This article presents novel solvent cast biocomposites of poly(lactic acid) (PLA), polyhydroxybutyrate-*co*-valerate (PHBV), and polycaprolactone (PCL) with enhanced barrier properties to UV light, oxygen, water, and limonene by means of incorporating an organomodified mica-based clay grade. The TEM results suggested a good clay dispersion but with no exfoliation in the three biopolyesters. In agreement with the crystallinity data, which was found to generally increase with increasing filler content, oxygen but specially water and D-limonene permeability coefficients were seen to decrease to a significant extent in the biocomposites and an optimum property balance was found for 5 wt % of clay loading in the three biopolymers. With increasing clay content, the light transmission of these biodegradable biocomposites decreased by up to 90% in the UV wavelength region due to the specific UV blocking nature of the clay used. As a result, these new biocomposites can have significant potential to develop packaging films, coatings and membranes with enhanced gas and vapor barrier properties and UV blocking performance.
 J Appl Polym Sci 118: 188–199, 2010

Key words: clay-based composites; packaging; barrier properties; biopolyesters

INTRODUCTION

Protection against light is a basic requirement to preserve the quality of many products, such as packaged foods. Metal and paper being opaque to the transmission of light, automatically provide this function. On the other hand, plastic films are often transparent materials to UV and Visible radiation of short wavelengths. Therefore, the protection of light sensitive goods, such as fruit and vegetable juices, vitamin and sport drinks, dairy products, and edible oils from UV-radiation when packaged in plastic containers has been widely investigated.[1–3]

The primary wavelengths of interest in, for instance, food packaging applications are those that fall between 200 and 2200 nm. This section of the electromagnetic spectrum can be divided into three components: the ultraviolet (UV) range (100–400 nm); the visible spectrum (400–700 nm); and the near-infrared range (700–2200 nm). Ultraviolet radiation accounts for only 3% of the total radiation that reaches earth, but it causes chemical reactions, weathering of polymers, fading of certain coloring, and even eye and skin damage. For this reason, UV light blocking is a very demanded property in polymers and also in the newcoming renewable and biodegradable polymers of interest in multisectorial applications.

Biodegradable and/or sustainable materials present a number of excellent properties for a number of applications, including packaging, automotive, and biomedical fields. Thermoplastic biopolymers, such as poly(lactic acid) (PLA), polyhydroxyalkanoates (PHA), and polycaprolactones (PCL), exhibit an excellent balance between barrier and mechanical properties, are water resistant and can be processed using conventional plastics machinery. Moreover, for the case of the first two, they originate from renewable resources, i.e., maize and microorganisms, respectively. Composites of biopolymers, often called nanobiocomposites, containing highly dispersed naturally derived layered additives, typically montmorillonite (MMT), are proving to be an excellent technology to design new materials with enhanced key properties while retaining the "bio" characteristics. Nanocomposites of biodegradable materials containing between 1 and 5 wt % of MMT have been claimed to exhibit significant improvements in barrier[4–9] and in mechanical properties[10,11]

Correspondence to: J. M. Lagaron (lagaron@iata.csic.es).
Contract grant sponsor: Spanish MEC project; contract grant number: MAT2006-10261-C03.
Contract grant sponsor: Spanish CONSOLIDER project FUN-C-FOOD; contract grant number: CSD2007-00063.
Contract grant sponsor: FPI program (GV associated to the MEC project); contract grant number: MAT2003-08480-C3.
Contract grant sponsor: NanoBioMatters S.L. (Paterna, Spain).

Journal of Applied Polymer Science, Vol. 118, 188–199 (2010)

JOURNAL OF AGRICULTURAL AND FOOD CHEMISTRY
ARTICLE

J. Agric. Food Chem. XXXX, XXX, 000–000 A
DOI:10.1021/jf1007659

Nanobiocomposites of Carrageenan, Zein, and Mica of Interest in Food Packaging and Coating Applications

MARIA D. SANCHEZ-GARCIA,[†] LOIC HILLIOU,[‡,§] AND JOSE M. LAGARON*,[†]

[†]Novel Materials and Nanotechnology Group, Instituto de Agroquímica y Tecnología de Alimentos (IATA), Consejo Superior de Investigaciones Científicas (CSIC), Av. Agustin Escardino 7, 46980 Paterna, Spain, [‡]Institute for Nanostructures, Nanomodelling and Nanofabrication (I3N), University of Minho, 4800-048 Guimaraes, Portugal, and [§]REQUIMTE, Faculty of Engineering, University of Porto, Rua Dr. Roberto Frias s/n, 4200-465 Porto, Portugal

The present study presents the development and characterization of biocomposites of a red-algae-derived carrageenan, mica, and their blends with zein prolamine obtained by solvent casting. The morphology of the blends was characterized by scanning and transmission electron microscopy (SEM and TEM), optical microscopy, and atomic force microscopy (AFM). Mechanical behavior, water barrier, water uptake, and UV−vis protection of the cast films were also investigated. The results indicated that the addition of 10 wt % glycerol to the blends resulted in a better dispersion of the additive and, for that reason, a better improvement for the studied properties. The composites were seen colored but transparent and exhibited the ability to block the UV−vis radiation because of the characteristic absorbing properties of the filler. Nevertheless, the main conclusion from the work is that the nanocomposites were seen to act as a reinforcing plasticizer and also led to significantly reduced water permeability and uptake. The clay was found to be more efficient in the latter aspect than the zein prolamine as an additive. As a result, these novel carragenan-based biocomposites can have significant potential to develop packaging films and coatings for shelf-life extension of food products.

KEYWORDS: Carrageenan; food hydrocolloids; nanocomposites; packaging; coatings

1. INTRODUCTION

Biopolymer films have been the focus of worldwide attention for the past few decades because they offer favorable environmental advantages in terms of sustainability and compostability compared to conventional synthetic polymeric films. Edible and biodegradable natural polymer films offer alternative packaging with lower environmental costs. The search for new renewable resources for the production of edible and biodegradable packaging materials and coatings has steadily increased in recent years. In particular, nonconventional sources of carbohydrates have been extensively studied. There are various unique carbohydrates that are found in marine organisms that represent a largely unexplored source of valuable materials. These nonconventional and underexploited renewable materials can be used as an interesting alternative to produce edible films and coatings.

The biopolymers studied in this work to produce edible films and coatings were κ/ι-hybrid carrageenan extracted from *Mastocarpus stellatus*, an underexploited red algae present in the Portuguese marine coast (*1*−*4*). Carrageenans are water-soluble polymers with a linear chain of partially sulfated galactans, which present high potentiality as film-forming material. Carrageenans are structural polysaccharides from red seaweed and have been used extensively in foods, cosmetics, and pharmaceuticals (*5*). Carrageenan biopolymer extracted from *M. stellatus* seaweeds was shown to be a κ/ι-hybrid carrageenan (*1*) with gel properties comparable to commercial κ-carrageenan gel formers (*2*, *3*). The use of carrageenan as edible films and coatings is already used in the food industry on fresh and frozen meat, poultry, and fish to prevent superficial dehydration (*6*), ham or sausage casings (*7*), granulation-coated powders, dry solid foods, oily foods (*8*), etc. but also to manufacture soft capsules (*9*, *10*) and, especially, nongelatin capsules (*11*). Polysaccharide and protein film materials are characterized by high moisture permeability, low oxygen and lipid permeability at lower relative humidities, and compromised barrier and mechanical properties at high relative humidities (*12*).

To tailor the properties and improve the water resistance of these biopolymers, it is often desirable to combine with, for instance, other biopolymers more resistant to water or with the addition of nanoclays. In the case of the addition of nanoclays, these layers are known to form impermeable shields. As a consequence, it is expected that the nanocomposite carbohydrate film will have substantially reduced water vapor permeability, thus helping to solve one of the long-standing drawbacks in the use of biopolymer films, i.e., water plasticization (*13*). Indeed, Lagaron et al. (*13*) showed that the dispersion of mica nanoclay layers into the biopolymer matrix greatly improved the overall water barrier without measurable impact in the biodegradability of the matrix, thus turning them into industrially attractive

*To whom correspondence should be addressed. E-mail: lagaron@iata.csic.es.

JOURNAL OF AGRICULTURAL AND FOOD CHEMISTRY
ARTICLE

J. Agric. Food Chem. **2010,** *58,* 12847–12857 **12847**
DOI:10.1021/jf102764e

Morphology and Water Barrier Properties of Nanobiocomposites of κ/ι-Hybrid Carrageenan and Cellulose Nanowhiskers

MARIA DOLORES SÁNCHEZ-GARCÍA,[†] LOIC HILLIOU,[§,#] AND JOSÉ MARÍA LAGARÓN*[,†]

[†]Novel Materials and Nanotechnology Group, IATA, CSIC, Apartado Correos 73, 46100 Burjassot, Spain, [§]Institute for Polymers and Composites/I3N, University of Minho, Campus de Azurém, 4800-058 Guimarães, Portugal, and [#]REQUIMTE-Faculty of Engineering, University of Porto, Rua Dr. Roberto Frias s/n, 4200-465 Porto, Portugal

The current study presents the development and characterization of novel carrageenan nanobiocomposites showing enhanced water barrier due to incorporation of cellulose nanowhiskers (CNW). CNW, prepared by acid hydrolysis of highly purified α cellulose microfibers, were seen to have a length of around 25−50 nm and a cross section of ca. 5 nm when dispersed in the matrix. The nanobiocomposites were prepared by incorporating 1, 3, and 5 wt % of the CNW into a carrageenan matrix using a solution casting method. Morphological data (TEM and optical microscopy) of the nanocomposites containing CNW were compared with the morphology of the corresponding biocomposites containing the original cellulose microfibers and the differences discussed. Thermal stability by TGA, water vapor permeability, and percent water uptake were also determined. The main conclusion arising from the analysis of the results is that the nanobiocomposites containing 3 wt % of CNW exhibited the lowest reduction in water vapor permeability, that is, ca. 71%, and that this reduction was largely attributed to a filler-induced water solubility reduction. This fully biobased nanoreinforced carrageenan can open new opportunities for the application of this biopolymer in food-packaging and -coating applications.

KEYWORDS: Carrageenan; food packaging; food coating; biocomposites; cellulose

INTRODUCTION

Biopolymer films have been the focus of worldwide attention for the past few decades because they offer favorable environmental advantages in terms of biodegradability compared to conventional synthetic polymeric films. Edible and biodegradable natural polymer films offer alternative packagings and coatings with lower environmental costs. The search for new renewable resources for the production of edible and biodegradable materials has steadily increased in recent years. In particular, nonconventional sources of carbohydrates have been extensively studied. There are various unique carbohydrates that are found in marine organisms that represent a largely unexplored source of valuable materials. These nonconventional and underexploited renewable materials can be used as an interesting alternative to produce edible films and coatings (*4*).

The biopolymers studied in this work to produce edible films and coatings were κ/ι-hybrid carrageenan extracted from *Mastocarpus stellatus*, an underexploited red algae present in the Portuguese marine coast (*1*−*4*). Carrageenans are water-soluble polymers with a linear chain of partially sulfated galactans, which present high potentiality as film-forming materials. Carrageenans are structural polysaccharides from red seaweed and have been used extensively in foods, cosmetics, and pharmaceuticals (*5*). Carrageenan biopolymer extracted from *M. stellatus* seaweeds was shown to be a κ/ι-hybrid carrageenan with gel properties comparable to those of commercial κ-carrageenan gel formers. The use of carrageenan as edible films and coatings already covers various fields of the food industry such as application on fresh and frozen meat, poultry, and fish to prevent superficial dehydration (*6*), ham or sausage casings (*7*), granulation-coated powders, dry solids foods, oily foods (*8*), etc., and also the manufacture of soft capsules (*9*, *10*) and especially nongelatin capsules (*11*). Polysaccharide and protein film materials are characterized by high moisture permeability, low oxygen and lipid permeability at lower relative humidities, and compromised barrier and mechanical properties at high relative humidities (*12*).

To tailor the properties and improve the water resistance of these biopolymers, it is often desirable to blend them with more water-resistant biopolymers or with nanoadditives. In the case of the addition of nanoclays, the nanocomposite films have been seen to substantially reduce water-vapor permeability, solving one of the long-standing problems in the production of biopolymer films and coatings (*13*).

More recently, cellulose nanowhiskers (CNW), also termed cellulose nanocrystals, are increasingly used as load-bearing constituents in developing new and inexpensive biodegradable materials due to their high aspect ratio, good mechanical properties (*14*), and fully degradable and renewable character.

*Author to whom correspondence should be addressed (e-mail lagaron@iata.csic.es).

Published on Web 11/12/2010

Cellulose (2010) 17:987–1004
DOI 10.1007/s10570-010-9430-x

On the use of plant cellulose nanowhiskers to enhance the barrier properties of polylactic acid

Maria D. Sanchez-Garcia · Jose M. Lagaron

Received: 4 May 2010 / Accepted: 22 June 2010 / Published online: 8 July 2010

Abstract Polylactic acid (PLA) nanocomposites were prepared using cellulose nanowhiskers (CNW) as a reinforcing element in order to asses the value of this filler to reduce the gas and vapour permeability of the biopolyester matrix. The nanocomposites were prepared by incorporating 1, 2, 3 and 5 wt% of the CNW into the PLA matrix by a chloroform solution casting method. The morphology, thermal and mechanical behaviour and permeability of the films were investigated. The CNW prepared by acid hydrolysis of highly purified alpha cellulose microfibers, resulted in nanofibers of 60–160 nm in length and of 10–20 nm in thickness. The results indicated that the nanofiller was well dispersed in the PLA matrix, did not impair the thermal stability of this but induced the formation of some crystallinity, most likely transcrystallinity. CNW prepared by freeze drying exhibited in the nanocomposites better morphology and properties than their solvent exchanged counterparts. Interestingly, the water permeability of nanocomposites of PLA decreased with the addition of CNW prepared by freeze drying by up to 82% and the oxygen permeability by up to 90%. Optimum barrier enhancement was found for composites containing loadings of CNW below 3 wt%. Typical modelling of barrier and mechanical properties failed to describe the behaviour of the composites and appropriate discussion regarding this aspect was also carried out. From the results, CNW exhibit novel significant potential in coatings, membranes and food agrobased packaging applications.

Keywords Cellulose · Nanobiocomposites · Mass transport properties · PLA

M. D. Sanchez-Garcia · J. M. Lagaron (✉)
Novel Materials and Nanotechnology Group, IATA-CSIC, Av. Agustin Escardino 7, 46980 Paterna, Spain
e-mail: lagaron@iata.csic.es

Introduction

Production of 'green materials' based on raw materials derived from natural sources of plant or animal origin are of great interest both in the academic and industrial fields. The most widely researched thermoplastic sustainable biopolymers for food agrobased packaging applications are starch, PLA and PHA's. From these, starch and PLA biopolymers are without doubt the most interesting families of biodegradable materials because they have become commercially available, are produced in a large industrial scale and also because they present an interesting balance of properties. Yet, the main drawbacks of this new family of polymers regarding performance are still associated to low thermal resistance, excessive brittleness and insufficient barrier to oxygen and/or to water compared to for instance other benchmark packaging polymers such as polyolefins and PET. It is,

ELSEVIER

Trends in Food Science & Technology 21 (2010) 528–536

TRENDS IN FOOD SCIENCE &TECHNOLOGY

Review

Natural micro and nanobiocomposites with enhanced barrier properties and novel functionalities for food biopackaging applications

Maria D. Sanchez-Garcia, Amparo Lopez-Rubio and Jose M. Lagaron*

Novel Materials and Nanotechnology Group, IATA, CSIC, Apdo. Correos 73, 46100 Burjassot, Valencia, Spain (Tel.: +34 963900022; fax: +34 963636301; e-mail: lagaron@iata.csic.es)

The incorporation of nanoclays, micro and nanofibers of cellulose and carbon nanofibers and nanotubes into bioplastics is attracting a great deal of research interest regarding improvement of general physical properties in plastics and bioplastics. The present overview shows, beyond the reviewed state of the art, nanobiocomposites specifically developed for food packaging applications, in which mainly cellulose biofibers, their highly crystalline building nanoblocks and food contact complying non-MMT (non-montmorillonite) nanoclays have been used in melt blending and solution casting processing routes to improve the barrier properties to gases and vapours and to impart additional functionalities to biopackaging plastics. Bar rier properties are known to be very strong limiting factors for the current widespread application of, mainly, biopolyesters in self-life extension of biopackaged foods. The paper specifically exemplifies on novel functionalities by showing novel nanobiocomposite films of biopolyesters with enhanced gas, vapour and UV barrier and simultaneously exhibiting controlled release capacity of an antimicrobial and antioxidant natural plant extract of interest in active antimicrobial food biopackaging applications.

* Corresponding author.

0924-2244/$ - see front matter © 2010 Published by Elsevier Ltd.
doi:10.1016/j.tifs.2010.07.008

State of the art

Biopolymers

There is a growing worldwide interest pushed by governments and societies to increment the responsible use of renewable resources in plastic commodity products in order to reduce the waste associated to their use, particularly in packaging applications (Petersen, Nielsen, & Olsen, 2001). The use of biodegradable plastics and resources are seen as one of the many strategies to minimise the environmental impact of petroleum-based plastics. The biological base of these new biopolymers provides a unique opportunity to incorporate a highly demanded property of these materials, i.e. compostability. Plastic recycling is not often economically viable due to contamination of the food packages. Therefore, compostability is a very interesting option that guarantees that new biomaterials will degrade mostly into carbon dioxide and water after disposal (Kijchavengkul, Auras, Rubino, Ngouajio, & Fernandez, 2006).

Biodegradable materials present a number of promising properties in a number of applications, including packaging, automotive and biomedical sectors. Specifically, thermoplastic biodegradable polymers, such as poly(lactic acid) (PLA), polyhydroxyalkanoates (PHA) and polycaprolactones (PCL), exhibit an excellent equilibrium of properties, apart from being processable using conventional plastics machinery and, for the case of the first two, they arise from renewable resources. PLA is a thermoplastic biopolyester produced from L-lactic acid, which typically comes from the fermentation of corn starch. Currently, PLA is being commercialized as a food packaging polymer in cups, containers and films for short shelf-life products (Auras, Singh, & Singh, 2006). Polyhydroxybutyrate (PHB) is a naturally occurring β-hydroxyacid (a linear polyester). The homopolymer, poly(hydroxybutyrate) PHB, and its copolymer with hydroxyvalerate, PHBV, are biodegradable thermoplastic polymers with important trade

NANOCOMPOSITES FOR FOOD PACKAGING

1. Introduction

Nanotechnology is by definition the creation and use of structures with at least one dimension in the nanometer-length scale that creates novel properties and phenomena otherwise not displayed by either isolated molecules or bulk materials. Since Toyota researchers in the late 1980s found that mechanical, thermal, and barrier properties of nylon-clay composite materials improved to a significant extent by reinforcement with less than 5% of clay (1), extensive research work has been performed in the study of nanocomposites for packaging application. The term "nanocomposite" refers to composite materials that contain typically low additions of some kind of nanostructured materials. Most nanocomposites being considered in the packaging sector are based in low additions, typically 1 to 7 wt%, of modified nanoclays.

2. Technology

Nanoscale structures display a high surface-to-volume ratio, which becomes ideal for applications that involve composite materials, chemical reactions, drug delivery, controlled and immediate release of substances in active and functional packaging technologies, and energy storage, for instance, in intelligent packaging (2,3).

Until recently, the most interesting packaging technology based on blending to generate barrier properties was the so-called oxygen scavengers. This technology is known to lead to relatively low levels of oxygen in contact with the food because it traps permeated oxygen from both the headspace and the outside. However, in carbonated beverages for instance, a barrier to carbon dioxide is also a requirement. As most commodity plastic packaging materials, eg, poly(ethylene terephthalate) (PET) and its main sustainable counterpart the PLA, are not sufficient barrier to these gases, multilayer structures had to be devised in which one layer (made of ethylene-vinyl alcohol copolymer (EVOH), MXD6, poly(ethylene naphthalene) (PEN), and nanocomposites of PA6) needs be high barrier to carbon dioxide and to oxygen. An alternative, technology is the use of oxygen scavenger but these only reduce O_2, and not CO_2, at the packaging headspace. The nanobio-composites technology can overcome this in monolayer solutions because barrier properties are usually not only to oxygen but also to other gases and low-molecular-weight components such as water vapor and food aroma components (4).

In general, the rationale behind the interest of the nanocomposites is that with low additions of the nanofiller, many relevant properties can be enhanced without a significant drop in interesting properties of the matrix such as transparency or toughness. As stated above, one property that has attracted more interest in the food-packaging area, because of its direct implication in food quality and safety issues, is the possibility of increasing the barrier properties to gases and vapors of plastics and bioplastics. Thus, by simple application of models such as the one of Nielsen, and for the case of laminar structures with

WOODHEAD PUBLISHING IN FOOD SCIENCE, TECHNOLOGY AND NUTRITION

Environmentally compatible food packaging

Edited by Emo Chiellini

3

Thermoplastic nanobiocomposites for rigid and flexible food packaging applications

J. Lagaron and M. Sanchez-Garcia, Institute of Agrochemistry and Food Technology, Spain; E. Gimenez, ESID, University Jaume I, Castellon, Spain

3.1 Introduction: plastic food packaging, sustainable materials and barrier properties

Over the last few decades there has been a significant increase in the amount of plastics being used in packaging applications. In fact, the largest application for plastics today is packaging, and within the packaging niche, food packaging constitutes the largest plastics-demanding application. This is because plastics demonstrate enormous advantages, such as thermoweldability, flexibility in thermal and mechanical properties, lightness and low price.[1–3] However, polymers do also have a number of limitations for certain applications when compared with more traditional materials such as metals and alloys or ceramics. Of these limitations, those relevant to this chapter are their impermeability to low molecular weight components, a comparatively low thermal resistance and a strong interdependence between the last two properties. In spite of this, use of plastic materials continues to expand and to replace the conventional use of paperboard, tinplate cans and glass, which have typically been used as monolayer systems. Initially, most plastic packaging was made of monolayer rigid or flexible materials but as the advantages of plastic packaging became more and more established and developed, the increasingly demanding product requirements found when plastics had to suit more and more different food products led, in conjunction with significant advances in plastic processing technologies, to more and more complex polymeric packaging formulations. This resulted in complex multicomponent structures such as the so-called multilayer packaging-based systems widely used today. However, there are significant advantages in terms of costs and other issues, such as ease of recycling, in